AN ABSTRACT OF THE THESIS OF

Austin R. Volk for the degree of Honors Baccalaureate of Science in Mechanical Engineering presented on March 6, 2014. Title: The Design, Manufacturing, and Testing of the 2014 Side-Pods for the Global Formula Racing Vehicle.

Abstract approved:

_____

Robert K. Paasch

For many years, engine overhearing has been the major cause for vehicle breakdowns and engine malfunctions for most teams in Endurance events at Formula Society of Automotive Engineers (FSAE) Series competitions. Additionally, with a growing importance of aerodynamics to the overall success of the *Global Formula Racing* at these events, in addition to an internal need for engine cooling, the side-pods have been a large focus of redesign for the 2014 season. The side-pods, which house oil and water radiators for engine cooling, are responsible for providing adequate airflow to maintain stable engine operating temperatures, while increasing downforce and reducing drag on the vehicle. This thesis details the complete design and manufacturing processes, followed by testing simulations and physical validation of the 2014 side-pods on the *Global Formula Racing* combustion and electric vehicles.

Keywords: Aerodynamics, Side-Pod, Cooling Duct, Formula SAE

Corresponding email address: ARV61291@comcast.net

The Design, Manufacturing, and Testing of the 2014 Side-Pods for the Global Formula Racing Vehicle

by

Austin R. Volk

A PROJECT

submitted to

Oregon State University

University Honors College

in partial fulfillment of
the requirements for the
degree of

Honors Baccalaureate of Science in Mechanical Engineering (Honors Scholar)

Presented March 6, 2014

Commencement June 14, 2014

Honors Baccalaureate of Science in Mechanical Engineering project of Austin R. Volk presented on March 6, 2014.

APPROVED:

_____

Mentor, representing Mechanical Engineering

_____

Committee Member, representing Mechanical Engineering

_____

Committee Member, representing Industrial and Manufacturing Engineering

_____

Chair, School of Mechanical, Industrial, and Manufacturing Engineering (MIME)

_____

Dean, University Honors College

I understand that my project will become part of the permanent collection of Oregon State University, University Honors College. My signature below authorizes release of my project to any reader upon request.

_____

Austin R. Volk, Author

ACKNOWLEDGEMENTS

I would like to thank my close mentor, Dr. Robert Paasch, for the continuous support, inspiration, wisdom and passion that he has so generously shared with me during this whole process. You have helped to inspire so much of the passion instilled in this work, as well as in my own personal engineering career. I look forward to our work together in the future.

I would also like to thank Dr. Toni Doolen for her time, expertise, and endless support and guidance in helping to make this thesis possible. I enjoyed our numerous conversations throughout my undergraduate career and I thank you for all the time you devoted to helping me find the right project.

To Dr. Nancy Squires, I thank you for always being so passionate about what you teach, and for always demonstrating the highest level of interest in your student's education. You have inspired my passion of aerodynamics and engineering and I am so grateful to have been able to learn from you.

I would also like to individually thank Phillip Arscott for his support and guidance during this endeavor, as well as my fellow team members at *Global Formula Racing* for their contribution to this project.

Finally, to my family and friends for their continuous love and support throughout my life and undergraduate career. Thank you for all of your advice, guidance, inspiration and for always being there to share the successes and hurdles associated with this work.

Table of Contents

List of Figures

List of Tables

The Design, Manufacturing, and Testing of the 2014 Side-Pods

for the Global Formula Racing Vehicle

1. Introduction

Since 1979, the Society of Automotive Engineers (SAE) have developed numerous competitions in which students from Universities around the world come together to race formula style vehicles. These cars have been designed, manufactured, and tested by undergraduate and graduate students from universities all around the World. The Formula SAE® Series (FSAE) competitions challenge students of multiple engineering disciplines, to collaborate to engineer and fabricate a small racing vehicle, which is supported by a strong marketing and business case. These teams work together as to represent a “design firm” engineering, fabricating, and testing prototype vehicles for the non-professional, weekend competition market that will later be “sold” to a “corporation” for future production [1].

Each different academic institution competes in various Static and Dynamic events through which the vehicle's engineering quality and performance is evaluated and tested. These students subject their vehicles to competitions against all of the other present Universities in order to gain the most points. These points determine the overall winner of the competition and will be discussed in more detail in Section 2.6. Although there are FSAE Rules that must be followed by each team, FSAE is designed to give maximum design flexibility and freedom of creativity and engineering in the complete vehicle design [1].

In 2009, Beaver Racing Team from Oregon State University *(Corvallis, Oregon, USA)* and BA Racing Team from Duale Hochschule Baden-Württemberg-Ravensburg, DHBW-R *(Friedrichshafen, Baden-Württemberg, Germany)* formed the first ever global collaboration between a U.S. and European team to design and manufacture two vehicles for formula style race events held across the globe. This global collaboration is known as *Global Formula Racing* (GFR). Every year GFR students design and manufacture a Combustion Car (cCar, OSU) and an Electric Car (eCar, DHBW-R) in which students from both institutions work together in building components for both cars despite the geographical separation.

With the growing importance of aerodynamics to the overall success of formula styles vehicles in racing events, this has been a rather large focus of design, development, and testing for the Global Formula Racing vehicles. In 2010, *Global Formula Racing* designed, manufactured, and implemented its first aerodynamics package, which helped to improve the overall performance of each vehicle. The notable success, measured by three consecutive national championships in Formula SAE® with the addition of aerodynamic elements, has motivated the *GFR* team to continue to improve these components. The 2014 combustion and electric vehicles will incorporate a redesigned aerodynamics, package which will include a front wing, undertray, side-pod, and rear wing.

Motivation

In recent years, engine overheating has been the major cause for vehicle breakdowns for many universities during endurance events at FSAE competitions,

including *Global Formula Racing* [13]. The side-pod plays a large role in the cooling performance of the engine components and was one of the primary goals in the development of this thesis. Additionally, the side-pod plays an important role in the aerodynamic performance of the vehicle, and with a relatively outdated design, this is the first new side-pod since 2011. The primary motivation for this thesis was to develop a new side-pod package to improve the aerodynamic and cooling performance of the combustion and electric vehicles, while also providing a large contribution to the overall appearance of the vehicle. As a student with interests in racing vehicle development, aerodynamics, and engine performance, this project and thesis provided all of the desired qualities of an interesting, yet tremendously challenging, engineering task.

This thesis will focus on the complete development of the side-pods for the 2014 combustion and electric vehicle for *Global Formula Racing.* This includes all of the design, manufacturing, and testing processes of the side-pod package and its internal components.

2. Background

The following section will provide an extensive overview of background knowledge necessary for understanding concepts and principles used to develop the 2014 side-pod package. This chapter will also cover limitations to the design including rules and regulations, and information on previous *Global Formula Racing* vehicles. Further information can be found in the sources cited in this thesis.

2.1 Side-Pod System

This section will outline the basics of the side-pod component and those characteristics related to aerodynamic concepts.

2.1.1 Side-Pod Functionality

Airflow around a race-car body is one that is extremely difficult to predict, but is crucial to the performance of the vehicle. The use of aerodynamic elements, such as wings and underbody devices such as an undertray, has helped in enhancing the aerodynamic performance of the vehicles. The side-pods play a unique role in the performance of the vehicle in areas of aerodynamics and heat management.

The *Global Formula Racing* combustion vehicle uses oil and water radiators that need to be cooled through the use of air convection. Much like the side-pods of Formula 1, the radiators are also housed within side-pod systems on each side of the vehicle. The side-pod duct allows the vehicle to utilize the energy of the incoming airflow to aid in the

cooling of engine components with minor aerodynamic losses [15]. See Figure 1 for an example of a typical side-pod duct.

Figure 1: Formula 1 style side-pod [15]

With the addition of the radiator in the open-stream comes resistance in airflow and thus increased vehicle drag [8]. The use of the side-pod helps dramatically to reduce the drag from radiators. In some cases, vehicles with side-pods have seen a reduction in drag, as much as 7 to 13 times less than in vehicles without side-pods [15].

Due to the slight airfoil shape of most formula style side-pods and a high pressure zone in front of the radiator at the inlet of the duct, there are potential lifting forces, which are both disadvantages to the side-pod component.

2.1.2 Aerodynamics – Lift, Drag and Downforce

Airflow over rigid bodies tends to produce aerodynamic forces in the vertical and horizontal direction of the free-stream airflow. These aerodynamic forces are known as lift and drag.

In regards to a race-car, these forces stem from the properties of the surrounding air and the disturbances caused by the motion of the vehicle [15]. As the vehicle travels, the air is accelerated as it deflects around the car. The forces caused by this acceleration can be broken down into vertical and horizontal components. For a race car, the emphasis is on downforce (negative lift) and drag seen in Figure 2 [15].

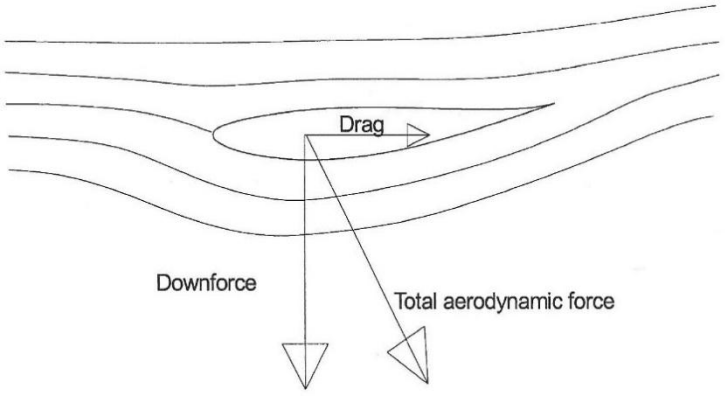

Figure 2: Main components of aerodynamic forces [15].

As an airfoil *(seen in Figure 2)* travels through a fluid, the forces on the object become stronger with increasing velocities. The wing pushes the air out of the way as it travels, causing the air to flow over both the top and bottom surfaces. Naturally, this air wants to follow the wing's curvature and to meet up at the trailing edge of the wing. In order for this to occur, Newton's law tells us that there must be a force acting on the air for this to happen, usually frictional forces due to fluid viscosity. This viscosity can be

thought of as a friction coefficient, or a measure of "stickiness" of a fluid against a surface. As the fluid closest to the surface begins to follow the curvature of the wing, the surrounding air is also influenced to behave similarly and accelerates towards the surface. This is caused by an external force, explained by Bernoulli's principle, as expressed by **Error! Reference source not found.**.

$$\begin{aligned} &\boldsymbol{Local\ Static\ Pressure + Dynamic\ Pressure = Constant} \\ &\boldsymbol{= Total\ Pressure} \\ &\boldsymbol{Static\ Pressure + \frac{1}{2}\ x\ Fluid\ Density\ x\ Fluid\ Velocity^2} \\ &\boldsymbol{= Total\ Pressure} \\ &\boldsymbol{P_{Static} + \frac{1}{2}\rho V^2 = Constant = Total\ Pressure} \end{aligned} \tag{1}$$

As velocity increases, or "dynamic" pressure increases, the "local static" pressure must decrease in order for total pressure to remain constant [15]. As the air begins to turn (accelerate) around the more curved surface, this causes velocity to increase, causing a decrease in "local static pressure". This causes a pressure gradient on the two sides of the inverted wing profile, with a higher pressure on the top surface than the bottom. This is the downforce experienced by the car.

Drag forces are similar in behavior, however drag acts because of frictional forces along the surface of the object, known as skin drag, as well as from flow separation, known as induced drag. When fluid flows over an object, the frictional forces caused by the viscosity tend to build up a "boundary layer". At the surface, the flow is very smooth and streamlined, or "laminar". This boundary layer gradually slows the fluid further away

from the surface. With this increase in friction, the air begins to lose its kinetic energy. When fluid does not have sufficient kinetic energy to flow from regions of high to low pressure, the fluid begins to "separate". This separation typically occurs at the rear of the vehicle, creating areas of chaotic, random, fast moving air or "turbulence". As seen from Bernoulli's principle, this high velocity air increases "dynamic" pressure while lowering "local static pressure". This creates a pressure gradient of high pressure in front of the moving object, and a low pressure region behind. This gradient produces a force in the direction of fluid flow, opposing vehicle motion, and creates drag. These boundary layer conditions can be seen in Figure 3.

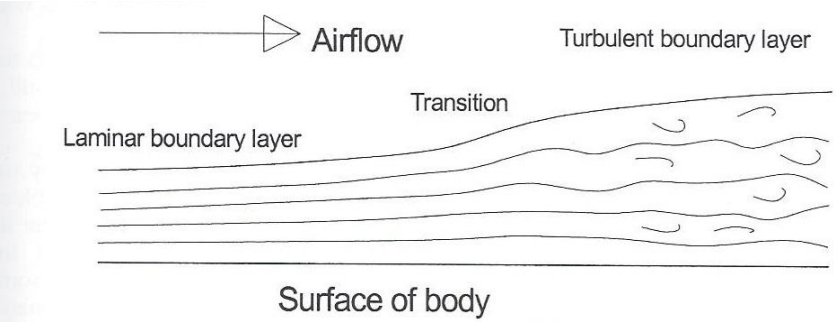

Figure 3: Boundary layer visualization of transition from laminar to turbulent flow [15]

An understanding of a general concept of the two forces is crucial in regards to vehicle design. With increased drag forces, a vehicle's engine must work harder to produce the necessary forward thrust to accelerate and move the car. With increased downforce the car experiences larger vertical forces, increasing the normal force of the tires in contact with the track. This increase in normal force increases the frictional forces, as well as the surface area (through tire compression), allowing for better traction or "grip" [15]. This increase in traction allows for greater acceleration, braking, and

cornering at higher speeds without overcoming frictional forces needed to maintain stability. As seen by Equation 2, an increase in downforce, increases normal force and directly relates to an exponential increase in the velocity that can be achieved around a given corner. This also indicates that with increases in downforce, the vehicle is also able to maintain the same velocity through corners with tighter radii.

$$\boldsymbol{Friction\ Force = Centripetal\ Force}$$

$$\boldsymbol{Frictional\ Force =}$$

$$\boldsymbol{Friction\ Coefficient\ x\ Vertical\ Normal\ Force} \tag{2}$$

$$\boldsymbol{Centripetal\ Force = \frac{Mass\ x\ Velocity^2}{Corner\ Radius}}$$

$$\boldsymbol{\mu * F_N = \frac{mV^2}{R_{corner}}}$$

These principles of aerodynamics and the encountered forces experienced by objects in air are crucial for proper racing vehicle design, especially in high-speed applications such as formula racing.

2.1.2.1 Airfoil Terminology

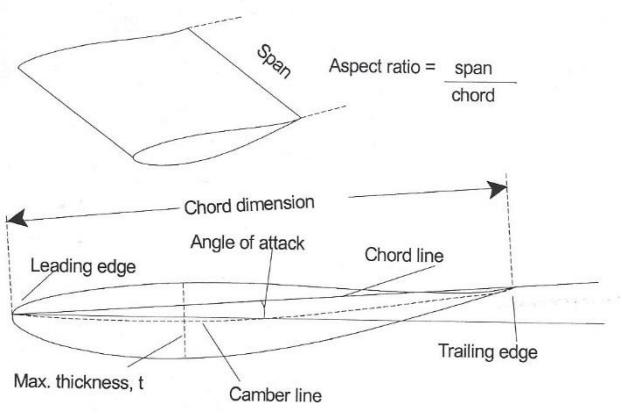

Figure 4: Wing terminology [15].

- **Leading edge**: Front part of the wing with radius shape.
- **Trailing edge**: Rearmost part of the wing, usually thin.
- **Chord line**: Distance from the leading edge to the trailing edge.
- **Maximum Thickness**: Denoted as percentage of overall chord length
- **Camber**: Wings that are asymmetric (most race-car wings) are said to have camber if one of the surfaces has more curvature than the other. In the case of the race-car wing in Figure 4, the bottom surface has much more curvature than the top, so this wing has *camber*. The camber of symmetric airfoils occurs along the mid-plane of the profile.
- **Camber Line**: Line drawn between the midpoints of the top and bottom surface at each point along the length of the wing.
- **Location of Maximum Camber**: Percentage of the chord length.
- **Span**: Width of the wing.

- **Angle of Attack (AoA)**: angle between free stream airflow and the chord line.

2.1.3 Automotive Cooling – Racing Vehicles

Traditional passenger cars are equipped with cooling and engine components concealed behind the front grill of the vehicle. In formula style vehicles, cooling component sizing and placement is much more difficult given the heavily restricted packaging space available. Given the high performance of these particular engines, these power plants traditionally produce a large amount power and heat. In order to maintain longevity in functionality and performance, this heat needs to be dissipated in order to prevent severe thermal stresses in the mechanical components of the engine [3]. In formula vehicles, this is done with a set of radiator coolers: oil and water.

2.1.3.1 Radiators – Location

As mentioned previously, sticking a radiator in the open will result in large amounts of drag. In order to improve both the thermal and aerodynamic efficiency of the cooling components, proper ducting design is required if the engineer is to provide adequate cooling with minor aerodynamic performance losses [15].

In many cases in Formula 1 history, the radiator was mounted in the front nose of the car, to capture clean, undisturbed air. In 1971, the Lotus 72 set the pace for side mounted radiators, and has been utilized ever since [21]. The Lotus 72 is shown in Figure 5.

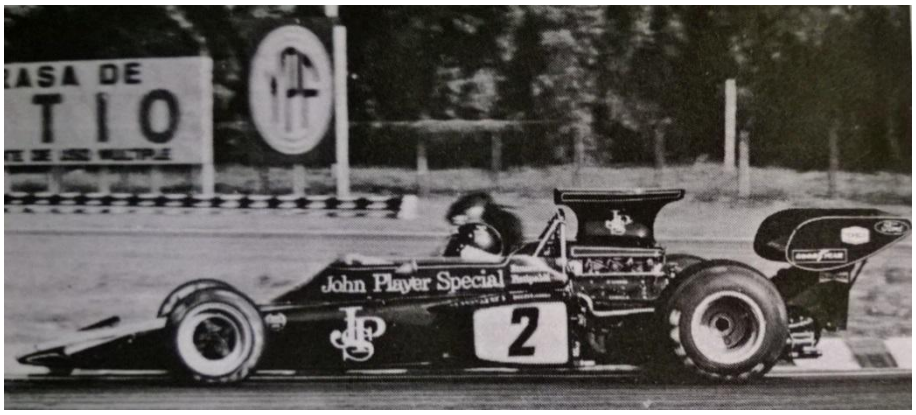

Figure 5: Lotus 72 with side mounted radiators [21]

In racing cars, with exposed wheels and suspension linkages and traveling along relatively high temperature track surfaces, it is fundamentally more difficult to cool the engine effectively [21]. Side mounting the radiators provides some potential drawbacks, as well as benefits. Given the suspension and wheels near the vicinity of the side-pod intake, the airflow becomes less favorable as it becomes rapidly disturbed by the rotation of the wheels and turbulent flow over the suspension links. However, in regards to vehicle dynamics, a low side-mounting radiator provides better vehicle performance given that it lowers the center of gravity, while allowing for housing in a much larger side-pod duct.

2.1.3.2 Radiator Functionality

The implementation of an effective cooling package for formula style race cars is imperative to the success of the vehicle. With an accurately paired engine and cooling system, the engine is able to reach an operating temperature that is high enough to ensure proper combustion, while remaining low enough to prevent any damage to the engine

block or cylinders [3]. The way this is obtained is through the use of oil and water radiators. These cooling systems rely on convective heat transfer, by forcing air through the radiator by the forward motion of the vehicle. This is necessary in order to remove heat output generated by the engine. Typically, radiators are packaged to match the cubic inch displacement of the engine so that the radiator will have adequate cooling capacity [14].

A radiator is a large heat exchanger that uses tubes, fins, and tanks, typically made of aluminum or other metal, to pass hot engine fluids and air through a system of channels to cool the engine [4]. The type of radiator used on the 2014 *Global Formula Racing* vehicle for both oil and water is shown in Figure 6.

Figure 6: 2014 GFR Radiators

Radiator functionality is rather simple but important for understanding effective cooling practices. In general, a radiator is a device that holds a large volume of liquid

(water or oil) in close proximity to a large volume of air, in order to induce convective heat transfer. A schematic of the basic radiator structure is seen in Figure 7.

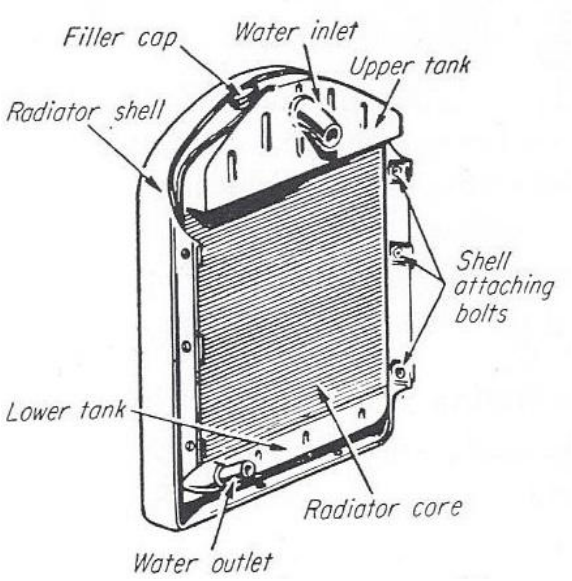

Figure 7: General radiator internal schematic [4]

The heated water or oil from the engine and transmission enter in through the top tank of the radiator and begin to transfer the heat to the radiator housing. The warm water passing through the radiator then becomes cool as air passes through the radiator, causing it to increase in density and sink to the bottom of the unit. As it sinks to the bottom tank, the water or oil travels through narrow passages formed by pairs of thin metal ribbons. These narrow fluid passages are separated by “fins” in the ribbon-cellular radiator core structure, seen in Figure 8.

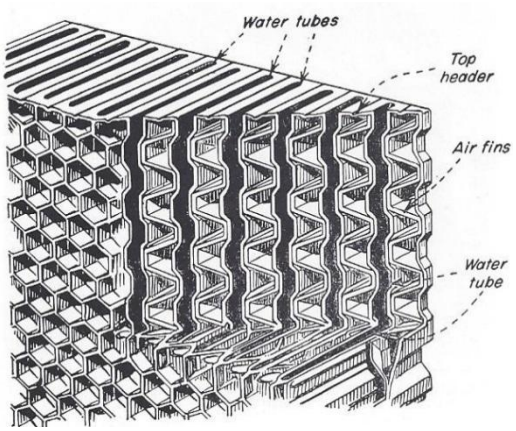

Figure 8: Radiator ribbon-cellular "fin" core structure [4]

Air flows between these fins in the direction of incoming airstreams, utilizing convection to force the air to absorb heat from the fins, which have already absorbed heat from the high temperature water moving through the metal ribbons. This hot air exits out the back of the radiator fins to ambient air, while the now cooled fluid leaves the bottom tank and travels back to the engine and transmission to further cool the engine block, cylinders, valves, gears, and more [4].

2.1.3.3 Radiator Heat Transfer

Radiators utilize the phenomena of convective heat transfer. Convection occurs because of two different mechanisms: random molecular motion and bulk fluid motion [2]. Convection occurs between a moving fluid and a contact surface over which the fluid flows, both at two different temperatures. In the event of a temperature difference, or gradient, the motion of the fluid alone allows for heat transfer. Boundary layers occur in moving fluids. In thermodynamics, the temperature throughout the air in boundary layer will develop a thermal boundary layer.

At the beginning of the boundary layer, the interface between the surface and the moving fluid, diffusion (random molecular motion) causes the majority of the heat transfer. At this point, the velocity is near zero and experiences conductive heat transfer which occurs between the two "still" bodies. As the fluid flows over the surface and the boundary layer forms, the heat transfer at the contact surface propagates downstream until the heat eventually is transferred to the air beyond the range of the boundary layer [2]. The thermal boundary layer principle is further illustrated in Figure 9.

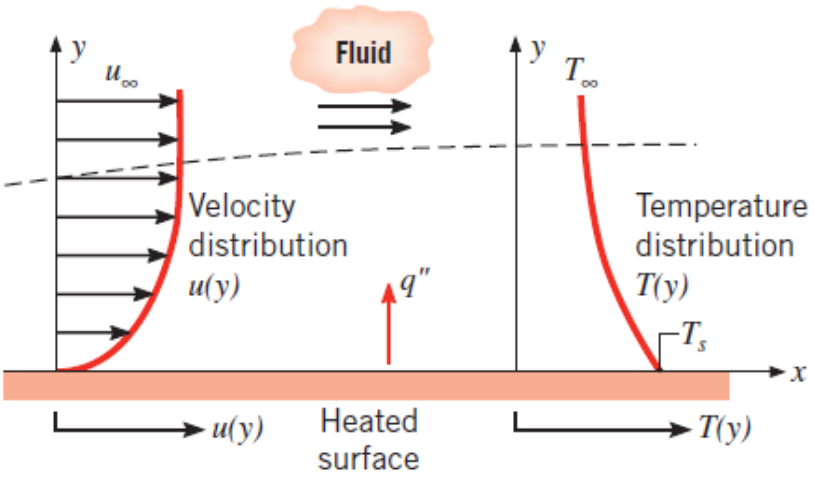

Figure 9: Velocity and thermal boundary layer development [2].

There are two types of fluid boundary layers: laminar and turbulent. Within a laminar boundary layer, the fluid is highly organized and streamlined. Turbulent boundary layer regions have large kinetic energy causing mixing as the high speed fluid travels towards the surface. Slow moving fluid is then thrown further out into the free stream as a result of this mixing. With these larger mixing capabilities and larger fluid velocities, the convective heat transfer coefficients are much larger than those for slower velocity, laminar flow. Thus, with increased turbulence, there is greater heat transfer [2].

2.1.3.3.1 Heat Transfer and Convection Coefficient

The general equation for convection heat transfer from the surface to the surrounding fluid is shown in Equation 3. Equation 3 identifies three different variables that can be manipulated to produce the correct amount of heat flow.

$$\boldsymbol{Q = hA(T_s - T_\infty)} \quad (3)$$

Where:

$$\boldsymbol{Q = Convective\ Heat\ Flow}\ ;\ \boldsymbol{h = Convection\ Coefficient};$$

$$\boldsymbol{A = Surface\ Area}$$

$$\boldsymbol{T_s = Surface\ Temperature};\ \boldsymbol{T_\infty = Ambient\ Fluid\ Temperature}$$

Equation 1: Heat transfer due to convection [2]

The first is the temperature gradient. As Equation 3 shows, the larger the temperature difference, the greater the heat transfer. Since the surface temperature of a radiator is based on the power output and operation of the engine, this temperature is an uncontrollable design constraint for the engineers. The ambient fluid temperature however is a variable that can be controlled in certain situations. The lower the temperature, the larger the temperature gradient, and therefore a higher level of heat exchange. For formula vehicles, it is rarely possible to change the surrounding air temperature. Normally this is representative of the ambient air on race-day and the air just above the surface of the track.

The second parameter is the convection coefficient, h. This parameter allows for the most flexibility in the design. The convection coefficient depends on material properties of the fluid, and most importantly in racing design, the velocity of the fluid. Many situations where *h* is fully maximized leads to insufficient heat transfer rates, or the costs of achieving a maximum convection coefficient is too expensive and outweighs the benefits gained [2]. In the case of formula cars, *h* can be maximized by increasing vehicle speed, however the maximization of the convection coefficient is limited by the power output of the vehicle's engine and the top speed it can achieve at full power.

The last variable is surface area. In racing vehicles, the space available for packaging provides a tight constraint on the overall design of the vehicle, especially for cooling components. Often there is little room for increases in area of the radiator, given the constraint of the side-pods, maximum vehicle width, height and so forth. There are however, ways in which engineers have increased the surface area available for convective heat transfer, such as by adding "fins".

2.1.3.4 Heat Exchanger Fins

The most common way for engineers to increase the surface area available for convection is through the addition of fins. This concept explains why automotive radiators utilize fins in the "ribbon-cellular" core mentioned to improve heat transfer for engine cooling. Fins add extra surface area and traditionally are designed with large thermal conductivities to minimize temperature variations from the base to the tip [2]. An example of a fin set up is shown in Figure 10.

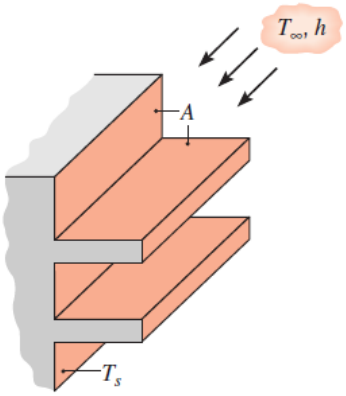

Figure 10: Fin schematic for improving convective heat transfer [2]

2.1.3.5 Air Fans

The last portion of the radiator package design for cooling enhancements is the radiator fan. Convection occurs naturally through changes in temperature and density which leads to circulation. Alternatively, the most common use of convection is forced convection. Forced convection is caused by external forces such as an electric fan, atmospheric wind speeds, as well as vehicle speeds and ram-air effects. In the case of forced convection, the speed of the air is controlled by an external source, which increases the convection coefficient, thus increasing heat transfer. Figure 11 illustrates this concept.

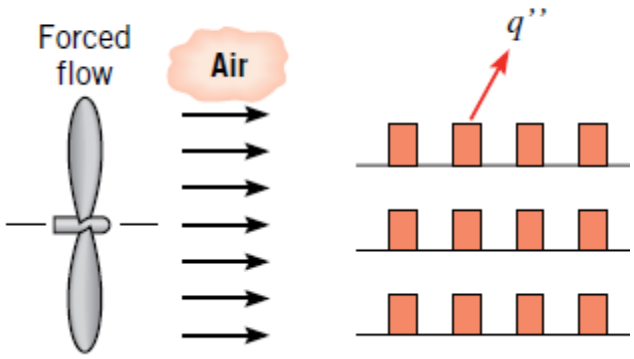

Figure 11: Force convection through auxiliary fans [2].

Fans are typically mounted on the back of the radiator and draw air from the outside environment at the opening of the side-pod, through the radiator core where it picks up heat from the high temperature engine fluid, and forces the air out an exit at the back of the duct. Airflow through each of these components has an influence on the flow through the main radiator and must be carefully controlled [17]. A schematic of this is shown in Figure 12.

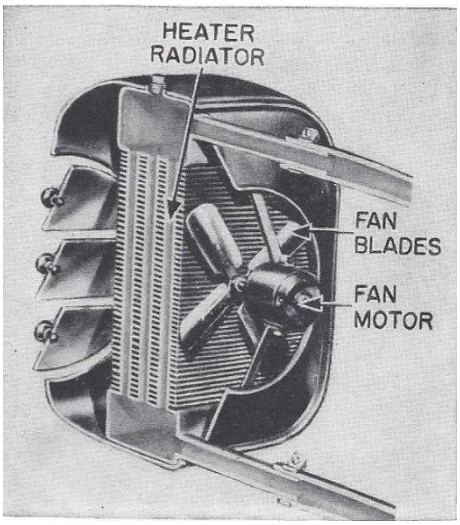

Figure 12: Radiator fan mounting schematic [4]

Some applications of radiator packages are equipped with fan shrouds that help to improve the cooling performance. Shrouds increase the efficiency of the fan by assuring that all airflow induced by the fan passes through the radiator core [4]. Ideally, air pressure in front of the radiator should be distributed evenly over the entire core to ensure proper cooling. Mounting a fan behind the radiator helps create a pressure drop in the rear of the duct that helps to further distribute the pressure over the front face of the radiator and assist in improved cooling capabilities [8].

2.1.4 Side-Pod Ducting Design

The shape and ducting design of the side-pod plays an important role on both aerodynamic and thermodynamic levels. Typical cooling ducts contain a small inlet, diverge to a wide-section at the location of the radiator, and then converge to a small exit at the rear of the duct. A small inlet reduces the ram-air pressure (forced air) needed to build up local static pressure in front of the radiator core for adequate airflow. [3].

The addition of a radiator and fan within the internals of the side-pod causes large pressure variations between the front and rear sections of the side-pods. As the nature of the radiator is to reject heat through convection, high velocity and thus higher mass flow rates correlate to larger values of heat transfer. The radiator and fan causes resistance of airflow and causes a pressure gradient. The gradients cause large variations in mass flow rate capabilities for cooling purpose depending on vehicle speeds and radiator flow restrictions caused by its internal finned core.

2.1.4.1 Fluid Flow through Ducts

Flow through the ducting core of the radiator requires a "pressure drop" to drive the air through the system. Bernoulli's principle and conservation of mass help to identify how fluid flows from areas of high to low pressure. For this reason, the ducting usually consists of a diverging section in which pressure at the inlet begins to increase in "local" static pressure as it slows through the opening. With a restricted opening and a diverging section, mass can be conserved. The equation for the conservation of mass in steady state conditions, assuming incompressible flow (constant density), is shown by Equation 4.

Mass Flow Rate In = Mass Flow Rate Out

$$\boldsymbol{Fluid\ Density_{Inlet}\ x\ Area_{Inlet}\ x\ Velocity_{Inlet}} = \boldsymbol{Fluid\ Density_{Exit}\ x\ Area_{Exit}\ x\ Velocity_{Exit}} \quad (4)$$

$$\boldsymbol{Area_{Inlet}\ x\ Velocity_{Inlet} = Area_{Exit}\ x\ Velocity_{Exit} = Constant\ Value}$$

From this relationship, it is observed that with incompressible flow (density remains constant); velocity varies inversely with changes in area as seen in Equation 5.

$$\frac{Area_{Inlet}}{Area_{Exit}} = \frac{Velocity_{Exit}}{Velocity_{Inlet}} = Constant \quad (5)$$

Now that the relationship between area and fluid velocity has been derived, it is important to combine this principle with Bernoulli's principle, in comparison to a small side-pod inlet, and diverging section at the front of radiator. At the inlet, the area is

relatively small corresponding to a high velocity at the inlet to maintain mass flow. With this increase in dynamic pressure at the inlet, the “local” static pressure drops, causing the side-pod to pull air through the opening and into the duct [15]. At the diffuser, the area is larger and requires a smaller velocity. According to Bernoulli’s principle, a low velocity corresponds to a low dynamic pressure. With low dynamic pressure, the “local” static pressure must increase to maintain constant total pressure. This is all due to air inside the ducting as being incompressible, which is true for most racing applications. This increase in “local” static pressure at the front of the radiator core is what drives airflow through the fins of the radiator for convective heat transfer.

Most inadequacies in proper cooling performance stem from an uneven pressure distribution across the face of the radiator. The use of front ducting within the internals of a side-pod can help create an equal pressure and velocity distribution over the radiator core. In order to effectively design a side-pod that provides the maximum airflow, it is important to consider the behavior of airflow at the exit, as well as the inlet. It is important to position the exit in an area of low static pressure zone, less than the pressure at the inlet. This will cause accelerated flow through the whole duct, resulting in larger mass flow rates. This can also be achieved by reducing the outlet size [15].

Of all the principles covered in this section of ducting design, the key factor that plays into adequate cooling is airflow. Radiator performance relies heavily on increased convection and demonstrates a direct relationship to mass flow rate of air passing through the car. Maximizing mass flow rate through a ducting system ultimately leads to maximum cooling performance for the design [3].

Computational Fluid Dynamics Simulation

The use of computational fluid dynamics (CFD) software has become increasingly popular in formula vehicle industries in efforts to test and validate aerodynamic designs. CFD allows for calculating theoretical values of downforce, drag, center of pressure, and much more with large computing power. The goal in any vehicle development program is to reduce the concept-to-production cycle time and the number of prototypes to still meet the design targets. [17]. The goal and time frame required by the *Global Formula Racing* schedule for production and attendance at competition requires heavy reliance on CFD models to validate designs.

CFD combines a systems analysis of fluid mechanics, heat transfer, and other processes through the use of computer-based simulations [15]. CFD simulations "converge" on a final result when the software gets close to a consistent answer repetitively for many iterations. Convergence in this thesis is defined by residuals, or differences between results, below 0.001. At this point, the values of forces, pressures, and mass flow rate through the radiators are stable [3]. Simulations typically converge after 3000 iterations. For aerodynamic simulations, the powertrain and other rear-end components (with the exception of wheels) were excluded from CFD simulations. This allowed for reduced computation time for meshing operations and simulations.

Once a design is made in CAD software, the 3D geometry (also referred to as a solid) is then imported into the CFD software. The software used by *Global Formula Racing* includes CATIA V5R19 by Dassault Systemes for CAD and STAR-CCM+ by CD-adapco for CFD. Once the solids are imported, the model is then put into virtual wind

tunnel with predefined conditions, parameters, and settings that establish the behavior of the simulation. The software then splits each surface and bodies into millions of three-dimensional cells of "bounded volumes" [15], in a process known as meshing. This allows the software to calculate real physical values using numerous engineering, physics, and mathematical equations and algorithms during simulations. Once the model has finished meshing, the simulation can then be run. The powerful aspect of the CFD software is in its post-processing capabilities. These post-processes allow for visualization and analysis of hundreds of aspects and results that help to depict the nature of the fluid flow, heat transfer, or chemical process that is being simulated.

2.2.1 Operation

The CFD software requires large computational power. In industry, such power is typically the result of clusters of super-computers. For this thesis and at *Global Formula Racing*, computation power is limited. Normal computation power includes one, half-car simulation (reduces computation time and assumes perfect symmetry of results) run on a 3.4 GHz 64-bit, 4-Core processor with 16 GB of RAM. Typical simulation times range from about 20-30 hours per simulation, with meshing sizes of about three-million cells.

2.2.2 Limitations

CFD is an important aspect of this thesis and played a huge role in the design and validation process of numerous side-pod concepts. There are however limitations to the accuracy in which the software can replicate real-world situations. There are settings,

parameters, and processes that have been excluded from this thesis. The complexity of the computational power of CFD simulation is enormous, and the difficulty in understanding how to replicate near-world scenarios is far beyond the level of the undergraduate knowledge of the author.

Notable limitations include the knowledge and understanding of various parameters and settings predefined for each individual simulation based on the scenario to be replicated. Other limitations come in the form of computation power, limiting the quality and sizes of the *mesh* characteristics that are possible. Even the most powerful computation machines are only able to mesh "cells" that are still slightly larger than the smallest scales of real fluid flow. This leads to false predictions of vortex development and flow behaviors [3].

Other limitations include flow around wheels, which is difficult to predict. Predefining parameters and settings to predict flow separation at the wheels becomes very challenging due to their rotational characteristics, shape, ground contact, and variable yaw angles [15].

Radiators also have limitations to the parameters and simulation settings. Without extensive knowledge of radiator behavior settings in CFD, it is very difficult to accurately model flow through a radiator core. For the purpose of these simulations, there is a default porosity associated with the radiator, modeled as an inlet and outlet and side-walls. Mass flow rate is relatively accurate for the modeling of the 2014 radiator and provides adequate insight for the purpose of this thesis. Pressure drop across the radiator as well as loss coefficients are important for accurate modeling. This component will be discussed in Section 2.4.

For purposes of simplification, radiator fans are excluded from the simulations in this thesis. Fan performance and parameter defining in CFD is beyond the knowledge of the author and would require years of experience. This would require more time than available to produce a working concept for the 2014 *Global Formula Racing* vehicles.

2.2.3 Wind tunnel layout

Figure 13 depicts the general layout of the virtual wind tunnel used in STAR-CCM+ by *Global Formula Racing.* This tunnel is approximately five vehicle lengths long, in order to avoid undesirable affects from the boundary walls. The wind tunnel floor is modeled as a moving wall to simulate vehicle motion. The tires are also predefined to rotate at 754.62 revolutions per minute given an 18 in. diameter wheel of a vehicle traveling at 65 kilometers per hour (~ 40 mph).

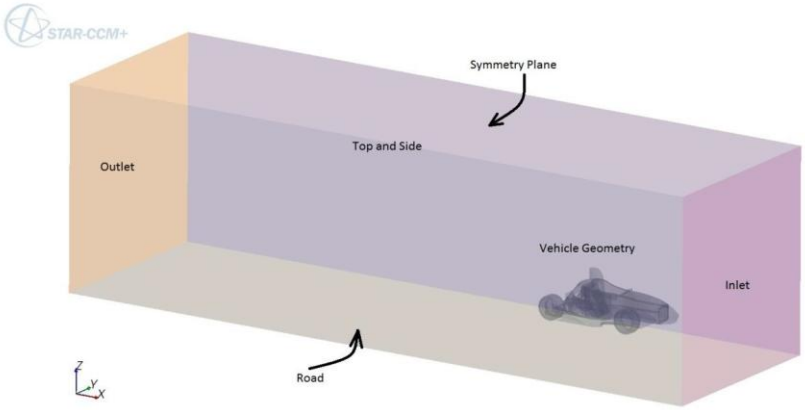

Figure 13: STAR-CCM+ virtual wind tunnel used by Global Formula Racing [12]

2.2.4 Settings

The following settings are common across all of the aerodynamic CFD simulations in this thesis and are similar to those used by 2013 Aerodynamics team with improvements to provide for more accurate results with faster simulation times.

Table 1: CFD Settings in STAR-CCM+

2014 Computational Fluid Dynamics Simulation Settings - STAR-CCM+			
Mesh Continuum		**Physics Continuum**	
Models		***Models***	
Prism Layer Mesher		Constant Density	
Surface Remesher		Gas - Air	
Surface Wrapper		K-Epsilon Turbulence	
Trimmer		Reynolds-Averaged Navier-Stokes	
Trimmer Mesh Type:	Hexahedra	Segregated Flow	
Trimmer Mesh Growth Type:	Simple	Segregated Fluid Temperature	
		Turbulent	
Reference Values		***Reference Values***	
Base Size:	1.0 m	*Maximum Allowable Wall Distance:*	1E-6 m
# of Prism Layers:	5	*Minimum Allowable Temperature:*	100 K
Prism Layer Stretching:	1.5	*Maximum Allowable Temperature:*	5000 K
Prism Layer Thickness:	50% of Base	*Reference Pressure:*	101325 Pa
Surface Growth Rate:	1.3		
Volumetric Controls		***Initial Conditions***	
Mesh Values		*Pressure:*	101325 Pa
Relative Size:	1.25% of Base	*Static Temperature:*	300 K
# of Prism Layers:	2	*Turbulence Intensity:*	0.01
Prism Layer Stretching:	1.5	*Turbulence Specification:*	Intensity + Viscosity Ratio
Prism Layer Thickness:	33.3% of Base	*Turbulent Velocity Scale:*	1.0 m/s
		Turbulent Viscosity Ratio:	10
		Velocity:	65 kph

An important setting noted in Table 1 is the use of a turbulence model. Flow over a vehicle is always turbulent. Using a k-epsilon turbulence model for momentum, kinetic energy, and dissipation rate has been proven to cause simulations to "converge" quicker than other turbulence model, significantly reducing simulation time. The k-epsilon model is used commonly in vehicle aerodynamics and gives relatively accurate results for the purpose of design [13].

2.2.5 Radiator Settings

The radiator in these simulations is modeled as a porous medium to account for a default pressure drop across the radiator. All the setting values in Table 2 were default, based on STAR-CCM+ tutorial for radiator modeling. Interior details of radiator core were neglected. The radiator was modeled as an inlet and outlet surface with porosity and pressure drop of Star-CCM+ default value, while radiator heat production from cooling fluid neglected. Fan contribution was also not accounted for.

Table 2: Radiator settings in STAR-CCM+

2014 Computational Fluid Dynamics Simulation Settings - STAR-CCM+: Radiator Settings		
Mesh Conditions	***Physical Conditions***	
Customize Prism Mesh	*Energy Source Option*	*None*
Volume of Interest Specification	*Initial Condition Option*	*Use continuum*
	Turbulence Specification	*Intensity + Viscosity Ratio*
	Physics Values	
	Motion Specification:	*Stationary*
	Porosity:	*1*
	Principle Tensors	
	Porous Inertial Resistance	
	XX-Axis Component:	*56.798 kg/m^4*
	YY-Axis Component:	*10000 kg/m^4*
	ZZ-Axis Component:	*10000 kg/m^4*
	Porous Viscous Resistance	
	XX-Axis Component	0.0 kg/m^3-s
	YY-Axis Component	10000 kg/m^3-s
	ZZ-Axis Component	10000 kg/m^3-s
	Solid Thermal Conductivity	
	Isotropic Tensor	*1.0 W/m-K*
	Turbulence Intensity	0.01
	Turbulent Viscosity Ratio	10

2.2.6 Vehicle Meshing Scenes

An example of CFD the meshing scene for the 2014 side-pod design illustrates general cell sizes, and surface boundary volumes. Figures 14-16 show cell size and meshing patterns for a half-car view, side-pod, and radiator mesh scene.

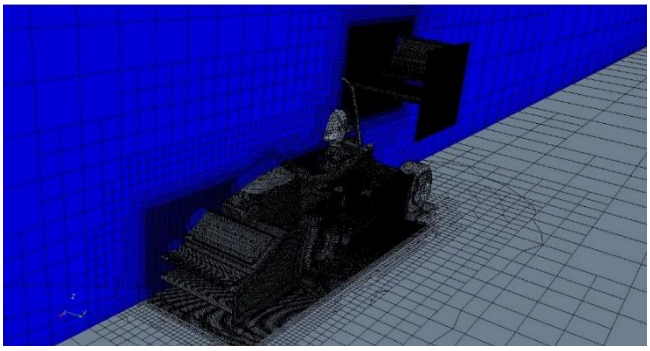

Figure 14: Half-car mesh scene

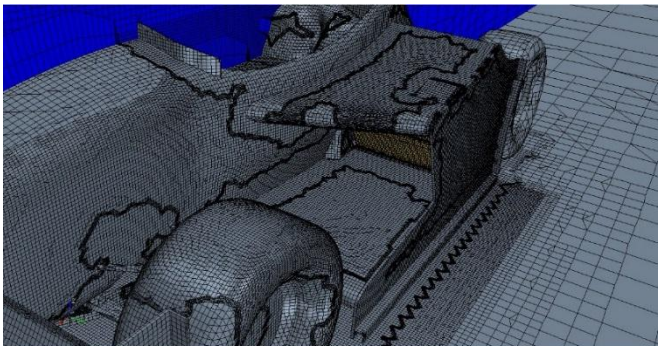

Figure 15: Side-pod mesh scene

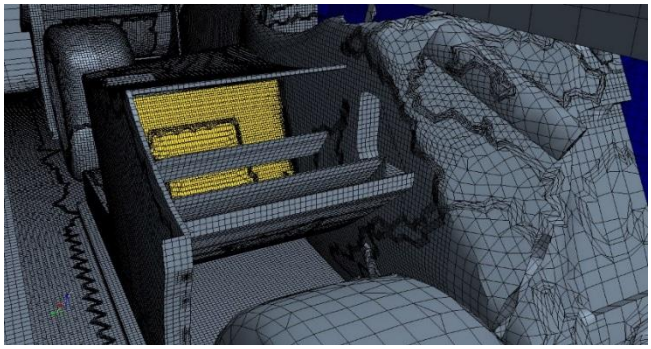

Figure 16: Radiator mesh scene

2.3 Composites

The use of composites by *Global Formula Racing* in the production of the FSAE vehicles is extensive. This section will provide brief background information regarding each major material and process used to produce the parts manufactured for this study.

2.3.1 Carbon-Fiber Pre-Pregs

Carbon-fiber pre-pregs are carbon fibers that are woven into fabrics and are *pre-impregnated* with epoxy matrix resin at the manufacturer. The parts used for this study were manufactured out of carbon-fiber composites because of its high specific strength [19]. Carbon-fiber is commonly used on race-car parts, and it allows for aerodynamic components to be extremely lightweight.

These pre-pregs are partially cured so that they are easy to handle while eliminating any resin leakage from the composite material during construction. This material must be kept at low temperatures (0°F) in order to prevent the hardening agents imposed in the resin, from prematurely curing. Pre-preg materials last about six months at this temperature [19]. Pre-pregs have a great degree of flexibility, which makes lay-up of rather complex parts much easier. This characteristic is known as *drape.* Pre-pregs also have a rather "sticky" surface because the resin is still only partially cured; this is known as *tack.* The tack of the pre-preg helps with placement and keeps pieces from shifting in the mold during lay-up.

2.3.2 Fabrics and Weaves

Fabrics and weaves are bundles of fibers arranged in specific orientations and made of many different materials. Fabrics can be used with resin matrix materials and provide the stiffness and rigidity usually desired by design with fiber composites. *Drape* is fabric flexibility. This flexibility allows the fibers to conform to the shape of the mold. The carbon fiber pre-preg used in this study was *plain weave*. Plain weave is the simplest of all weaving patterns. It is constructed of repetitious over-under patterns. This provides maximum stability and firmness with little to no fiber "slippage" during lay-up. Plain weave provides uniform strength from in-plane stresses from shear forces, and is typically the stiffest weave [19]. Plain weave design can be seen in Figure 17.

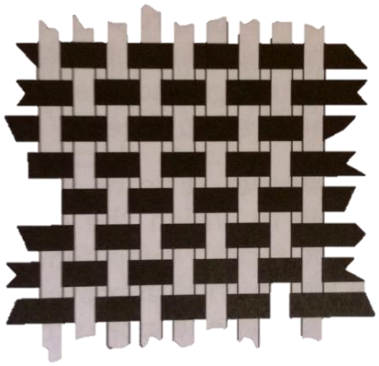

Figure 17: Plain weave fabric [19]

2.3.3 Sandwich Structures

In engineering applications, where forces are applied out of the plane of the composite material, the fibers and resin matrix have very little ability to resist these stresses. In this case, composite products tend to incorporate a sandwich structure. This sandwich structure consists of two face sheets of carbon-fiber pre-preg, core material, and

adhesive sheets to hold the core and laminate together [19]. The thickness of the core adds to the bending and flexural strength of the composite. Typical core materials include honeycomb core made from balsa wood, aluminum, foam, paper, and many other materials. The parts in this thesis were manufactured with Rohacell ® low density close packed cell foam.

The most important part of the sandwich structure is the bonding strength of the core and composite laminates. The adhesive sheets must be strong enough to transfer the loads to the core and laminate in order to eliminate the chance of *debunking,* or separation, from the surface of the core. The adhesive must be thick enough over the entire surface; however it should not be so thick that it becomes a point of failure [19]. Figure 18 shows the schematic of a typical sandwich structure.

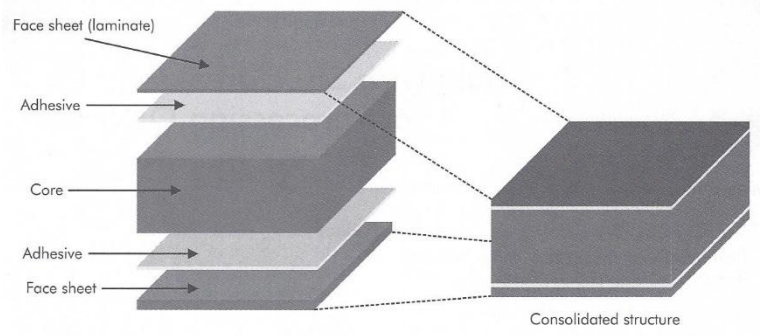

Figure 18: Composition of a sandwich structure [19]

2.3.4 Lay-Up

The lay-up process of composite manufacturing is extremely important to the overall performance of the part. The orientation of the fibers plays a large role in the strength and direction capabilities of stress tolerance.

Pre-preg Layup - Issues

Difficulties with pre-pregs are the potential for contaminants on the surface of the composite. Silicone contaminants are the worst for pre-preg surfaces. Experience shows that if silicone is present on the surface of the carbon, the ability for it to bond to subsequent plies is compromised [19].

2.3.5 Vacuum Bagging

The vacuum bagging portion of composites manufacturing with pre-pregs is undoubtedly the most important process. The purpose of vacuum bagging of carbon pre-pregs is to initiate the movement and flow of the resin matrix during the curing stage. The vacuum bag helps to pull the partially cured resin through the fibers when subjected to pressure and temperature. This molten resin moves between the layers, or *plies,* and into layers of absorbent fabric used in the bagging process. Vacuum and temperature processing of carbon-fiber pre-pregs eliminates the possibility for boundaries to exist between layers and cause potential delamination [19], as shown in Figure 19.

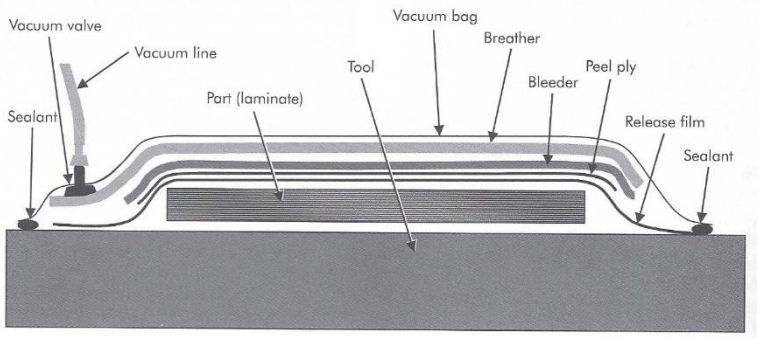

Figure 19: Vacuum bagging component schematic [19]

2.3.6 Bridging

Typical issues with carbon-fiber composites and molds that were experienced in the development of parts for this thesis included a common problem, known as *bridging*. Bridging occurs when the shape of the part does not allow the vacuum bag to press against all surfaces of the mold and composite. These areas are not properly compressed during curing and can lead to delamination of plies. This problem also prevents the transfer of pressure to the rest of the part.

There are three techniques that can be used to help avoid any issue of bridging. The first is the intentional use of pleats in the bagging material. These pleats allow for excess bag in areas where bridging may occur due to taut bagging materials. These pleats allow for bags to conform against all surfaces of the part and mold [19].

The second way to eliminate bridging is by chamfering core materials at an angle, to allow for bags to come in better contact with side surfaces. Chamfering at a 45° angle versus a 90° wall for example allows for better contact between the bag and the composite. This chamfer can be seen in Figure 20.

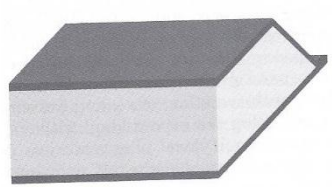

Figure 20: Composite edge chamfering to prevent bridging [19]

The third option is to use what is known as a pressure intensifier. Pressure intensifiers are objects that fit in the places that are difficult for the bag to reach. For example, the use of an aluminum block in the bend of an L-bracket would act as a pressure intensifier once vacuum is pulled on the bagging system. A pressure intensifier schematic is shown in Figure 21

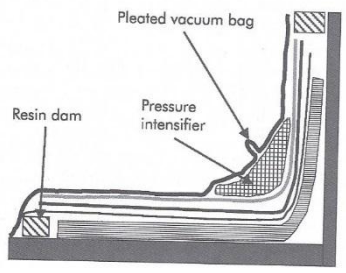

Figure 21: Pressure intensifier [19]

2.4 *Testing*

In the design process, validation through software simulation provides limitations to the engineer depending on the knowledge and ability of the user to correctly predefine conditions and parameters within virtual environments such as those of computational fluid dynamics software. It is important to further validate these concepts through physical testing and real-world data collection. Correctly modeling radiators in CFD requires extensive empirical data. For the nature of the side-pod, this empirical data stems from the fluid behavior through real products, such as the 2014 radiators. Predicting flow through radiators in various scenarios requires knowledge of the pressure drop across the radiator and the loss coefficients due to its porosity and the airflow restrictions at its core interface.

The empirical data acquired from physical testing is rather simple, yet vital for proper replication. Unfortunately in this thesis, this empirical data was not collected in time to include in the simulation, requiring default radiator settings provided by STAR-CCM+ to be used for simulation purposes. This is an area for future research.

In order to adequately model the radiator, pressure drop across the radiator must be measured experimentally. This can be done using Pitot-tubes placed before and after the radiator core to measure the pressure differential at various velocities in a wind-tunnel. This pressure drop, ΔP_R, is assumed to be proportional to the dynamic head of the fluid with additional loss coefficients, k_L. Due to the nature of the moving fluid, this pressure drop is equivalent to the dynamic pressure caused by the moving fluid and the loss coefficient is included as a reduction factor in this equation. As mentioned in Section 2, the dynamic pressure is equivalent the following equation:

$$Dynamic\ Pressure = \frac{1}{2}\rho V^2 \quad (6)$$

In terms of a radiator's dynamic head the above equation becomes:

$$\Delta P_R = k_L \frac{1}{2}\rho V^2 \ [7] \quad (7)$$

Where

$$k_L = \sum_{n=1}^{N} r_n V^{n-1} \ [7]. \quad (8)$$

Equations 6, 7 and 8 incorporate the fluid velocity, V, at the inlet. This velocity traditionally is measured with hot wire anemometers. In a study at the University of Melbourne, five anemometers were used on the radiator surface to measure the average velocity normal to the inlet of the radiator [13]. This also allows for mass flow rates to be calculated through the radiator. Once the pressure drop is measured with respect to changing inlet velocities normal to the surface, the loss coefficient can be determined given the amount of data collected. The value, n, in Equation 8, is representative of the number of velocities at which data is collected. In the case of the University of Melbourne, five velocities were measured, requiring that this to be a fourth-order equation with a polynomial line to be fitted to the data points, given the exponent of velocity, n-1. This allows for an empirical equation for the loss coefficient that can then be included in Equation 7 to solve for the pressure drop at any inlet velocity. Once this pressure drop is known, the parameters for different vehicle speeds can then be defined in STAR-CCM+ CFD simulations. The next two subsections will provide a brief overview of the testing equipment that can be used for measuring the airspeed and pressure variations in the side-pod.

2.4.1 Anemometers

A hot wire anemometer is a very fine wire heated between two small probes measuring rapidly fluctuating airflow. These wires can be operated at either constant current such that resistance varies as a function of velocity; or with constant resistance, so that current becomes a measure of velocity. In the case of constant resistance, this is allows the operator to have only a single temperature measurement. For the case of anemometers used in radiators and automotive airflow, temperature often plays an important role in understanding the airflow and cooling capabilities of the vehicle's side-pod. Thus it is most common that current remains constant, and resistance fluctuates with changes in velocity. The output of these probes is not linear and thus requires internal *linearizers* in order to produce usable velocity data to the operator [24].

2.4.2 Pitot Tubes

A Pitot tube is a small tube that can be aligned with the direction of fluid flow in order to measure pressure differentials. The importance of a Pitot tube is that it allows the operator to place them in different locations and allows for relatively high levels of accuracy due to little friction at the small diameter of the tube. A frictionless measurement device is important since Bernoulli's equation is used to determine the pressure and velocity at the point of the Pitot tube, and does not account affects due to fluid viscosity. One disadvantage of the Pitot tube is that it must be closely aligned with the flow direction, which may be unknown in certain applications and requires a high level of precision [24].

Limitations for the Pitot tube include yaw angles greater than 5°, which produce substantial errors in the measurements. Another limitation to the Pitot tube is that it is relatively ineffective at low-velocities. The pressure differential at low-velocities is too small in gas flows and does not provide a high enough resolution for the operator to make any sort of analysis [24].

2.5 *Global Formula Racing*

At *Global Formula Racing*, the design and engineering development of all vehicle components is guided by an overarching team philosophy: *to win competitions through simplicity, reliability and simulation validated by physical testing.* All of the designs and manufacturing are guided by this idea, and this idea is the foundation behind all concepts in this thesis.

2.5.1 Engine Selection

At *Global Formula Racing,* the combustion vehicle uses a one-cylinder Honda CRF 450X motorcycle engine. Due to the limited top-speed capabilities of the courses at FSAE competitions, having a larger engine, such as a 600cc four-cylinder engines used by many competitors, adds unnecessary weight for unusable power gains. Having a smaller engine allows the drivers of *GFR* to be able to utilize a higher percentage of full-throttle engine performance, resulting in faster accelerations and quicker response time, with a much lighter engine configuration.

The downside of using a small engine displacement in the GFR vehicle is that the engine tends to produce a lot of heat given the more strenuous running environment than typically experienced by this engine. This makes optimizing engine cooling extremely important and difficult to accomplish. Given that this engine is made for a motorcycle application, using the engines to power a heavier vehicle at a high level of performance produces much larger amounts of heat. Since the vehicle runs at lower vehicle speeds than required for cooling, this requires high performance heat rejection strategies [13]. To

account for this, *Global Formula Racing* purchased radiators designed for 450cc All-Terrain-Vehicles to provide additional cooling power, and provide a much larger "core" area.

2.5.2 Aerodynamics Background

In 2010, *Global Formula Racing* designed, manufactured, and implemented its first aerodynamic package, which improved the overall performance of each vehicle. The 2010 aerodynamics package included an undertray and windshield gurney, and a singular side-pod. As a result of a student built lap-time simulation, the importance of a high performing aerodynamics package to improve vehicle performance and efficiency in Autocross and Endurance dynamic events has motivated the GFR team to continuously improve the aerodynamic components over the years.

With a well-designed aerodynamics package, the downforce creates an increase in traction between the tires and track, allowing for much better handling and faster responses to necessary changes in direction and higher cornering speeds. These components are extremely important because they add little to the overall weight of the vehicle, while providing a much higher level of performance. For the aerodynamics package, it is a tradeoff between slight increases in mass for a certain level of gain in downforce. With high performance aerodynamic elements in events such as Autocross and Endurance, the vehicles are able to maneuver with high lateral acceleration in all directions due to large amounts of downforce.

The side-pods of the vehicle play a crucial role in the overall cooling of the

vehicle, however they and have become increasingly more integrated into the aerodynamics package at *Global Formula Racing*. The addition of a larger front wing to the 2014 vehicle restricted airflow to the coolers. As a result, the side-pods required design strategies that would provide as much airflow as possible for effective cooling of engine components. The side-pods were designed to be used on both sides of the vehicle to house water and engine oil coolers. This was a particularly difficult challenge given that air flow over the large front wing tended to reduce the amount of available air accessible to the cooling components. The intent of the side-pods are to direct all available air into the internal ducting in order to increase airflow through the radiator core. To improve the airflow through each side-pod, the radiators are assembled with a rear-mounting fan to improve heat rejection.

For *Global Formula Racing*, side-pod design has been rather difficult to understand in terms of airflow patterns and cooling capabilities. Given the absent documentation and justification for previous design strategies of the side-pods, past teams tried to utilize an externally mounted "louver" concept to help increase airflow to the side-pods. The goal of the "louvers" was to increase the outlet area to extract the air through the radiator using a vacuum type function. The goal of this design was to promote a higher pressure gradient through the cooler, effectively increasing the mass flow rate through the core for improved cooling. In the recent years, the side-pods have struggled to provide efficient airflow to both the water and oil radiator and have provided very minimal performance enhancements in cooling the engine.

In 2011 and 2012, the side-pods were able to provide sufficient cooling to the engine, however in the 2013 season, the engine temperature rose to extreme levels and

nearly caused the car to fail from overheating. In 2013, the implementation of a new undertray forced the radiators and side-pod surfaces much higher than in past years. As a result of this height increase, the packaging for the radiator was much more restricted.

This resulted in a steep mounting angle for the radiators in order to fit within the packaging requirements of the side-pod. This steep angle (acute in relation to incoming airflow) led to the cooling problems. The nature of radiators to cool properly has much to do with the amount of airflow propagating through the cooling fins. Maximum heat transfer occurs when the airflows perpendicular to the front surface of the radiator, minimizing restriction. The 2013 side-pod design also encountered some additional airflow stall characteristics that reduced cooling. In CFD simulations, the air was seen flowing over the vehicle's front tires and into the opening of the side-pod, where large amounts of air collected and stalled. This air then exited from the side-pod inlet, flowing underneath the undertray instead of passing through the radiators. This was largely due to the shape and location of the side-pods, as well as the decreased angle of the radiator causing restrictions to airflow.

For the *GFR* 2014 vehicle, the side-pods needed to be completely redesigned. In order to improve engine cooling and performance, new radiators were purchased and integrated into the engine's cooling system. This had a direct impact on the shape and structure of the side-pod, which ultimately led to a complete redesign. The new cooling system uses a square radiator that allows the team to reduce the mounting angle of the radiators to help promote more orthogonal air flow. With this, the goal of the new side-pod design configuration is to improve airflow internally for the vehicle's cooling system, as well as externally to help increase the aerodynamic performance in terms of

overall vehicle downforce and drag reduction.

Through recognition of problems associated with side-pod designs for the 2011-2013 vehicles and translating these issues into engineering design goals for the 2014 vehicle, the *GFR* team was able to improve designs tremendously. Such improvements benefitted the vehicle cooling capabilities, aerodynamic performance, vehicle construction, integration, manufacturability, and aesthetics.

2.6 *FSAE Competition Breakdown*

FSAE competitions all follow the same general format in terms of the types of events that each team must complete. The FSAE events are broken up into two different categories: Static and Dynamics events. The events of the two categories will be described below and will provide further detail relating the impact of the aerodynamics team in contributing to the overall success of *Global Formula Racing* in receiving maximum points at competition.

The following breakdown of the Formula Student Competition requirements illustrates a high level overview of the different competition events and how they directly relate to the goals of the Aerodynamics team within the *Global Formula Racing* organization.

2.6.1 Formula SAE Competition Requirements

- *Static Events (325 Points Total)*
    - *Presentation (75 Points):* Each team develops and presents a business case in efforts to sell their product to the executives of a corporation. Teams must sell demonstrate its product best meets the requirements of target market: Weekend competition racers.
        - The aerodynamics package is a large aspect vehicle composition. The aerodynamics team must be able to

design a high performing aerodynamics package that will enhance the vehicle performance and raise driver enjoyment in order to better appeal to the target market. In doing so, this package must contribute to the overall image and aesthetics of vehicle in a positive way.

- *Engineering Design (150 Points):* This section critiques the engineering technical design aspects of the vehicle. Judges will critique the processes and strategies used to implement a design that would appeal to this target market.
    - This portion is heavily influenced by the aerodynamics team, and provides a significant opportunity to showcase the aerodynamics evolution of the GFR vehicle over the years. It allows GFR to display a significant level of understanding of fluid mechanics, and aerodynamics design to justify the GFR 2014 aerodynamics package.

- *Cost and Manufacturing Analysis (100 Points):* At this event, Judges will critique the cost benefits of all components of the vehicle based on overall advantages and enhancements to the vehicle.
    - Given the extensive amount of aerodynamic

components on the vehicle, the Aerodynamics team must work to manufacture parts effectively and efficiently to reduce costs, and manufacturing time while still producing improved high performance parts.

- *Dynamic Events (675 Points Total)*
    - *Acceleration (75 Points):* At this event, the car is accelerated in a straight line to assess the straight-line acceleration abilities of the vehicle.
        - The aerodynamics team must produce a lightweight package that can be adjusted for low drag situations to improve the vehicles acceleration and top speed.
    - *Skid-Pad (50 Points):* In this event, the vehicle is driven in a constant-radius turn on a figure-8 course and scored based on its cornering ability.
        - The aerodynamics package must still be lightweight and adjustable to effectively produce downforce even at low speed maneuvers to help vehicle traction and cornering performance
    - *Autocross (150 Points):* This event evaluates the overall performance of the vehicle including speed and

maneuverability on a tight course. Each car performs during its own allotted times as to eliminate hindrance from any other competition vehicles running at the same time.

- This requires that the aerodynamics package provide a high level of downforce and low drag while all of its components remain lightweight.

- *Endurance (300 Points):* During this event, the vehicles durability and reliability is tested. The vehicle is put under high stress conditions for the longest period of time during the competition and evaluated on its performance.
  - The aerodynamics package must be structurally strong, provide high down force, low drag, and adequate airflow for effective cooling to engine components during endurance run.

- *Efficiency (100 Points):* In addition to the reliability, the fuel efficiency of the vehicle during the Endurance event will be evaluated.
  - The aerodynamics team must design a lightweight package that provides a level of low drag.

2.7 *Rules and Constraints Analysis*

In the overall design of the overall vehicle, there are particular rules pertaining to the aerodynamics package that provide certain limitations to the design of each component. In relation to the side-pod design, the following rules constrain the component design:

2.7.1 2014 FSAE Rules

The following is an excerpt of the 2014 FSAE Rules applicable to the side-pod design for Formula SAE.

ARTICLE 2: GENERAL DESIGN REQUIREMENTS [1]

T2.1 Vehicle Configuration

The vehicle must be open-wheeled and open-cockpit (a formula style body) with four (4) wheels that are not in a straight line.

Definition of "Open Wheel" – Open Wheel vehicles must satisfy all of the following criteria:

1) *The top 180 degrees of the wheels/tires must be unobstructed when viewed 68.6mm (2.7 inches) above the plane formed by the tops of the front and rear tires.*

2) *The wheels/tires must be unobstructed when viewed from the side.*

3) *No part of the vehicle may enter a keep-out-zone defined as a circle 68.6mm (2.7 inches) larger radially than the outside diameter of the tire with the tires steered straight ahead with a 77 kg (170 pound) driver seated in the normal driving position. The inner sidewall of the tire (vehicle side) is not included in this assessment. See Figure 22 below.*

Note: The dry tires will be used for all inspections. For technical inspection the keep-out-zone may be inspected by use of a tennis ball fastened to the end of a stick. The ball will have the 68.6mm (2.7

inches) diameter and must be able to be freely moved around the outside of the tire without contacting any portion of the car other than the tire.

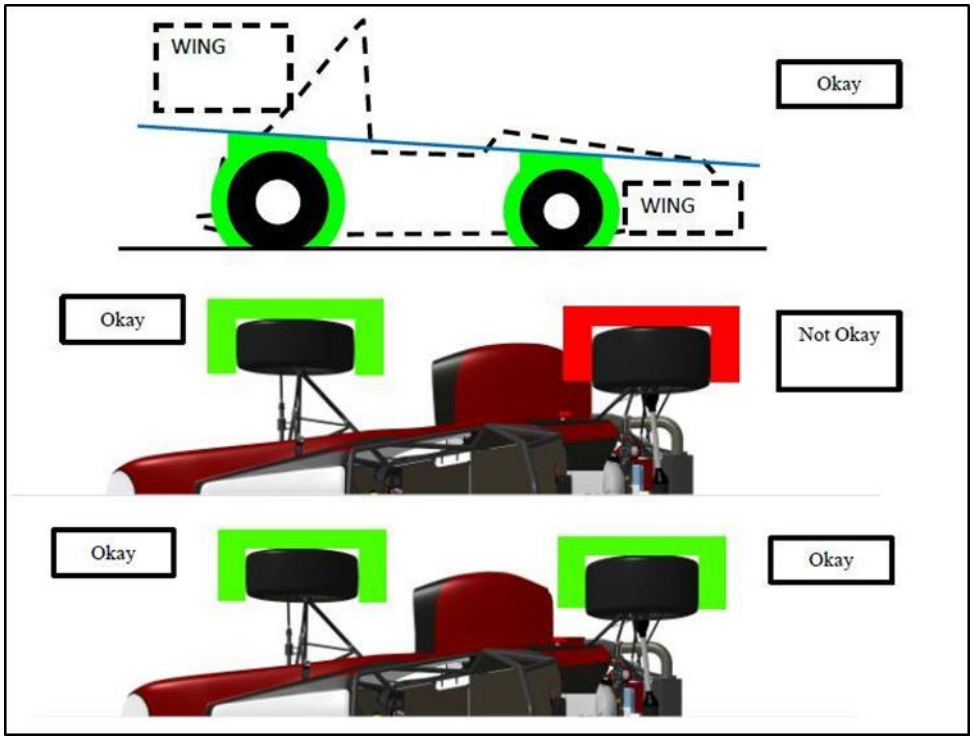

Figure 22: "Keep-Out-Zone" [1]

There were some major design constraints to the side-pod in addition to the total aerodynamic package [1]. Particularly in reference to the *"Vehicle Configuration" rules*, the side-pod needed to account for the necessary 2.7 inch extra diameter from the outer radius of the tire, in both design and positioning in the fore/aft direction of the vehicle, as seen in Figure 22. This provided a challenge in creating a successful side-pod duct that does not interfere with the *"Keep-Out-Zone"* while still managing to provide as much *useful* airflow as possible through the cooling radiator systems.

ARTICLE 9: AERODYNAMIC DEVICES

T9.1 Aerodynamics and Ground Effects – General
All aerodynamic devices must satisfy the following requirements:

T9.2 Location

T9.2.1 In plain view, no part of any aerodynamic device, wing, under tray or splitter can be:

a. Further forward than 762 mm (30 inches) forward of the fronts of the front tires

b. No further rearward than 305 mm (12 inches) rearward of the rear of the rear tires.

c. No wider than the outside of the front tires or rear tires measured at the height of the hubs, whichever is wider.

As stated in [T9.2.1c] - "*Aerodynamic Devices - Location",* the side-pods needed to remain within the dimensional constraints provided by the furthest distance outboard of the tire surfaces. This limited the overall shape of the side-pod, and had to be considered when dealing with external dimensional constraints from the new "square" shaped radiators.

T9.3 Minimum Radii of Edges of Aerodynamic Devices

T9.3.1 All wing edges including wings, end plates, Gurney flaps, wicker bills and undertray that could contact a pedestrian must have a minimum radius of 1.5 mm (0.060 inch).

With respect to the *"Minimum Radii of Edges of Aerodynamic Devices"* rule, this requires any components that could come in contact with a pedestrian, including side-pods to have a minimum radius on its outer surfaces in order to eliminate personal injury in the event of accidental human contact on or off the course.

T4.8 Driver Egress

All drivers must be able to exit to the side of the vehicle in no more than 5 seconds. Egress time begins with the driver in the fully seated position, hands in driving position on the connected steering wheel and wearing the required driver equipment. Egress time will stop when the

driver has both feet on the pavement.

T9.5 Driver Egress Requirements

T9.5.1 Egress from the vehicle within the time set in Rule T4.8 "Driver Egress," must not require any movement of the wing or wings or their mountings.

T9.5.2 The wing or wings must be mounted in such positions, and sturdily enough, that any accident is unlikely to deform the wings or their mountings in such a way to block the driver's egress.

In accordance with the Driver Egress rules as stated above in [T4.8] and [T9.5], the driver must be able to exit the vehicle in no more than 5 seconds, and required that the side-pods not restrict the driver from being able to quickly exit the car. This was accounted for in overall side-pod height, location, and shape design in order to provide as little restriction for entering and exiting the vehicle as possible.

2.7.2 2014 Formula Student Germany

IC2.7 Tank Filling Requirement [10, 11]

IC2.7.1 The fuel tank must be capable of being filled to capacity without manipulating the tank or the vehicle in any manner. During fueling or refueling the vehicle may only be touched by the fuel crew and officials. The tank will be filled to the fill line, or if a filing system is used, to the automatic stop point. If, for any reason, the fuel level changes after the team has moved the vehicle, then no additional fuel will be added.

As stated in the 2014 rules for the Formula Student Germany competitions, no part of the vehicle may be manipulated in any manner during fuel filling. This directly affected the design of the side-pod as it eliminated the need for any type of removal section of the side-pod to be included in the design. The fuel cap must be completely

accessible at all times and requires that a section of the side-pod must not block this channel. This effectively altered the outlet area seen by the internal airflow and will had an overall effect on the airflow speed at the exit of the side-pod.

At *GFR*, the design of all components must satisfy the general rules of all competitions in which the vehicles are intended to complete in efforts to create designs that provide commonality and comply to the rules for each individual competition.

3. Design Requirements

The particular requirements of the aerodynamics package on the FSAE vehicles are extremely important to the overall success of the vehicle performance and the points gained at competitions. The aspect of points and competition success ultimately drives design decisions that are made early on in the development process. The purpose of the GFR 2014 Aerodynamics team is to create a lightweight package that produces a high level of downforce to improve vehicle handling and reduce lap times. This combination allows the car to score the most points during the competition, and was the primary goal in working to implement significant improvements to previous *GFR* vehicle designs. All aerodynamic components were designed for high downforce, low drag, and a well-balanced center of pressure, as well as to help improve manufacturing processes.

The side-pods of the *GFR* 2014 vehicles have particular requirements that affected the design strategy in order to maximize competition points through improved vehicle performance. For this particular aerodynamic component, the main design focus was to improve the airflow through the radiators on both sides of the vehicle. In 2014, the vehicle included a new set of radiators that were square shaped. Although they contain the same amount of surface area as the 2013 radiators, they are designed to have a much shorter but wider profile, which allowed for more vertical mounting. This allowed the radiators to be mounted more orthogonally to the incoming airflow which was projected to increase vehicle cooling capabilities.

The 2014 car also includes much larger fans that needed to be properly mounted on the rear-fin area of the radiator to improve cooling. The larger fan will help to improve

the airflow through the side-pods at all times, but most significantly when ambient air speed is low. Due to the relatively low speeds of vehicles at FSAE competitions in comparison to Formula 1 type races, the need for fans during Dynamic events is crucial to help pull in enough air to adequately cool the systems. In Formula 1, the vehicle travels at high speeds where the velocity of the car provides adequate airflow rate to cool the engine components without the need for a fan. With these larger radiator and fan packaging requirements, the 2014 needed to be bigger and re-designed although it added mass to the car, and decreased points [5].

Another aspect of the 2013 design of the side-pod was its tendency to create lift. The requirement of this year's side-pod design was to incorporate a new design to reduce weight, improve overall downforce of the vehicle and to reduce drag. The center of gravity of the vehicle is also an important characteristic that will be considered locating the final position of the radiator. The increase in downforce, reduction of drag, and lower center of gravity can all be related to competition points according to Figure 23 for both cCar and eCar.

1 kg vehicle mass	Acceleration	Skidpad	Autocross	Endurance	Fuel	Total
FSAE	-0.15	-0.12	-0.57	-0.64	-0.04	-1.52
FSUK	-0.15	-0.12	-0.57	-0.64	-0.04	-1.52
FSG / FSA	-0.15	-0.12	-0.38	-0.88	-0.29	-1.82
Average	*-0.15*	*-0.12*	*-0.51*	*-0.72*	*-0.13*	-1.62

1 N-m engine torque	Acceleration	Skidpad	Autocross	Endurance	Fuel	Total
FSAE	0.68	0.00	0.62	0.70	-0.45	1.54
FSUK	0.68	0.00	0.62	0.70	-0.45	1.54
FSG / FSA	0.68	0.00	0.41	0.96	-0.25	1.80
Average	*0.68*	*0.00*	*0.55*	*0.78*	*-0.38*	1.63

10 mm CG height	Acceleration	Skidpad	Autocross	Endurance	Fuel	Total
FSAE	0.62	-0.43	-1.58	-1.78	0.00	-3.18
FSUK	0.62	-0.43	-1.58	-1.78	0.00	-3.18
FSG / FSA	0.62	-0.46	-1.06	-2.44	-0.67	-4.00
Average	*0.62*	*-0.44*	*-1.40*	*-2.00*	*-0.22*	-3.45

10 N aerodynamic downforce	Acceleration	Skidpad	Autocross	Endurance	Fuel	Total
FSAE	0.02	0.15	0.73	0.83	-0.06	1.68
FSUK	0.02	0.15	0.73	0.83	-0.06	1.68
FSG / FSA	0.02	0.18	0.49	1.13	0.24	2.06
Average	*0.02*	*0.16*	*0.65*	*0.93*	*0.04*	1.80

10 N drag	Acceleration	Skidpad	Autocross	Endurance	Fuel	Total
FSAE	-0.25	0.00	-0.12	-0.14	-0.06	-0.56
FSUK	-0.25	0.00	-0.12	-0.14	-0.06	-0.56
FSG / FSA	-0.25	0.00	-0.08	-0.19	-0.11	-0.63
Average	*-0.25*	*0.00*	*-0.11*	*-0.16*	*-0.08*	-0.55

Figure 23: Equating Design Parameters to Points [9]

This particular project within the aerodynamics package required a substantial amount of collaboration with team members working directly on the undertray, Chassis, and cPowertrain in terms of component placement, mounting, and interference issues. The collaboration required that combustion powertrain members to work with the undertray and side-pod engineers to create an integrated cooling system that provided the best possible airflow, and allowed for ease of manufacturing and assembly for the radiator, side-pod and undertray.

The goal of the side-pod development was to design a final product that provided the best aerodynamic performance with a large consideration for ease of manufacturing.

From an Aerodynamics team standpoint, the success of the side-pods, as well as

all other components of the aerodynamics package, required strong teamwork, efficient member relationships and a balance of members' strengths and weaknesses to offset the vast range of skills and expertise of other members. The success of this particular product required excellent communication skills from a variety of different team inputs, from fellow Aerodynamics team members, cPowertrain, and Chassis members to help make the integration of this component one that was an improvement over previous models, and contributed to a high level of performance for the 2014 GFR vehicle. The sub-team interaction required in the development is outlined in Table 3.

Table 3: GFR Sub-Team interactions summary

● Aerodynamics - Undertray: Close communication and design considerations/inputs due to undertray-side-pod relationship on GFR vehicle. Required communication and design perspectives from both members for successful integration including assembly, mounting and positioning.
● cPowertrain - Cooling Systems: Strong collaboration in radiator placement, component housing and assembly, as well as design iterations for optimal cooling effects for engine performance.
● Chassis - Monocoque: Integration of the side-pods and factors affecting overall shape due to monocoque profile changes and other aspects including assembly. Chassis team was consulted consistently in order to coordinate the attachment methods for a high level of structural and aerodynamic performance, as well as ease of manufacturing.

In terms of competition events, the side-pods play a major role in all events however there seems to be a much larger impact on vehicle performance particularly in the Autocross, and Endurance events. Within the Endurance event most importantly, proper airflow through the side-pods is most important due to the strenuous demand of the engine to perform for much longer periods of time; approximately twenty minutes. This Endurance event causes the engine to produce large amounts of heat, and requires

adequate cooling performance to guarantee the vehicle engine systems do not fail.

In terms of aerodynamic performance, the side-pods were designed to maximize design parameters that induced the least amount of vehicle drag for improvements in the Endurance event. It looked towards improving downforce production required by Autocross events where large accelerations in all directions are necessary. In terms of the Endurance event, with less drag and better airflow through the side-pods, the vehicle will have less resistance and the engine will be able to run cooler, which will ultimately lead to an improvement in vehicle efficiency; a major portion of points for the endurance event.

In review of the purpose of the design changes for the 2014 side-pod, the goal was to create a part that produced maximum downforce with minimal drag, and increased airflow to the radiator and cooling system. Additionally, more goals were to reduce weight through manufacturing techniques, and improve assembly time with part simplification.

4. Current State Analysis and Benchmarking

4.1 Current State Analysis

In 2010, an undertray design and windshield gurney was introduced into the vehicle design to improve overall vehicle performance by improving downforce capabilities. This marked the beginning of the aerodynamics package and provided a solid foundation for future aerodynamics team to build from.

In 2011, a complete aerodynamics package was introduced into the design of the overall vehicle including a newly designed undertray and the previously designed windshield gurney. This new aerodynamics package included multiple new components such as a front mounted wing, redesigned side-pods, and a rear wing. The vehicle's performance in events such as Autocross and Endurance improved significantly providing solid evidence of the need of an aerodynamics package that provided a high level of downforce and low drag.

4.1.1 GFR Side-Pod Evolution:

2010: With the help of Daimler Trucks North America, a rather large side-pod was designed to house a radiator responsible for cooling the engine motor oil. DTNA supported the *GFR* team by allowing vehicle aerodynamics testing on the 2009 vehicle, in the DTNA Wind Tunnel, located on Swan Island in Portland, Oregon. The following year, DTNA engineers provided helpful suggestions in a detailed airflow and cooling analysis that helped drive the design for 2011, using the 2010 side-pod as a benchmark.

This side-pod was critiqued by individuals at DTNA who analyzed the characteristics of the airflow and made suggestions for radiator mounting strategies for improved performance. In 2010, the GFR car only had one side-pod that housed both a water and oil cooler in a single unit, as seen in Figure 24.

Figure 24: Side-Pod from GFR 2010 Car [6].

2011-2012: For the GFR 2011-2012 vehicles, the side-pods were redesigned to incorporate a symmetric pair of side-pods that were positioned on both sides of the vehicle, in mirror images of each other. For this particular design, the inlet shape was changed to allow low-flowing air into the duct by lowering the side-pod inlet. It also included a redesigned outer shell of the side-pod to return towards the monocoque at a much steeper angle, allowing the air to be exit faster. The addition of the louvers on the top portion of the side-pods were created to induce a "vacuum" action to pull the air out of the radiators through the production of a low pressure zone on top of the side-pod caused by fast moving air. This can be seen in Figure 25. These were later removed due to cooling hindrances caused by the louver design. There is little empirical data for this

generation of side-pods due to design completion in Germany, however according to graduate students of *Global Formula Racing*, it has been noted that the cooling system was extremely inefficient and engine cooling needed tremendous improvement. The comparison of the 2011 and 2012 side-pods can be seen in Figure 26.

Figure 25: 2011-2012 Side-pods - CATIA V5

Figure 26: 2011 (right) and 2012 (left) side-pod designs

2013: The GFR 2013 car utilized the same side-pod design as the 2011/2012 vehicle however the angle of the radiator was more acute, which restricted airflow through the radiator. As mentioned previously, engine operating temperatures decreased during physical testing when the louvers were removed. There has been little

investigation into numerical data verifying this, but it is an area of further recommendation for the *GFR* 2015 Aerodynamics team. For the 2013 design, there was a large section cut-out in the side-pod, directly behind the location of the fan to improve airflow through the side-pod, as shown in Figure 27. Due to the space claim restrictions of the radiators within the side-pod, the radiators were mounted at much shallower angles with respect to the income airflow. As will be discussed later, the low mounting angle was a huge factor in the inability for the radiators to properly cool the engine components, nearly prevented *GFR* from finishing multiple Endurance events in the 2013 season.

Figure 27:2013 Side-Pod with Louvers Removed

4.1.2 Current State and SWOT - Side-Pods

The side-pods have not changed since the GFR 2011 car and due to the need for new cooling system components and an overall improvement of airflow, the 2014 side-pods needed to be completely redesigned. The new design of the side-pods required new

geometry, positioning, and mounting strategies to produce the most effective cooling for the vehicle. With the introduction of a four-element front wing, the side-pod design needed to extract air from very *limited* flow coming from over the large front wings and direct it into the side-pods to ensure maximum cooling. This required collaboration between the side-pods and the cPowertrain team to agree on proper positioning of the radiator and side-pod to provide an adequate solution. This also required numerous design iterations and extensive analysis through CFD, from both the Aerodynamics team as well as the cPowertrain team to identify the incoming airflow and cooling performance of the radiators. This required airflow studies where the best final design was chosen based on airflow and performance of the entire vehicle rather than only one of the subsystems (i.e. side-pod, cPowertrain).

The current 2013 cooling system is positioned in a way that does not particularly benefit the engine performance of the vehicle and limits its cooling capabilities. The radiator is mounted at an extremely shallow angle in order to compromise for the packaging limitations of the side-pod and radiator with the addition of a rather large and newly designed undertray. Due to the size of the new undertray, the space available for mounting the cooling components was significantly limited. The new undertray provided extremely high levels of downforce that greatly improved the vehicles performance and was a necessary addition to the vehicle despite its restrictions to the mounting of the radiator. As seen in Figure 28, the radiators are mounted at approximately a 35° angle with respect to the vehicle motion and incoming airflow.

Figure 28: Radiator mounting angle with respect to incoming airflow and vehicle motion.

Another component of the current cooling package used on the 2013 GFR vehicle was a fan mounted behind the radiator. This fan, as seen below in Figure 29, is much too small for the size of the radiator to have any great effect on the airflow through the cooling system.

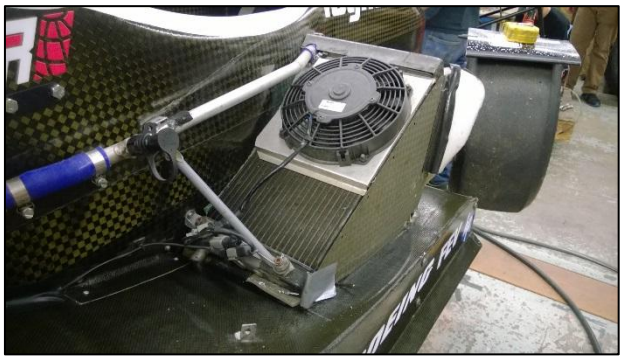

Figure 29: Rear fan radiator mounting for 2013 GFR vehicle.

This particular component was also changed for the 2014 GFR vehicle and a much larger fan was paired and mounted to the new radiator. This had a dramatic effect on the aerodynamic design of the side-pod in terms of space claim for the cooling

package within the internals of the side-pod cavity.

The 2014 side-pod looked to improve the internal ducting to become a completely integrated part of the overall side-pod design rather than the current system which utilizes pieces of foam, tape, and carbon to block air from flowing around the radiators as seen in Figures 30-32.

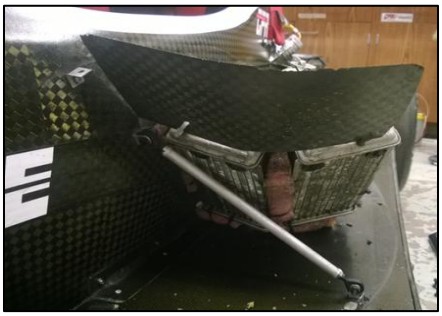

Figure 30: Radiator Carbon-Fiber Ducting (Front View).

Figure 31: Radiator Carbon-Fiber Ducting (Side-View)

Figure 32: Radiator Carbon-Fiber Ducting with Gorilla Tape

As mentioned above, the 2013 side-pod is contoured in a way that required some extra post-processing additions to “seal” off escaping airflow from around the edges of the radiator. The goal of the 2014 side-pod with internal ducting was to eliminate the need for additional post-processing of cut-to-fit pieces after the side-pod has been mounted. This made it easier to reassemble in fewer steps. This improved assembly and integrated to better fit the shape of the side-pod as shown in Figure 33.

Figure 33: Driver side, side-pod with post-processing manufacturing additions using foam and tape to further seal and direct the air towards radiators.

The 2013 side-pods are extremely lightweight and made with one layer of T800 Carbon-Fiber – ¼” Honeycomb core, and another layer of T800 Carbon-Fiber. The 2014 GFR side-pod further investigated the potential for decrease in material use for structural reasons which could potentially result in an even further weight reduction of the part.

4.1.3 SWOT Analysis

Results from a Strengths, Weakness, Opportunities, and Threats (SWOT) analysis for the side-pods summarized in

Figure *34* and provides a basis for understanding the 2014 GFR side-pod design strategy.

Internal	*External*
Strengths: ● Strong CATIA V5 design experience with complex part shape design ● Manufacturing of carbon fiber lay-ups ● Miniscule drag effects ● Aerodynamic, Thermodynamics and Fluid Mechanics conceptual knowledge and understanding	**Opportunities:** ● cPowertrain working to optimize cooling systems and studying airflow effects ● Resources and people with knowledge of Star-CCM+ for CFD ● Resources for F1 style side-pod design and cooling
Weaknesses: ● Currently produces lifting force rather than down force ● Lack of quantitative data for airflow into side-pod and heat dissipation ● Current designs have poor cooling effects ● Lack of knowledge of CFD program operations	**Threats:** ● Lack of airflow present due to new, larger front wing design ● Unable to route air into side-pods for sufficient cooling ● Time limitations to run physical airflow tests to validate CFD ● Insufficient time to manufacture completely new molds for complex shape designs

Figure 34: SWOT Analysis

4.1.4 Goals for GFR 2014 Vehicle - Side-pods:

- Improve airflow through side-pod with variations in inlet/outlet geometry, positioning, and internal ducting design.
- Focus on radiator positioning and angle to improve airflow through cooling

system for maximum heat transfer effects. Design shape to accommodate placement and maintain styling characteristics consistent with chassis shape and overall vehicle image.

- Work with cPowertrain to maintain clearance and component compatibility for cooling space claim.
- Investigate variation in side-pod shape and feature additions to increase downforce and reduce lift while maintaining low levels drag.

4.2 Benchmarking

In order to further understand how the 2014 *GFR* side-pods could be improved in the process of the redesign, benchmarking prior years was a valuable process. In Section 4.1, the current state of the prior side-pods were evaluated and analyzed through visual inspection, knowledge shared from previous senior project reports, and through qualitative analysis. Based on the previous SWOT analysis, one of the biggest weaknesses of the side-pod component for the *GFR* vehicle is the lack of quantitative data, validation through physical testing, and lack of knowledge of airflow characteristics and heat dissipation abilities. This section will introduce more quantitative data, as well as a more technical approach for manufacturing, assembly, and design of previous side-pods.

4.2.1 Side-Pods

In 2011, the side-pods and molds were designed and manufactured in Germany. There was little documentation from these previous designs. There has been little work done to provide any technical data regarding design and justification, and there is especially little knowledge about the airflow through the side-pod and its effect on cooling performance. In terms of manufacturing, the molds were manufactured in Germany and brought to Oregon State University by a German exchange student. The aerodynamics team at Oregon State University in 2011 only assisted in the manufacturing process, thus little documentation of manufacturing and implementation was completed.

The design of the side-pods did not change from the GFR 2011 to *GFR* 2012 car,

and in 2013 the *GFR* car experienced minor aesthetic changes. In 2011, the side-pods were manufactured out of carbon-fiber and a core material; whereas in 2012 the side-pods were made of Kevlar. In 2013, the side-pods were re-manufactured using carbon-fiber once again using a 1-core-1 lay-up, with louvers removed as mentioned earlier. The other changes made to the 2013 side-pods were: a larger exit created by shortening the outlet location, and wider inlets. This was done during the manufacturing process as the entire mold was utilized for lay-up versus previous years in which the side-pods were manufactured 65 mm away from the width edge and 10 mm away from the height edge of the mold.

This increase in height to the 2013 side-pod was instituted due to a much longer radiator than used in the previous years. This caused the side-pods to increase slightly in size, however in order to offset the height change as much as possible, the radiators were mounted at extremely low angles in relation to the flow of air. The 2013 side-pod was also mounted to a completely redesigned undertray wing structure as seen in Figure 35.

Figure 35: 2013 Side-pod and undertray

Physical benchmarking of previous side-pods for 2011-2013 can be seen in Table 4. These measurements were physically taken during the benchmarking process during the initial phases of the design in October of 2013 and were documented for further use in years to come and used as a guideline for the 2014 side-pod.

Table 4: Side-pod specification comparison of measured dimensional parameters as well as physical side-pod mass.

Side-Pod Specification Comparison	2013	2012	2011
Length	580 mm	580 mm	580 mm
Inlet Width	360 mm	295 mm	295 mm
Outlet Width	180 mm	200 mm	200 mm
Inlet Height	310 mm	300 mm	300 mm
Outlet Height	190 mm	230 mm	230 mm
Mass	444.4 g	453.56 g	471.22 g

As demonstrated by Table 4, the length and width of the 2013 side-pod increased as a result of utilizing the entire mold to create the physical side-pod for this race year. It can also be seen that although the overall size of the side-pod increased, the mass decreased by 9.16 grams from the previous design. This is due to multiple aspects of the manufacturing process. Weight was reduced because of the removal of the louvers, the shortening of the side-pod outlet in the longitudinal direction of the vehicle, as well as the material lay-up. From 2012 to 2013, the side-pod weight was reduced due to the lay-up schedule of one layer of carbon-fiber, honeycomb core material, and a final layer of carbon-fiber. The differences between the 2012 and 2013 side-pod structure can be seen in Figure 36.

Figure 36: 2012(left) and 2013(right) Side-Pods illustrating difference between louver removal and exit area.

4.2.1.1 Side-Pod Structure Comparison

Throughout the evolution of the side-pods on the GFR cars from 2011 to 2013, there have been some slight changes to the way the side-pods have interfaced with other components of the vehicle. Table A 1 in Appendix A illustrates the differences between the oil and water radiators for the last three years, detailing different aspects such as mounting techniques, component interfaces, assembly structure and strategies, assembly notes documenting strengths and weaknesses, internal and external design features, and lastly the structure of the side-pods internal ducting systems.

4.2.2 Radiator

As noted in prior sections, the airflow through the side-pods of the 2011 and 2012 *GFR* cars was sufficient in providing enough cooling to allow the engine to operate

normally. The change to the 2013 and its inability to cool properly was largely due to the change in radiator angles from the previous years as well as the addition of a much larger front wing. The comparison of the vehicles from years 2011-2013 can be seen in Table 5 below. This table illustrates the different mounting angles for both the oil and water radiators over the various years.

Table 5: Oil and Water radiator mounting angles for the GFR 2011-2013 vehicles with respect to incoming airflow.

Radiator Specifications	2013		2012		2011	
	Oil	Water	Oil	Water	Oil	Water
Radiator Mounting Angle	28.8°	38.4°	29.5°	34.2°	55.1°	48°

As seen in Table 5 above, both the oil and water radiators began to decrease in angle each year. The reason for this is unknown from 2011-2012, however as mentioned previously, the decrease in oil radiator angle for the *GFR* 2013 car to its lowest point was due largely to the size constraints of the new longer radiator, although the water radiator was able to increase from the previous year with the increase in height of the 2013 side-pod.

4.2.3 *Side Pod Airflow Engineering Analysis*

A critical aspect of the side-pods on the GFR vehicles has much to do with the airflow through the internals of the side-pod and through the radiator components for cooling purposes. There has been little analysis of this aspect of the side-pods, and because it is relatively difficult to prove, little knowledge has been documented over the years. In order to provide any engineering analysis to the new design of the 2014 side-

pod, it was necessary to first categorize some basic theoretical parameters regarding the flow through previous side-pods based on principles discussed in Section 2.

In order to simplify the overall analysis, it is important to state that for the case of airflow through the side-pods, the law of conservation of mass must be met, stating that the mass that flows through the entrance must leave out of the exit. With the assumption that all of the incoming air passes through the side-pod, the mass flow rate can be broken down into a fluid's density, velocity, and the cross sectional area through which it travels. This allows for an observation of ratios of velocity to the ratios of the inlet and outlet areas through which the fluid travels. For racing applications, it is understood that the density of the fluid, in this case air, remains constant throughout the flow.

According to the law of conservation of mass for a steady state system:

$$\textit{Mass flow rate in} = \textit{Mass flow rate out} \tag{9}$$

Relating mass flow with the fluid's velocity, density, and the cross-sectional area, the equation can be written in terms of its inlet and outlet properties:

$$\rho_i A_i V_i = \rho_o A_o V_o \tag{9.1}$$

Assuming the fluid is incompressible during this flow allows for simplification as density remains constant over the course of the flow; this simplifies to:

$$A_i V_i = A_o V_o \tag{9.2}$$

Rearranging the variables to demonstrate the ratio of inlet and outlet areas to the corresponding velocities at the inlet and outlet, the parameters can be rearranged as seen

in Equation 10, which can be used for geometrical comparison of flow velocities of various designs simply from deriving the conservation of mass above.

$$\frac{A_i}{A_o} = \frac{V_o}{V_i} \tag{10}$$

Some caveats must be mentioned in regards to the above calculations. These equations do not account for choked flow, pressure drops across a radiator, or back-pressure from restricted fluid flow out of the exit as could be expected from a real life situation.

This analysis is solely used for quick calculations to analyze the effects of varying the inlet and outlet sizes affects flow velocity based on the law of conservation of mass. These calculations provide basic insight into how the flow increases/decreases with changes in inlet/outlet cross sectional areas design concepts. Only physical testing would be able to provide the most realistic results to determine how such parameters and characteristics are influenced, although these ratio relationships help with preliminary designs.

The above calculations have been performed for the last three years of side-pod designs analyzing both the oil and water side-pods. It can be noted that the same values were used for both the oil and water (given they are identical side-pods). Lastly, the *velocity ratio* is simply the ratio of the exit velocity to the inlet velocity, as calculated by dividing the inlet area by the outlet area. In these particular calculations, the louver area on the rear of the side-pods was considered to have its own outlet area "seen" by the flow of air and was added to the total exit area of the side-pod.

Table 6: Flow area analysis of 2011-2013 side-pods comparing velocity ratios

Side Pod Flow Area Analysis	2013		2012		2011	
	Oil	*Water*	*Oil*	*Water*	*Oil*	*Water*
Inlet Area (mm^2)	72,000	72,000	76,000	76,000	76,000	76,000
Outlet Area (mm^2)	38,000	38,000	62,000	62,000	62,000	62,000
Louver Area (mm^2)	3,600	3,600	4,000	4,000	4,000	4,000
Total "Seen" Exit Area	41,600	41,600	66,000	66,000	66,000	66,000
Velocity Ratio*	**1.731**	**1.731**	**1.152**	**1.152**	**1.152**	**1.152**

**A disclaimer to the "Velocity Ratio" is that it is simply a calculation of the ratio of inlet area to outlet area size, providing an associated velocity multiplier. For example, for the 2013 Oil Radiator, the ratio of inlet area to outlet area = 72,000/38,000 = 1.731. This means that in the absence of backpressure, and ignoring pressure drop across a radiator, the velocity at the outlet is 1.731 times greater than the velocity at the inlet according to 1.731 = V2/V1; V2 = 1.731 x V1*

As is shown in the data above, the 2013 side-pod had the largest *Velocity Ratio*, providing that it its geometry provided for the largest increase in fluid velocity, and mass flow rate, at the exit of the side-pod. As it was mentioned earlier, the 2013 was the least effective at providing proper airflow to the cooling components. Although we understand the relationship of the inlet and outlet sizes that should theoretically produce the best results for incompressible flow, it can be seen that many other factors such as pressure drop across the radiator and mounting angle are large contributors to the effectiveness of the airflow cooling capabilities.

The above calculations were made by measuring the inlet and outlet areas in CATIA V5 for each side-pod design for 2011, 2012, and 2013. An example of the inlet and outlet areas from the CAD model is shown below in Figure 37.

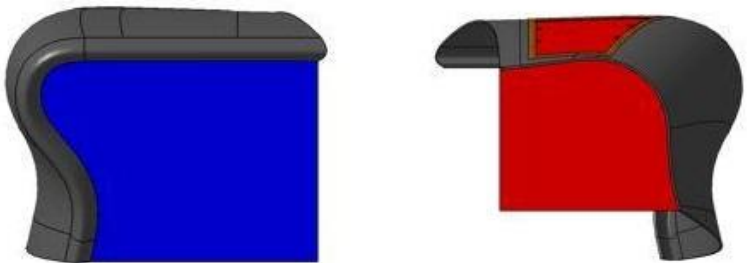

Figure 37: Geometry created in CATIA V5 to calculate Inlet (left) and Outlet (right) areas, including louvers, for the 2011-2013 Side-Pods

4.3 Competition Benchmarking

In order to better understand side-pod designs, it was important to look externally for benchmarking and ideas for improvement. Looking within the FSAE competition realm, two competitors stand out amongst other Universities: Tu Graz FSAE Racing and Monash Motorsport FSAE.

4.3.1 Tu Graz FSAE Racing

Figure 38: Tu Graz FSAE Racing Car [23]

Figure 39: Tu Graz FSAE Racing Car [23]

As seen in Figure 38 and Figure 39, Tu Graz FSAE Racing teams have utilized a rather rigid looking side-pod appears much more robust with its sharp lines, and rigid body shape. The team does a very nice job of contouring the side-pod to the shape of the chassis in its appearance as one uniform body. The cooling package of this particular side-pod is exposed at the outlet of the side-pod. This design shows potential benefits with the location of the inlet being close to the chassis body for undisturbed flow. It appears to catch air from over the a-arms and suspension links of the front wheels, rather than only the turbulent air coming from the tires.

Figure 40: 2006 Tu Graz FSAE Racing Car [23]

In 2006, Tu Graz FSAE Racing implemented a side-pod design very similar to the design of the 2013 *GFR* vehicle seen in Figure 40 above. These particular side-pods were extremely similar in shape, included a rather large inlet, and incorporated louvers mounted on the rear of the side-pod, similar to *GFR* 2011 and 2012. Benefits of this design include streamline part shapes that add to the aesthetics of the vehicle. This image also shows the rather vertical mounting of the radiators within the side-pod which is

crucial for effective cooling, given orthogonal airflow through the core. Tu Graz Racing switched to the more “squared design” change to the side-pods style shown above in Figure 38 and Figure 39 back in 2007. Tu Graz could have experienced similar issues, leading to the vehicle change in 2007 shown in Figure 41 below. This design strategy has been used ever since.

Figure 41: Tu Graz FSAE Racing - Tankia 2007 with “squared” pod design [23]

4.3.2 Melbourne Monash FSAE

Figure 42: Monash Motorsport Vehicles [16]

Figure 43: Monash Motorsport Vehicles [16]

Melbourne Motorsport has a very unique body and shape design to all of the vehicle elements; however their aerodynamics package is on the same scale as the GFR vehicle. This could also provide insight into potential engine cooling issues much like those of Global Formula Racing. For this particular design, the radiator is mounted within a side-pod design that does not enclose the cooling components. As can be seen in

Figure 43 above, the Monash vehicle uses air flowing around the chassis body and underskirts to channel the air along the length of the underbody skirt and into the radiator housing. This particular design seems to allow more air to come in contact with the radiator given the "openness" of the design. However, there definitely seems to be some flaws with the radiator mounted outboard rather than perpendicular to the flow of incoming air as it travels down the underskirt channel. This most likely looks like the result of packaging constraints, given that the side-pod extends to the edge of the tires illustrating that they are using the maximum space claim possible for the width of their undertray and side-pod components.

4.4 Side-Pod Analysis: Daimler Trucks North America

In 2010, Daimler Trucks North America engineering team was able to look at the GFR 2010 side-pod and radiator design, and provided a rather detailed analysis, including suggestions for future designs.

Figure *44* below shows a detailed PowerPoint slide provided by DTNA to GFR, illustrating problems with the current design at that time.

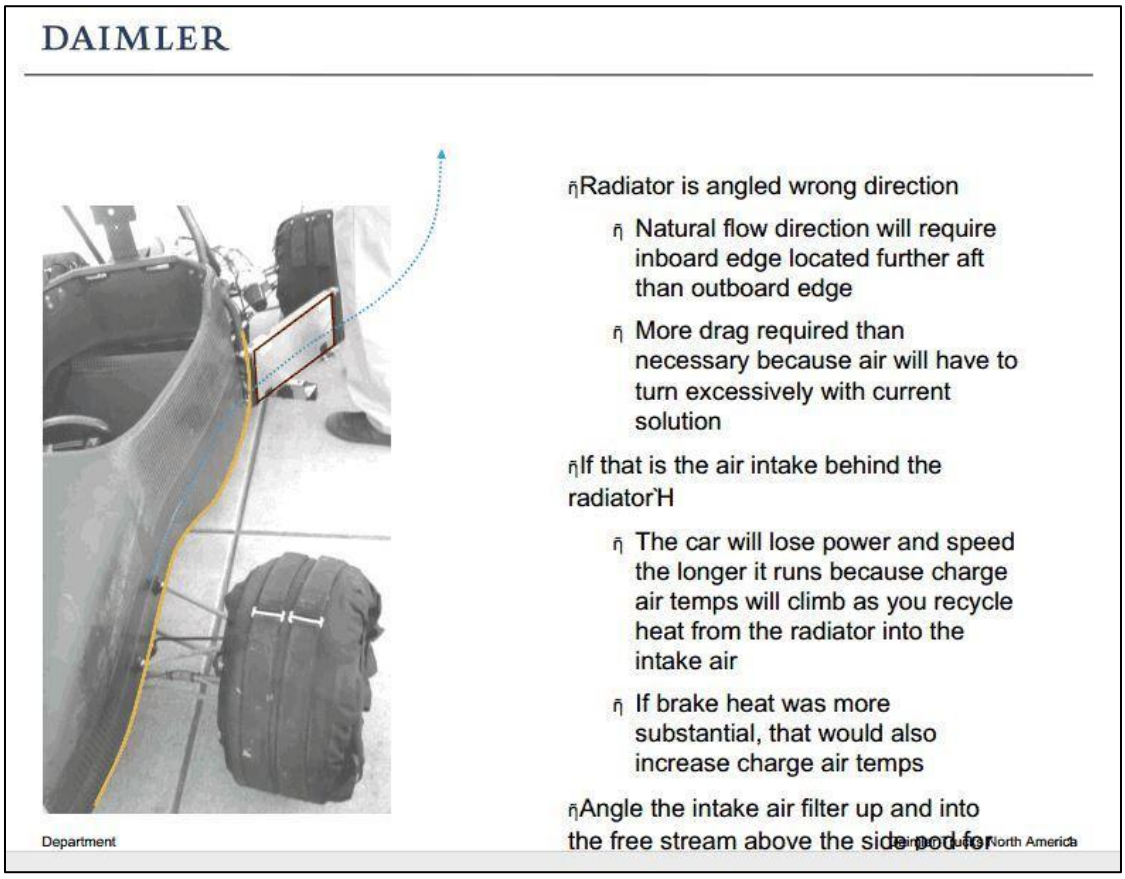

Figure 44: The above slide was provided by DTNA analyzing the 2010 vehicle radiator design [5]

As seen in the above image similar to the mounting strategy of Monash

Motorsport, the radiator is angled in the wrong direction to capture enough air for proper cooling. This was changed in the *GFR* 2011 car that included radiators mounted with no outboard angle, but instead utilized angles in the only the vertical directions.

Daimler Trucks North America provided some recommendations of new design concepts that could be utilized for future side-pod radiator configuration packages seen in Figure 45.

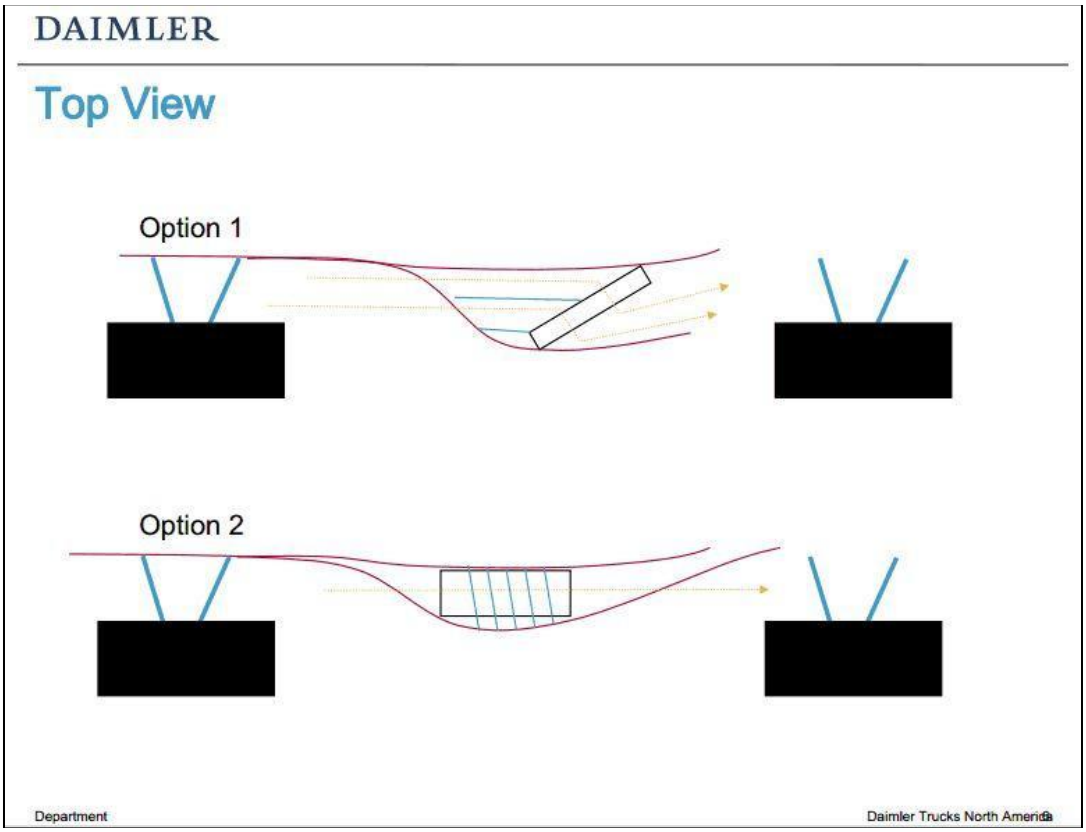

Figure 45: DTNA recommendations for future radiator positioning [5]

4.5 Side-Pod Manufacturing

As a result of the side-pod design staying relatively consistent since 2011, the manufacturing process has allowed for repetitive mold. The molds were originally manufactured in Germany and consisted of three different components: the main body shape, the leading edge radius, and a third surface used for a bottom panel. The molds can be seen in

Figure 46 [18].

Figure 46: Side-pod molds used for the 2011-2013 GFR vehicle [18].

The above photo shows the complete assembly of the left and right side-pod molds. The three individual pieces are all held together to create the final shape. The 2011 side-pods utilized the bottom surface panel, as the 2011 side-pod did not attach to any undertray component, and instead housed a radiator with its own flooring connected to the rest of the side-pod body. In 2012, the side-pod was mounted to the undertray which spanned the entire width of the vehicle. Lastly the 2013 model mounted directly to the newly designed undertray wing components on both sides of the vehicle. These two designs still utilized the leading edge radius, held on by bolts at numerous locations on the mold; however they did not require the floor panel in the construction.

In the 2012 and 2013 side-pods, the assembly utilized plastic hex head bolts for reduced weight, and used small L-shaped metal brackets to attach the 2013 side-pod to the chassis and undertray structures with epoxy. This provided for ease of manufacturing in eliminating extra processes to design carbon-fiber attachment flanges.

Figure 47: L-Bracket (left) for Side-pod - Undertray attachment (right).

All of the benchmarking data represented in this section of this thesis was used to

make improvements for the 2014 side-pod package.

5. Conceptual Design Analysis

This next section presents some initial design concepts for the 2014 side-pod. Each design concept will be analyzed in accordance to the design goals set for the 2014 aerodynamics package by *Global Formula Racing*. This section will outline the characteristics of each design that were potential strengths and weaknesses in accordance to customer requirements, design goals, and the previously discussed SWOT analysis components. This section will outline the direct customers of the 2014 side-pod, and cover aspects of each design including manufacturability, airflow characteristics, aerodynamic forces from CFD results, and CFD simulations.

An important aspect of the design analysis includes the overall design goals of the 2014 Aerodynamics team. These exist as a high-level view of the basic principles and requirements that the side-pod design must fulfill. They are outlined as such:

Design Goals of 2014 Aerodynamics Team (Side-Pods)

- The side-pods must be able to be installed and removed without modifying any other system or vehicle component with which it interacts or interfaces.
- Must allow for proper airflow to provide effective cooling capabilities to both an oil and water radiator.
- It must create a reduction in the lift forces as caused by the side-pod in previous years. The design must work towards achieving the highest value of downforce as possible while minimizing drag effects.

- 2014 side-pod must seek to improve the overall vehicle performance through potential weight reductions, increased downforce, reduced drag, and provide effective airflow to improve engine performance and efficiency as required by Autocross and Endurance events.
- Must allow for re-filling of oil and water radiators without removal of entire side-pod assembly.
- Must not require any panels of side-pod to be removed in order to fill fuel tank during competitions *(according to FSG rule IC 2.7)*

Secondly, the customers and customer requirements must be outlined in order to help understand who is affected by the side-pod design, and what the requirements are in order to successfully accomplish the design goals.

The customers and customer requirements of the 2014 side-pods are:

1. 2014 *Global Formula Race Team*

a. cPowertrain Team

i. cPowertrain Cooling Components Team

1. Provide effective airflow for cooling purposes

b. Aerodynamics Team

i. Add to the overall aerodynamic performance

1. Incorporate side-pod outlet near trailing edge of undertray wing component to improve downforce by delaying separation and also reducing drag

ii. Easily manufactured

c. Management Team - TA's
    i. Design, manufacture, and build a running vehicle by Spring Break of 2014 (March 22-29, 2014)
d. GFR Vehicle Competition Driver
    i. Safe and reliable shielding of radiator fluid from coming in contact with driver.
e. Pit-Team
    i. Easily removable and serviceable for any troubleshooting and/or maintenance during competition or in the off-season.

2. Competition Events
a. Competition points determined by success and overall improvement to vehicle handling in dynamic events, as well as design and justification for static events.
b. Must be aesthetically pleasing in order to gain static competition points

3. FSAE & FSG Event Judges
a. Must adhere to all design and performance rules as stated by FSAE and FSG rules for 2014 competition.

4. Future Global Formula Race Teams
a. Provide physical testing and validation to support CFD simulations. Aim to provide recommendations for future designs and areas of focus to further improve knowledge of airflow characteristics and cooling capabilities in order to design more effective side-pod systems.

All of the goals and customer requirements listed above can be summarized by the basic engineering components outlined in the following radial process diagram of Figure 48 . Each of these aspects played a large role in the design aspect and were all characteristics that needed to be evaluated. This designed required tradeoffs that provided for the most suitable design for the 2014 side-pod.

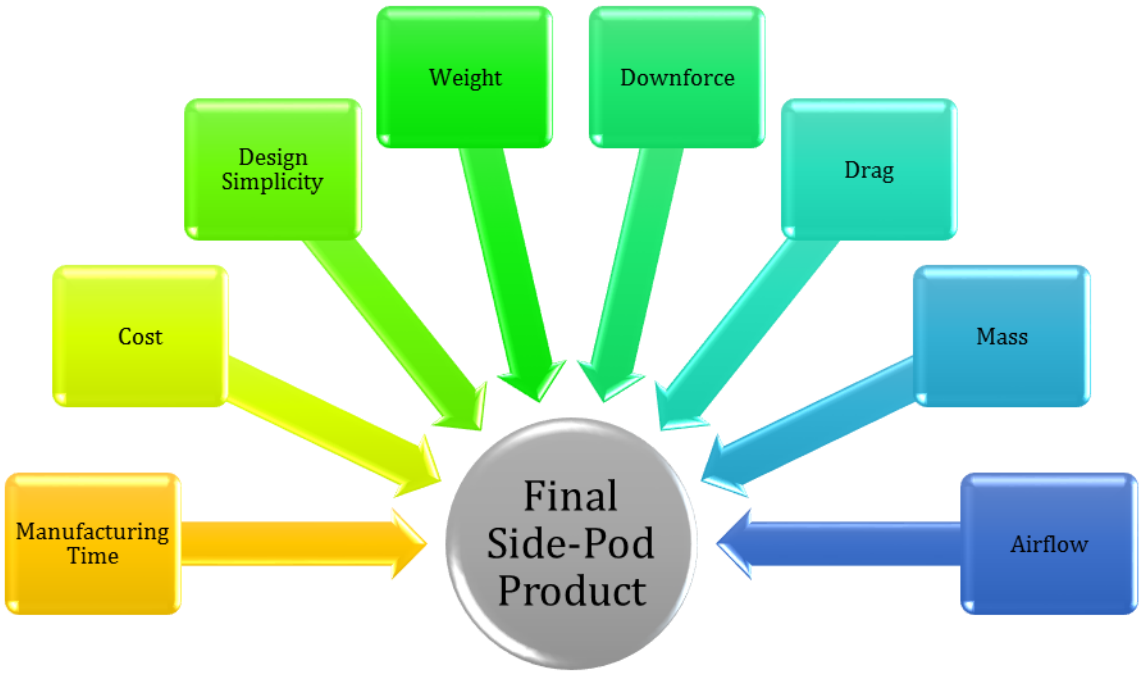

Figure 48: Design components incorporated into 2014 side-pod design

Each component in the figure above played a large role in the design decisions that were made by upper management and the author of this thesis. Significant compromises were made to provide the most effective solution given the current design requirements as well as the limited manufacturing time due to competition schedule.

5.1 Initial Design Phase – Concepts Considered

The following concepts were created during the initial design phase in the fall of 2013. In this section, the concepts will be listed in terms of the design evolution of the GFR 2014 side-pod initial concepts, along with some basic data relating to the projected performance. During the second half of the design phase, the side-pod design was focused in a different direction utilizing a different design strategy. This secondary design phase led to an increase side-pod performance, ease of manufacturing, part complexity reduction, and allowed for more design emphasis on internal ducting and mounting assembly. These concepts will be discussed in Section 5.2. In this section, none of the following concepts were validated using CFD simulations, due to the reprioritization and refocus of the design goals for the 2014 side-pod.

5.1.1 Design Concept Iterations

The following figures illustrate the side-pod design concepts that were initially considered before a reprioritization of the side-pod manufacturing.

Concept 1: 10_41_201_PRT A

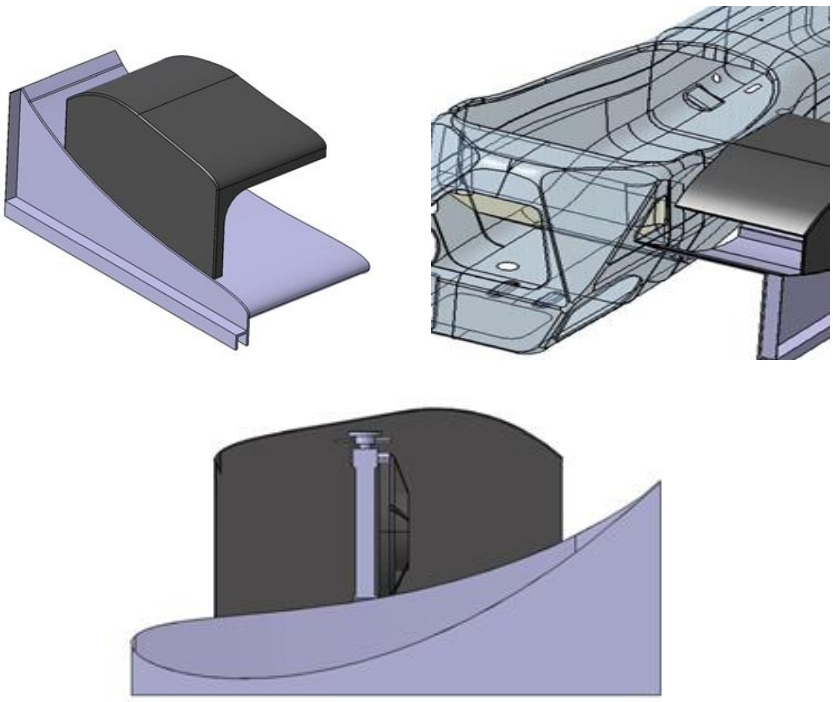

Figure 49: Side-Pod Concept #1

Concept 2: 10_41_201_PRT B_It1

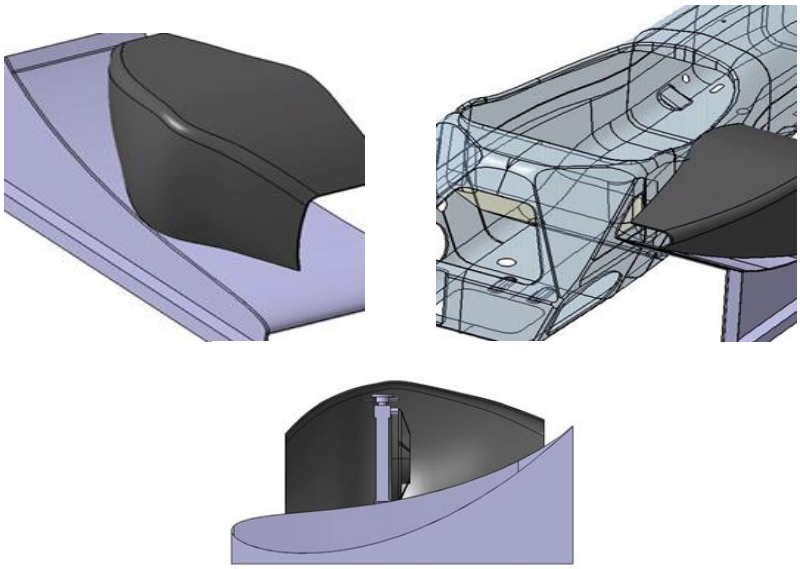

Figure 50: Side-Pod Concept # 2

Concept 3: 10_41_201_PRT B_It2

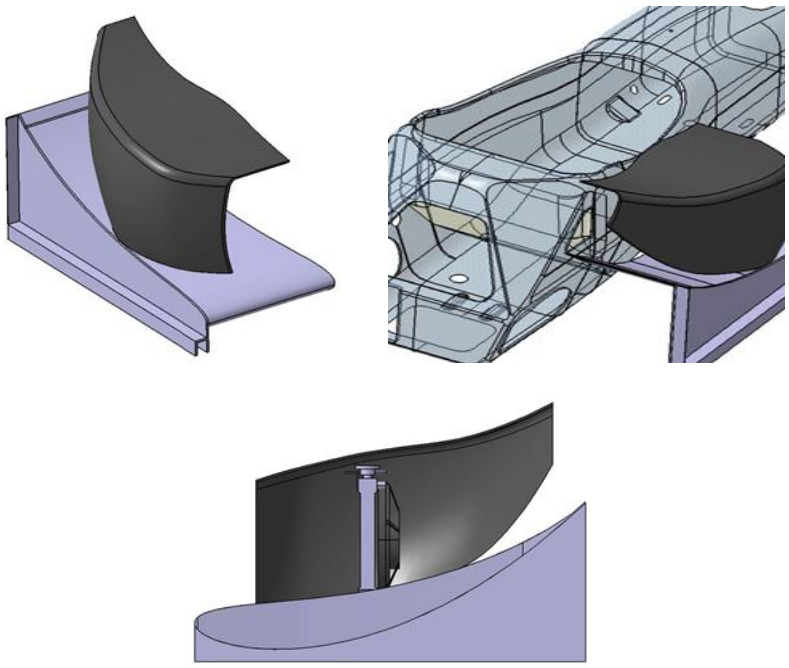

Figure 51: Side-Pod Concept # 3

Concept 4: 10_41_201_PRT C

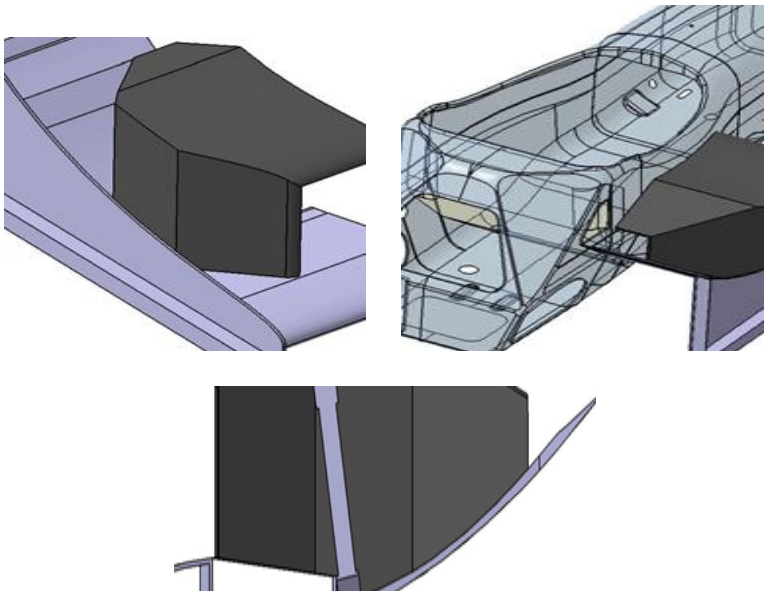

Figure 52: Side-Pod Concept #4

As will be discussed at the end of this section, the radiator and undertray surface were altered to promote better airflow through the radiator. The concept in above Figure 52: Side-Pod Concept #4 shows the incorporation of this design into the side-pod shape.

Concept 5: 10_41_201_PRT D_It2

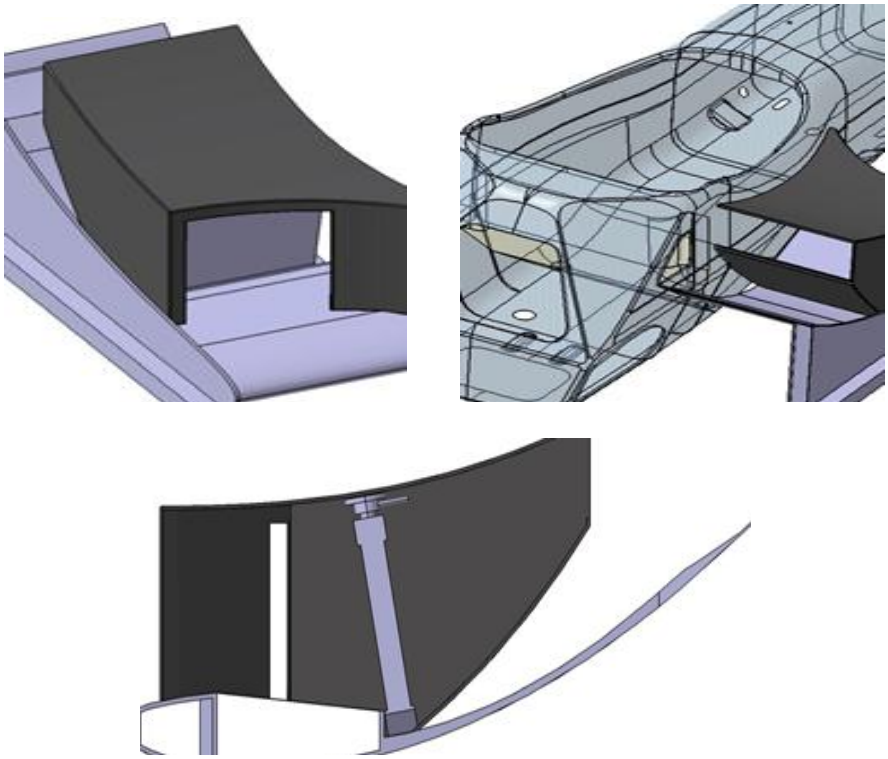

Figure 53: Side-Pod Concept #6

Airflow Analysis Summary of 2014 Design Concepts

Table 7: Side-pod flow area analysis for all five primary design iterations described in above section.

Side-Pod Flow Area Analysis	2014 - Design Phase 1				
	201_PRT A	201_PRT B_IT1	201_PRT B_IT2	201_PRT C	201_PRT D_IT2
Inlet Area (mm^2)	90000	50000	69000	55000	55000
Outlet Area (mm^2)	50000	9000	18000	9000	44000
Velocity Ratio*	1.80	5.56	3.83	6.11	1.25

All of the above concepts are summarized in Table A 2, in Appendix A. It can be noted that 10_41_201_PRT_C has the least added mass to the total vehicle. This would help increase points for the GFR competition car in the greatest measurable way. Aerodynamic performance of each of the above side-pods has not been analyzed but is a recommendation for further investigation.

5.2 Airflow Study: Radiator Re-Positioning

After an investigation into the airflow over the undertray, using a baseline 2014 Aerodynamics CFD simulation without a side-pod or radiator, it was determined that ambient air flowing over the undertray was not flowing orthogonal to the ground and path of travel as was initially predicted. As seen in Figure 54 below, the airflow is seen to flow more parallel to the curvature of the top surface of the undertray.

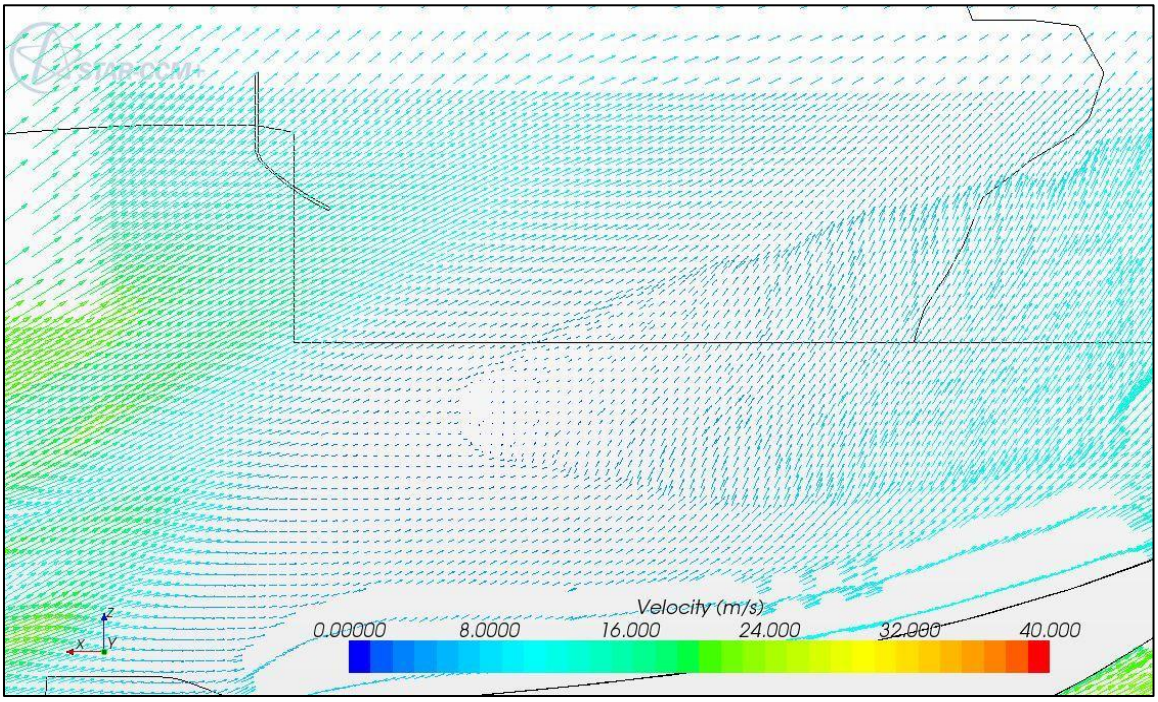

Figure 54: Airstream vectors showing parallel flow to undertray surface.

As a result of the above findings, communication with the cPowertrain and undertray engineers led to a redesign of the undertray to allow for a repositioning of the radiator. This repositioning is seen in the Figure 55 below.

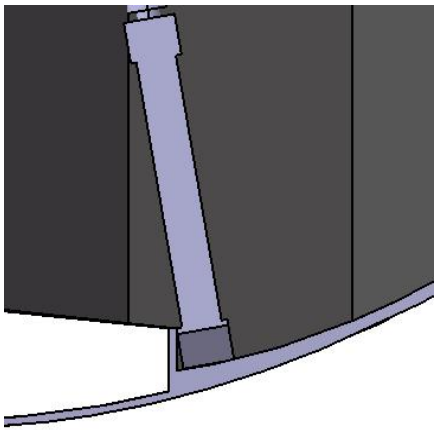

Figure 55: Removal of top surface of the 2014 undertray to account for lower radiator positioning and angle.

In the above figure, the solution to this was to remove a section of the top surface of the undertray to allow for lower positioning of the radiator. The idea was to allow the radiator core "fin" area to be flush with the leading contact surface of the undertray. This change allowed for the air to flow more orthogonally through the radiator fins to help aid in cooling performance. This also would improve vehicle handling by creating a lower center of gravity due to the lowering of the cooling elements.

Determining the proper placement of the radiator has been a crucial part of the design of the 2014 side-pod and undertray components. The placement of the radiators was a huge area of improvement over the recent years designs and helped significantly in solving the past cooling problems and inefficient airflow. The final location for the 2014 radiator for the cCar is shown below in Figure 56.

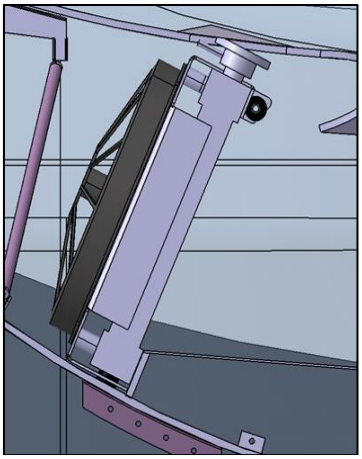

Figure 56: Radiator positioning and integration with undertray and side-pod top element

This particular positioning and angle of mounting has significantly contributed to the mass flow rate of air within the radiator core and it is a tremendous improvement that will be discussed in more technical detail in the upcoming section. This mounting angle also allows for filling of the water radiator without having to worry about any bubbles getting trapped in the top corners of the radiator. This angle was tested by filling the radiator with water and viewing the displacement caused when air bubble were released when tipped vertically. There were little to no air bubbles that escaped after complete filling, and provided an acceptable fill angle for servicing purposes. This is shown in Figure 57 below.

Figure 57: Radiator water fill and air bubble check at desired mounting angle.

The final positioning was established, through physical experimentation outlined above for the air bubble check, and cPowertrain and Aerodynamics agreed that 65° would be the acceptable mounting angle. This angle was chosen through various placement iterations and through compromises between side-pod height, undertray construction, and for cPowertrain routing line requirements, maintenance and regulatory service requirements. The angle is shown below in Figure 58.

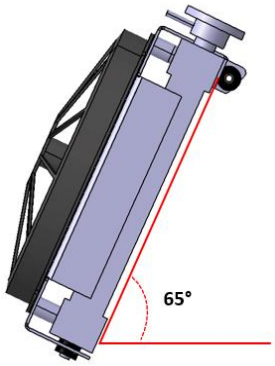

Figure 58: Radiator mounting angle

In order for the radiator to mount effectively to the undertray, the positioning needed to account for 2 mm of clearance for a rubber grommet to be placed on the lower positioning pins. This grommet spacing is shown in Figure 59 below.

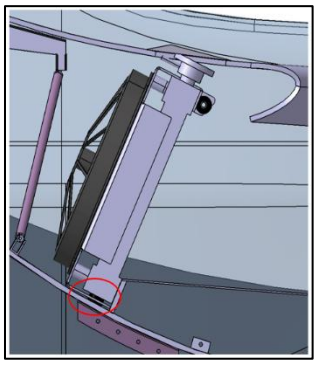

Figure 59: Rubber grommet spacing (2mm)

5.3 Secondary Design Phase – Concepts Pursued

In this section, the secondary design phase produced completely different concepts than those discussed in Section 5.1. These concepts involved a design strategy change to use current wing profiles that would allow for ease of manufacturing, part complexity reduction, ease of assembly, and reliability. Utilizing current Joukowski wing profiles for the side-pod allowed for use of the 2013 undertray mold during manufacturing. Using current undertray molds for a side-pod profile allowed for significant reductions in manufacturing time. This eliminated time for mold development, CNC programming, and physical fabrication times.

The general approach to the design of the 2014 side-pod was an iterative process. This process flow is seen in Figure 60. This diagram outlines the overarching process of design iteration created in CAD, followed by analysis of the results of the CFD simulations. Further changes to the designs were made based on these results, and again subjected to simulation to view the impact on aerodynamic performance and airflow. This process was repeated until a satisfactory result was produced.

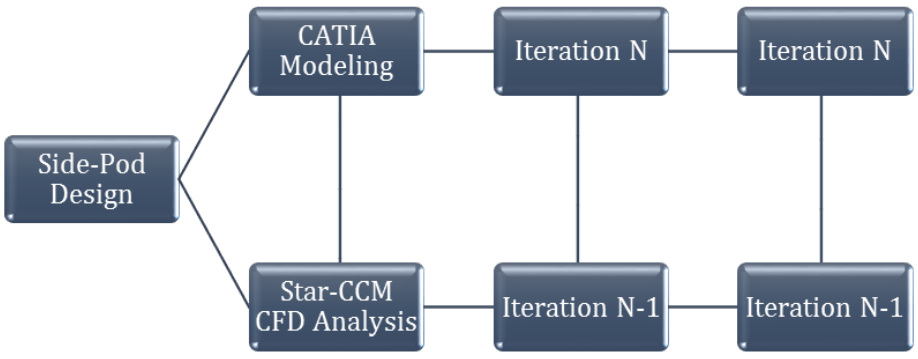

Figure 60: Design process flow for 2014 concepts

For each concept below, a brief description will be provided, all concepts will be tabulated to show CFD results, and the total aerodynamic performance of the entire vehicle will be related to competition points.

The following side-pod concepts were designed with similar wing profile characteristics to that of the 2014 undertray. The chord lengths have been altered slightly; however the thickness and camber have remained the same percentage of the 2014 undertray chord length. The airfoil data of the 2014 undertray is listed in the following table.

Table 8: Undertray wing profile data used to design side-pod

Undertray	**GFR 2014**
Profile	Joukowski
Thickness	12%
Camber	10%
Chord Length	1000 mm
Angle of Attack (AOA)	17°

Although CFD simulations were only run on half-car models, all performance data listed in the following sections is representative of full car performance.

GFR_14_10_41_201_E

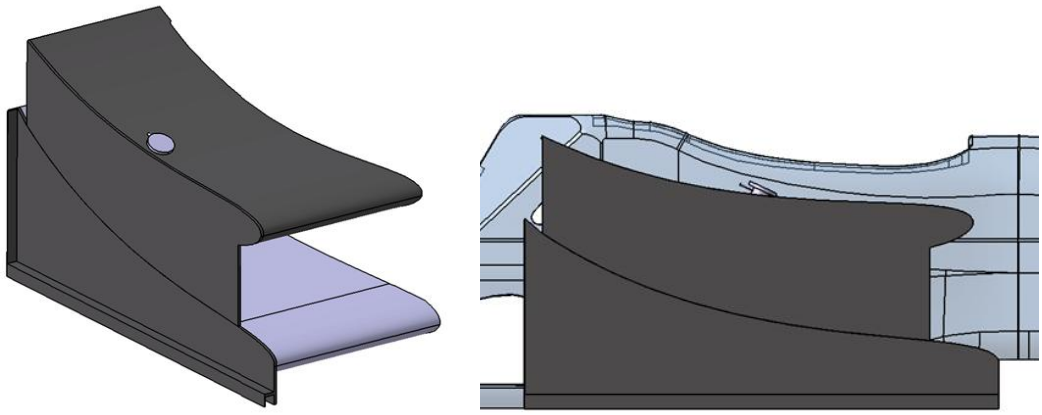

Figure 61: Side-Pod with leading edge offset 50 mm from leading edge of 2014 undertray, at same angle of attack (17 degree AOA) as undertray. (Isometric View)

Table 9: Side-Pod wing profile data

Side-Pod	**GFR 2014**
Part Number	*GFR_14_10_201_E*
Profile	Joukowski
Thickness	12% of Undertray
Camber	10% of Undertray
Chord Length	874 mm
Angle of Attack (AOA)	17°

Description and Results Analysis:

This side-pod concept was the first of the *GFR* 2014 concepts to be tested with CFD simulations. Since there was no prior simulation or previous knowledge of performance, this concept was used as a baseline for later concepts. This side-pod surface is mounted at the same angle of attack as the 2014 undertray; however its leading edge is

offset by 50 mm from the leading edge of the undertray. Its trailing edge is also shortened to prevent airflow restriction at the exit of the duct.

The goal for this concept was to increase downforce as much as possible by extending the wing profile as far rearward as possible to follow the surface of the undertray and utilize a large chord length. The reason for the offset was to allow air coming from over the large front wing profile to have space to be directed downward into the radiator cavity. As summarized in Table 10: Design summary of aerodynamic performance from CFD and projected weight calculations., this particular design created a total of 7.8 N of lift on the full car, and a 74.8% reduction in lift from the 2013 side-pod, which produced 31N of lift as shown in Appendix A. This concept allowed for a mass flow rate of 0.43 kg/sec according to CFD results tabulated in Table 10. This concept had the greatest addition of mass to the entire vehicle, approximately 1.35 kg, which provides the greatest reduction in competition points in this particular category of all the secondary design concepts. Figure 62 shows the streamline visualization of this concept using Star-CCM+™.

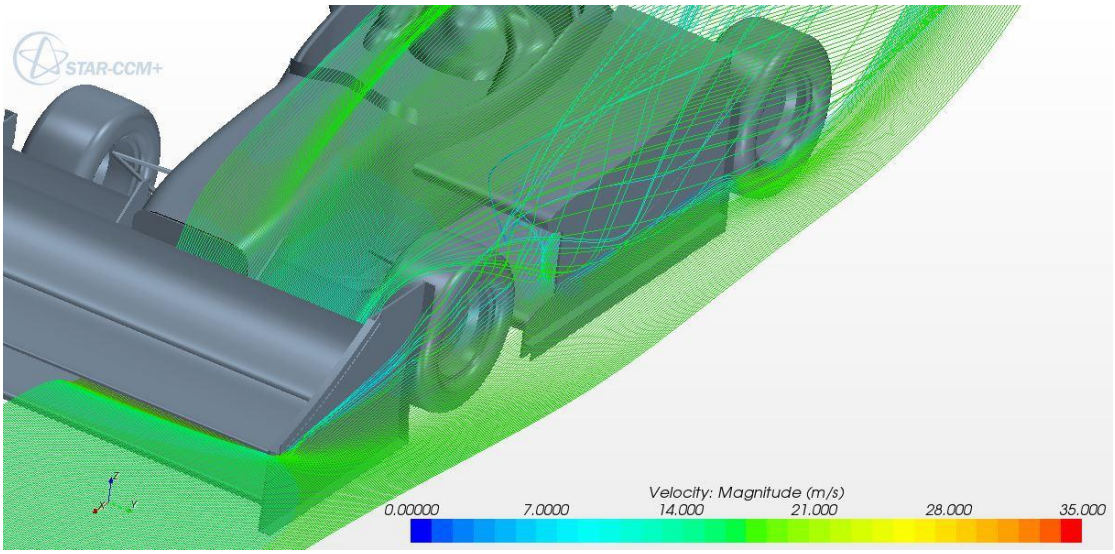

Figure 62: CFD streamline visualization (300 mm from floor) showing majority of air by-passing side-pod inlet. Significant airflow from front wing projected over side-pod inlet.

Design Summary:

Table 10: Design summary of aerodynamic performance from CFD and projected weight calculations.

Side-Pod	201_E	2013	Delta (2013-2014)
Downforce	*-7.6 N*	*-30.6 N*	*+75.2%*
Drag	*2.4 N*	*-0.2 N*	*-1300%*
Mass Flow Rate	*.43 kg/sec*	*0.05 kg/sec*	*+760%*
Mass	*1060 g*	*444.4 g*	*-138%*

Concept Summary:

Table 11: Concept summary of GFR_14_10_201_E

Design Assessment:	Initial iteration validated by CFD simulation. High level of uncertainty into validity of results and required further design changes to view effects on performance.
Reasoning:	CFD simulation shows majority of air by-passing side-pod inlet. This visualization does not seem to correlate well with mass flow rates obtained by CFD calculations. Provides uncertainty into the validity of the calculation of downforce values as well.
Investigation:	Inspired new iteration with shortened entrance, and larger entrance to see if it was possible to capture more air coming from the front wing.

GFR_14_10_41_201_F

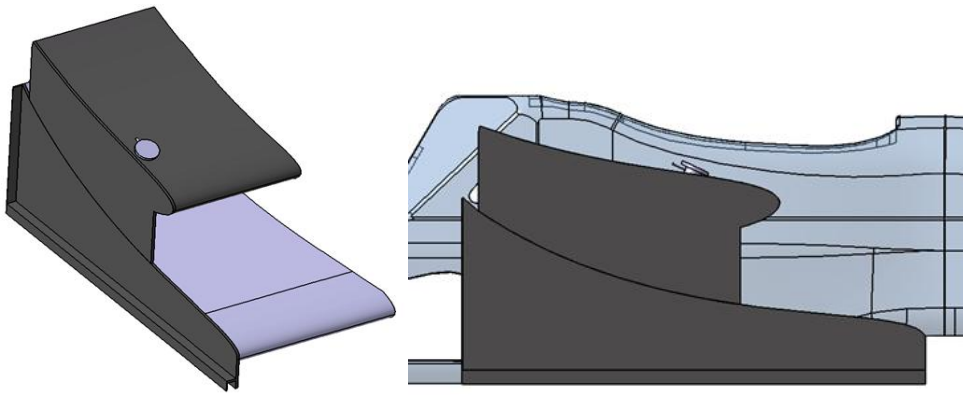

Figure 63: Side-Pod with leading edge offset 250 mm from leading edge of 2014 undertray, at same angle of attack as undertray. (Isometric View)

Table 12: Side-Pod wing profile data

Side-Pod	**GFR 2014**
Part Number	*GFR_14_10_201_F*
Profile	Joukowski
Thickness	12% of Undertray
Camber	10% of Undertray
Chord Length	640 mm
Angle of Attack (AOA)	17°

Description and Results Analysis:

This design concept utilized a much shorter side-pod with its leading edge offset 250 mm from the leading edge of the undertray. This side-pod configuration also utilizes the same angle of attack as the undertray in order to as much downforce performance as the previous iteration. The reasoning for a much shorter side-pod was to investigate

whether it was possible to capture more airflow through the ductwork of the side-pod and into the radiator. This was done by moving the entrance further aft on the vehicle length in order to catch as much available air as possible along the chassis line, as well as any air coming over the front wing and wheels.

As predicted, this configuration allowed for the greatest mass flow rate of air through its internal ducting, 0.49 kg/s according to CFD results shown in the below summary performance chart. Due to the nature of the short entrance distance between the inlet of air and the front core of the radiator this value for mass flow rate is significantly higher than what would be expected in real on-track situations. The side-pod does not have enough space to adequately pressurize and slow down the air at the inlet as needed for effective performance [15]. Thus, it would not produce as high of mass flow rate in real situations when compared to CFD results, due to limitations in CFD simulation properties and error.

After a further understanding of the principles behind adequate side-pod design, it was decided that this concept would not be implemented in the final design. However, looking at aerodynamics performance from simulations, this concept produced 11N of lift, with a 64.5% reduction in lift from the 2013 side-pod. Due to its shorter length, this side-pod consequently has the least addition of mass to the car, adding only 1.01 kg to the entire car. One thing to note about this concept is a less than 1 value of the velocity ratio of the particular design. For this design, the outlet area was larger than the inlet even though it had the largest mass flow rate of the secondary design phase concepts. This also led to some uncertainty about the validity of the velocity ratio and CFD simulation in respect to real life situations. .

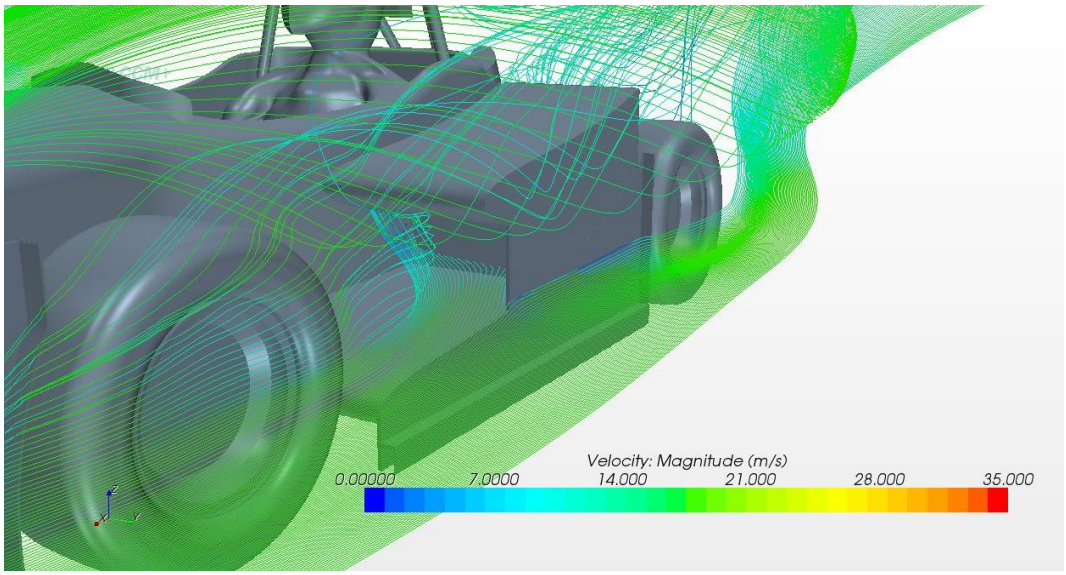

Figure 64: CFD streamline visualization (300 mm from floor) of short entry side-pod.

Design Summary:

Table 13: Design summary of aerodynamic performance from CFD and projected weight calculations.

Side-Pod	201_F	2013	Delta (2013-2014)
Downforce	*-11 N*	*-30.6 N*	*+64%*
Drag	*-0.14 N*	*-0.2 N*	*-30%*
Mass Flow Rate	*.49 kg/sec*	*0.05 kg/sec*	*+880%*
Mass	*730 g*	*444.4 g*	*-64.3%*

Concept Summary:

Table 14: Concept summary of GFR_14_10_201_F

Design Assessment:	Second iteration to be run in CFD simulation. High level of uncertainty of this design due to CFD results and design calculations.
Reasoning:	After further background research into recommended side-pod designs, and SAE publications, short entrance to radiator proves to be inefficient design in real-world racing situations [15]. Although large mass flow values from CFD, there are limitations to the accuracy of CFD simulation due to GFR lack of prior knowledge of accurately modeling pressure drop across radiator. Design provides a fractional velocity ratio (<1) indicating the side-pod would be acting as a diffuser and slowing down the air as it moves from the entrance to the exit; opposite of desired design.
Investigation:	Future concepts should pursue compromise between a long entry vs. short entry to combine the benefits of both previous concepts. Pursue medium length entry for realistic pressurization of incoming air for increased pressure gradient across radiator.

GFR_14_10_41_201_H

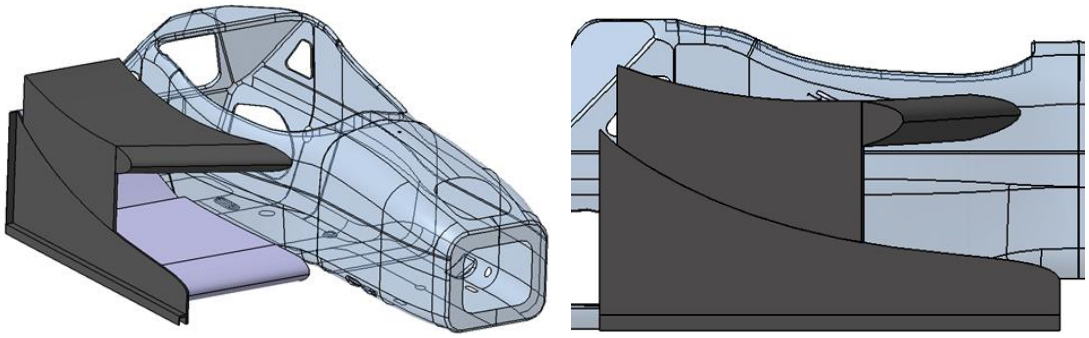

Figure 65: Side-Pod with slanted leading edge offset from leading edge of 2014 undertray, at lower angle of attack (AOA) than undertray. (Isometric View)

Table 15: Side-Pod wing profile data

Side-Pod	GFR 2014
Part Number	*GFR_14_10_201_H*
Profile	Joukowski
Thickness	12% of Undertray
Camber	10% of Undertray
Chord Length	470 mm
Angle of Attack (AOA)	17°

Description and Results Analysis:

As seen by the above CFD simulations of the previous concepts, the amount of available air to enter the side-pod is extremely limited, as most of the air flows above the side-pod due to the new front wing design. The streamlines of the previous simulations show that the majority of the air is flowing from around the outside of the tires and around the side of the vehicle. As mentioned previously, this design was intended to be a

compromise between the first two concepts (201_E and 201_F) that utilized a longer profile to improve downforce, while maintaining a slight offset in opening position to gather more airflow. This led to a design change implementing a slanted opening to provide benefits from both styles.

This concept captures substantially more air from the outboard area of the vehicle and directs it into the side-pod and radiator. The resulting concept is shown in Figure 65. This concept maintains the same angle of attack as the undertray; however the top surface is split at a 35 degree angle to capture more of the outboard flowing air. This concept provided 20N of lift, only a 35% reduction from the 2013 vehicle, with a mass flow rate of 0.45 kg/sec and an associated velocity ratio of 1.45. This concept produced more lift than desired, however it captured more air from the proper areas. The endplate associated with this particular concept was vertical in the front, and seemed to restrict airflow to the radiator slightly. This led to a further increase in the angle of attack that improved downforce and air flow.

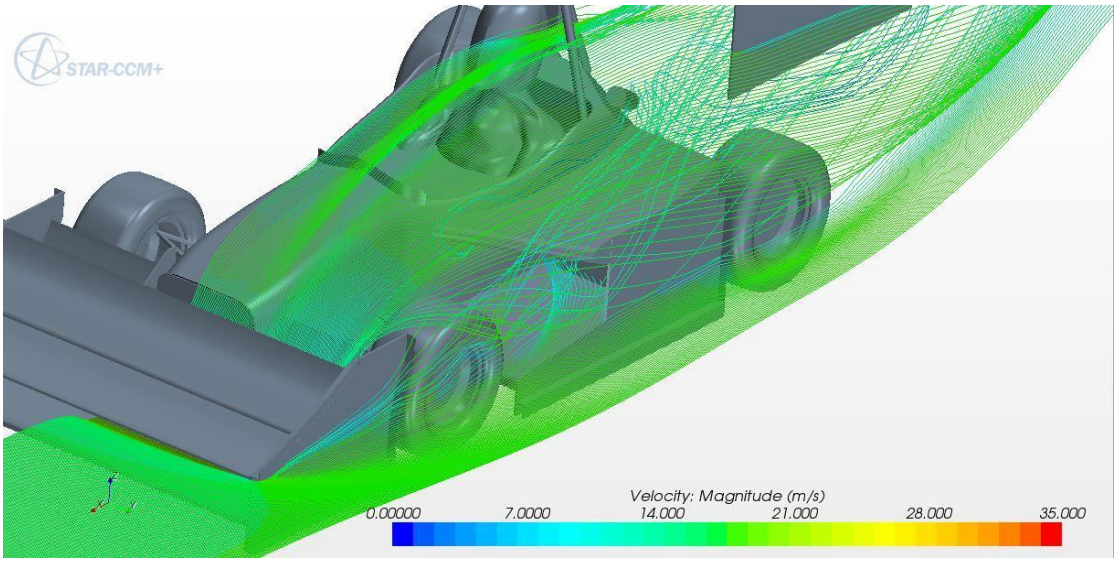

Figure 66: CFD streamline visualization (300 mm from floor) of GFR_14_10_41_201_H showing more streamlines being pulled into the side-pod from outboard areas of vehicle.

Design Summary:

Table 16: Design summary of aerodynamic performance from CFD and projected weight calculations.

Side-Pod	201_H	2013	Delta (2013-2014)
Downforce	*-20 N*	*-30.6 N*	*+34%*
Drag	*-3.4 N*	*-0.2 N*	*-1500%*
Mass Flow Rate	*.45 kg/sec*	*0.05 kg/sec*	*+800%*
Mass	*791 g*	*444.4 g*	*-78%*

Concept Summary:

Table 17: Concept summary of GFR_14_10_201_H

Design Assessment:	Still not optimal solution for aerodynamic performance. Mass flow rate acceptable but revisions to the endplate could be beneficial to improve airflow to the radiator.
Reasoning:	As seen by the CFD results in Table 16, this side-pod concept produces rather large amounts of lift. This concept needs revision in order to be significant improvement from 2013. Mass flow seems realistic given that this design allows for better capturing of outboard streamlines. Endplate needs to be improved to match angle of radiator mounting. Also need investigation into addition of gurney flap on trailing edge of undertray to improve airflow through side-pod, while improving downforce on undertray system. Needs final verification of rear endplate shape to comply with "Keep-out zone" of 2014 Formula SAE Rules.
Investigation:	Next concept should focus on new angle of attack of side-pod, slanted endplate opening at the front. Should also verify with simulations that additions of gurney slot and flap on outboard surface of endplate could produce benefits as seen by 2013 car. Alter aft endplate edge to include wheel contour for rules compliance.

GFR_14_10_41_201_J

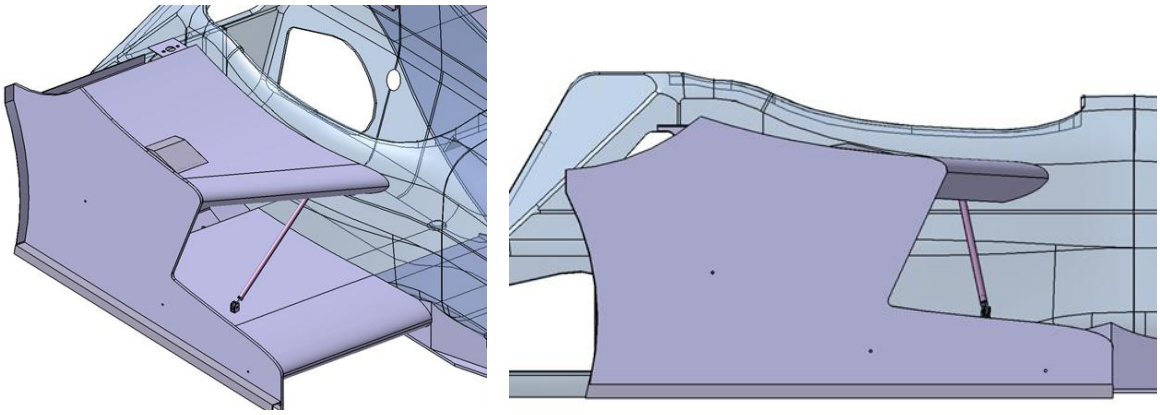

Figure 67: Side-Pod with slanted leading edge offset from leading edge of 2014 undertray, at larger angle of attack than undertray. Endplate angled to allow for improved outboard airflow.

Table 18: Side-Pod wing profile data

Side-Pod	GFR 2014
Part Number	*GFR_14_10_201_H*
Profile	Joukowski
Thickness	12% of Undertray
Camber	10% of Undertray
Chord Length	470 mm
Angle of Attack (AOA)	20°

Description and Results Analysis:

In the final iteration of the side-pod, GFR_14_10_41_201_J, the endplate was reshaped to become more parallel to mounting angle of the radiator package. This endplate change allowed for a larger opening. The angle of attack of the side-pod surface

was also increased to improve downforce. With an increase in angle of attack, the side-pod was able to be lowered slightly, without interfering with the radiator. This allowed an increase in the velocity ratio 2.02, the largest of the design concepts of this secondary design phase (concepts outlined in Section 3.2). The mass flow rate associated with this design was 0.45 kg/sec and produced only 12 N of lift, a 61% reduction from 2013.

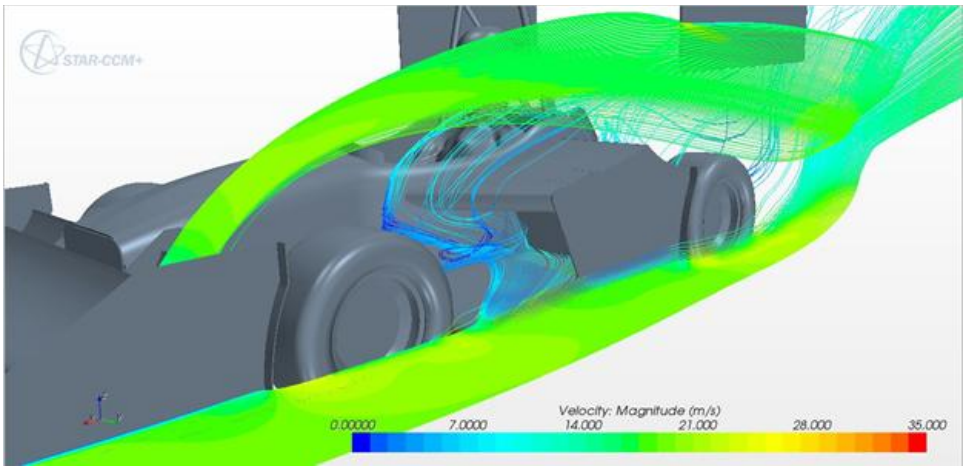

Figure 68: CFD streamline visualization (200 mm from floor) showing air availability in outboard regions. Image shows air from front wing element going over side-pod inlet.

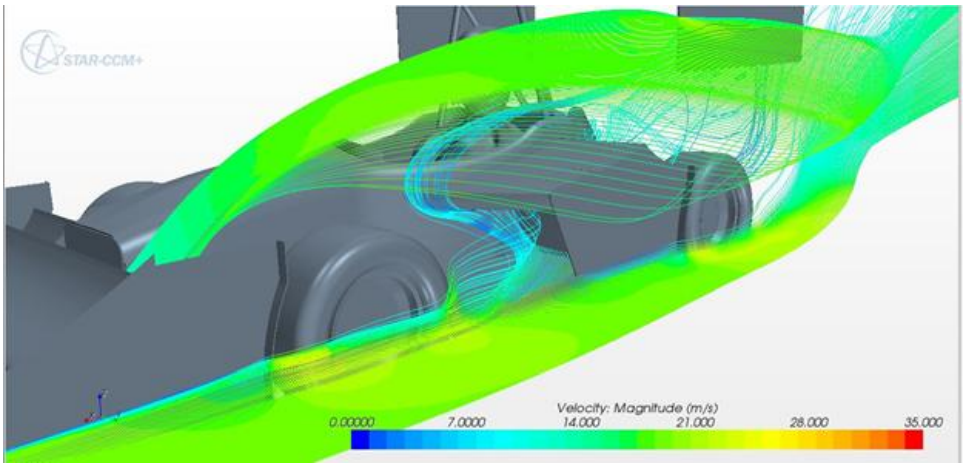

Figure 69: CFD streamline visualization (300 mm from floor) showing abundance of air entering side-pod inlet from around front tire.

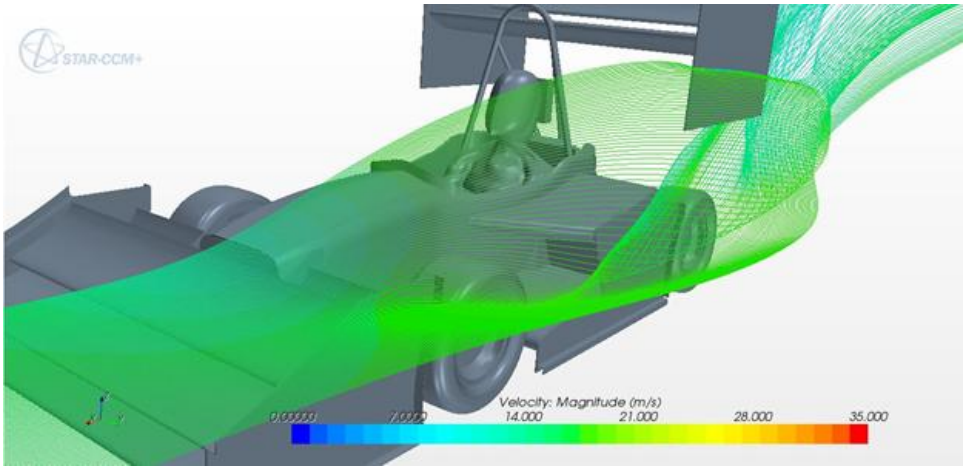

Figure 70: CFD streamline visualization (550 mm above ground) showing no air entering side-pod at this height.

Design Summary:

Table 19: Design summary of aerodynamic performance from CFD and projected weight calculations.

Side-Pod	201_J	2013	Delta (2013-2014)
Downforce	*-12 N*	*-30.6 N*	*+61%*
Drag	*-0.4 N*	*-0.2 N*	*+100%*
Mass Flow Rate	*.45 kg/sec*	*0.05 kg/sec*	*+800%*
Mass	*780 g*	*444.4 g*	*-75.6%*

Clearance Issues

One important design parameter that was taken into consideration during the side-pod design stage was the need for easy access to the fuel tank fill neck. This component exists on the left-hand side of the vehicle, and had to be accounted for on both side-pods in efforts to make symmetric parts. As seen in Figure 71 below, the side-pod is shortened to make sure there is access to the fuel tank fill neck during refueling. The image below is

of the right-hand side of the vehicle, however it can be seen that the side-pod is cut short of the triangular cutout in the chassis in order to maintain clearance from the fuel tank which is exposed on the left-hand side of the vehicle.

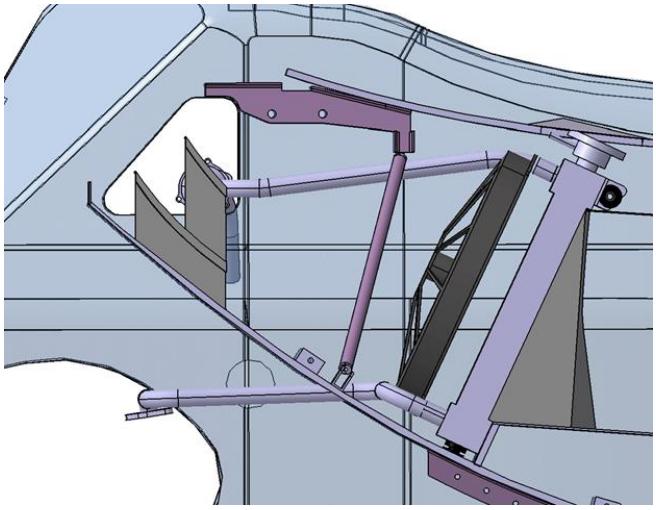

Figure 71: Side-pod top profile shorted to accommodate fuel tank fill neck on left-hand side (Right-hand side shown)

Endplate Design:

The endplate of this side-pod design incorporates the more slanted opening along the entrance of the side-pod to allow more outboard air to enter into the radiator. This endplate also includes a gurney slot and gurney flap on the outboard edges to aid in proper airflow and increased downforce. A CFD pressure plot of the gurney slot can be seen in Figure 72 below.

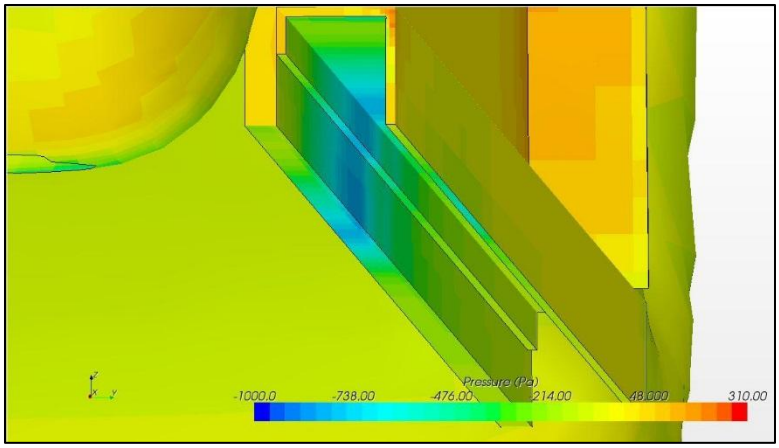

Figure 72: Pressure plot of the gurney slot on the outboard edge of the 2014 side-pod/undertray endplate.

The goal behind the design of the gurney slot is to prevent outside air from entering the low pressure regions under the undertray wing surface and disturbing the pressure gradient. If air is allowed to flow under this region, it limits the amount of downforce the undertray can achieve. This slot induces a region of local vortices that travel along the length of the channel. As noted by the light blue colored region, this is a low pressure zone in which a vortex has formed and escaped the slot, flowing into the area of the undertray. Unfortunately, this design does not provide adequate guiding of the vortices along the outboard edges as it theoretically should hold the vortices in the channel for a longer period. The air streamlines through the slot can be seen in the Figure 73.

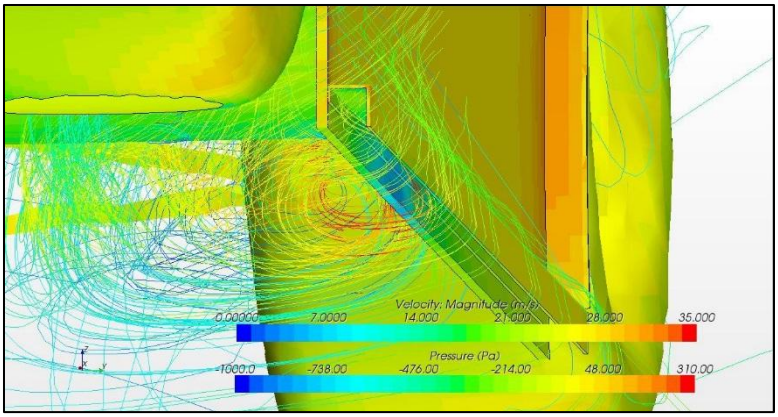

Figure 73: CFD streamline image of airflow through the endplate gurney slot.

As seen in the above image, the airstream continues down the channel until the vortices gains too much momentum and escapes the channel and into the undertray airflow. The low pressure region (blue), show a corresponding increase in airflow velocity (red) streamlines representing an increase in velocity during this low pressure region as is to be expected given the nature of aerodynamics [15]. This design does eliminate a large portion of the outside air from flowing beneath the undertray, although the image above strictly depicts the streamlines at the beginning of the channel. Without the slot, the endplate would not be able to deflect outboard air from entering this low pressure region.

Lastly, the gurney flap on the aft portion of the endplate is highlighted with a high pressure zone in Figure 74 below. This high pressure region creates additional downforce on the overall side-pod and undertray system.

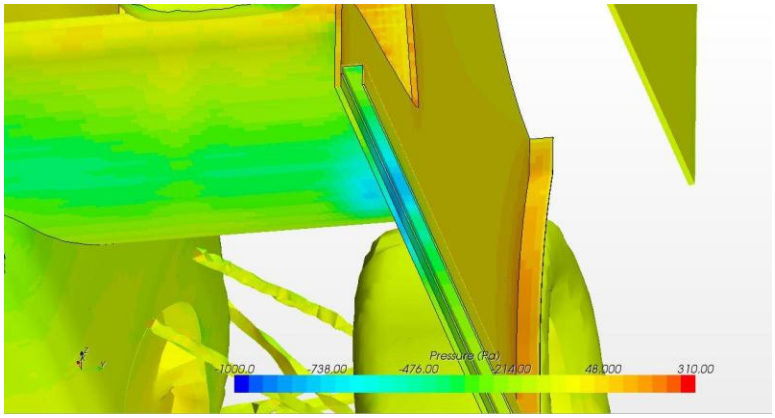

Figure 74: Pressure plot of the endplate gurney flap at the rear section.

As seen in the above image, the orange/red colors, as noted by the legend, represent high pressure zones, creating downforce.

Concept Summary:

Table 20: Concept summary of GFR_14_10_201_J

Design Assessment:	Final design candidate for 2014 side-pod and endplate shape/design. Provides significant improvements over 2013 design. Airflow drastically improved, as well as sufficient improvement in aerodynamic performance.
Reasoning:	As seen in Table 19 above, the aerodynamic performance is greatly improved along with projected mass flow for cooling abilities. Implements all components to be investigated as noted in 201_H concept summary. Although weight is increased in comparison to 2013, significant reductions will be made based on carbon fiber layup and core lattice patterns to be discussed section 4.3
Investigation:	Further investigation into other components to be integrated into the side-pod package, including front entry and exit ducting fins to improve airflow and aerodynamic performance.

Iteration Summary

The performances of the above concepts are outlined in Table A 3 and Table A 4, found in Appendix A. This table outlines each concept's individual mass additions, aerodynamic performance such as downforce and drag, and the contribution of each concept to competition points for full vehicle set-ups. Additionally, each concept's results are shown graphically in Figure 75: Downforce comparison of 2014 design concepts-Figure 78: Mass addition comparison of 2014 design concepts.

Graphical Results Comparison:

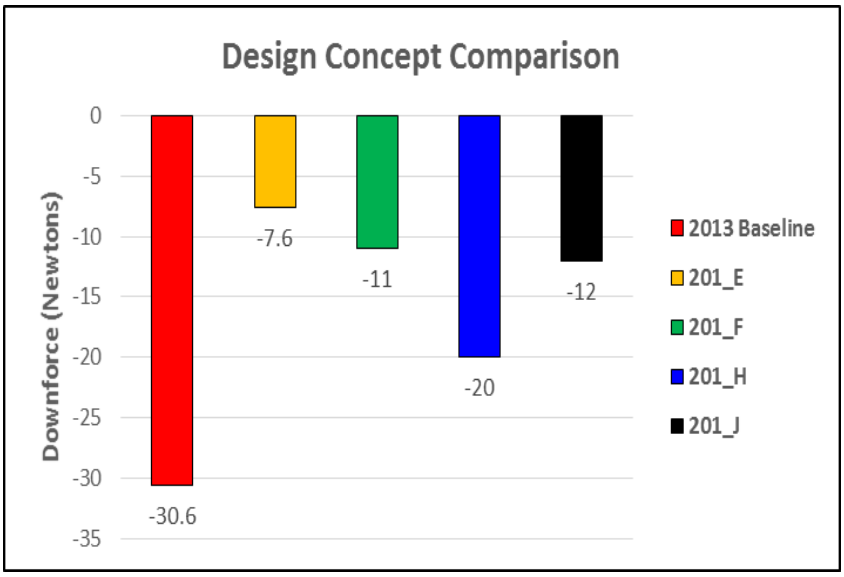

Figure 75: Downforce comparison of 2014 design concepts

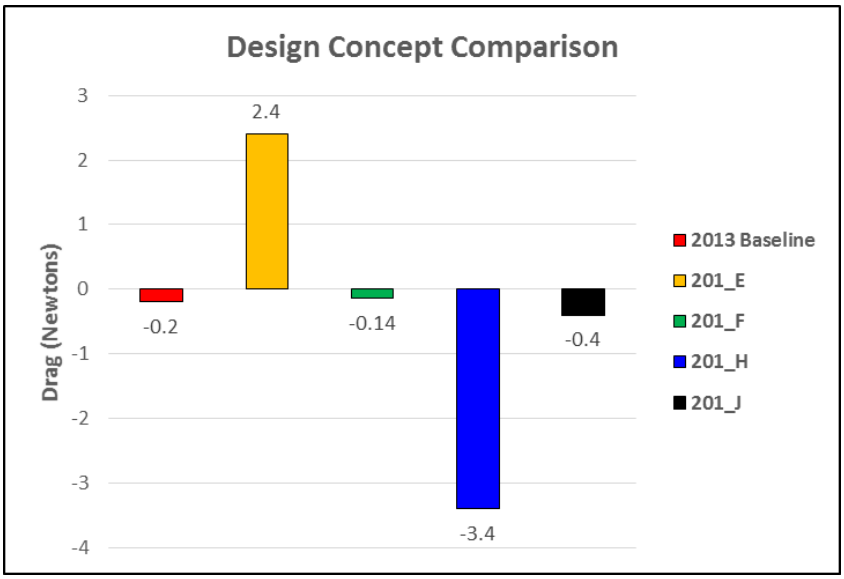

Figure 76: Drag comparison of 2014 design concepts

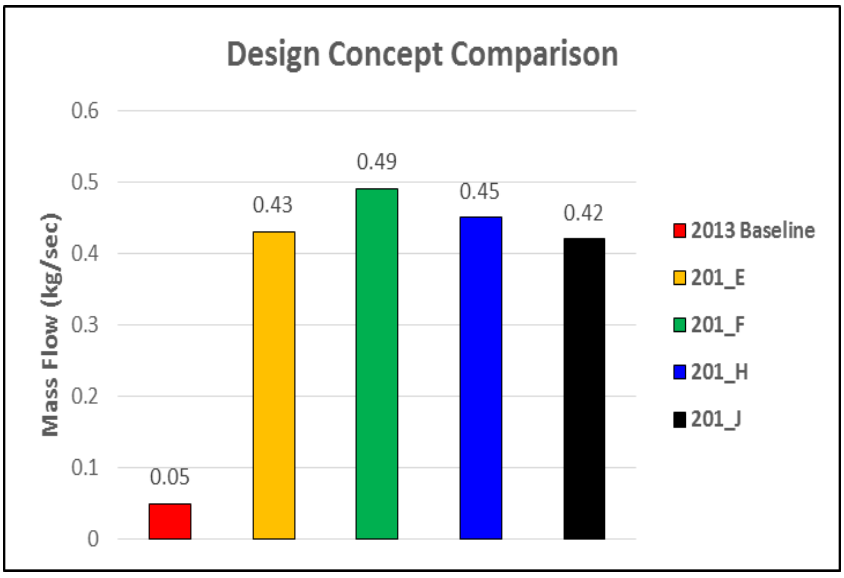

Figure 77: Mass flow rate comparison of 2014 design concepts

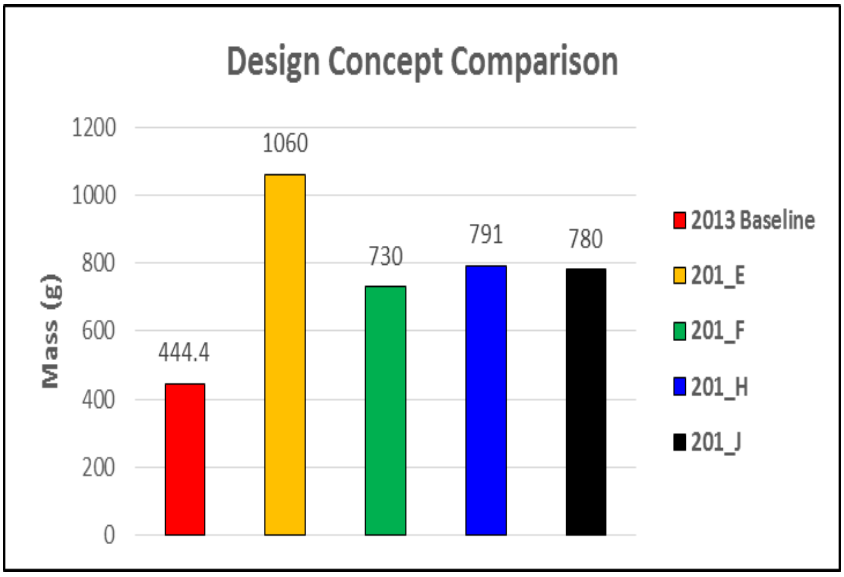

Figure 78: Mass addition comparison of 2014 design concepts

5.4 Internal Ducting Design

The next portion of the side-pod package was the internal ducting. The ducting system was intended to direct all incoming air to the core of the radiator components, and to help direct exiting airflow in the right direction to improve mass flow, improve downforce, and delay flow separation for reduced drag. The manufacturing goal for this ducting design was to eliminate the need for foam and tape pieces to be used as post-processing options. This current design is extremely inefficient and is difficult to maintain accurate repositioning after service.

This particular component will rely heavily on the shape of the side-pod to provide boundaries for the internal ducting. Initially, the design plan was to create a rather simple shaped duct, formed by simple layers of carbon over a removable foam mold for manufacturing. Ideally, this would be customized to fit and assembly easily and effectively to the side-pod housing. The general ideas that were considered were relatively simple cross-sectional designs with sides drafted at angles to accommodate for a small opening transitioning to a relatively large radiator section as seen in Figure 79 below.

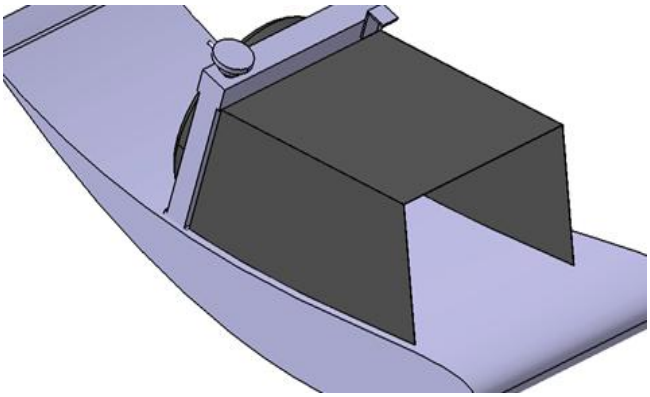

Figure 79: Initial cross-sectional style ducting concept.

This concept proved to be more than needed to properly duct the air into the entrance of the radiator core. This led to further designs outlined in the upcoming subsections.

5.4.1 Front Ducting

Only two concepts for the front ducting were considered due to the simplicity of the design requirements to provide adequate directional control of airflow to the radiators. Both concepts are very similar in design functionality, but differ in size leading to weight reductions with equivalent performance.

Front Ducting Concept #1

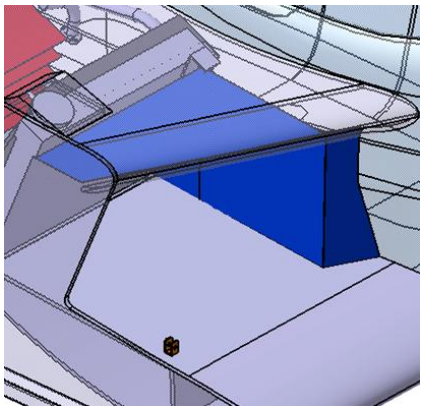

Figure 80: GFR 2014 front ducting concept #1 with extended side-wall

The above Figure 80 illustrates the first iteration of the front ducting that was considered for the 2014 side-pod design. This design utilized a rather large front entry piece running along the chassis line of the vehicle. The goal of this concept was to grab air from along the surface of the chassis and direct it into the side-pod channel. This utilized a three piece system, a top piece for sealing the internal portion of the side-pod and the radiator core, a flat side-panel that would allow for straight airflow into the radiator core at the correct mounted angle, and a third entrance piece that would seal off any air pockets from forming in between the flat side-panel and the chassis. This particular ducting added roughly 131 grams to the entire weight of the vehicle. This ducting was rather large for the simple function. The next and final iteration looked at simplifying the shape and reducing size and weight.

Front Ducting Concept #2

The final concept for the front ducting was designed to better seal off airflow from escaping around the sides and top of the radiator body in order to improve and direct more air through the core for cooling. This front ducting was constructed using the 3D contours of the chassis body for better sealant to eliminate air from flowing around the radiator body. This can be seen in Figure 81 and Figure 82. It also is designed to directly interface with the top profile of the side-pod, and utilize the leading edge as a place for consistent mounting.

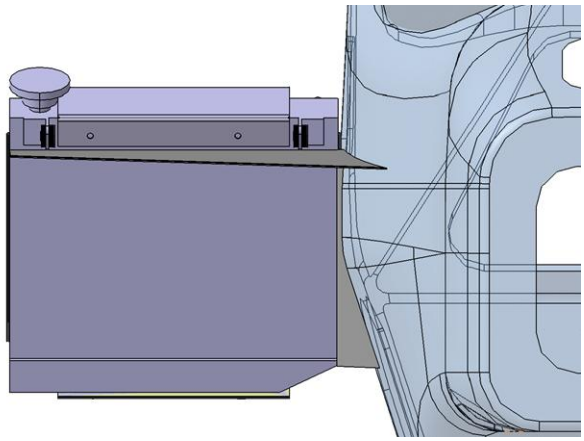

Figure 81: Front ducting interface with chassis contours to direct airflow through core.

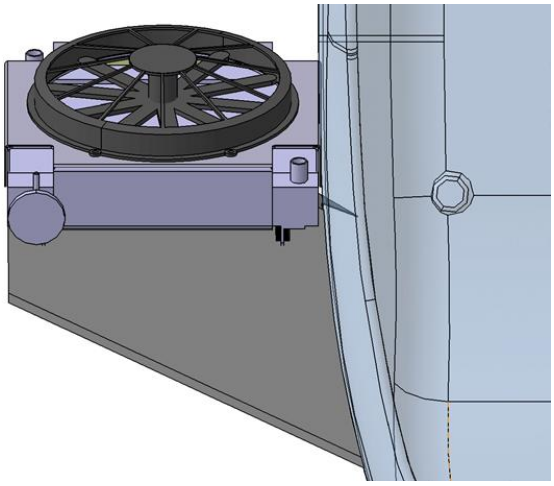

Figure 82: Front ducting showing use of chassis body to outline shape of ducting

The front ducting concept #2 shown in the above figures features a shortened side-wall piece that was significantly reduced from the original ducting of concept #1 as seen in Figure 83 below. The wall was shortened to reduce weight by 22%, while improving airflow.

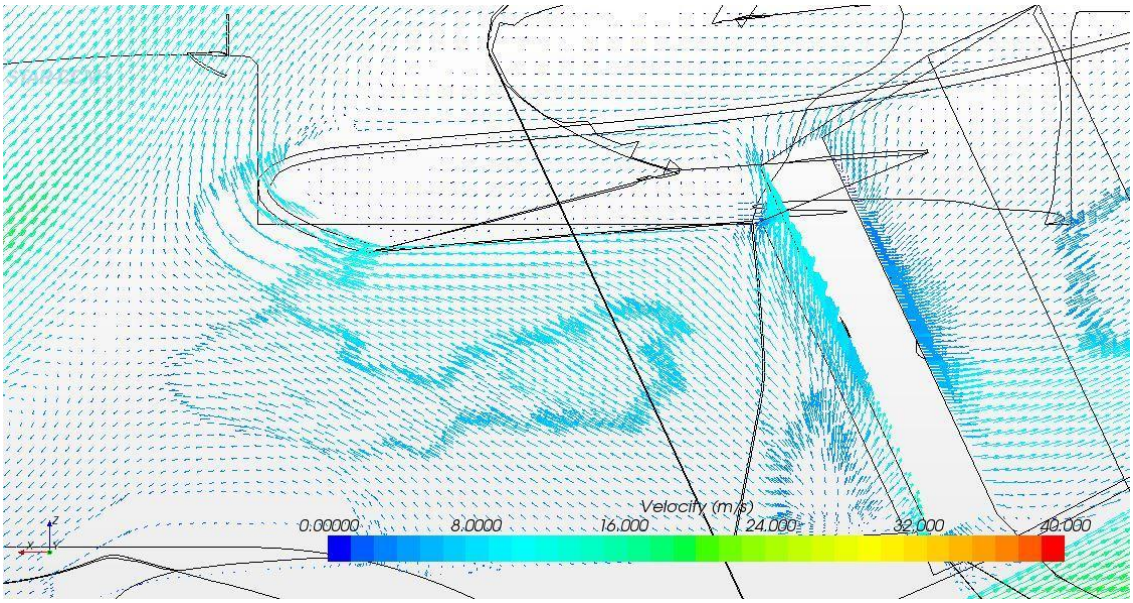

Figure 83: CFD simulation section of 2014 finalized front ducting at chassis line illustrating flow velocity through the side-pod and radiator.

In the above figure, the section top section of the image indicates the sealant of air around the chassis inboard face of the radiator. This shows the front ducting properly sealing the air from escaping around the top and sides of the radiator. The ducting protruding from the leading edge to the radiator helps to focus the majority of the airflow into the core. This ducting also helps to reduce any backflow up inside of the leading edge and around the top of the radiator, as seen by the minimal amount of flow vectors near the leading edge and top of the side-pod.

Front Ducting Concept Comparison and Competition Points:

The following Table 21 details the weight of the two front ducting concepts. This helped in finalizing the design by understanding how the design would affect competition points since this component's function is only to direct and seal airflow, thus minimizing mass was very important.

Table 21: Weight comparison for 2014 front ducting design concepts

	GFR 2014 Front Ducting: Concept 1	GFR 2014 Front Ducting: Concept 2
Surface Area (m^2)	0.1956	0.152
Weight (kg)	0.13107	0.10184
Total Vehicle Weight Addition (kg)	0.26214	0.20368

The benefits of front ducting are difficult to relate directly to competition points. The following table shows the added mass of the ducting to the whole vehicle and its relation to competition points. The addition of the front ducting is crucial to the success of the cooling capabilities of the vehicle but there is no way to directly relate those to competition points.

Table 22: Comparison of competition points for 2014 front ducting concepts

Vehicle Mass to Total Points	GFR 2014 Front Ducting: Concept 1	GFR 2014 Front Ducting: Concept 2
FSAE	-0.398	-0.310
FSUK	-0.398	-0.310
FSG/FSA	-0.477	-0.371
Average	-0.425	-0.330

As seen in the above table, Concept #2 provides the least reduction in competition points due to its decreased surface area, and corresponding reduction in weight. Both concepts weight were calculated using a 2-ply carbon-fiber lay-up schedule.

5.4.2 Rear Ducting

In the first design phase, only front ducting was considered to be a necessary addition. After external investigation into race car aerodynamic elements, rear ducting was investigated. With inspiration from the 2008 Audi A4 DTM (*Deutsche Tourenwagen Masters*, German Touring Car Masters) fender wings seen in Figure 84 and Figure 85 below, the GFR side-pod package incorporated wing-shaped ducts to be located in the exit region.

Figure 84: Audi A4 DTM fender-wing elements (Autoblog.com)

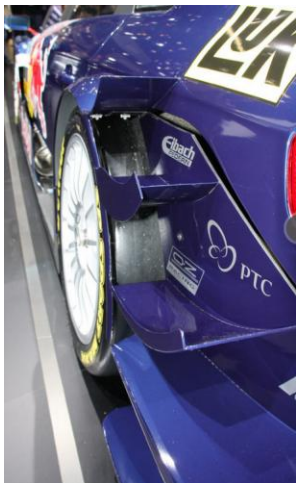

Figure 85: Audi A4 DTM fender wing element close-up

After further investigation, it was found that rear exit ducting could provide positive benefits to the downforce of the entire vehicle as well as the airflow through the side-pod and with positive downstream effects on airflow over the rear wing.

Initially, the rear ducting was designed to have five wing elements to direct the airflow upwards above the trailing edge of the undertray in efforts to help delay flow separation. Delaying flow separation would help reduce drag and effectively increase downforce. This concept is shown in Figure 86 below.

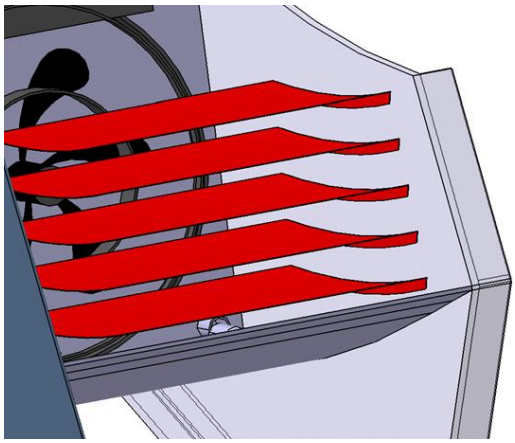

Figure 86: Initial design concept for rear ducting of side-pod

The concept in Figure 86 was designed with ease of assembly in mind. The five elements of the rear ducting attach directly to the endplate for simple removal with the endplate design. This allows for consistent placement in preparation for competition without having to deal with tape and foam, as done in previous years. This concept was discarded, due to large additions of unnecessary weight, and complexity without the projection of added benefits. With five elements, the angle of attack was not large enough to cause any major aerodynamic benefits. This led to simpler designs which implemented fewer wing-style elements. This led to multiple iterations with two or three elements in which the angle of attack was varied.

Rear Ducting Concept #1

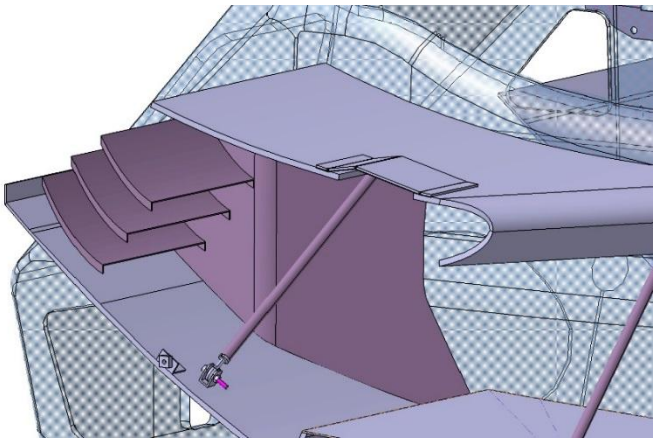

Figure 87: Concept # 1 showing three element style of ducting with fuel neck shield.

This particular concept was designed using a three element design, and a fuel neck shield. With this shield, the goal for this concept was to direct the air from the exit of radiator, without any interference from the cooling lines, fuel neck cap and other components in the rear of the side-pod. The idea was also to effectively “reduce” the

outlet area in an attempt to further accelerate the flow through the side-pod. This particular concept did not prove to be beneficial to the design of the car, as it restricted air flow, and created lift. The results of this design concept are shown in

Table 23 below.

Table 23: Effect on Aerodynamic and Airflow Performance of 2014 Side-Pod

Rear Ducting: Concept #1	**2014**
# of Elements	3 (plus shield)
Angle of Attack (AOA)	49°
Downforce (Side-Pod)	-21 N
Drag (Side-Pod)	-2.5 N
Mass Flow (Side-Pod)	.422 kg/sec

This concept was not beneficial to the performance of the side-pod design. This led to a new design which eliminated the shield and investigated the use of only two elements.

Rear Ducting Concept #2:

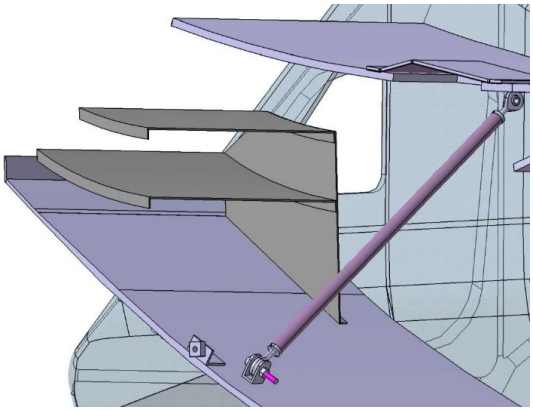

Figure 88: Concept #2 with low angle of attack and large separation between undertray surfaces

The second concept focused on the development of a two element design. This particular design incorporated a lower angle of attack, with large separation from the undertray surface. This was raised in an attempt to reduce the potential for restricted airflow over the top surface of the undertray. A restriction would lead to an increase in pressure, and would create a pressure gradient that promotes lift, with low pressure on the top of the elements, and high pressure on the bottom surfaces. This pressure gradient would induce lift rather than downforce [15]. This did not prove to be the case. The results are seen in Table 24.

Table 24: Effect on Aerodynamic and Airflow Performance of 2014 Side-Pod

Rear Ducting: Concept #2	**2014**
# of Elements	2
Angle of Attack (AOA)	20°
Down Force	-12 N
Drag	-1.06 N

Mass Flow	.43 kg/sec

This design shows no improvement in downforce performance in CFD simulations, and it restricted airflow through the side-pod as seen by the reduction in mass flow rate from .45 to .43 kilograms per second. This led to an increase in angle of attack and separation distance in the next iteration.

Rear Ducting Concept #3

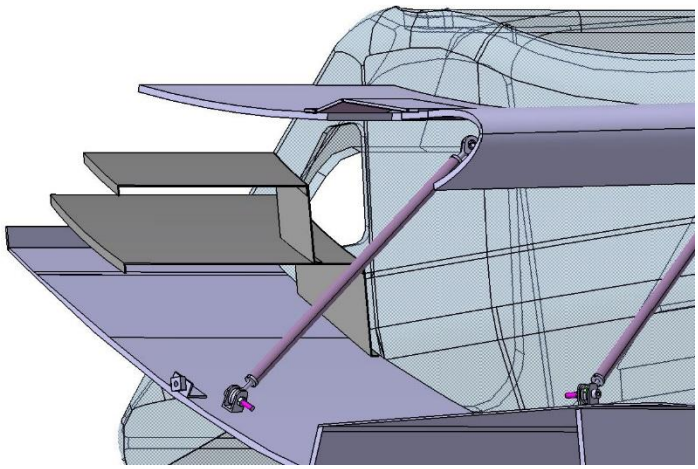

Figure 89: Concept #3 with larger angle of attack and offset top element.

The third iteration of the ducting was slightly enhanced from the previous designs in that the spacing between the undertray and bottom element was the same as that between the top and bottom element of the ducting. This concept maintained a larger angle of attack, and an offset design of the top element to account for interferences between the fuel neck. With an increase in angle of attack and equal spacing, the initial

prediction was that downforce may increase slightly. This also, was incorrect. The results are seen in Table 25.

Table 25: Effect on Aerodynamic and Airflow Performance of 2014 Side-Pod

Rear Ducting: Concept #3	**2014**
# of Elements	2 (top element offset)
Angle of Attack (AOA)	40°
Down Force	-12.1 N
Drag	-0.011 N
Mass Flow	0.438 kg/sec

This concept also proved to be a hindrance on the performance of the 2014 side-pod. The lift created by this ducting actually reduced the performance of the side-pod slightly, while also reducing the mass flow rate through the radiator. This led to the final design concept in which an even larger angle of attack was implemented.

Rear Ducting Concept #4

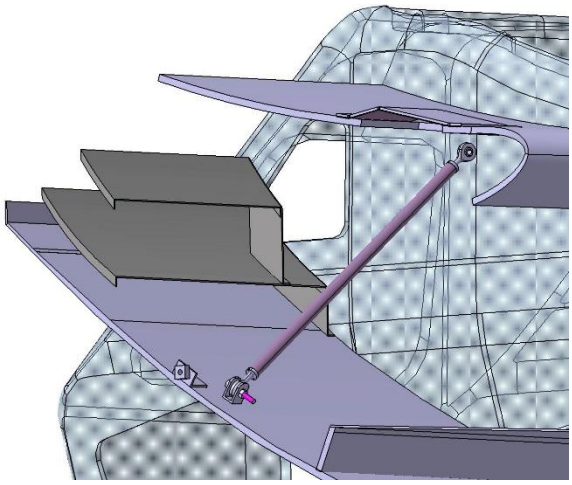

Figure 90: Concept #4 with larger angle of attack and top element offset.

This final concept combined all of the iterations above and found the compromise of each. The angle of attack for this design was increased from 40° to 45°, but reduced form the initial 3 element concept (Concept #1) which was mounted at 49°. This particular concept improved the performance of the side-pod the most, and was a design worth implementing. The results are shown in Table 26 below.

Table 26: Effect on Aerodynamic and Airflow Performance of 2014 Side-Pod

Rear Ducting: Preliminary Concept	**2014**
# of Elements	2 (top element offset)
Angle of Attack (AOA)	45 degrees
Downforce (Side-Pod)	-10.4 N
Drag	-0.08 N
Mass Flow	0.465 kg/sec

This design proved to be the most beneficial of the rear ducting concepts considered above. The rear ducting decreased lift by 0.5 N, and increased airflow by approximately 0.015 kilograms per second (30% of 2013 total mass flow rate). Not only did this ducting improve the side-pod performance, it also had the greatest effect on total downforce and drag of the car due to the nature of the fluid separation being delayed, and an acceleration of airflow on the underside of the undertray and rear wing, leading to a higher pressure gradient experienced by both elements.

Rear Ducting Summary

The design progression between the concepts for the rear ducting can be seen in Figure 91 and the comparison of downforce values of undertray and rear wing can be seen in Table 27 below.

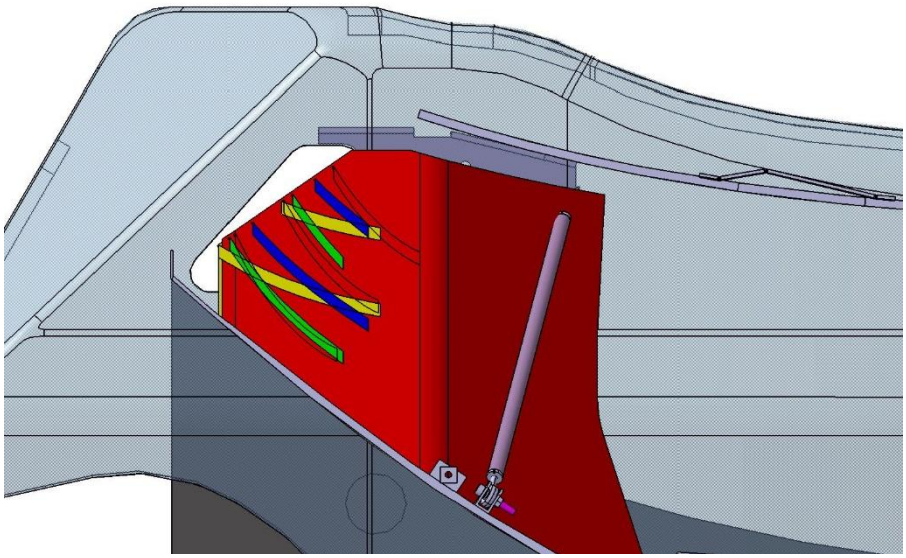

Figure 91: Rear ducting progression: Concept #1 (Red), Concept #2 (Yellow), Concept #3 (Blue), Concept #4 (Green).

Table 27: Rear Ducting Effect on Undertray and Rear Wing Downforce Values

Rear Ducting - Downforce Effects	***Undertray***	***Rear Wing***
Concept #1 (Red)	208 N	424.4 N
Concept #2 (Yellow)	211 N	430 N
Concept #3 (Blue)	208.5 N	424 N
Concept #4 (Green)	223.4 N	433 N

This data shows that even though the angle of attack and spacing adjustments between designs were very minimal, the changes had a very drastic effect on the other aerodynamic components of the vehicle such as rear wing and undertray. This is largely due to flow separation and changes in the direction of the airflow caused by the rear ducting undertray trailing edge flap. This separation can be seen in the CFD airflow vector image shown below.

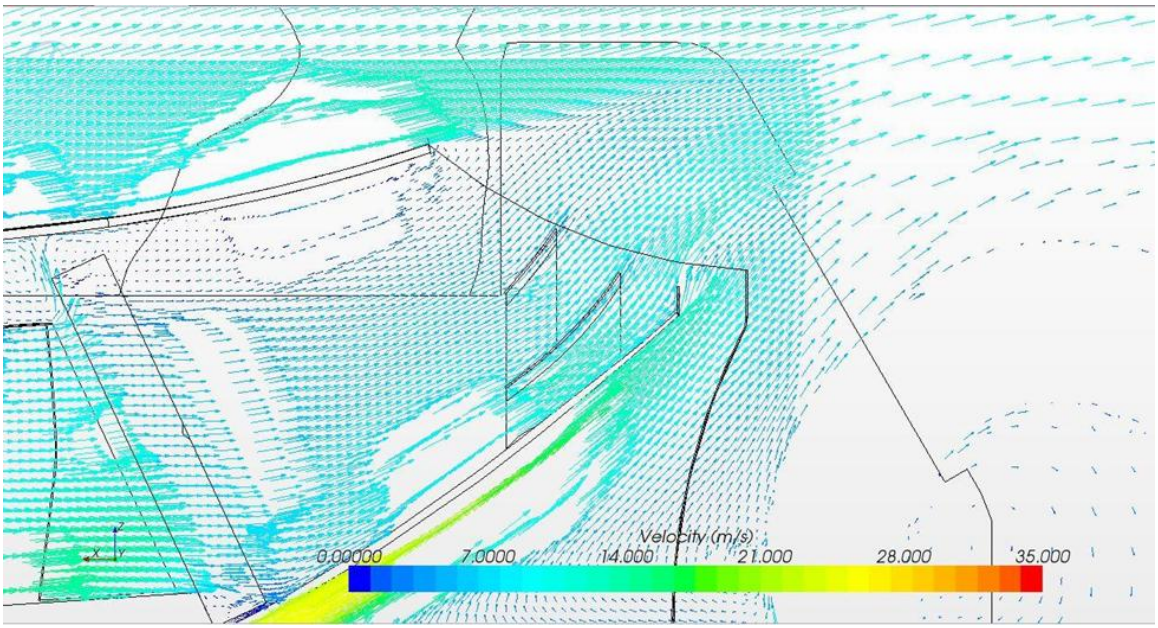

Figure 92: CFD vector scene illustrating velocity vectors and flow over the rear ducting and trailing edge gurney flap.

As seen in the CFD image above, the flow over the top of the side-pod is redirected to a sharper upward angle with the help of the rear ducting. The trailing edge gurney flap also redirects a lot of the flow and helps add to the downforce created by the undertray. The trailing edge gurney flap can be seen in Figure 93.

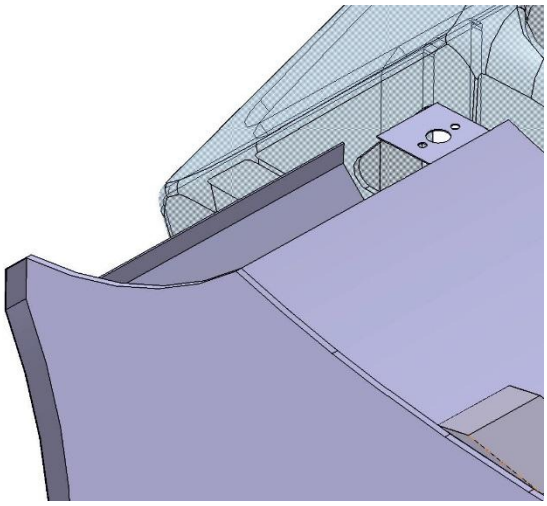

Figure 93: Trailing edge gurney flap addition to the 2014 undertray design.

A pressure plot from Star-CCM+ of the rear ducting is shown in Figure 94 and Figure 95.

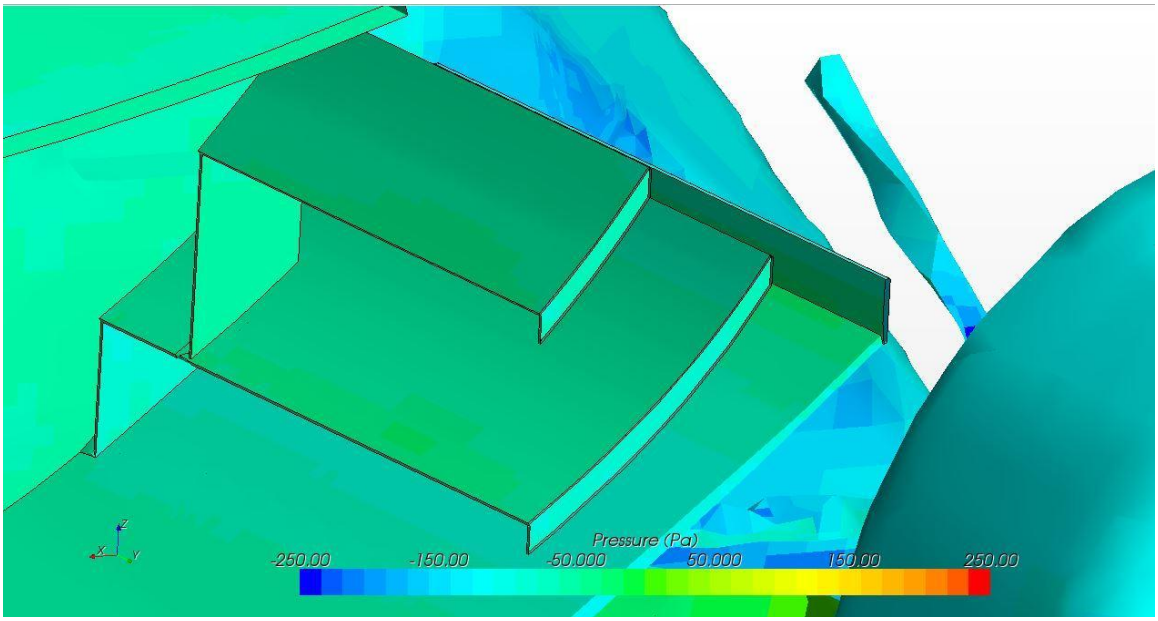

Figure 94: Pressure plot of upper surface of wing elements of rear ducting

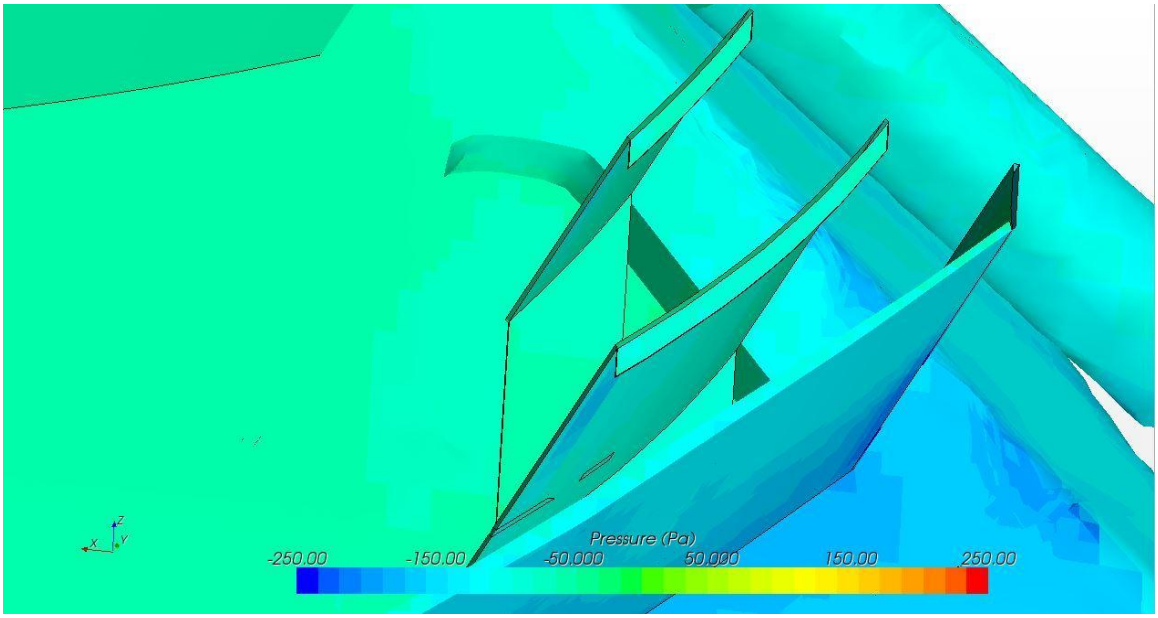

Figure 95: Pressure plot of lower surface of wing elements of rear ducting

From observation of the two images above, it is clear that there is a small but distinguishable pressure differential between the top and bottom surfaces of the rear ducting. The difference is visible in the color scheme of the pressure plot. The higher pressure zones on the top surface (green) and lower pressure zone on the bottom (blue) are indicative of higher velocity air on the bottom, also seen by the cluster of velocity vectors in Figure 92. This shows that the rear ducting is in fact contributing to the downforce created by the side-pod and undertray system, as well as increasing the mass flow through the side-pod channel. The addition of the undertray trailing edge flap also led to a pressure gradient as noted by the lower pressure region (blue) on the flap in Figure 96 below.

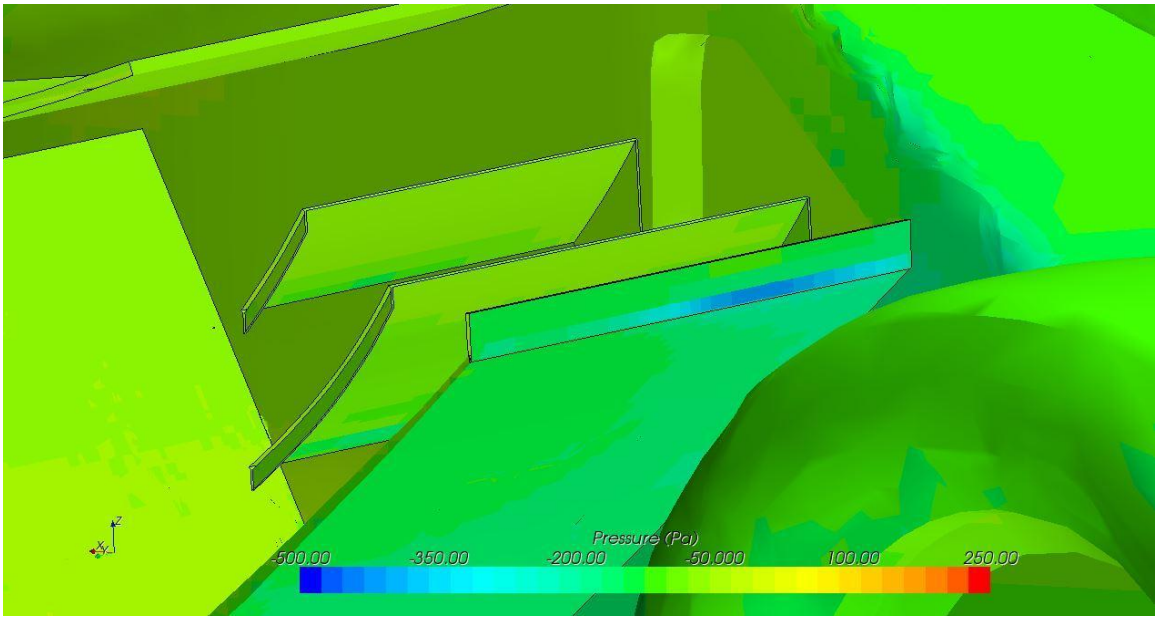

Figure 96: Pressure plot of gurney flap

The high pressure region in of the trailing edge flap seen in the ducting image of Figure 94 above, and the low pressure zone created on the reverse side of the gurney flap, shown in Figure 96, illustrate an important pressure gradient that causes additional downforce.

Weight Addition and Competition Points:

The following tables outline the weight of the final rear ducting design and its effect on the competition points of the GFR 2014 vehicle.

Table 28: Weight parameters of final ducting design

	GFR 2014 Rear Ducting: Final Design
Surface Area (m^2)	0.138
Weight (kg)	0.13869
Total Vehicle Weight Addition (kg)	0.27738

Table 29: Effect of rear ducting on competition points gained

Vehicle Mass to Total Points	GFR 2014 Rear Ducting: Final Design
FSAE	-0.422
FSUK	-0.422
FSG/FSA	-0.505
Average	-0.449

5.5 Final Side-Pod System Aerodynamic Performance Analysis

In Section 5.2, CFD simulation streamline images showed the availability of air from the outboard regions of the vehicle. As noticed by the streamlines coming off of the large front wing element, the air from above bypasses the side-pod inlet. The majority of the air at these heights around 200-550 mm above ground (Figure 68 and Figure 69), flow around the externals of the tire and into the side-pod inlet. There also exists a limit, approximately 550 mm above ground (Figure 70) where no air enters the side-pod. This led to the design change of the side-pod to include a slanted inlet to allow for capture of this airflow from around the front tires. This significantly improved cooling capabilities, as well as downforce. Through analysis into the aerodynamics of the final design were scrutinized carefully using various scalar, vector, and streamline scenes in Star-CCM+. These scenes are seen and discussed next.

5.5.1 Airflow Velocity Vectors

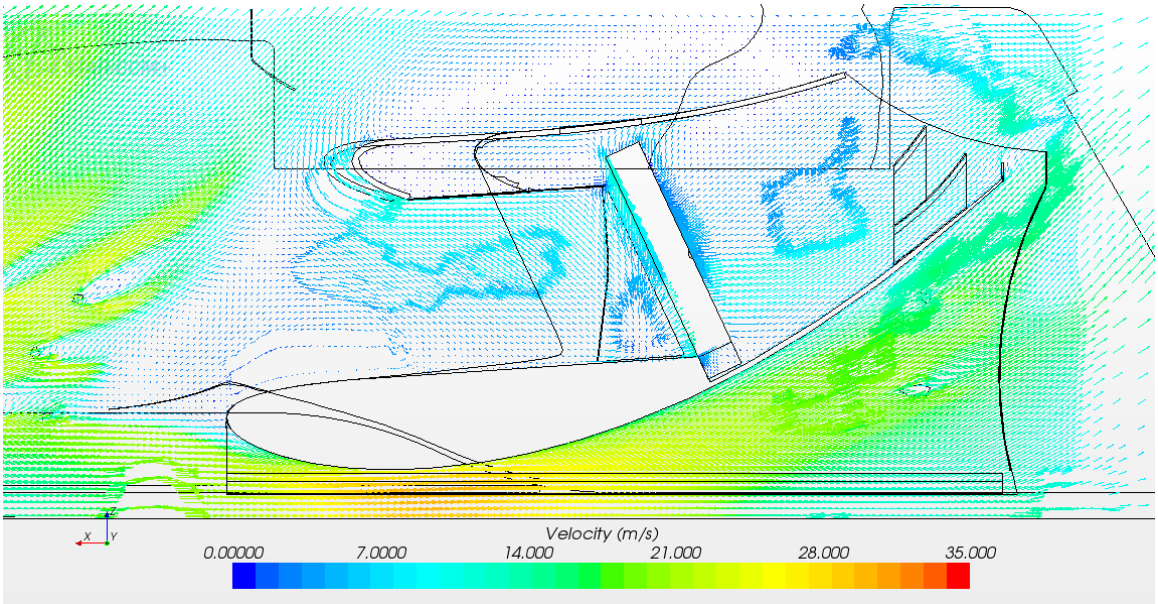

Figure 97: CFD simulation section at chassis tangent line of flow velocity through final 2014 side-pod design.

In Figure 97 above, it is seen that very low speed airflow (blue region) occurs near the chassis line of the vehicle in front of the radiator. This is what is to be expected giving the proper front ducting design preventing the airflow from escaping along the chassis line. At this point, the air is further directed into the radiator core rather than allowing air to flow around the sides and top. It is also observed that there is a small amount of air escaping out of the inlet of the side-pod at this point, as seen in Figure 98 below.

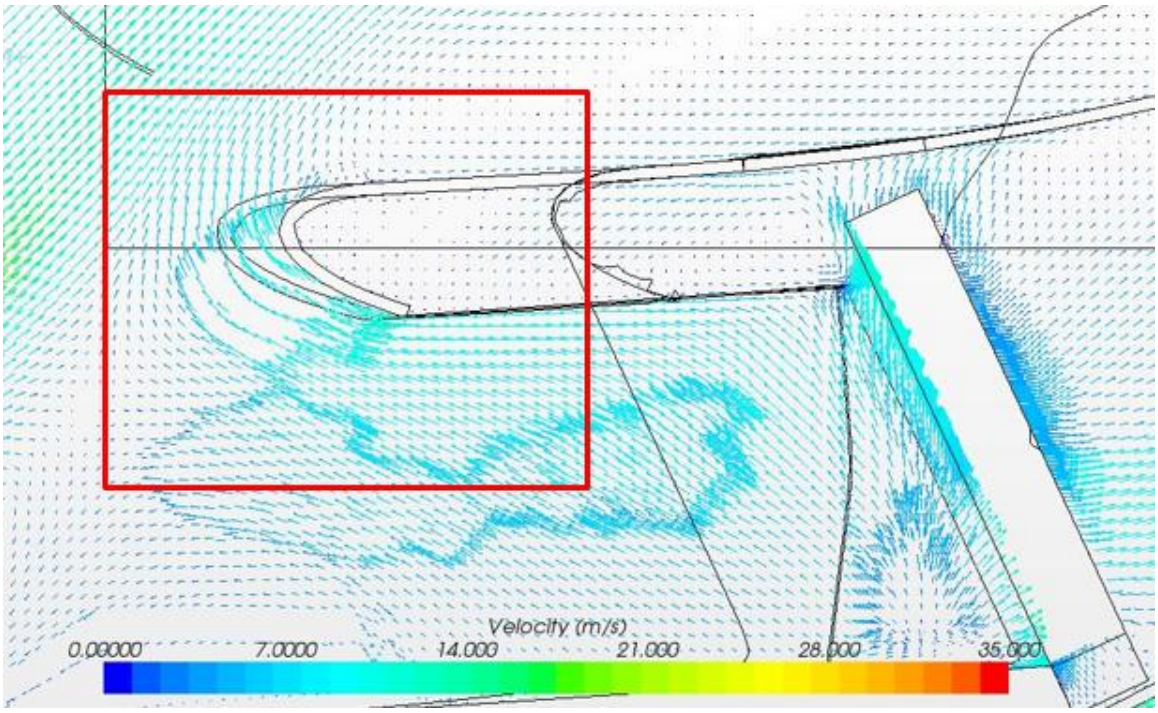

Figure 98: Noted regions of zero air from ducting and air escaping out of the inlet

The next portion of the side-pod to analyze was the middle of the system at the center of the radiator core. This can be seen in Figure 99.

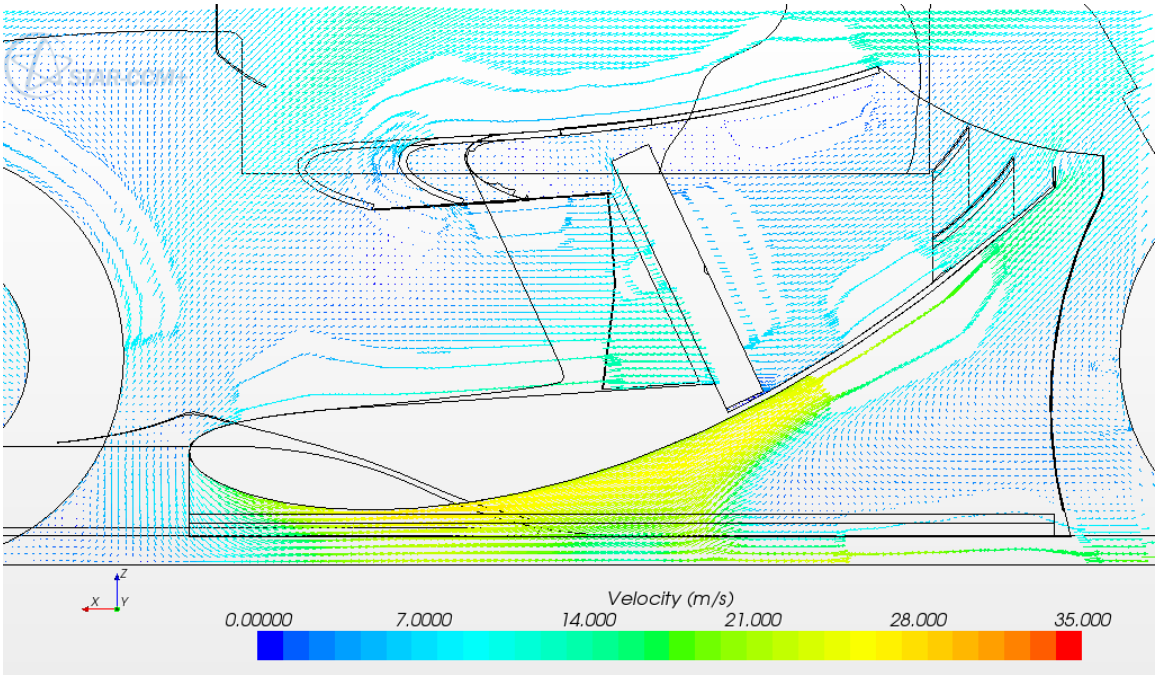

Figure 99: CFD simulation section at radiator mid-line of flow velocity through final 2014 side-pod design.

In Figure 99 above, this section is split by an x-z plane through the middle of the radiator. This allows for visualization of the airflow through the central core of the radiator. Here it can be seen that the flow is accelerated through opening of the side-pod and then slows as it enters through the core of the radiator and out the exit. This can be noted by the color gradient scale below the vector scene. It also begins to increase in velocity as it reaches the rear ducting and out over the trailing edge flap of the undertray.

The next step was to look at the airflow at the side-pod endplate interface. This is shown in Figure 100.

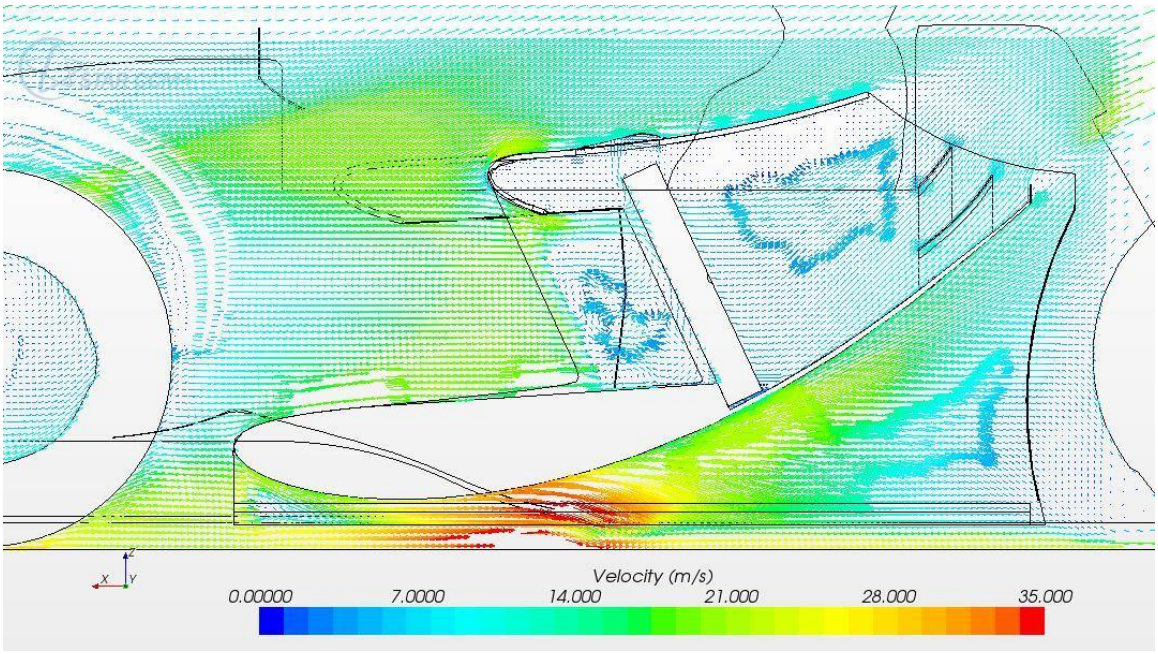

Figure 100: CFD simulation section at side-pod/endplate interface of flow velocity through final 2014 side-pod design.

Lastly, the above figure shows a plane parallel to the y-axis direction at the interface of the side-pod top profile and the endplate. At this location, the air velocity has increased significantly at the inlet of the ducting. This is largely due to the outboard airflow as shown by the streamline figures. The air is moving at large velocities and is slowed by the core of the radiator as to be expected after acceleration to the entrance of the core as shown by Figure 99 at the radiator midline. The flow also is seen to accelerate at the end of the trailing edge gurney flap of the undertray. These CFD images help provide a good understanding of the velocities and flow behaviors of the air within and outside of the side-pod. This helped to verify that the final design is contributing to the aerodynamic performance of the entire vehicle more so than the previously discussed concepts.

5.5.2 Scalar Scenes

5.5.2.1 Radiator Pressure Plot

Due to the nature of the side-pod there are some tradeoffs between aerodynamics performance and mass flow of air through the cooling system. In order to increase the downforce of the side-pod, there must be higher pressure on the top of the side-pod, and lower pressure on the inside. The tradeoff comes with the need for increased mass flow rate. As mentioned before, mass flow rate increases with increasing pressure gradient from in front of the radiator to the exit of the radiator. With a desire for increased pressure in front of the radiator, this creates a high pressure region on the inside of the side-pod profile. This creates lift on the side-pod rather than the desired downforce [13]. The final design to be used for 2014 manages to provide adequate results for both of these major customer requirements. A pressure plot of the front and rear of the radiator from CFD simulations of the final configuration is shown below.

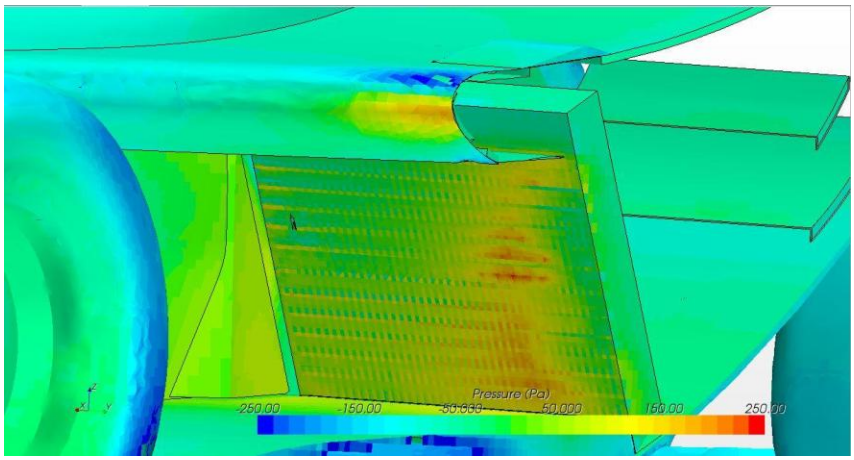

Figure 101: Pressure plot of front radiator core within 2014 final design configuration.

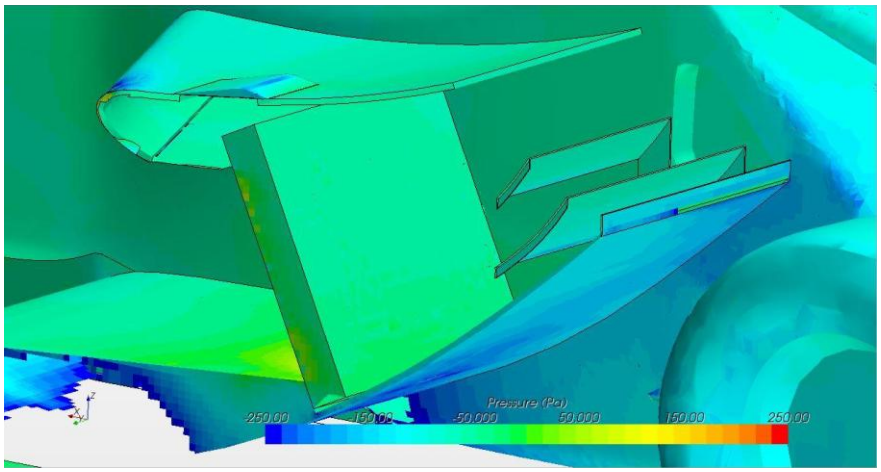

Figure 102: Pressure plot of the rear radiator core within the 2014 final design configuration

The above pressure distribution seen from the front and rear images of the radiator core, illustrate that a pressure drop certainly occurs across this radiator in CFD simulations. This aspect is important due to the nature of radiators and increased heat exchange. The pressure gradient on the front of the radiator core also illustrates that airflow coming from the outboard edges as seen in Section 5.2, creates the highest pressure at the outboard edge of the radiator.

In terms of the CFD accuracy of this radiator model, this is significant in calculating the mass flow rate through the side-pod as it must be able to take into account the porosity and restriction of airflow through the radiator core. This pressure gradient would not be present in the simulation results if the settings were changed to model the radiator as a "measuring volume" with dimensions, rather than a solid body with porosity.

5.5.2.2 Side-Pod System Pressure Plot

Another important tool for analyzing the design of a side-pod on a formula style race-car is to view the pressure plots over the entire system. This tool is unique in the fact that it is much easier to identify changes in pressure over the entire system rather than small velocity vectors that are difficult to see and understand. This sub-section identifies some of these key pressure locations in describing the performance of the side-pod package.

Figure 103 shows a pressure plot from -250 to +250 Pascals of pressure over the entire system. This allows for ease of visualization in identifying key regions where side-pod performance aspects are developed. This plot shows a region of a small amount of low pressure on the top surface of the side-pod. This is to be expected given the small amount of lift known to be created by the side-pod. This image also shows a frontward angle of the pressure gradient across the front face of the radiator core.

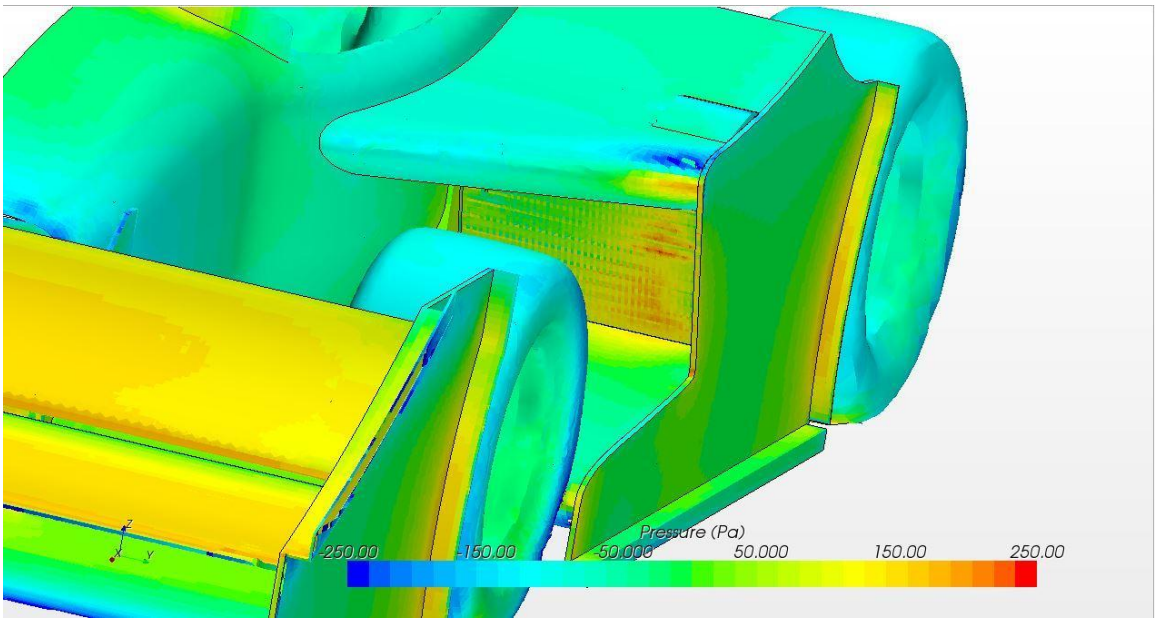

Figure 103: Pressure plot of the selected final side-pod system.

Figure 103 helps to identify key characteristics of the airflow over and around the side-pod system. With this angle of slant of the side-pod profile and opening, this "swept-back" wing style side-pod would most likely produce vortices that travel along the leading edge. Due to this angle, the vortices spin along the leading edge to the lowest point, which in this case occurs at the endplate interface. At this point, the vortices spin off the leading edge and off into the outboard air. At this point, the velocity is much larger than the surroundings, leading to a decrease in pressure locally. This is seen in Figure 104 as the dark blue region at the furthest outboard point on the leading edge. Also note the airflow at the chassis line directly in front of the side-pod/chassis interface shows a change from high to low pressure. This illustrates an increase in velocity, or acceleration of flow over the top of the surface of the side-pod. This also helps to identify why the side-pod is creating a small amount of lift.

Figure 103 also shows a high pressure region on the front wing of the vehicle, representing a large amount of downforce experienced by the front wing of the car. The tires are also highlighted by a low pressure region, much like the side-pod, due to the fast rotation of wheels increasing the velocity of the air and decreasing the pressure. A lot of this disturbed air is captured by the side-pod, one of the main downsides to low radiator mounting positions [21]. Figure 104 shows a pressure plot shown from higher above the vehicle.

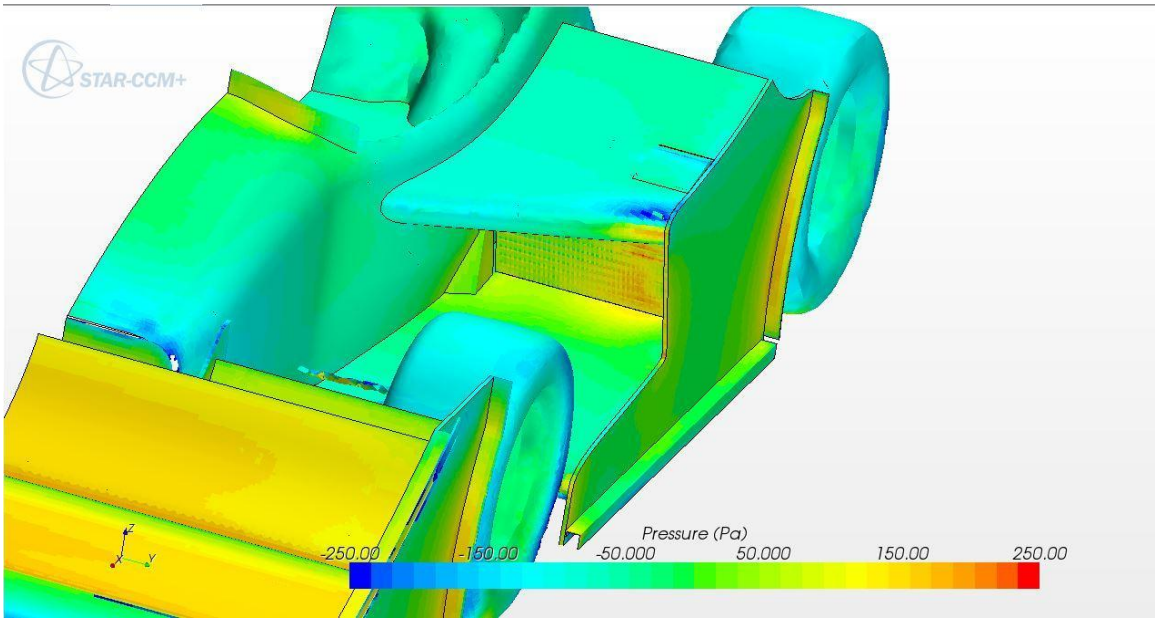

Figure 104: Pressure plot of the side-pod system.

The angle of this pressure plot helps to further visualize the pressure gradient across the top surface of the undertray leading up to the radiator core. Notice also the high pressure zone experienced by the front ducting, also leading to a conclusion that the front ducting is doing a sufficient job at sealing the air from flowing around the radiator. The gurney flap also shows a region of high pressure leading to an increase in downforce

from airflow along the side of the endplate. Lastly, Figure 105 shows the pressure distribution across the endplate, including the previously mentioned gurney flap high pressure region at the rear.

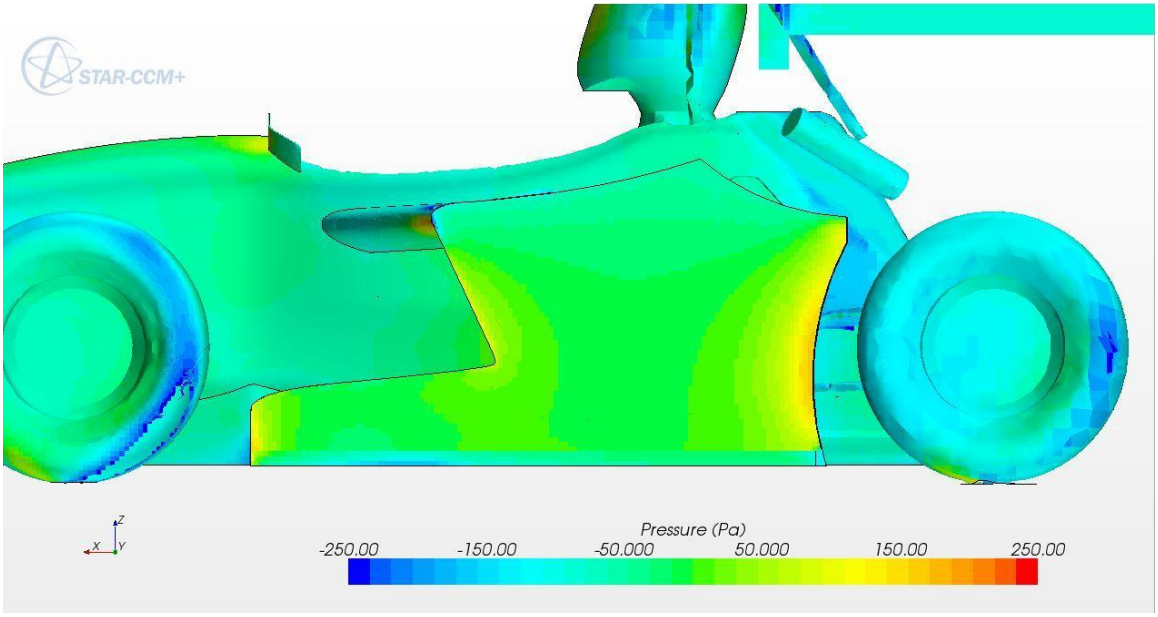

Figure 105: Pressure plot of side-pod/endplate.

All of the above pressure plots help to illustrate different aspects of the aerodynamic performance of the side-pod system in helping to further analyze and evaluate the effectiveness of the design.

5.5.3 Yaw Conditions

During the majority of its time on the race-track, the Formula SAE vehicle spends most of its time travelling around corners and turns. With this, the car spends a large amount of time in a yawed position. The majority of the CFD simulation and testing done

during the design of the 2014 side-pod was done by analyzing the straight line motion of the vehicle to determine its performance. Although the Global Formula Racing Aerodynamics team has limited knowledge about properly running CFD simulations in a yawed condition, the following section will cover some brief analysis of the performance of the side-pod in a yawed condition. The following figures demonstrate the positioning of the vehicle through cornering conditions.

5.5.3.1 Yaw Simulation:

5 Degree Corner Turn / 12 Degree Wheel Angle / 2G Lateral Acceleration

This particular yaw condition represents cornering at a 5 degree angle, with the front wheels turned 12 degrees, representative of an over-steering condition.

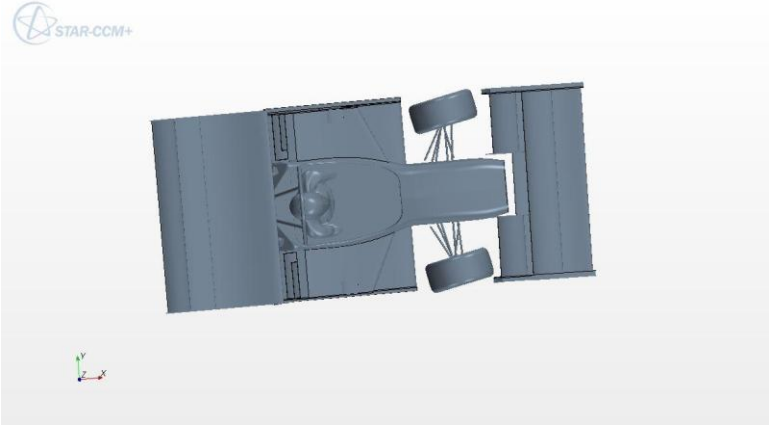

Figure 106: Top view of the yaw condition of the 2014 side-pod package. 5 degree corner turn with 12 degree wheel angle at 2-G of lateral acceleration.

Figure 107: Front view of the yaw condition of the 2014 side-pod package. 5 degree corner turn with 12 degree wheel angle at 2-G of lateral acceleration.

5.5.3.2 Yaw Simulation:

45 Degree Corner Turn / 30 Degree Wheel Angle / 1G Lateral Acceleration

This particular yaw condition represents cornering at 45 degrees, with the front wheels turned 30 degrees, representative a loss of grip and corrective steering scenario.

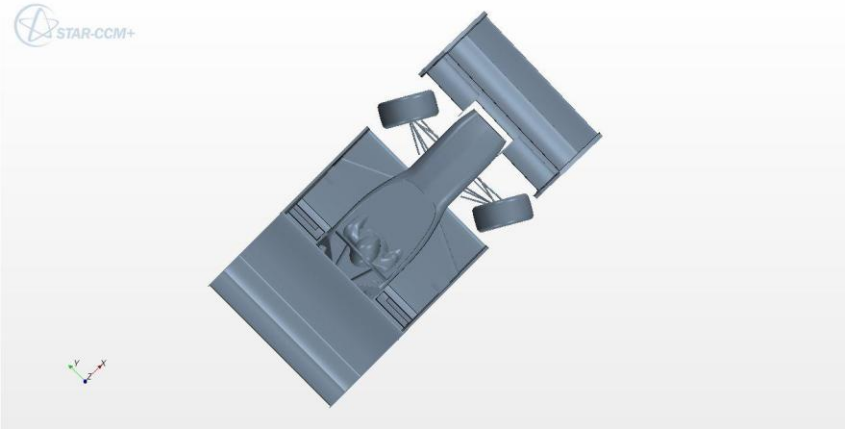

Figure 108: Top view of the yaw condition of the 2014 side-pod package. 45 degree corner turn with 30 degree wheel angle at 1-G of lateral acceleration.

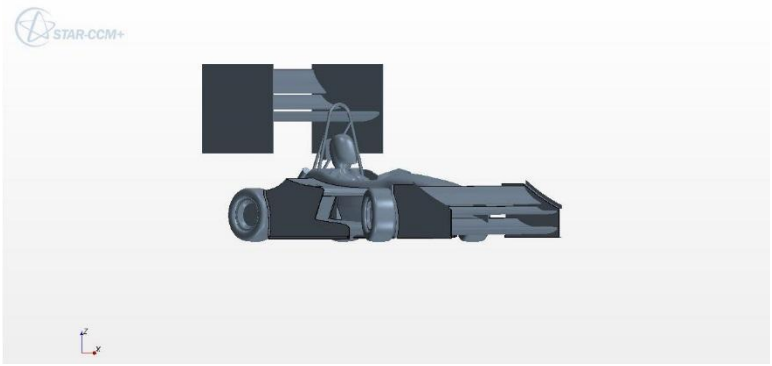

Figure 109: Front view of the yaw condition of the 2014 side-pod package. 45 degree corner turn with 30 degree wheel angle at 1-G of lateral acceleration.

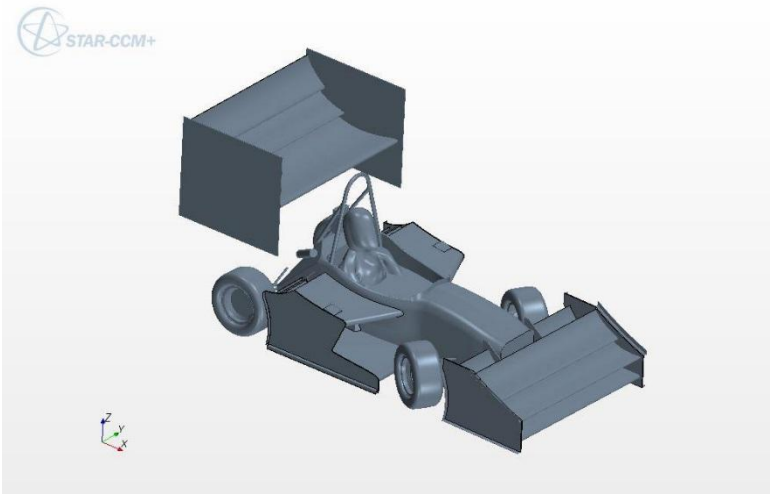

Figure 110: Isometric view of the yaw condition of the 2014 side-pod package. 45 degree corner turn with 30 degree wheel angle at 1-G of lateral acceleration.

5.5.4 Side-Pod Airflow Streamlines - Yaw Conditions

The following sub-section provides visual images into the conditions of airflow in a yawed condition during Endurance and Autocross type races. These streamline images are broken up into two different cornering and steering angle configurations.

5.5.4.1 Yaw Simulation:

5 Degree Corner Turn/ 12 Degree Wheel Angle / 2G Lateral Acceleration

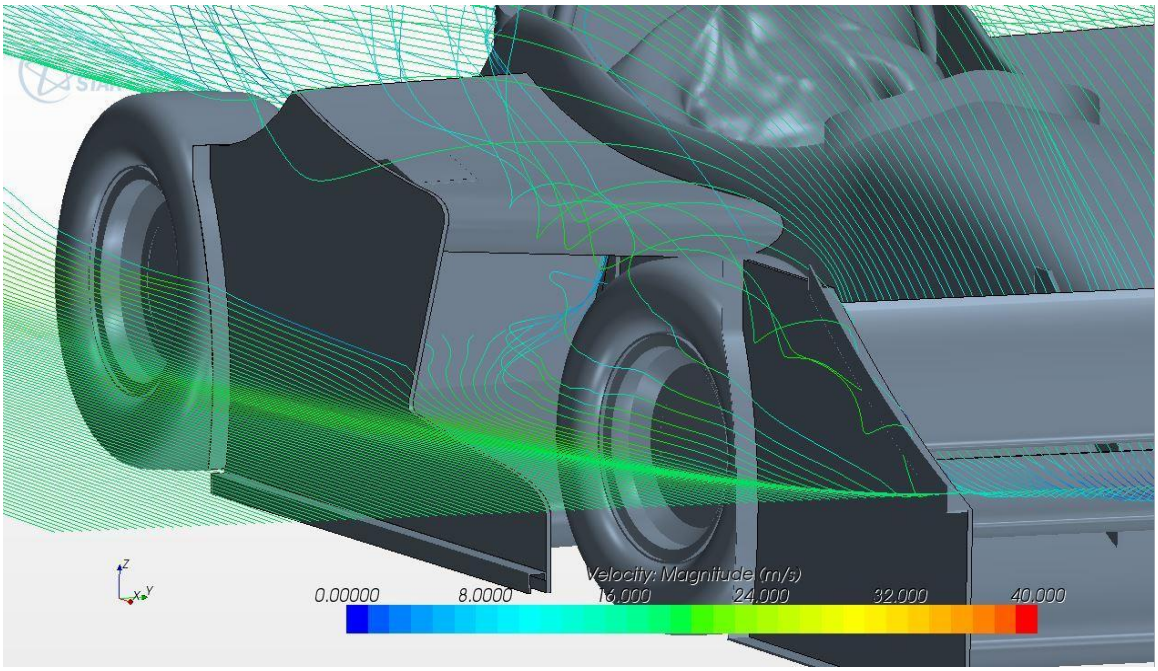

Figure 111: Streamline scene from Star-CCM+ of airflow through side-pod and radiator system.

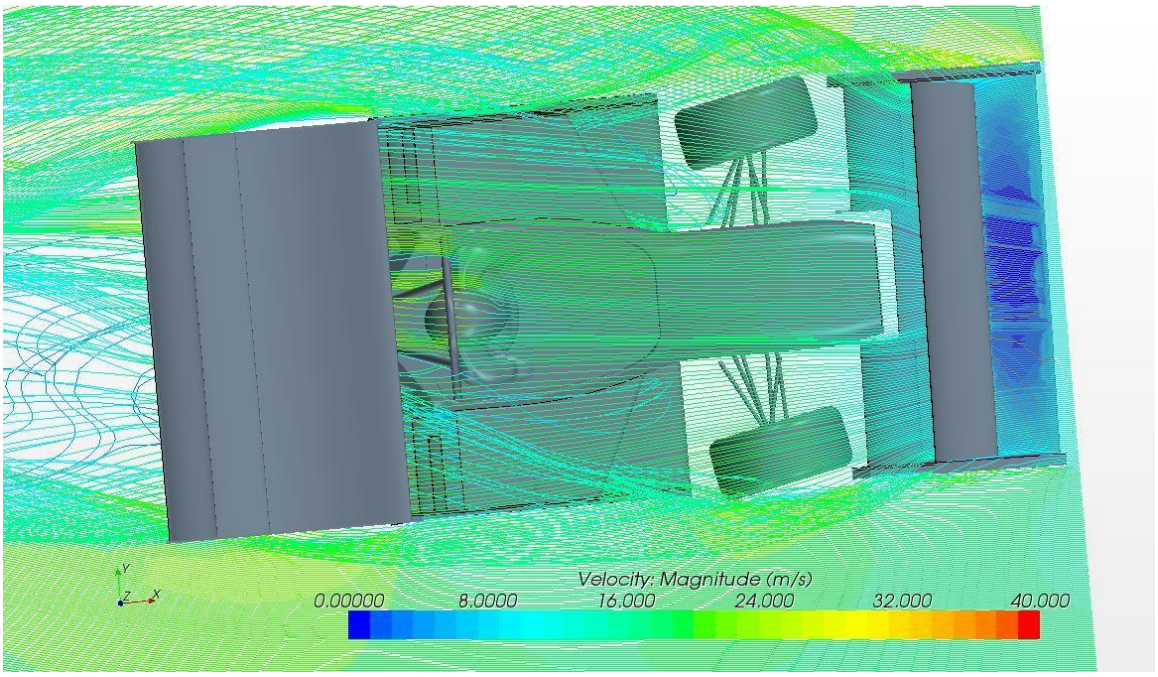

Figure 112: Top view of airflow streamline through side-pod in yawed conditions.

In the particular streamline images of Figure 111 and Figure 112, the side-pod airflow is rarely affected during these cornering conditions. As shown by Figure 112, the airflow through the side-pod is rather consistent with that of a straight line case, as seen by the large amount of streamlines in both figures, entering the side-pod system.

5.5.4.2 Yaw Simulation:

45 Degree Corner Exit / 30 Degree Wheel Angle / 1G Lateral Acceleration

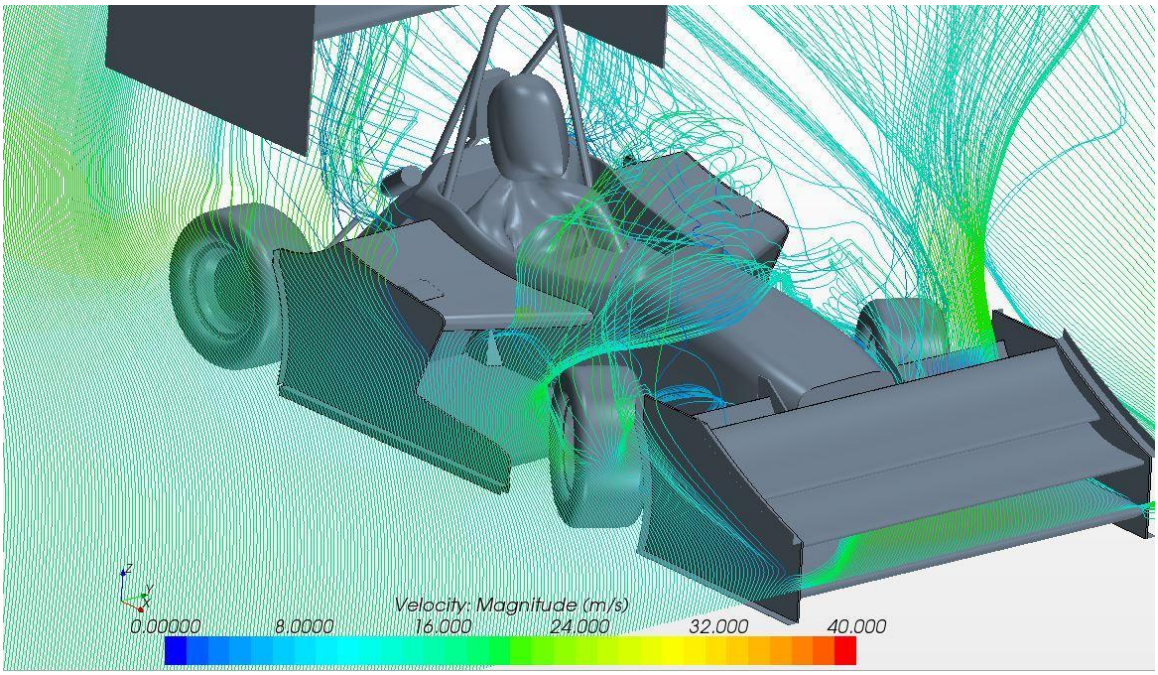

Figure 113: Isometric view of airflow streamline through side-pod in yawed conditions (150 mm above ground).

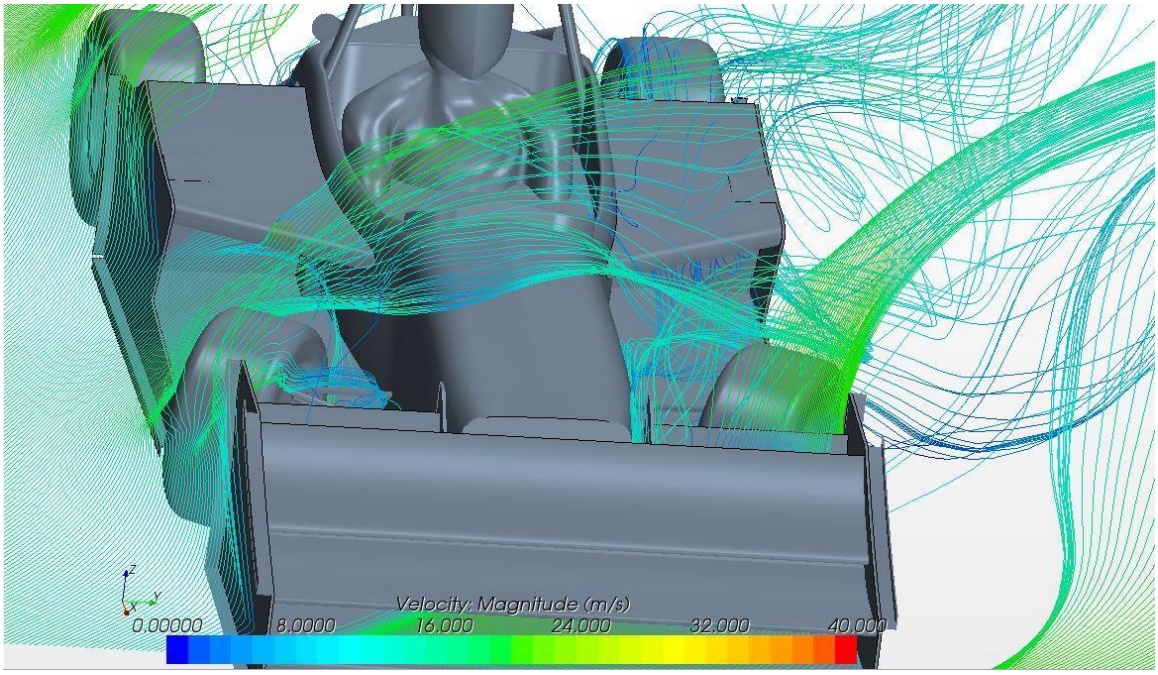

Figure 114: Front view of airflow streamline through side-pod in yawed condition (150 mm above ground).

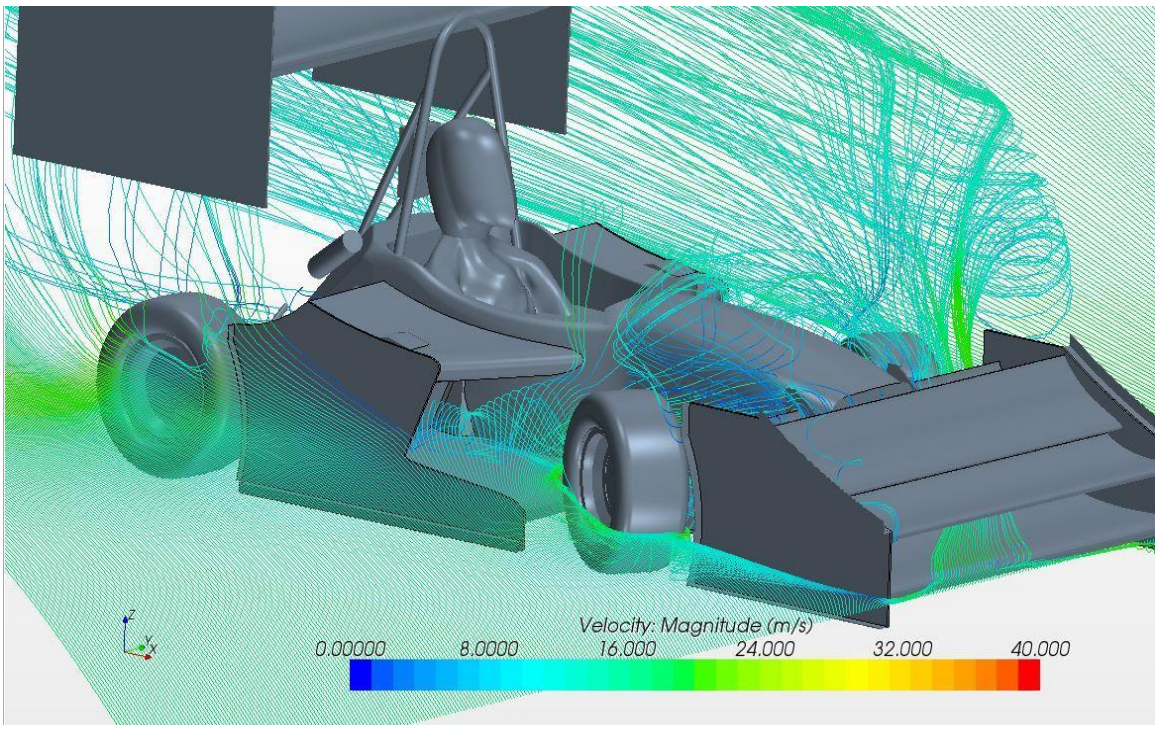

Figure 115: Isometric view of airflow streamline through side-pod in yawed conditions (100 mm above ground).

In the previous images, the airflow through the side-pod and radiators at this particular cornering and steering angle show very different results than those streamline figures in straight driving conditions. Figure 113 shows rather chaotic airflow over the top of the right side-pod and chassis, and very limited airflow through the left side as seen in Figure 114 in which the majority of the air enters and then escapes out of the inlet. Thus during this condition, the left-side pod would experience a steep decline in airflow through the radiator. The fan package (discussed in the upcoming section) will help tremendously in improving airflow during these conditions. Lastly, in Figure 115 at lower heights, the right side-pod airflow is not greatly affected by the turning conditions. This had a large influence in the design of the side-pods to have a slanted back design for the opening to allow for more outboard air in both straight line and yawed conditions to flow through the radiator.

The "swept back wing" style of the 2014 side-pod allows for more consistent airflow through various turning and straight line vehicle motion. This is important for the GFR vehicle in which cooling failure has been an issue. This helps provide reassurance that adequate airflow will be achieved in various driving conditions.

The results of aerodynamic performance of the side-pod, including downforce, drag, and air flow (mass flow rate) are summarized in Table 30 below. *Note: Due to errors in the current aerodynamics CFD simulation for yawed conditions, only the mass flow rate values were measured through one side-pod.*

Table 30: Aerodynamic and Airflow Performance of 2014 Side-Pod in Yaw Conditions

2014 Side-Pod Yaw Results	***12/05/2G***	***-30/45/1G***
Downforce	-5.9 N	-4 N
Drag	0.34 N	-1.2 N
Mass Flow Rate (Left)	N/A	0.56 kg/sec
Mass Flow Rate (Right)	0.21	N/A

The results of Table 30 indicate that during cornering, the side-pod that is on the vehicle side that went into the incoming free-stream air, experienced mass flow rates that improved tremendously from the straight line condition: from 0.465 to 0.56 kilograms per second. All of the CFD mass flow rates are measured without a fan. With the presence of a fan, the side-pod opposite the incoming free-stream, will still receive adequate cooling based on proper fan sizing with the radiator component. As a summary, this design will provide adequate cooling even in the events of cornering in which the mass flow rate could drop to as significantly low as 0.21 kilograms per second, especially with the inclusion of a radiator fan. As noted in Table 30 as well, the lift created by the side-pod is reduced dramatically during yaw-conditions, most likely due to the decrease in velocity of the vehicle during cornering conditions. In summary, the slanted side-pod is projected to provide adequate airflow in various conditions expected during Autocross and Endurance style races.

This concludes the aerodynamic performance analysis section of this thesis. The next sections will highlight other important component designs included in the 2014 side-pod package.

5.6 Cooling Fan and Shroud

An additional area of design for the side-pod of the 2014 GFR car included modeling the radiator component in CAD, as well as the modeling of a fan for mounting purposes. Originally, the radiator and fan were modeled as shown in Figure 116.

Figure 116: Original fan-radiator package in CATIA V5

The model was later updated to show the final purchased fan system by the 2014 management team. The fan package that is included on the GFR 2014 car is shown below in *Figure 117: 10" SPAL fan to be mounted on the rear of each radiator*.

Figure 117: 10" SPAL fan to be mounted on the rear of each radiator

The above OEM fan was designed in CATIA V5 for the GFR 2014 vehicle using the below engineering drawing provided by SPAL Automotive.

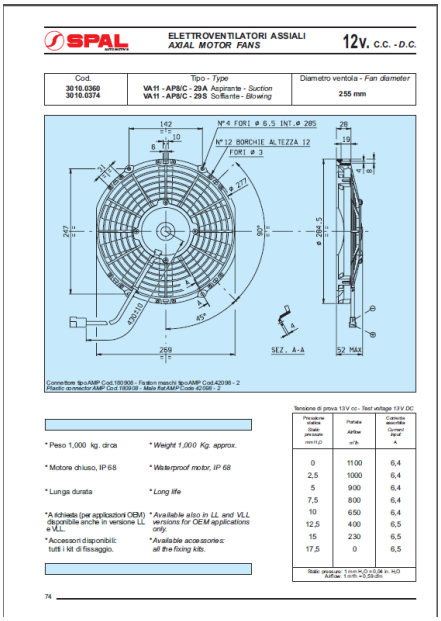

Figure 118: SPAL Automotive 10" fan engineering drawing

The updated CAD model of the final radiator and fan package is shown in Figure 119.

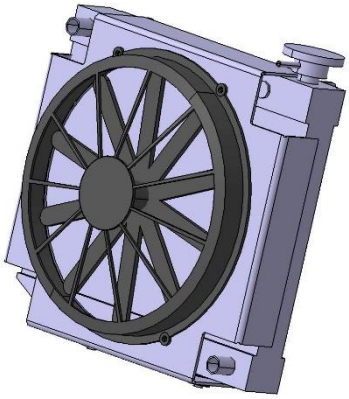

Figure 119: Radiator, fan and shroud updated CAD model

This portion of the cooling package was incorporated into the side-pod system design, because the need for a fan shroud was extremely important in efforts to securely fasten the fan to the radiator and promote as much airflow through the radiator core as possible. The requirement for the fan shroud was to allow for a 1" separation between the fan and radiator core. This fan and shroud package is a shared design for both the oil and water coolers of the *GFR* cPowertrain system. The final fan shroud is shown in Figure 120 below.

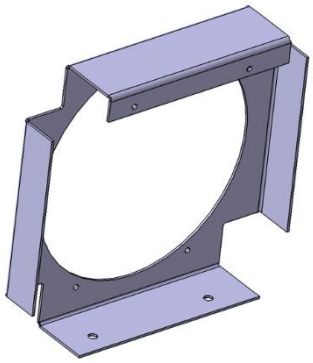

Figure 120: 2014 fan shroud design for attachment of fan to radiator unit

Weight Addition and Competition Points:

Below is a table illustrating the surface area of the fan shroud used to calculate the weight of the shroud, and the total addition to vehicle weight according to a composites weight calculator designed for the aerodynamics group.

Table 31: Fan shroud individual and total weight

	GFR 2014: Fan Shroud
Surface Area (m^2)	0.216
Weight (kg)	0.27872
Total Vehicle Weight Addition (kg)	0.55744

The added mass of the fan shroud and its result on competition points is seen below in Table 32.

Table 32: Fan shroud competition points

Vehicle Mass to Total Points	GFR 2014: Fan Shroud
FSAE	-0.847
FSUK	-0.847
FSG/FSA	-1.015
Average	-0.903

5.7 Brackets, Inserts, and Fasteners

5.7.1 Front Mounting Brackets

An important component of the side-pod system is the mounting strategy that will be used to secure all of the components together properly and in accurate locations. Initially, basic L-shape brackets were to be designed to mount the side-pod to the chassis and endplate. Instead, the 2014 side-pod package included universal brackets that allow for mounting of the side-pod as well as the undertray rods. The bracket design is shown in Figure 121 below.

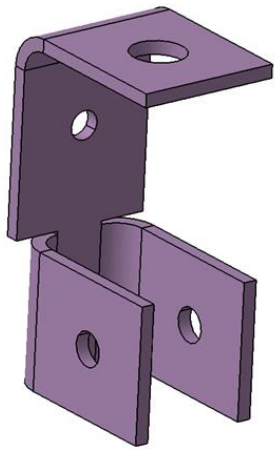

Figure 121: Carbon-fiber front mounting bracket.

This design utilizes composite potted inserts that fit into small, pre-drilled holes in the chassis body. The integration of both the side-pod and undertray rod mounting locations can be seen in Figure 122.

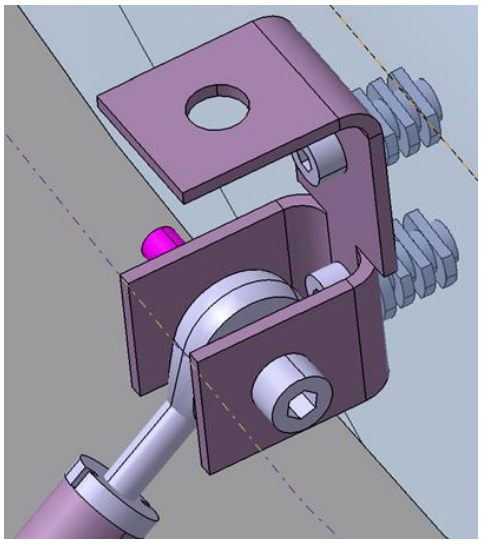

Figure 122: Front mounting bracket shown with rod ends, potted inserts and fasteners

The front mounting brackets are to be used with M4 x 12 mm bolts through customized potted inserts provided by Marketing Masters. The rod ends attach to the bracket using an M5 bolt. The side-pod utilizes the top hole which incorporates nylon push-style rivets from Fun Country for easy assembly and removal.

Weight Addition and Competition Points:

The weights and competition points for the above front mounting bracket are shown below.

Table 33: Weight addition of front bracket.

	GFR 2014: Front Bracket
Surface Area (m^2)	0.006
Weight (kg)	0.01206
Total Vehicle Weight Addition (kg)	0.02412

Table 34: Front bracket competition points

Vehicle Mass to Total Points	**GFR 2014: Front Bracket**
FSAE	-0.037
FSUK	-0.037
FSG/FSA	-0.044
Average	-0.039

The concepts were designed to be 1.2 mm thick, which requires approximately six plies of carbon-fiber. This lay-up schedule was used to calculate the above weights.

5.7.2 Side-Pod Endplate Brackets

The connection of the side-pod and endplate interface required separate brackets to be designed. These brackets were designed to be small in order to reduce weight, while providing structural strength to withstand the loads from the side-pod and endplate. These brackets includes an 8 mm hole to allow for push rivets to be used for attachment, while the other side of the bracket will be epoxied to the endplate. This bracket can be seen in Figure 123 below.

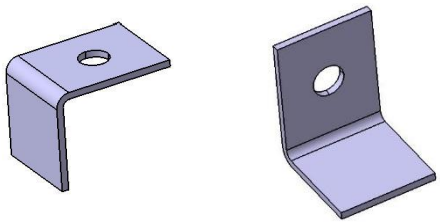

Figure 123: Side-Pod endplate mounting bracket with 8 mm hole for plastic rivets.

Weight Addition and Competition Points:

There will be four of these brackets on the cCar and two on the eCar. These brackets were made with six plies of carbon, which was used to calculate the weights and competition points for both the cCar and eCar listed below.

Table 35: Bracket weights for 2014 cCar and eCar

Endplate/Side-Pod Bracket Weights	GFR 2014: cCar	GFR 2014: eCar
Surface Area (m^2)	0.003	0.003
Quantity	4	2
Weight (kg)	0.00603	0.00603
Total Vehicle Weight Addition (kg)	0.02412	0.01206

Table 36: Competition point relationship to endplate bracket for 2014 cCar and eCar

Vehicle Mass to Total Points	GFR 2014: cCar	GFR 2014: eCar
FSAE	-0.037	-0.018
FSUK	-0.037	-0.018
FSG/FSA	-0.044	-0.022
Average	-0.039	-0.020

5.7.3 Potted Inserts

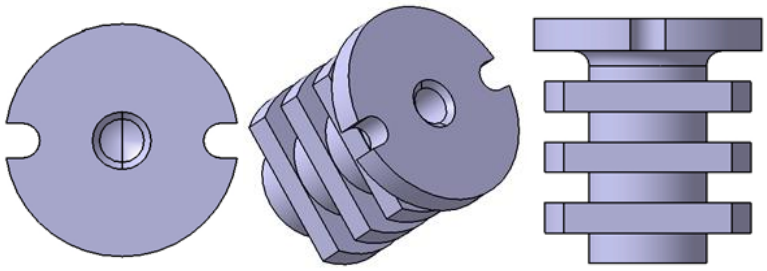

Figure 124: M4 potted inserts custom made for GFR 2014 provided by Marketing Masters.

These potted inserts were custom made to fit M4 style bolts used for the *GFR* 2014 cars. These potted inserts fit into custom drilled holes in the chassis body and are secured with epoxy. The epoxy is shot into the chassis and fills the ridges of the insert. This is a secondary process completed once the side-pod and undertray are correctly positioned. These potted inserts hold the front brackets into the chassis as seen in Figure 122 in the above bracket section.

5.7.4 M8 Honda Style Nylon Pry Rivets

These nylon pry rivets will be used to attach the side-pod to the endplate brackets and the front brackets. In the past, plastic socket hap caps screws and washers were used to secure the side-pod to the undertray and chassis. These were extremely difficult to remove and increased the assembly time required. Due to the low level of lift on the side-pod, these pry rivets provided plenty of clamping force to securely fasten the side-pod. These rivets are seen in Figure 125 below.

Figure 125: Nylon rivets (Image "A"). Image provided by Western Power Sports

5.7.5 Rear Mounting Brackets

In the rear of the vehicle, a universal bracket was designed to attach the side-pod, rear undertray rod, and main switch to the chassis body. This bracket was designed to be able to be used for both the cCar and eCar. One bracket was made to account for all of these components on both vehicles and accounts for both the internal roll hoop of the

cCar, as well as the external mounted roll hoop of the eCar. This rear bracket utilizes a current mounting bracket used for the roll hoop and minimized the need for additional mounting fasteners by utilizing those currently in place. This bracket is directionally designed, and has a mirrored design on the left hand side of the vehicle, opposite of what is shown in Figure 126. This design is used on the left side of the vehicle to hold the undertray and side-pod to the chassis. For ease of manufacturing, reduction of part complexity and design simplification, this bracket design is utilized on both sides of the vehicle despite the small amount of additional weight of the bracket on the left side where switches are not mounted.

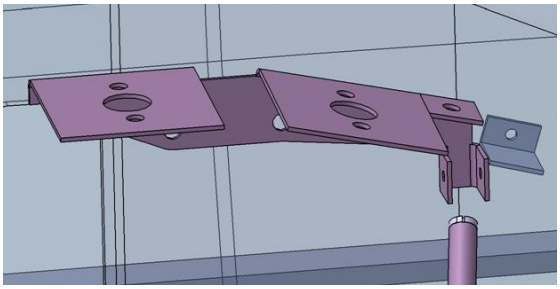

Figure 126: Rear ducting compatible with both cCar and eCar roll hoops and main switch, undertray rod end brackets and side-pod fastener hole.

As seen in Figure 126, this bracket accounts for the slope in the side-pod wing profile, as seen by the right side of the image with a negatively sloped flange.

5.7.6 Fasteners

For all the fastener requirements of the side-pod system, both M4 and M5 style screws will be utilized where large amounts of support are required, such as in the front and rear brackets at the potted insert-chassis interface, and for rod end mounting of the

undertray. All M4 and M5 style fasteners for the mounting brackets, potted inserts, and rod-ends will be provided by Portland Screw.

Weight Addition and Competition Points:

Weight and competition points can be seen in the tables below.

Table 37: Fastener weights for 2014 eCar and cCar

Fastener Weight Addition	GFR 2014: cCar	GFR 2014: eCar
Fastener Weight (kg)	0.0018	0.0018
# of Fasteners	4	4
Total Vehicle Weight Addition (kg)	0.0072	0.0072

Table 38: Fastener competition points for 2014 eCar and cCar

Fastener Mass to Total Points	GFR 2014: cCar	GFR 2014: eCar
FSAE	-0.011	-0.011
FSUK	-0.011	-0.011
FSG/FSA	-0.013	-0.013
Average	-0.012	-0.012

5.8 Fill Cap Cover

This particular piece is very minimal yet important in order to meet the requirements outlined by the FSAE rules and customer requirements for the 2014 aerodynamics package. Due to the protrusion of the radiator fill cap extending beyond the external surface of the side-pod; this requires a cover in order to protect the driver and any officials or crew members from accidental exposure to hot water in the event of a radiator cap malfunction. The fill cap cover can be seen in Figure 127 below.

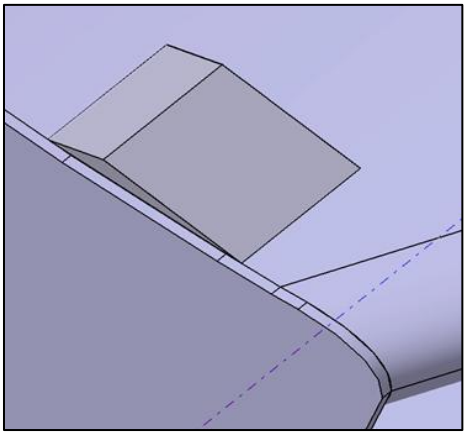

Figure 127: Radiator fill-cap cover attached to the top of the side-pod

This piece of the side-pod construction has very limited technical data that can be discussed.

Weight Addition and Competition Points:

The following tables illustrate part weight and the relationship to competition points.

Table 39: Fill cap cover weight

	GFR 2014: Fill Cap Cover
Surface Area (m^2)	0.013
Weight (kg)	0.00871
Total Vehicle Weight Addition (kg)	0.01742

Table 40: Fill cap cover relationship to competition points

Vehicle Mass to Total Points	GFR 2014: Fill Cap Cover
FSAE	-0.026
FSUK	-0.026
FSG/FSA	-0.032
Average	-0.028

5.9 Benchmarking of 2014 vs. 2013 Side-Pod System

This section will briefly summarize the results of the 2014 side-pod design, and will compare it to the performance characteristics of the 2013 Global Formula Racing vehicle. All of the previously discussed components are considered as part of this analysis. The entire final package will be recapped in the upcoming section and is considered here for comparison to the 2013 vehicle.

The following table illustrates the aerodynamic and airflow performance comparison of the 2014 projected results from CFD simulations to the 2013 CFD simulation results.

Table 41: Aerodynamic and Airflow Performance Comparison

Performance Characteristic	GFR 2014	GFR 2013	% Improvement
Weight (no endplate)	211.13 g	444.4 g	52%
Weight (including endplate)	1,007 g	444.4 g	127%
Mass Flow Rate	0.465 kg/sec	0.05 kg/sec	830%
Total Vehicle Downforce	1176.6 N	844.2 N	39%
Total Vehicle Drag	423.2 N	396.2 N	7%
Side-Pod Downforce	-10 N	-31 N	-68%
Side-Pod Drag	-0.8 N	-0.2 N	300%

As seen in Table 41, the weight of the 2014 side-pod is slightly larger than the 2013. This is because the 2013 side-pod was its own modular component, whereas the 2014 design integrates the undertray endplate into the vertical wall of the side-pod

system. From an airflow perspective, the mass flow rate has been increased by 830% over the 2013 vehicle. This is a strong representation that the cooling system will receive adequate airflow to maintain sufficient engine cooling during Autocross and Endurance events. The 2014 side-pod also creates much less lift than the 2013 side-pod which was a huge goal for this year's design. As a whole, this side-pod package helps tremendously in the improvement of the overall aerodynamic performance. The 2014 vehicle simulation results projects nearly 1200 N of downforce in comparison to 844 N of 2013 aerodynamic simulations. These performance improvements in relation to competition points can be seen in Table 42.

Table 42: Correlation of Aerodynamic Performance of CFD Results to Competition Points

	GFR 2014: 14_SP_1.19	GFR 2013: 14_Baseline_Trimmer 3	Points Improvement
Total Downforce Points	212.14	152.21	59.93
Total Drag Points	-24.84	-23.26	-1.58
Net Points	187.3	128.95	58.35
Side-Pod Downforce Points	-1.88	-5.409	3.529
Side-Pod Drag Points	0.05	0.01	0.04
Side-Pod Net Points	-1.83	-5.40	3.56

The mass addition of the 2014 side-pod and endplate package in comparison to the 2013 car is seen in Table 43, which represents competition point deductions of both years. Although this is not a completely level comparison (given the 2014 modular

integration with the undertray), it gives a good representation into the point breakdown for each year.

Table 43: Side-Pod Mass and Competition Point Comparison

Vehicle Mass to Total Points	GFR 2014 (kg)	2014 Competition Points	GFR 2013 (kg)	2013 Competition Points	Point Increase
FSAE	1.007	-1.53	0.4444	-0.68	0.86
FSUK	1.007	-1.53	0.4444	-0.68	0.86
FSG/FSA	1.007	-1.83	0.4444	-0.81	1.02
Average	1.007	-1.63	0.4444	-0.72	0.91

Although the point deduction for mass of the side-pod is higher than the 2013 vehicle, the mass points are negligible in comparison to the increase in competition points gained from aerodynamic performance.

5.10 Design Summary

Table 44 provides a brief summary of the total competition points gained from the complete 2014 side-pod package. This table includes points from both aerodynamic performance (downforce and drag) as well as negative points from mass of all parts.

Table 44: Competition points gained from 2014 side-pod package

Total Points Gained at Competition	GFR 2014: cCar
FSAE	184.583
FSUK	184.583
FSG/FSA	184.046
Average	184.404

6. Design Selected

In this next section, the final designs selected for the 2014 *GFR* vehicle, as described thoroughly in the previous section, will be reviewed in summary. This upcoming section will include finalized designs in relation to customer requirements and team goal, a recap of performance results of the final design, engineering justification, technical data and drawings, manufacturing plans, molds, and vendor supplied parts.

This upcoming section is broken into three sections, *Rationale for Selection, Technical Specification, and Manufacturing Plan.* Each of these three sections are broken up into sub-sections, detailing the different components designed within the side-pod project itself. This includes the side-pod, endplate design, front/rear ducting, fan shroud, radiator placement, fill cap cover, bracket design, fasteners and mounting components.

6.1 Rationale for Selection

The side-pod package for the *GFR* 2014 car is a significant improvement on many different levels for the aerodynamics package. A lot of design work has gone into creating an aerodynamically effective side-pod which improves the overall performance of the vehicle. This improvement comes from an increase in downforce, reduced drag, a decrease in total system weight, and significant improvements in airflow to the cooling package. The new side-pod system will be reviewed with a brief overview of the changes made to this year's side-pod package and relate them to goals of the 2014 aerodynamics team, as well as the engineering and customer requirements outlined in Section 5.

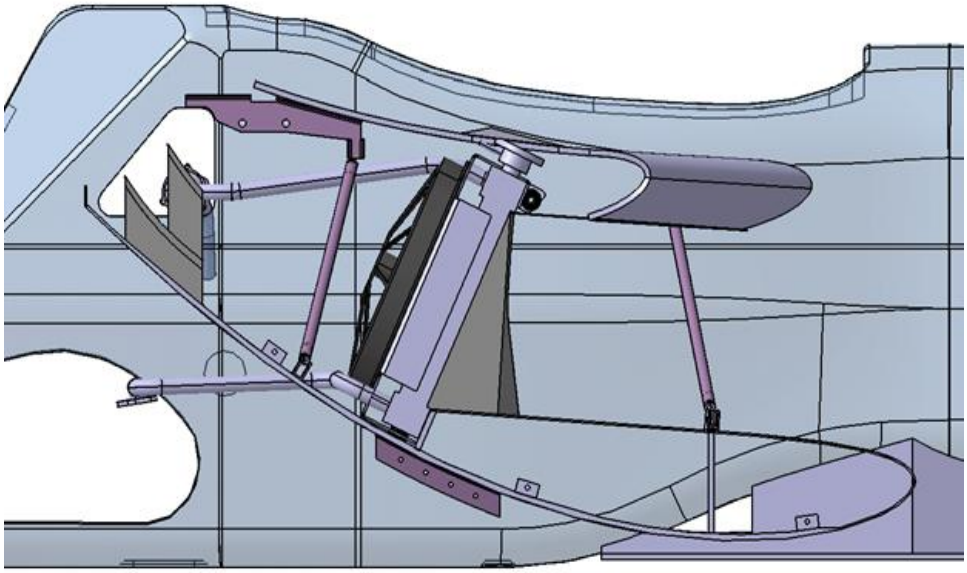

Figure 128: Final side-pod package with fan shroud, brackets, ducting, and mounting components (shown without endplate to display internals)

The 2014 side-pod package seen in Figure 128 was designed from multiple iterations and numerous CFD simulations to help narrow down shape and design that would produce the most downforce and air flow. As outlined in Section 3, many

additional components were added to improve the overall performance and improve possible competition points for the *GFR* vehicle. An overview of all of these components within the side-pod package can be seen in the Figure 128. This package is a balance between ease of manufacturing and assembly time, while providing beneficial trade-offs by being a lightweight design, with a significant improvement in downforce and tremendous increases in airflow from the 2013 design.

After numerous iterations, it was decided that simplifying the side-pod could be one of the best solutions for the *GFR* 2014 car. This resulted in the one piece side-pod shown in Figure 128. The advantages to this design are simple yet significant. A design goal of this year's side-pod was to integrate the undertray endplate to be used as the outboard wall of the side-pod as shown in Figure 129 below.

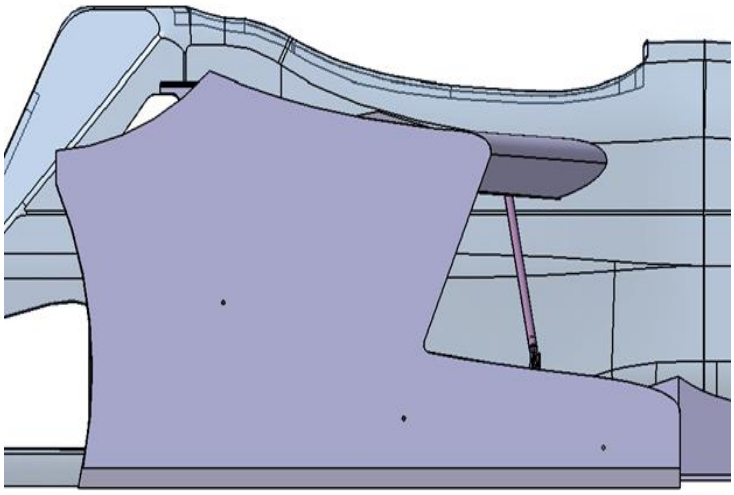

Figure 129: Undertray endplate used as outboard wall of side-pod

Integrating the endplate into both the side-pod and undertray design allows for ease of assembly, reduced manufacturing, and less weight for the entire vehicle, which is important to the overall customer requirements and team goals for 2014. This particular

side-pod also integrates some unique features including an identical Joukowski wing profile as the 2014 undertray, with an increased angle of attack of 20° in comparison to the 17° angle of the undertray. This wing profile and angle of attack used for the side-pod increased the amount of downforce created for the overall vehicle by effectively reducing the amount of side-pod lift in comparison to the 2013 side-pod.

As mentioned previously, this side-pod profile and endplate design allows for the best of both solutions for downforce and airflow into the radiators. With the particular shape of the side-pod, lift is significantly reduced; with the internal ducting, endplate, and inlet design, the mass flow rate has improved tremendously.

The 2014 side-pod meets all of the design goals of the Aerodynamics team. These include installation without modification of any vehicle components (besides the removal of the endplate), providing effective airflow for cooling, creating more downforce than 2013 (or less lift), and allowing re-filling of radiators without removal of the entire side-pod assembly (due to the radiator fill cap protruding beyond the top of the side-pod, enclosed by a removal fill cap cover).

6.2 Technical Specification

In this section, the complete side-pod package will be outlined in terms of technical justification, performance improvements to the *GFR* vehicle, and detailed information regarding competition points, and aerodynamic performance from CFD simulations.

6.2.1 Side-Pod Profile

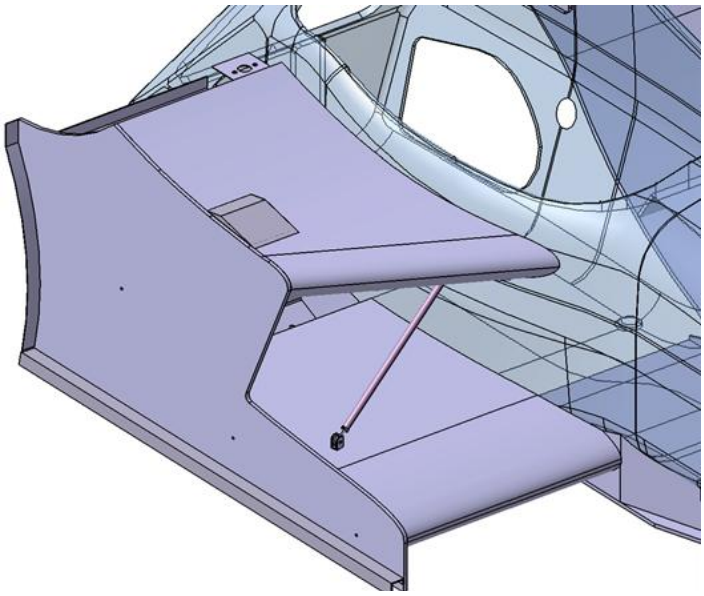

Figure 130: 2014 Side-Pod inverted-wing profile

The profile of the 2014 side-pod utilizes the Joukowski profile of the 2014 Undertray. The reason for this design was due to the desire for ease of manufacturing. One of the design goals for the 2014 side-pods was to reduce manufacturing time, and was done so for this year by eliminating the need to develop new molds. Instead, it was designed utilizing profiles of molds of existing aerodynamic components, and in this

case, the 2013 undertray mold. This profile helps reduce lift, and increases mass flow rate through the radiator. This design was chosen for 2014 due to the slanted opening design allowing for more outboard air to flow into the radiator during both straight line and yaw conditions.

6.2.2 Endplate Design

The 2014 undertray/side-pod endplate integrates a gurney slot along the bottom edge to help reduce vortices from disturbing the airflow below the undertray, as well as a gurney flap at the rear of the endplate to improve downforce. This particular endplate integration with both the undertray and side-pod allows for ease of assembly. With one piece used for both components, this will allow for easy access to both components between competitions. The endplate can be removed with three fasteners, and will allow full access to all radiator and fan components, cooling lines, and ducting. In addition, the rear ducting will be epoxied to the inside of the endplate for consistent removal and reassembly without the need for tape. This endplate design meets the customer requirements by contributing to the improved airflow, and reducing weight while maintaining ease of assembly for easy servicing. This provides easy access to all cooling components with only three fasteners. It is also easily manufactured using laser cut sheet-metal molds provided by GK Machine as a template for carbon-fiber lay-up.

6.2.3 Front Ducting

The front ducting of the 2014 car has been an important component of the design process. In past years, it has been a last minute component that has been cut-to-fit with little emphasis on proper mounting strategies and effective ducting practices to improve the airflow. This new ducting allows for better sealant to prevent air from bypassing the radiator, and does a sufficient job of directing as much air as possible to the core of the radiator. The finalized ducting can be seen in Figure 131 below.

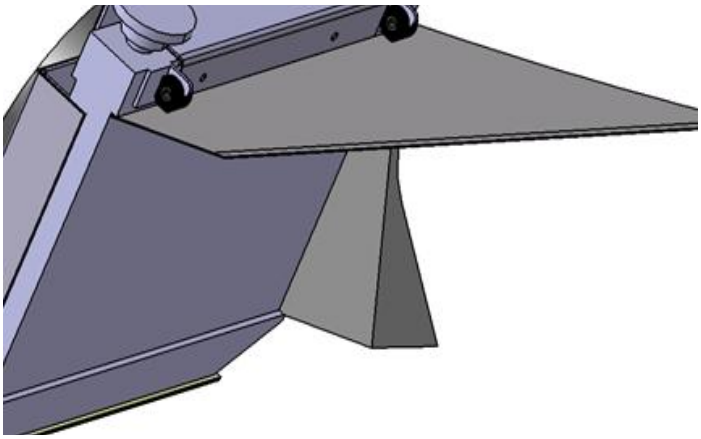

Figure 131: 2014 front ducting design

This design reduced the weight from the first ducting concept for 2014, and eliminated the need for any excess cut-to-fit foam pieces secured and fastened with tape to various components. This particular ducting will be made of two plies of carbon-fiber. This ducting does not require the manufacturing of any molds, and will be made using printed templates for carbon cutting.

6.2.4 Rear Ducting

Towards the end of the design phase of the 2014 side-pod, the need for rear ducting quickly became a necessity. With investigation into the effects of rear ducting as mentioned in Section 5.4, it showed promising results on the aerodynamic performance and mass flow rate of the vehicle with its incorporation. This led to numerous design iterations including the final ducting design which utilizes the front wing flap profile and mold for its manufacturing. This allows for use of current molds in combination with printed templates used for cutting the carbon-fiber. The new rear ducting is a two element ducting, with a top element that is shorter than the bottom for clearance and interference issues of the fuel neck, and cooling lines in addition the main electrical switch positioning with the new universal rear brackets. The rear ducting had a positive effect on the airflow leaving the undertray and entering the rear-wing region. Overall, the addition of this rear ducting improved the downforce capabilities of the 2014 aerodynamics package from a full-vehicle standpoint. This ducting is shown below in Figure 132.

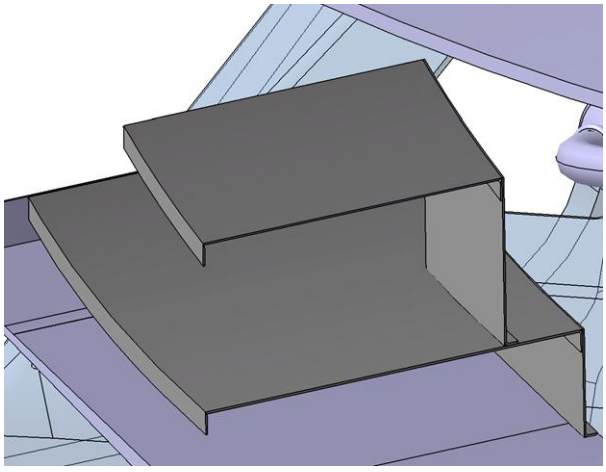

Figure 132: Rear ducting for 2014 side-pod utilizing front wing-flap profile

In the final design selection, it was decided that the best angle of attack for the flap elements was approximately 45°. This angle provided the best mass flow rate as seen from CFD simulation results of "14_SP_1.19" from Table A 3 and Table A 4 in Appendix A. Both the top and bottom flap have the same front-wing flap profile mounted parallel to each other. This angle is shown in Figure 133 below.

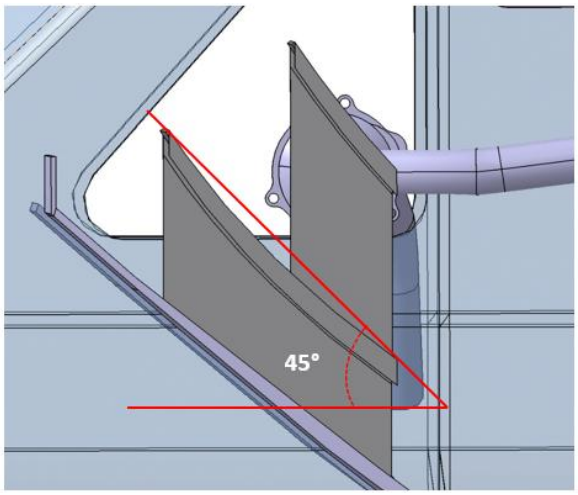

Figure 133: Rear ducting wing element mounting angle of approximately 45°

This ducting allows the air to be directed more vertically as to help delay flow separation and extract more air from the bottom of the undertray with its vertical momentum. This ducting also creates accelerated flow on the bottom of the ducting, contributing a small portion to total downforce on the vehicle given the wing element shape and angle of attack. When analyzing the whole vehicle, this ducting also helps the rear wing to create slightly more downforce given that the air is also further accelerated on the underside of the wing element where the low pressure zones are further influenced.

For ease of assembly, this ducting will attach directly to the endplate in a permanent fashion for ease of assembly in both removal and reassembly to ensure the ducting is repeatedly placed in the proper position for improved performance. The inboard flaps of the ducting will be attached using small Velcro strips on the upper surface of the undertray. This ducting will be made of three plies of carbon to minimize weight and increase strength and stiffness.

6.2.5 Fan Shroud

In addition to the side-pod package, assembly and attachment of the cooling components have become an important aspect of this project. One area of improvement that was focused on was the fan shroud. The 2014 fan will be attached to a carbon-fiber shroud a similar composition to that of the side-pod. This shroud attaches to current mounting positions of the new radiators and allows for accurate positioning with respect to the rear of the radiator using pre-designed mounting holes compatible with the new 2014 cooling fan. The shroud can be seen in Figure 134 below.

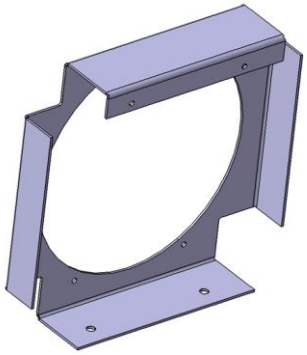

Figure 134: 2014 fan shroud with attachment holes for radiator and cooling fan

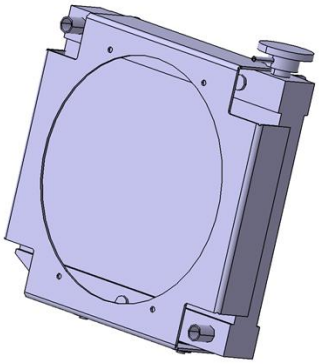

Figure 135: Fan shroud attachment to 2014 radiator with predetermined fan mounting holes.

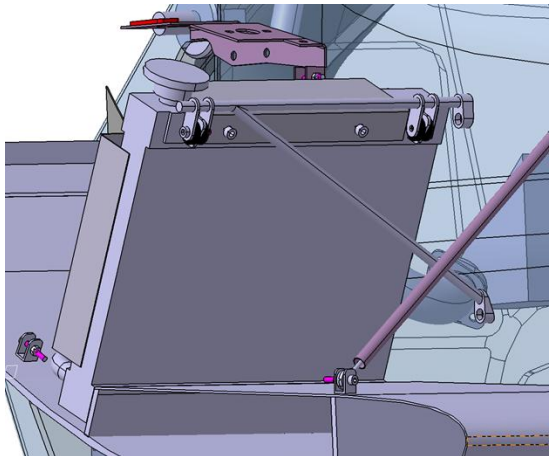

Figure 136: Radiator features used for shroud mounting

Installation

The following process diagram shows the step by step installation of how the fan shroud will work with the radiator and fan package, which utilizes current mounting points on the radiator as well as pre-designed mounting holes on the OEM fan.

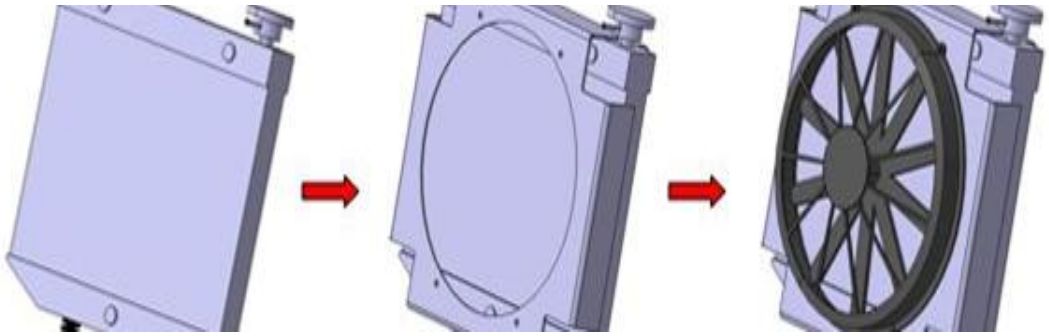

Figure 137: Installation process and integration of fan and shroud components with 2014 radiator.

In order to manufacture this fan shroud, GK Machining helped to laser cut and bend a sheet-metal mold that will be used for carbon-fiber lay-up. This shroud consists of ⅛" foam wrapped with two layers of carbon fiber for increased stiffness and reduced weight, rather than ten or more layers of carbon that would be needed to support the weight of the fan. The holes on the front of the shroud accommodate M6 size bolts for proper mounting into the radiator. The fan attaches to the fan shroud with ¼" bolts and will require nuts to secure the fan to the shroud.

6.2.6 Bracket Design, Fasteners, and Mounting

6.2.6.1 Front Bracket

The mounting strategy of the 2014 side-pod and undertray was an area that proved to be an area for improvement in terms of commonality and simplification. The front of the side-pod is attached to a customized bracket that encompasses two potted inserts attaching to the main chassis while also allowing the rod ends of the undertray to mount to the chassis simultaneously. A picture of the front mounting bracket system is shown below in Figure 138.

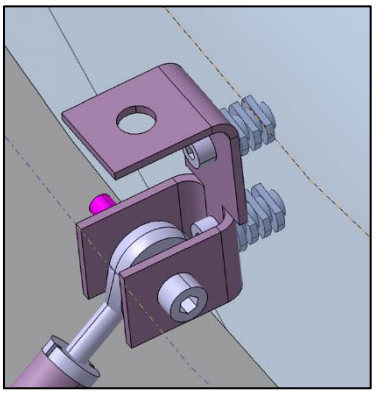

Figure 138: Front mounting bracket used by side-pod (excluded from image), undertray rod ends, and potted inserts into the chassis body.

6.2.6.2 Rear Bracket

In the aft portion of the side-pod and undertray system, the two components attach to the rear of the vehicle using a customized, universal bracket that additionally houses an electrical switch, with a position for the cCar and eCar, as well as a slot for the externally mounted roll hoop of the eCar. This particular bracket will be made of carbon-fiber

utilizing a sheet-metal mold being laser cut and bent by GK Machining, one of GFR's sponsor vendors. This part will be made for both RH and LH sides of the vehicle using two different molds. This rear bracket is shown in Figure 139 below.

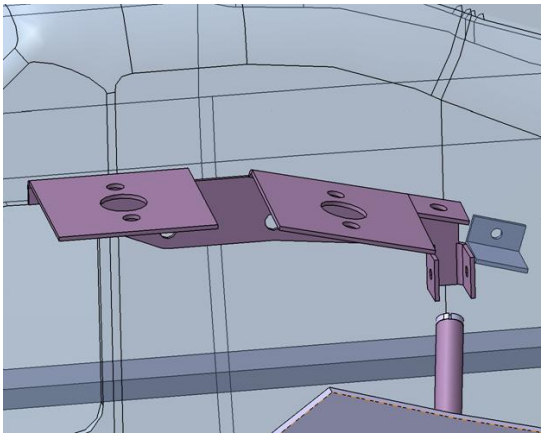

Figure 139: Rear bracket compatible with both cCar and eCar roll hoops and main switch, undertray rod end brackets and side-pod fastener hole.

6.2.6.3 Side-Pod/Endplate Bracket

The side-pod and endplate mounting brackets were designed to be a simple as possible to manufacture, and to properly secure the two components together. This bracket will attach to the side-pod with an M8 nylon pry rivet for easy removal, while remaining permanently epoxied to the endplate. This bracket will consist of six plies of carbon-fiber to provide structural support. This bracket can be seen in Figure 140.

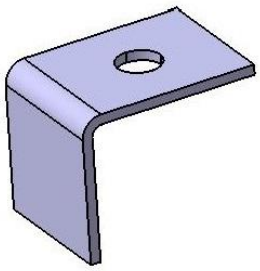

Figure 140: Final side-pod/endplate bracket design

6.2.6.4 Potted Inserts

The potted inserts to be used for assembly of components to the chassis are shown in Figure 141. These are provided to GFR from a full-sponsorship from Marketing Masters. These potted inserts are made of composite material, for customized M4 fasteners.

Figure 141: Customized composite inserts provided by Marketing Masters

6.2.6.5 M8 Nylon Pry Rivets

The nylon pry rivets used to attach the side-pod to the front, rear, and endplate brackets are shown in Figure 142. These allow for easy assembly and removal of aerodynamic components in the side-pod package. These will also be utilized on the 2014 undertray splitter skirts.

Figure 142: Nylon pry rivets components assembled (left) and disassembled (right)

6.2.7 Fill Cap Cover

This is a simple piece to be manufactured out of carbon-fiber similar to that of the ducting. This piece will simply be attached to the side-pod using small strips of Velcro for easy removal and access for quick filling, while enclosing the radiator cap. This will be manufactured using sheet-metal molds laser-cut and bent by GK Machining for carbon-fiber lay-up.

6.2.8 Electric Car

The 2014 eCar was a rather difficult task to include during the design of the side-pod and undertray components. For simplification purposes, the side-pods and endplates will be the same for the RH side of the eCar as that of the RH side of the cCar. On the LH side of the eCar, it will utilize the 2014 undertray with a simple endplate that does not extend above top of the undertray. The LH side of the eCar does not include a side-pod due to less cooling components than required by the cCar. The brackets take into account

the external roll hoop of the eCar given the two switch locations and middle slot. The external mounted roll hoop can be seen in the Figure 143 below of the 2014 eCar.

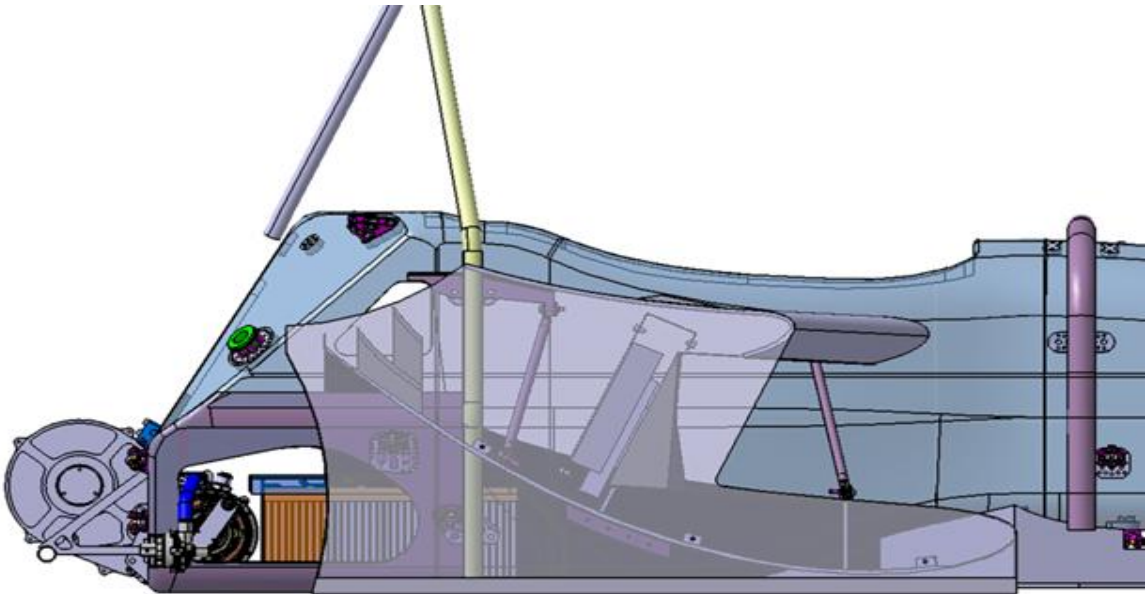

Figure 143: 2014 eCar external mounted roll hoop interaction with side-pod and rear mounting bracket.

6.2.9 Final Side-Pod System and Performance

As mentioned in Section 4.1, the final design of this concept (10_41_201_J) proved to be the most promising on all three levels of performance: aerodynamics, cooling, and weight addition; as well as for ease of manufacturing.

The slanted entry of these designs allows for greater entrance of air from outboard regions where air is available, while maintaining a large enough wing profile length to provide adequate downforce. The difference between H and J are a slanted endplate design parallel to the radiator angle in efforts to allow for more external airflow for cooling. 201_J has a slightly larger angle of attack than the undertray which allowed for

the greatest aerodynamic performance of the vehicle in terms of competition points. The interaction between the airflow and performance of the final side-pod concept, as shown in the right image of Figure 144, with both the undertray and rear wing, provided much more substantial results when analyzing the aerodynamic performance of the entire vehicle, leading to its selection for the final 2014 *GFR* vehicle.

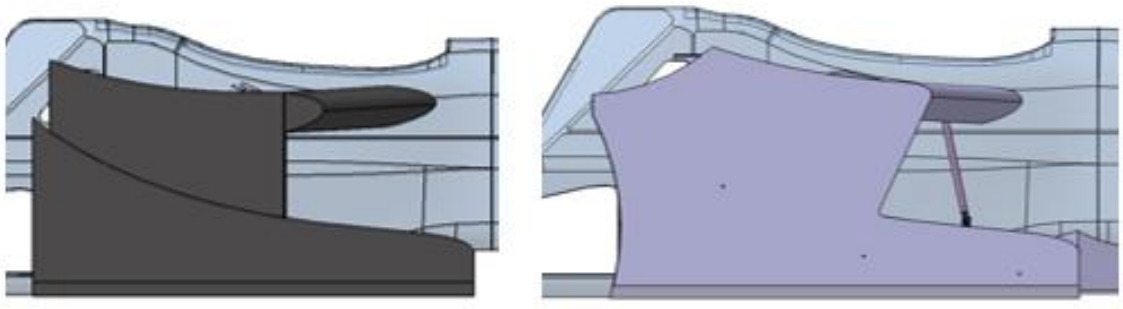

Figure 144: Comparison of endplate shapes of final iteration 10_41_201_J (right) and initial slant concept 10_41_201_H (left)

2014 Final Design Performance:

The final design for the 2014 side-pod will be a rather simple design utilizing the same wing profile as the undertray. The CFD results of the final side-pod design with finalized rear ducting, front ducting, and endplate design can be seen in Table 45: Final side-pod design in relation to total vehicle aerodynamic performance competition points gained. below. This table also outlines the complete aerodynamic performance of the full-vehicle and the total points gained at competition.

Table 45: Final side-pod design in relation to total vehicle aerodynamic performance competition points gained.

	Part #/ Aero Run-Ran Code	Iteration Name	Leading Edge Offset from Undertray Leading Edge	Side-Pod End Plate SA (m^2)	Undertray Endplate SA (m^2)	Total Endplate SA (m^2)	Side Pod Top SA (m^2)	Side Pod Bottom Leading Edge Radius SA (m^2)	Total Surface Area of Side-Pod/Complete Endplate (m^2)	Part Weight (kg)	Weight Addition to Full Car (kg)	Velocity Ratio
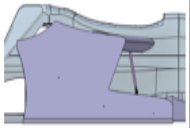	201_J 14_SP_1.19	2014 Final Side-Pod/Endplate	-83 mm to front edge	0	0.337	0.337	0.186	0.035	0.558	0.53	1.07	2.03

Part #/ Aero Run-Ran Code	Side Pod (Description)	Mass Flow Kg/s	DF	DR	Points DF	Points DR	Net Points	Total DF N	Total Drag N	L/D	Total Points DF	Total Points DR	Total Car Net Points
201_J 14_SP_1.19	new small front ducting, Rear Ducting Iteration 5 - Lowered, Final Side-pod location, Final Endplate, Undertray trailing edge gurney	0.465	-10.4	-0.8	-1.87512	0.04696	-1.82816	1176.6	423.2	2.78	212.14	-24.84	**187.30**

Benchmark Comparison and Competition Points:

The 2014 side-pod is a tremendous improvement in many different areas. In terms of cooling capabilities, the final design provided the highest mass flow rate of any design iteration considered for this year's vehicle, 0.465 kg/sec. In terms of aerodynamic performance, the final side-pod design had one of the lowest individual lift values of all the iterations -10 N, produced 0.8 N of thrust and was a great improvement in respect to the 2013 side-pod. Although it was only the second lowest lift value of the concepts considered, the interaction with the entire vehicles aerodynamic performance was by far the best solution when also considering weight, and cooling performance. The improvements of *GFR* 2014 in comparison to *GFR* 2013 are listed in the table below.

Table 46: Performance characteristic changes between 2014 and 2013 GFR vehicles

Performance Characteristic	GFR 2014	GFR 2013	% Improvement
Weight (no endplate)	211.13 g	444.4 g	52%
Weight (including endplate)	1,007 g	444.4 g	127%
Mass Flow Rate	0.465 kg/sec	0.05 kg/sec	830%
Total Vehicle Downforce	1176.6 N	844.2 N	39%
Total Vehicle Drag	423.2 N	396.2 N	7%
Side-Pod Downforce	-10 N	-31 N	-68%
Side-Pod Drag	-0.8 N	-0.2 N	300%

The above table shows significant improvement in the side-pod in comparison to the 2013 vehicle. The above values above that are listed as decline in performance are

indicated in red.

Minimizing weight is an important goal for the 2014 side-pod package. In order to do this, the parts need to be designed to have as minimal mass effects on the total car. The following table illustrates a weight breakdown of all of the components within the side-pod package for both the cCar and eCar.

Table 47: Carbon Fiber Component Weight Breakdown

Carbon Fiber Parts	Surface Area (m^2)	# Plies	% of Full Core Design	Core Thickness (mm)	Individual Weight (g)	cCar Vehicle Weight Addition (g)	eCar Vehicle Weight Addition (g)
Side-Pod	0.222	2	25%	6.35	183.17	366.34	183.17
Endplate	0.337	2	25%	6.35	278.05	556.11	278.05
Endplate Gurney	0.01	2	0%	6.35	6.70	13.40	6.70
Endplate Slot	0.058	2	0%	6.35	38.86	77.72	38.86
Front Ducting	0.152	2	0%	6.35	101.84	203.68	101.84
Rear Ducting	0.138	3	0%	6.35	138.69	277.38	138.69
Fan Shroud	0.216	2	50%	3.18	211.72	423.44	211.72
Front Bracket	0.006	6	0%	6.35	12.06	24.12	24.12
Rear Bracket LH/RH	0.038	6	0%	6.35	76.38	152.76	152.76
Endplate Bracket (each)	0.003	6	0%	6.35	6.03	24.12	12.06
Fill Cap Cover	0.013	2	0%	6.35	8.71	17.42	8.71
					Total cCar Side-Pod Package Weight	2.14 kg	
					Total eCar Side-Pod Package Weight		1.16 kg

In regards to weight, the new side-pod shares a common endplate with the undertray and led to a larger weight product than that seen on the 2013 car. In 2013 the side-pod was a completely modular piece. Although this does show an increase in weight of 127%, the ease of manufacturing, aerodynamic performance, and mass flow rate completely outweigh the negatives caused by the addition to weight in terms of competition points. The point breakdown for weight is shown in the table below [9].

Table 48: Mass addition of side-pod to 2014 vs. 2013 vehicle in comparison to competition points

Vehicle Mass to Total Points	GFR 2014 (kg)	2014 Competition Points	GFR 2013 (kg)	2013 Competition Points	Point Increase
FSAE	1.007	-1.53	0.4444	-0.68	0.86
FSUK	1.007	-1.53	0.4444	-0.68	0.86
FSG/FSA	1.007	-1.83	0.4444	-0.81	1.02
Average	1.007	-1.63	0.4444	-0.72	0.91

Even though the weight averages to an additional 1.63 points deducted from GFR competition points total, the increase in points from aerodynamic performance alone is more than enough to justify the offset. As found from Table A 4, in Appendix A, "SP_1.19" the interaction between the side-pod and the rest of the aerodynamic elements greatly increased the amount of points that will be gained at competition in the 2014 year in comparison to 2013 and can be seen in the table below.

Table 49: Aerodynamic performance results in relation to competition points

	GFR 2014: 14_SP_1.19	GFR 2013: 14_Baseline_Trimmer 3	Points Improvement
Total Downforce Points	212.14	152.21	59.93
Total Drag Points	-24.84	-23.26	-1.58
Net Points	187.3	128.95	58.35
Side-Pod Downforce Points	-1.88	-5.409	3.529
Side-Pod Drag Points	0.05	0.01	0.04
Side-Pod Net Points	-1.83	-5.40	3.56

With a thorough investigation into improving the aerodynamic performance of the side-pod and improving mass flow rate of air through the cooling systems using CFD, it was found that much of the air available for cooling into the side-pod was coming from the outboard regions of the vehicle during travel. Early in the design stage, much emphasis was focused on capturing as much air as possible traveling up and over the new, much larger front wing elements. With this investigation, it was found that the air above the side-pod was extremely limited by this front wing, and that the majority of the air available for flow into the side-pod was coming from around the front tires in the outboard regions of the vehicle rather than from above. The CFD results that helped determine this are visualized in Figure 68, Figure 69, and Figure 70.

As seen in the above table, the 2014 side-pod contributes to a significant increase in the aerodynamic performance of the entire vehicle. Even though it is producing a minimal amount of lift, this is an acceptable compromise in relation to the mass flow rate that will be provided to the cooling components and led to a much more reliable car when it comes to endurance type events in the 2014 season. Additionally, the effects of the side-pod have greatly increased the downforce effects of the undertray, and with the addition of ducting, the rear wing is experiencing higher downforce values as well. The *GFR* 2013: 14_Baseline_Trimmer 3 CFD results include all components used on the current 2013 *GFR* car used for competition. This car is chosen for comparison to keep our benchmarking consistent in verifying the 2014 design as an improvement from 2013.

Design Summary and Competition Points

The following table provides a brief summary of the project total competition points gained from the complete 2014 side-pod package. Table 50 includes points calculated from both aerodynamic performance (downforce and drag) values, as well as negative points from the mass addition of all parts.

Table 50: Competition points gained from 2014 side-pod package

Total Points Gained at Competition	GFR 2014: cCar
FSAE	184.583
FSUK	184.583
FSG/FSA	184.046
Average	184.404

6.3 Manufacturing Design

The following section will outline the manufacturing details of the previously described components outlined in Section 6.1 and 6.2. This section will include engineering drawings (if applicable), vendor parts, templates (if applicable), a detailed parts list including fasteners and brackets, carbon-fiber lay-up schedules, and core lattice information.

Manufacturing Overview:

The side-pod profile will be manufactured with a 1-core-1 lay-up in order to minimize the weight of the components. It will also only utilize the core in a specific core lattice pattern that will be described in the manufacturing plan of Section 6.3.1.

This side-pod design has greatly simplified the manufacturing process by eliminating the need for new molds to be CNC machined and fabricated, and will utilize current molds used for the 2013 undertray in combination with printed templates. The leading edge will be manufactured using existing joggle molds made on the undertray mold and will be attached to the side-pod top profile using epoxy. This side-pod will utilize push-pin inserts for attachment to mounting brackets. This design meets all of the customer requirements as outlined in Section 5 by providing effective airflow, improving downforce, is easily manufactured, and is easily removable for servicing.

6.3.1 Side-Pod, Leading Edge, and Endplate

The 2014 side-pods allows for the utilization of the 2013 undertray molds for the manufacturing process. This mold is not wide enough in its current state, but will not

require completely new manufacturing and fabrication of molds for use on 2014. This design utilizes a slight offset in a template style carbon lay-up strategy using printed templates. This design also utilizes the identical molds and manufacturing processes for creating the undertray and the leading edges. The 2013 undertray mold can be seen in the Figure 145 below.

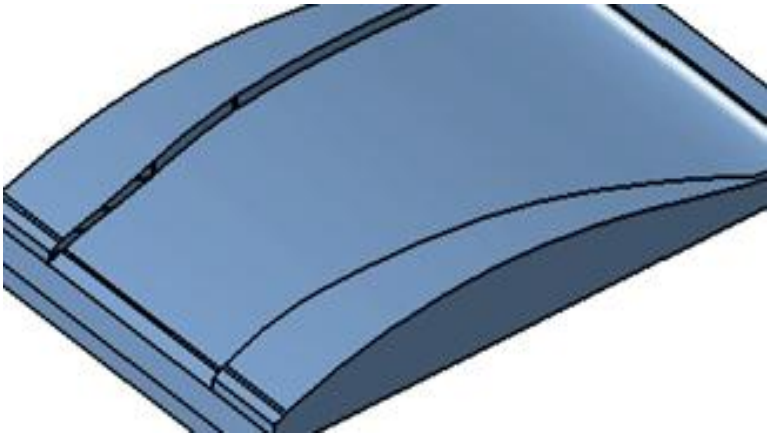

Figure 145: 2013 undertray mold from CATIA V5.

Toray T800 Carbon-fiber Pre-preg

The 2014 side-pod, endplate, and leading edge are manufactured with a 1-core-1 lay-up schedule. These components will utilize Toray T800 Plain Weave Carbon-Fiber [22]

Rohacell® Low-Density Foam Core

The aerodynamics elements of the 2014 car used a new type of foam core, Rohacell IG 31, rather than the previous used Hexcel HRH-10-1/8-3.0 honeycomb core

on the 2013 vehicle. The material properties for this foam are provided by the manufacturer, Evoniks Industries AG [20]. Rohacell Industrial Grade (IG) foam is 6mm thick, closed cell foam (polymethacrylimide) which is commonly used for pre-preg processing, similar to the carbon-fiber pre-preg construction used by *GFR* [22]. It is easy to machine and shape, thus will be greatly utilized on the complex parts of the aerodynamics system, particularly on this side-pod.

Lay-Up Schedule

The sample lay-up schedule can be seen in the Figure 146 below.

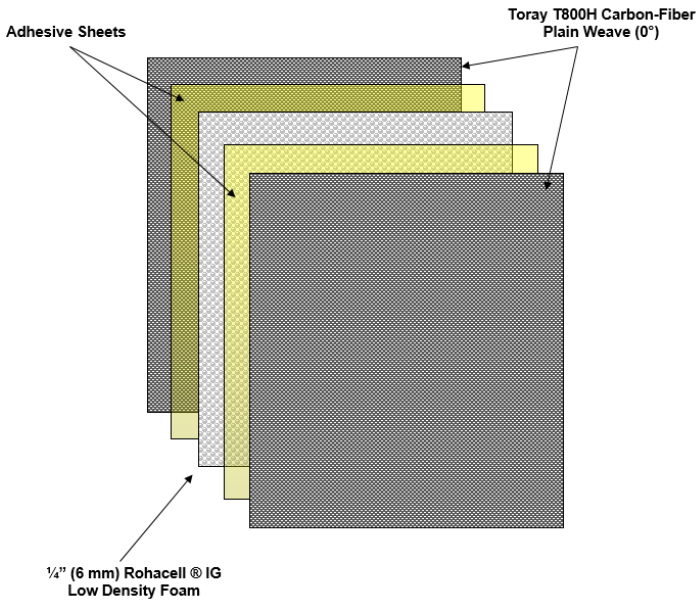

Figure 146: 1-Core-1 lay-up schedule with adhesive sheets.

Lattice Structure

Reducing weight on the 2014 aerodynamics package, required investigations into the benefits of a core "lattice" structure to use for component structural support. An

example of the lattice structure that is used on the 2014 side-pod and endplate is shown below in Figure 147.

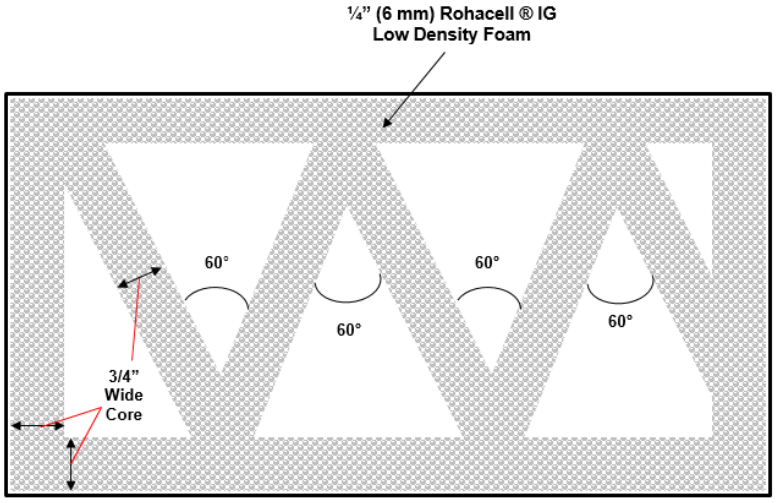

Figure 147: Foam core lattice lay-out for 2014 Side-Pod, Endplate, and Leading Edge.

The lattice structure above provides stiffness and rigidity to any torsional forces the component may experience, while allowing for a weight reduction due to the reduction in the amount of core used. The components will also have core around the perimeters to provide strength in the event of impact as well as for other structural purposes.

Side-Pod

Carbon-Fiber Cutting/Positioning Template

The template to be used for the lay-up of the side-pod in relation to the layout template of the 2014 undertray can be seen below.

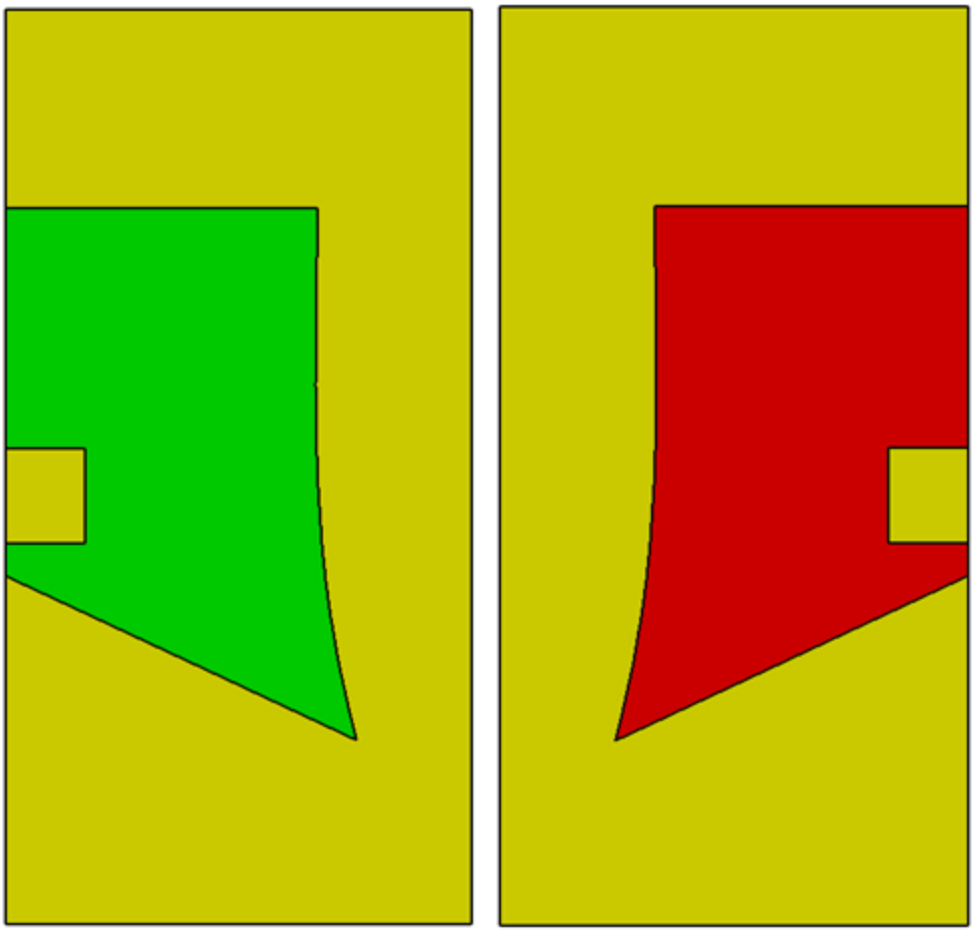

Figure 148: Carbon-fiber printed template to be used for 2014 side-pods. Left hand side-pod mold (left) and right hand side-pod mold (right) are shown.

In the above template, the yellow region is the unfolded top surface of the 2014 undertray, which will be used when locating the side-pod template for proper profile shape and size. The red and green regions specify the side-pod carbon-fiber lay-up region. This engineering drawing can be found in Figure B 1: Three view engineering drawing of 2014 side-pods., in Appendix B.

Endplate

The 2014 endplate will be manufactured using a carbon-fiber lay-up schedule and

foam core lattice structure as shown in Figure 146 and Figure 147. This particular component will be manufactured using carbon-fiber, laid up on a sheet-metal mold laser-cut to match the identical size, shape, and hole cut-outs for fasteners to hard point locations. A drawing of this A36 steel 12 gauge sheet-metal mold manufactured by GK Machining is shown in Figure B 2 of Appendix B. This mold can be used for both the right-hand and left-hand endplates, although this can only be used for one endplate at a time.

Endplate Gurney Flap

The vertical gurney that attaches to this endplate will be made using a custom CNC manufactured mold by the Aerodynamic Manufacturing Engineer. This will consist of six plies of Toray T800 PW (0°) lay-up schedule similar to that of the rear and front brackets.

Endplate Gurney Slot

The endplate gurney slot on the bottom of the endplate will be manufactured by laying carbon-fiber over a square aluminum block. This will give us the sharp inside corners of the “h” shape. This will also be manufactured with an 8 plies lay-up schedule shown in Figure 149.

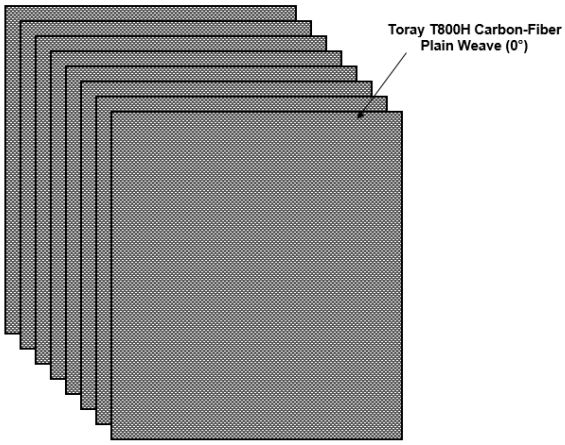

Figure 149: 8-ply carbon fiber endplate gurney slot lay-up schedule

The hard points of the endplate will be located with screws placed in the through-hole locations in the sheet metal mold, and will be built up to correspond to the hard points located on the internals of the undertray.

Side-Pod Leading Edge

The side-pod leading edge will be constructed using similar methods to the side-pod top profile in regards to a printed template. This particular leading edge will be cut in such a way that the split line shown in Figure 140 will be lined up with the split between the joggle molds. An example of the leading edge template is shown below in Figure 150.

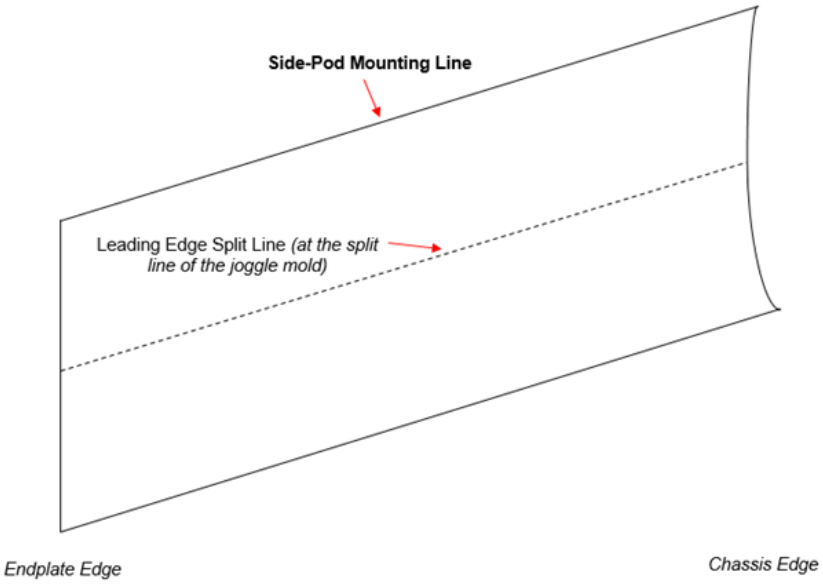

Figure 150: Printed template showing leading edge features used for cut-out and placement in the undertray mold.

This leading edge will utilize a three carbon-fiber ply lay-up schedule shown in Figure 151.

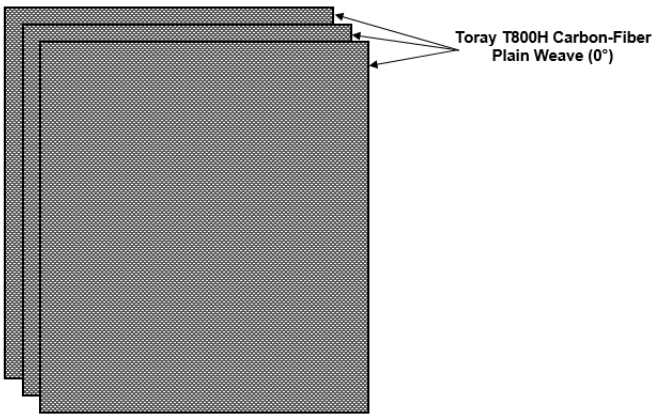

Figure 151: Three ply carbon-fiber lay-up schedule for the leading edge

The following Figure 152 is a view of the side profile of the joggle mold currently

on the 2013 undertray mold that will be used to create the leading edge.

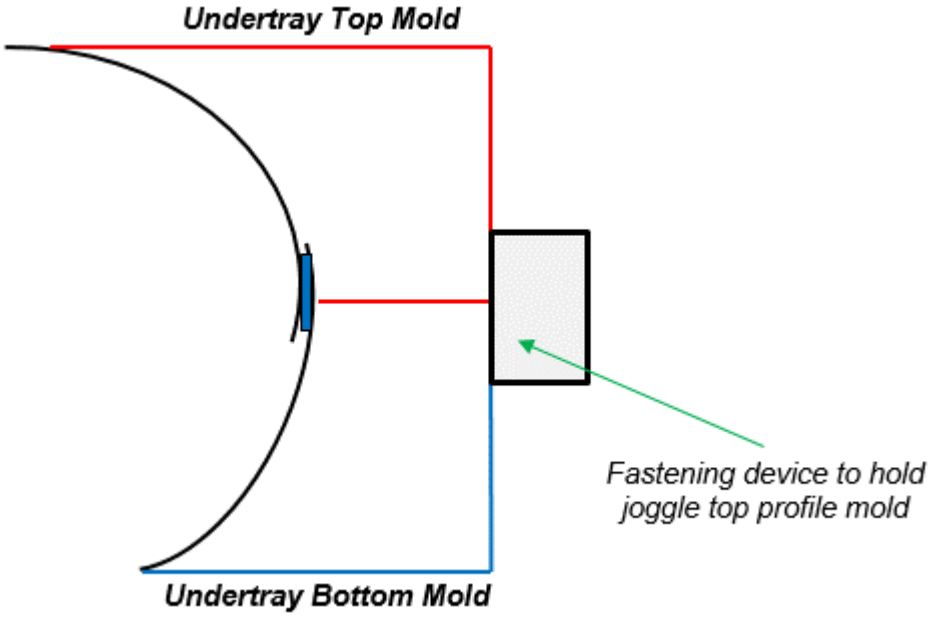

Figure 152: Joggle mold and leading edge construction schematic

6.3.2 – Front Ducting

The front ducting will be made using printed templates much like that of the side-pod. This will be constructed in a two-piece construction process. The two pieces will be constructed on sheet-metal plates in the composites lab, and will be epoxied together after curing. The engineering drawing below gives a brief overview of the overall shape and interface with the radiator. The carbon templates can be seen in Figure C 2 and Figure C 3, in Appendix C.

This front ducting is composed of three layers of Toray T800 Plain Weave Carbon-Fiber shown in the lay-up schedule below.

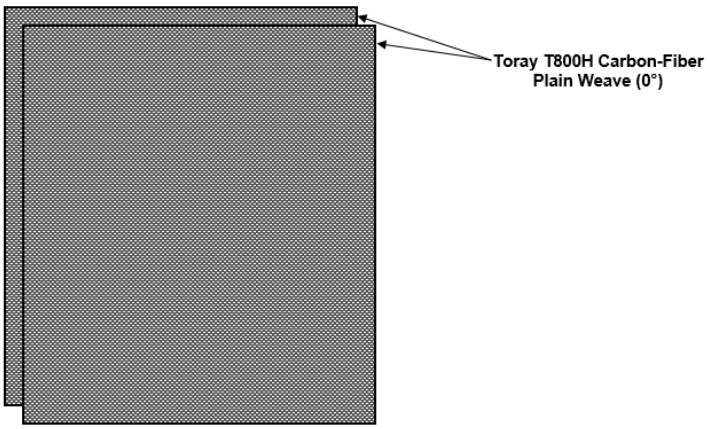

Figure 153: Lay-up schedule of carbon-fiber for front ducting.

6.3.3 – Rear Ducting

The rear ducting will be made using the 2014 front wing flap molds. They will also incorporate a printed template for location matching of wing profile. An engineering drawing of the rear ducting is shown in the Figure B 4, in Appendix B.

The rear ducting will be made in multiple processes. The top and bottom flap elements will be made separately using the front wing mold. The vertical supports will both be manufactured individually, as well as all of the attachment flanges, using printed templates. Each flange will be epoxied to the vertical supports, which will then be epoxied to the top flap elements. All components of the rear ducting will be constructed using three layers of Toray T800 Plain Weave Carbon-Fiber. This lay-up schedule is shown in Figure 154.

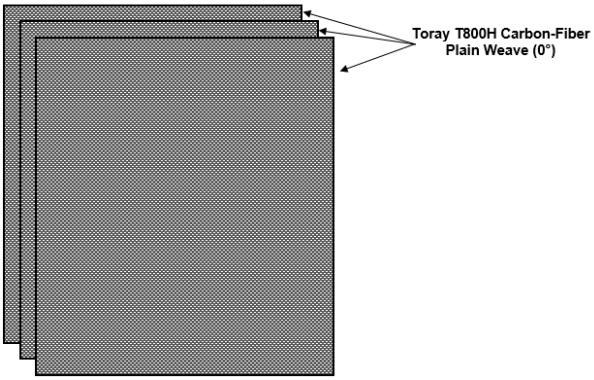

Figure 154: Three ply lay-up schedule for rear ducting

The vertical supports and flange templates, and wing flap size and placement are shown in the Figure C 4 of Appendix C. These templates will be placed in the front wing mold. The outer edge of the template is the front of the bottom mold of the front wing flap element. This template will be used to correctly space the carbon-fiber during lay-up to achieve the correct wing profile for the rear ducting.

6.3.4 – Fan Shroud

The fan shroud for the 2014 cooling package will be constructed using carbon-fiber. This sheet-metal mold is laser-cut and bent by GK Machining. The carbon-fiber will be laid up on the outside of the mold to give the desired shape and dimensions. This particular component will utilize two plies of carbon-fiber and a special ⅛” low density foam. The 1-core-1 lay-up schedule for the fan shroud can be shown in the Figure 155 below.

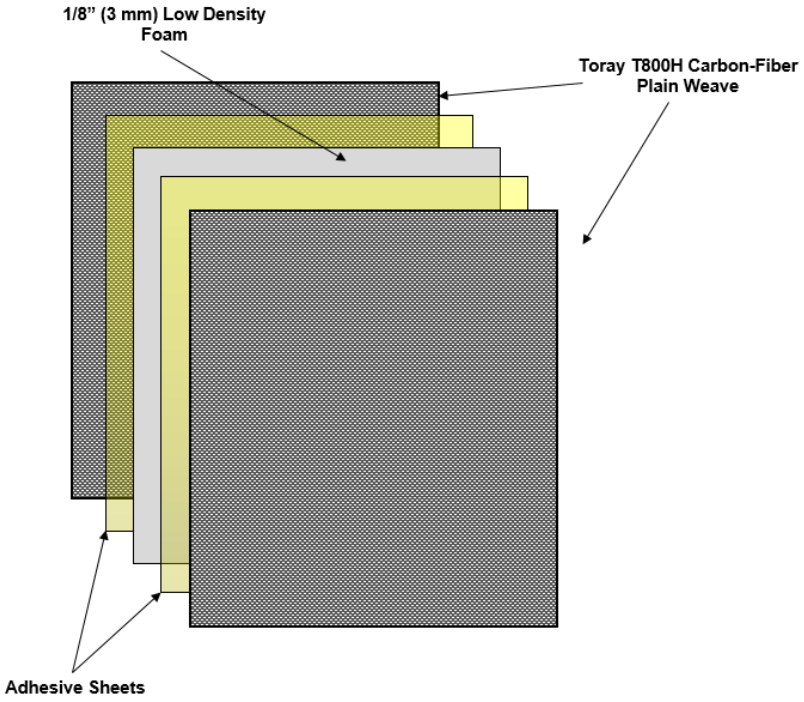

Figure 155: Fan shroud lay-up schedule.

The engineering drawing for the fan shroud can be seen in the Figure B 5, in Appendix B. The carbon will be cut, folded, and laid up on the GK mold using the template shown in Figure C 5, in Appendix C.

6.3.5 – Fill Cap Cover

The fill cap cover is a relatively simple piece to make, and will be manufactured out of two plies of Toray T800 Plain Weave Carbon-Fiber. The mold used to make this piece will be constructed out of sheet-metal, laser-cut and bent by GK Machining. An engineering drawing for this part is shown in Figure B 6, in Appendix B.

This mold includes bends to create accurate flanges during carbon-fiber lay-up as to keep the same shape as that in the GFR14 CAD model. These flanges will be the

support for the Velcro attachment strips. The “unfolded” view of the above engineering drawing illustrates the necessary dimensions for the carbon-fiber to be cut. The carbon lay-up of this cap cover can be seen in Figure 156. The carbon will be laid up on the underside of the mold.

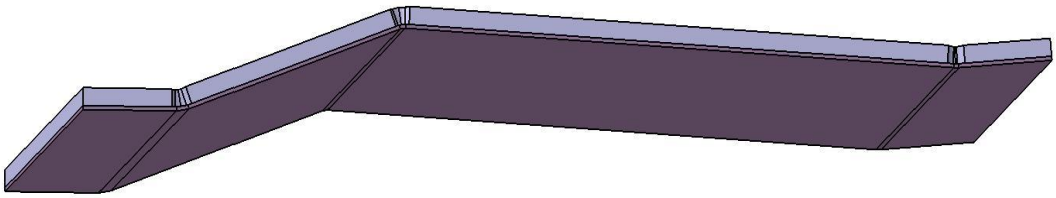

Figure 156: Fill cap cover mold with carbon-fiber pre-preg lay-up.

The lay-up schedule for this part consists of two plies of carbon-fiber pre-preg, shown in Figure 157.

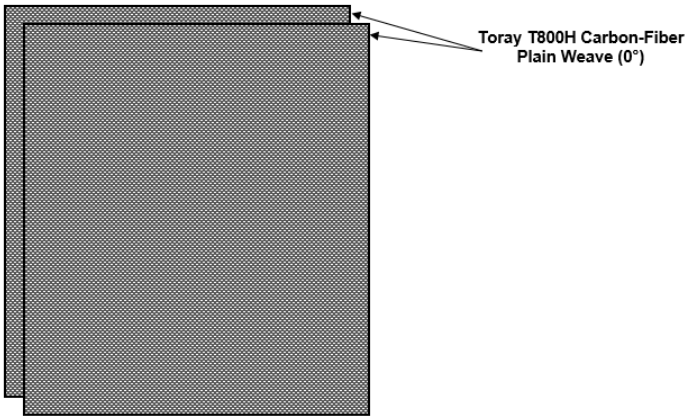

Figure 157: Two ply carbon-fiber lay-up schedule for fill cap cover.

6.3.6 – Brackets, Fasteners, and Mounting

6.3.6.1 Front Bracket

The front attachment bracket for the side-pod and undertray rod ends will be made using a sheet-metal mold for carbon-fiber lay-up. This mold is laser-cut and bent by GK Machining. The engineering drawing can be seen in Figure B 7, in Appendix B.

The sheet-metal mold is to be used as the base for the carbon-fiber lay-up. These brackets will be made of six plies of Toray T800 Plain Weave Carbon-Fiber for structural strength in supporting the loads of the undertray and side-pod. Figure 158 demonstrates the CAD model of the finished carbon-fiber bracket laid up on the sheet-metal mold. This bracket with six plies will be approximately 1.2 mm thick.

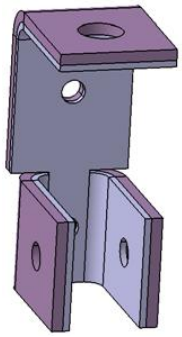

Figure 158: Carbon-fiber (purple) bracket laid up on the sheet-metal mold (grey).

This mold was designed to account for 1.2 mm of carbon to provide the correct final dimensions of the carbon-fiber bracket once all the plies have been placed and cured. This mold provides the exact inner dimensions desired for the rod-ends, and allow for room to place extra carbon-fiber on the inside of the mold area once the first part has cured. This will allow for manual placement of carbon-fiber plies on the rod-end

connection area to reduce any play that the rod-end may experience.

6.3.6.2 Rear Bracket

The rear mounting bracket required two separate sheet-metal molds for carbon-fiber lay-up. This particular bracket is not symmetric, thus there was a need for handed parts. Although the parts are identical in size and shape, one mold is needed for both the left and right-hand side of the vehicle. This bracket is laser-cut and bent by GK Machining. The engineering drawing can be seen in Figure B 8, in Appendix B.

This bracket is also designed to account for a 1.2 mm offset of four plies of T800 Plain Weave Carbon-Fiber (0°) and two plies of Toray T800 Plain Weave (45°) to account for shear stress from twisting the main switch on. This can be seen in the image below in which the carbon-fiber is placed on the correct side of the mold to produce the correct dimensions.

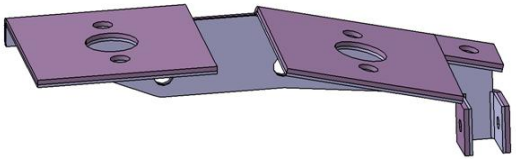

Figure 159: Rear bracket manufactured using carbon-fiber (purple) laid up on sheet-metal mold (grey).

The lay-up schedule for this bracket can be seen in Figure 160.

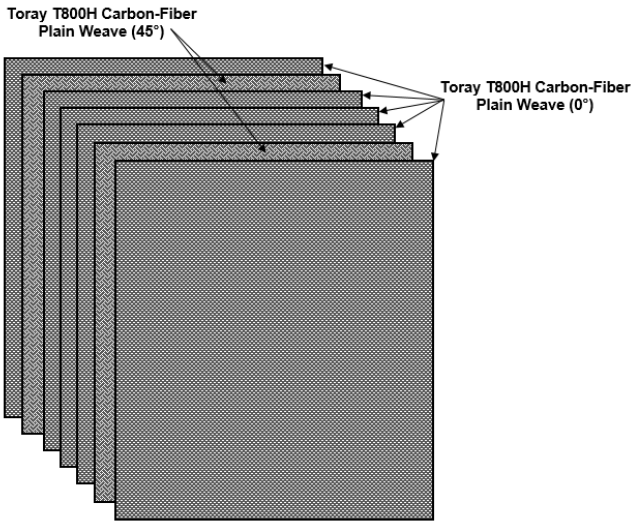

Figure 160: Six ply carbon-fiber lay-up of four plies of Toray T800 Plain Weave (0°) and two plies of Toray T800 Plain Weave (45°) for rear brackets.

6.3.6.3 Side-Pod/Endplate Bracket

The endplate and side-pod interface brackets are manufactured using one mold which produces ten brackets in one curing cycle. These brackets are produced using six plies of Toray T800 Plain Weave carbon-fiber, laid up on a sheet-metal mold laser-cut and bent by GK Machining. The lay-up schedule for this bracket is identical to the lay-up schedule of the front and rear brackets. The mold is shown in the Figure 161 below.

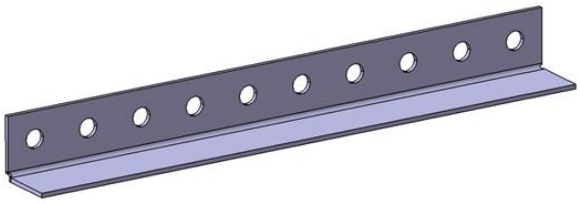

Figure 161: Sheet-metal mold for side-pod/endplate bracket construction.

This particular mold allows for more effective and efficient bracket

manufacturing given the amount of brackets that can be made from one mold. Each bracket is properly spaced to give the correct dimensions given the rivet whole locations. The engineering drawing for the above mold is shown Figure B 9, in Appendix B. The carbon-fiber for this bracket will be laid up on the insider of the above mold. This will allow for trimming of carbon-fiber to produce the same dimensions as necessary to align correctly with the fastener holes on the side-pod top surface.

6.3.7 Manufacturing Part Summary

All of the above parts are to be manufactured by the 2014 aerodynamics team using multiple molds provided by GK Machining. Other parts are to be manufactured using printed templates for carbon-fiber ply placement and as templates for cutting. To provide a summary of all of the manufacturing needs for the 2014 side-pod package, the following Table 51 provides an extensive list of all parts manufactured, sponsor provided, and/or purchased.

Table 51: 2014 side-pod complete parts and required material breakdown

Part/Component	cCar Quantity	eCar Quantity	Material	Origin	Supplier
Side-Pod	2	1	T800 Plain Weave Carbon-Fiber	Manufactured	GFR14
Leading Edge - Mold	1	1	Renshape Tooling Board	Manufactured	GFR14
Endplate	2	2	T800 Plain Weave Carbon-Fiber	Manufactured	GFR14
Endplate - Mold	1	2	12ga A36 Steel	Laser-Cut and Bent	GK Machining
Front Ducting	2	1	T800 Plain Weave Carbon-Fiber	Manufactured	GFR14
Rear Ducting	2	1	T800 Plain Weave Carbon-Fiber, Paper Foam, Adhesive Sheet	Manufactured	GFR14
Rear Ducting - Mold	1	1	Renshape Tooling Board - Front Wing	Manufactured	GFR13
Cooling Fan	2	N/A	N/A	Purchased	A1 Electric
Fan Shroud	2	N/A	T800 Plain Weave Carbon-Fiber, Paper Foam, Adhesive Sheet	Manufactured	GFR14
Fan Shroud - Mold	2	N/A	12ga A36 Steel	Laser-Cut and Bent	GK Machining
Fill Cap Cover	2	1	T800 Plain Weave Carbon -Fiber	Manufactured	GFR14
Fill Cap Cover - Mold	4	1	12ga A36 Steel	Laser-Cut and Bent	GK Machining
Front Bracket	2	1	T800 Plain Weave Carbon -Fiber	Manufactured	GFR14
Front Bracket - Mold	6	2	18ga A36 Steel	Manufactured	GK Machining
Rear Bracket	2	1	T800 Plain Weave Carbon -Fiber	Manufactured	GFR14
Rear Bracket - Mold	6	2	18ga A36 Steel	Manufactured	GK Machining
Side-Pod/Endplate Bracket	4	2	T800 Plain Weave Carbon -Fiber	Manufactured	GFR14
Side-Pod/Endplate Bracket - Mold	1	N/A	14ga A36 Steel	Manufactured	GK Machining
Potted Insert	4	2	Composites	Manufactured	Marketing Masters
M8 Nylon Pry Rivet	8	4	Nylon	Purchased	WPS
M4x12mm bolt	4	2	Steel	Sponsored	Portland Screw
M4 nut	4	2	Steel	Sponsored	Portland Screw
M5x8mm bolt	4	N/A	Steel	Sponsored	Portland Screw
1/4-20 bolt	8	N/A	Steel	Sponsored	Portland Screw
1/4" nut	8	N/A	Steel	Sponsored	Portland Screw
Toray T800 PW Carbon-Fiber	N/A	N/A	90° Carbon Fiber	In Stock	OSU Composites Lab
Hexcel Honeycomb 1/4" Core	N/A	N/A	Honeycomb Core	In Stock	OSU Composites Lab
Film Adhesive	N/A	N/A	Film Adhesive	In Stock	OSU Composites Lab
Vacuum Bag	N/A	N/A	Vacuum Bag	In Stock	OSU Composites Lab
Release Film	N/A	N/A	Release Film	In Stock	OSU Composites Lab
Peel Ply	N/A	N/A	Peel Ply	In Stock	OSU Composites Lab
Cotton Breather	N/A	N/A	Cotton Breather	In Stock	OSU Composites Lab
Adhesive Sheet	16	6	Adhesive Sheet	In Stock	OSU Composites Lab
Thin Paper-Foam Sheet	4	1	Foam Sheet	In Stock	OSU Composites Lab
Velcro	N/A	N/A	Velcro	Purchased	GFR14

6.3.8 Manufacturing Schedule

All the parts to be included in the 2014 side-pod system are manufactured in-house, from carbon-fiber. The following is a schedule for manufacturing the side-pod components.

Table 52: Manufacturing Schedule for 2014 side-pod

Manufacturing Task	Start Date - Finish Date
Sand Undertray Mold	Week 1 (1/7) - Week 2 (1/18)
Print Templates: Side-Pod, Leading Edge, Brackets, Ducting, Fan Shroud, Fill Cap	Week 3 (1/19)
Side-Pod (RH) Manufacturing - Carbon Cutting, Core Cutting/Chamfering + Cure	Week 4 (1/19)-Week 5 (2/8)
Side-Pod (LH) Manufacturing - Carbon Cutting, Core Cutting/Chamfering + Cure	Week 6 (2/10-2/16)
Leading Edge Manufacturing	Week 4 (1/19), Week 5 (2/8), Week 6 (2/12), Week 7 (2/19)
Endplate (RH) Manufacturing - Carbon Cutting, Core Cutting/Chamfering, Hard points countersinking + Cure	Week 4 (1/26) - Week 6 (2/14)
Endplate (LH) Manufacturing - Carbon Cutting, Core Cutting/Chamfering, Hard points countersinking + Cure	Week 6 (2/15) - Week 7 (2/21)
Ducting Manufacturing - Front and Rear	Week 6 (2/10-2/16)
Fan Shroud Manufacturing - Carbon cutting, core cutting	Week 4 (1/30) - Week 7 (2/22)
Front Bracket Manufacturing	Week 4 (1/30) - Week 6 (2/13)
Rear Bracket Manufacturing	Week 4 (1/30) - Week 6 (2/13)
Side-Pod Endplate Bracket Manufacturing	Week 4 (1/30) - Week 6 (2/13)
Fan Shroud and Radiator Assembly	Week 6 (2/14)
Radiator/Undertray Side-Pod Assembly	Week 8 (2/23-2/28)
Side-Pod/Undertray Assembly: Car Ready	Week 9 (3/8)
Full Car Assembly/Troubleshooting	Week 10 /11 (3/9) - (3/29)

7. Manufacturing Implementation

This section will cover the process used to manufacture the complete side-pod package for 2014.

7.1 Mold Preparation

As discussed in Section 6.3, the design of the 2014 side-pod utilized previous molds designed for the 2013 undertray. These molds however, we outdated for 2014 design of both the side-pod and undertray and needed modification. The molds would maintain the same profile; however the 2014 parts were designed to be much wider, thus requiring a widening of the molds. This is described in the following sub sections. The undertray molds can be seen in Figure 162.

Figure 162: 2013 undertray molds to be sanded down for 2014 manufacturing

7.1.1 Sanding Undertray Molds – Top and Bottom

Rather than subjecting the RenShape® molds to a secondary CNC operation and in order to reduce manufacturing time associated with producing G-code and scheduling machine time, the molds were widened using a sanding operation. The sanding was done using pneumatic, dual-action orbital sander. This mold modification process required six sanding operations.

Initial roughing operations for widening mold by removing the edges and removing excess RenShape® was done with 40 grit paper and an orbital sander.

Figure 163: Mold removal with initial 40-grit roughing operation

Once the majority of the material was sanded down to about 1/8” from milled surface, the molds were hand-sanded using 80 grit paper. Using a long sanding block, the edges were ground down until initial scratching began to appear on the smooth surface, indicating that these surfaces were level.

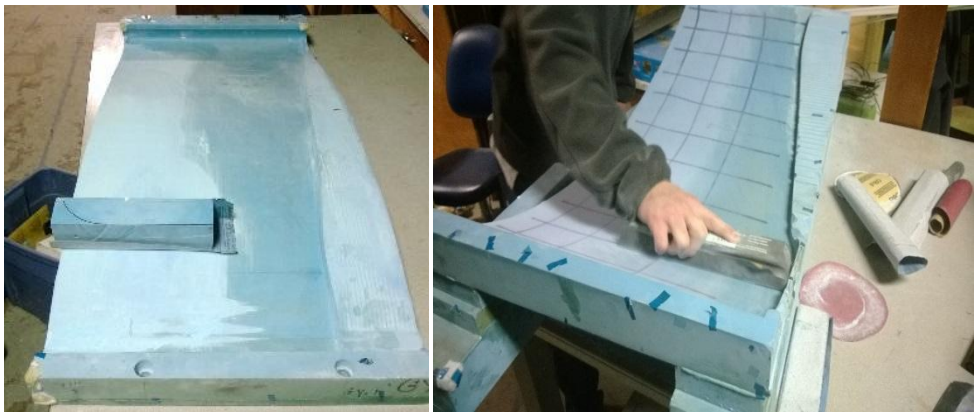

Figure 164: 80-grit sanding operation to level mold surfaces

Any low regions were filled with specialized Ren-Weld® Resin and hardener. These areas were filled in and flushed with surrounding regions and made level with a long, spreader. This is shown in Figure 165.

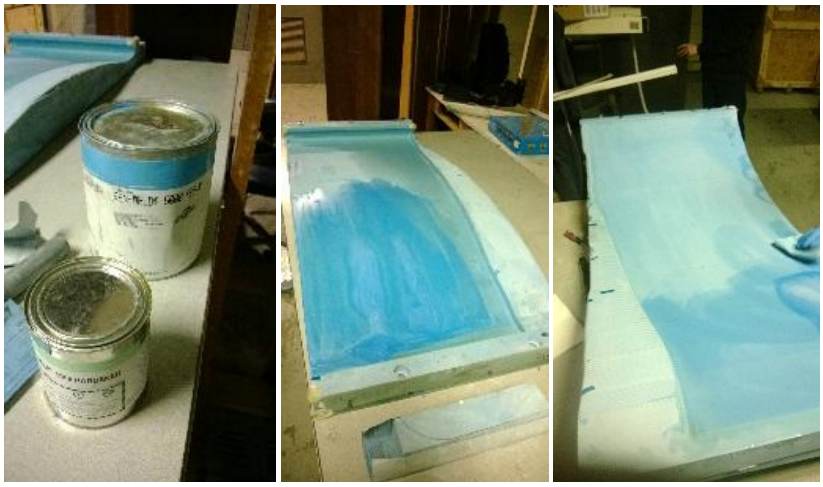

Figure 165: Filling low areas with Ren-Weld epoxy resin

These surfaces were then re-sanded with 80 grit to remove excess epoxy resin build up. This is seen in Figure 166.

Figure 166: Re-sanding surfaces to remove excess epoxy resin

The entire mold surface was then stepped-down and sanded with 200 and 250 grit to increase the smoothness, and was finished with a 600 grit dry and wet-sand to provide a polished surface. Once the sanding was complete, the molds were then sealed with five coats of a RenShape® mold sealant solution.

Each coat was spread into an even thin film layer with a cotton rag. This was a necessary process to allow the molds to be used for carbon-fiber lay-up without the risk of resin absorption into the tooling board composite foam of the RenShape® mold. The finished mold surfaces can be seen in Figure 167.

Figure 167: Final top and bottom undertray profile molds

7.2 Supplier Molds - GK Machine

This section will strictly outline the molds that were machined by GK and how we planned to use them for the carbon lay-up. This will be a brief run through of the different molds they made for the different parts of the side-pod system. I will also discuss the process of preparing these molds for use with carbon fiber and in the oven (All molds need to be cleaned with acetone, and layered with at least 10 layers of mold release, etc.)

The majority of parts had associated molds that were manufactured by GK Machine and used for carbon fiber lay-up. These molds were made of A36 grade steel which were laser cut and bent to specifications of the engineering drawings as seen in Appendix A. Each mold is outlined in this section, along with a designation detailing which side would be used to lay-up carbon in order to provide accurate part dimensions that matched the CAD models.

7.2.1 End Plate Mold

This mold was laser cut to shape to match the profile of the side-pod and included holes for proper line-up of hard points for mounting and integration with the undertray.

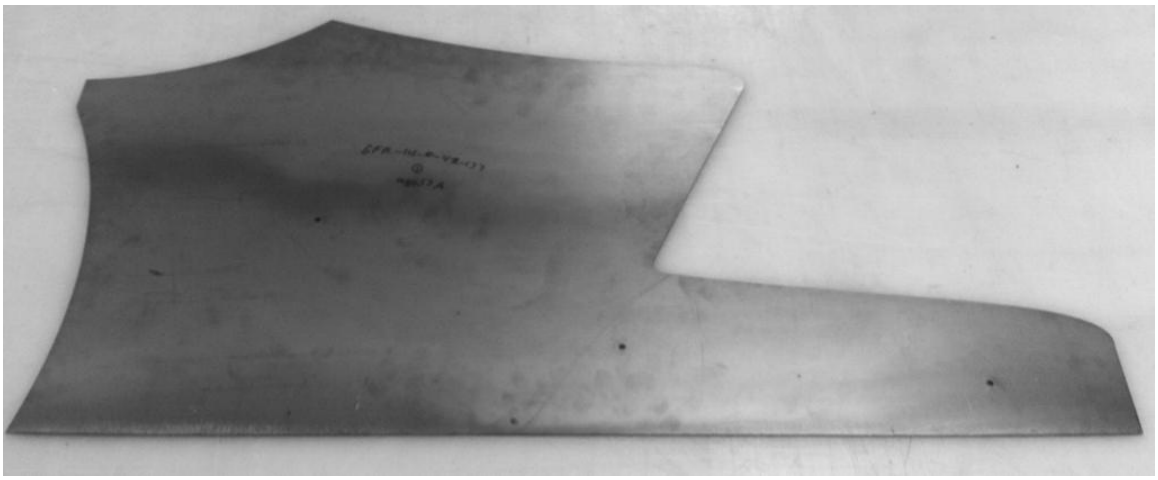

Figure 168: Endplate mold provided by GK Machine

Carbon was laid up on the corresponding side in which the endplate was to be positioned on the vehicle. This mold was universal; meaning the surface shown in Figure 168 represented a right-handed endplate, whereas the reverse side corresponded to the left-hand side of the vehicle.

7.2.2 Fan Shroud Mold

GK Machine provided two fan shroud molds which allowed for an increase in production by allowing two fan shrouds to be produced during a single oven cure cycle. Given the large quantity of fans on the vehicle, as well as back-up fans in stock in case of failure, four fan shrouds were manufactured.

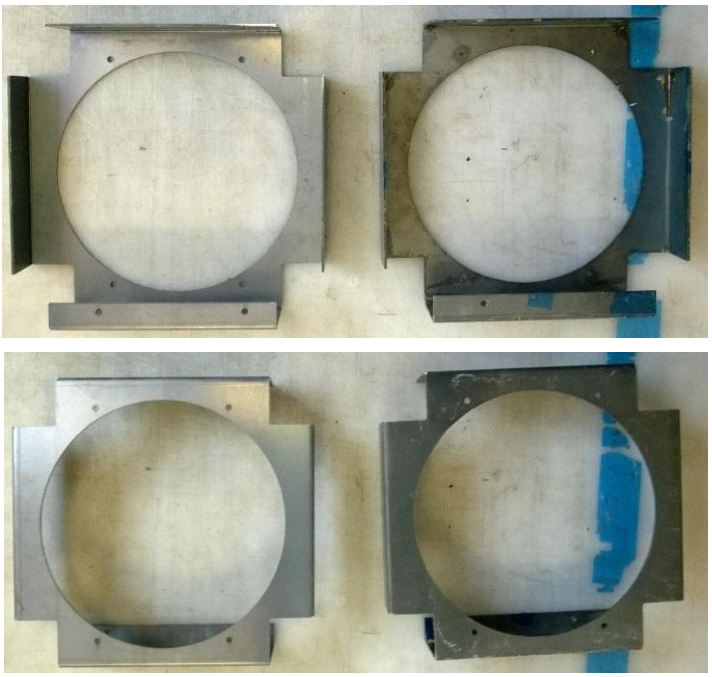

Figure 169: Fan shroud molds provided by GK Machine

The dimension of these two shrouds was offset in design to allow for carbon lay-up on the outer surface of the bends and flanges.

7.2.3 Front Bracket Mold

Due to the rather complex shape of the front bracket design, these molds were also laser cut and bent to be used with carbon fiber. There were a total of eight molds to be used, which allowed for enough brackets for use on both the cCar and eCar with four additional spares, in one cure cycle. This greatly improved manufacturing time, and allowed for focus on other more time consuming aspects of fabrication.

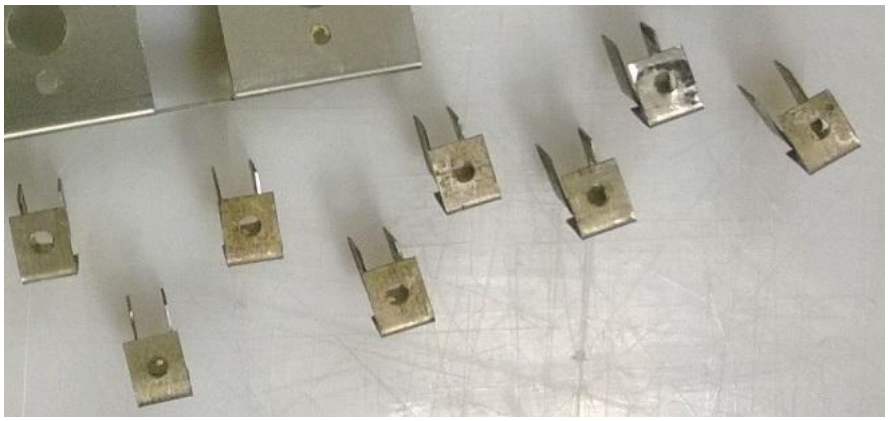

Figure 170: Front bracket molds (eight) provided by GK Machine

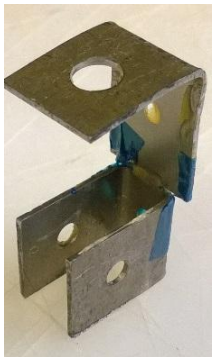

Figure 171: Front bracket mold provided by GK Machine

These bracket molds were used to lay-up carbon on the outer surfaces of the sheet-metal and were designed with an offset to provide accurate final dimension according to CAD model designs.

7.2.4 Rear Bracket Mold (RH/LH)

This particular bracket was a last minute design that needed to implement a mounting strategy for the main power switch, undertray rods, and side-pod. In order to

reduce design time, these molds were made as mirror images for the left and right hand sides of the vehicle, even though no switches exist on the left hand side. These molds were outsourced for manufacturing due to the complexity the design including multi-angled bends that could only be done accurately using professionals machine equipment.

Figure 172: Rear Bracket (right-hand shown) provided by GK Machine

Figure 173: Comparison of left and right handed rear bracket molds

These molds were also designed for offsets due to material thickness of carbon fiber lay-up on the outer surface, in order to match specifications of the CAD model.

7.2.5 Side-Pod Endplate Bracket Mold

This mold was machined to allow for manufacturing of ten brackets in one cure cycle. The holes were also machined so that they could be easily located and sized during post-processing operations.

Figure 174: Side-pod/endplate bracket mold provided by GK Machine

These molds required lay-up on the internal bend of the metal, which required trimming of carbon-fiber before curing. This guaranteed that each bracket would be 1”x1” and could be cut evenly to 1” width.

7.2.6 Fill Cap Cover Mold

This mold was designed to incorporate the downward slope of the side-pod profile, while maintaining an apex at the projected location of the radiator.

Figure 175: Fill cap cover mold provided by GK Machine

Figure 176: Fill cap cover mold (side-view)

7.3 Material

This section will briefly cover the materials used in all/most of the parts and how to properly use them/why we use them.

The fabrication of the components used in the side-pod package are all constructed of composite structures, mainly carbon-fiber, with additional use of core material for strengthening purposes. These materials will be shown in the following subsections.

7.3.1 Carbon Fiber

All of the parts seen in this thesis are constructed of Toray T800 Plain Weave carbon-fiber pre-preg. This is shown in Figure 177.

Figure 177: Toray T800H plain weave (0°) carbon-fiber pre-preg

For additional applications in which there may be torsional stresses, in the case of the rear bracket caused turning the main power switch, Toray T800 Plain Weave 45° carbon-fiber pre-preg was used. This is shown in Figure 178.

Figure 178: Toray T800H plain weave (45°) carbon-fiber pre-preg

7.3.2 Adhesive Sheets

The adhesive sheets used for adhering carbon-fiber to the foam core material are shown in Figure 179. This adhesive, ACG MTA241 by Advanced Composites Group Ltd., provides a way to adequately bond the two materials together in the event of a sandwich panel construction, as discussed in Section 2.3.3.

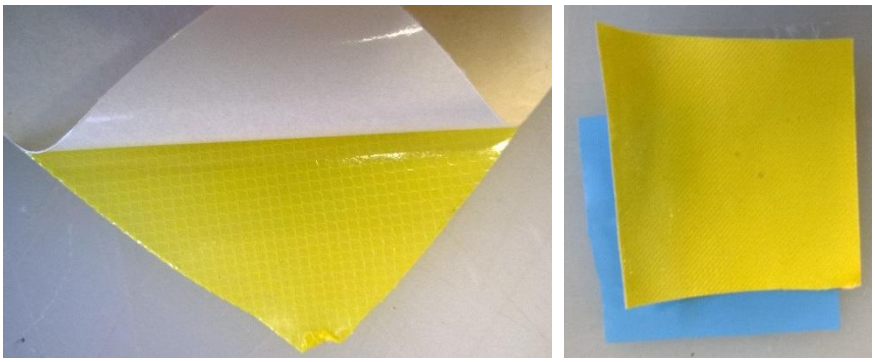

Figure 179: ACG MTA241 adhesive sheets

7.3.3 Rohacell® Foam Core

Initially, the manufacturing plan for the side-pod utilized honey comb core material. Due to tedious machining operations in shaping the core, the design transitioned to use Rohacell® a closed-cell foam core, with the same density of 2 lbs/ft^3 as the honey comb core used in previous aerodynamics packages.

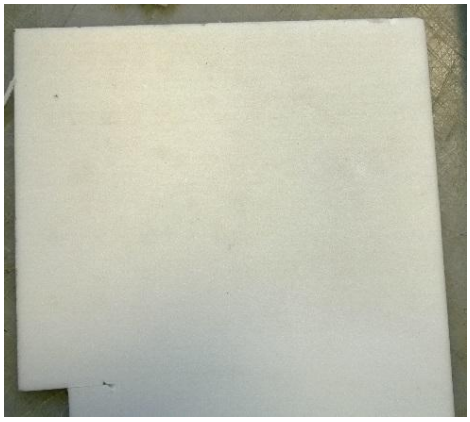

Figure 180: Rohacell foam sheet used as core material

7.4 Vacuum Bagging

This section will briefly detail the process used in the vacuum bagging of all of the carbon-fiber parts, materials that were used, and the issues that were encountered.

7.4.1 Materials

The materials used in the vacuum process are described in this section.

1. **Acetone:** Solvent solution used for cleaning tools, metals, molds, and removing any oils, grease or dirt.

2. **Mold Release:** Silicone dry lubricant that prevents the carbon-fiber from adhering to the mold surface.

Figure 181: Aerosol mold release agent used for carbon-fiber manufacturing

3. **Peel Ply:** Typically a porous fabric for absorption during resin flow, with a high strength to resist tearing during vacuum pull.

Figure 182: Peel ply porous material

4. Release Film: Smooth film material used to provide simple method of removing part after curing. This material keeps the bag from sticking to the resin pulled during vacuum and absorbed by the peel ply.

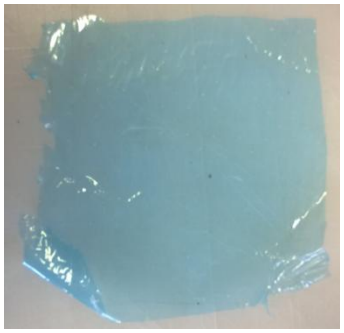

Figure 183: Release film

5. Cotton Breather: Also known as a breather material, the cotton acts as a distributor for the vacuum and for escaping gasses. Also is used to act as a buffer between the bag pleats/wrinkles and the part surface. Typically high porosity and strong enough to not collapse under vacuum.

Figure 184: Cotton breather

6. Vacuum Bag: Strong polymeric film material used to cover the entire part surface and apply vacuum pressure to all areas of the part and withstand pressure from the vacuum without tearing. The material is flexible enough to conform to the shape of the part and withstand curing temperatures. The vacuum bag is the last material laid up on the part.

Figure 185: Vacuum bag

6. Sealant Tape: Highly adhesive polymeric tape available in thin strips on large rolls. The sealant is placed around the entire part assembly to create an

airtight seal around the part to prevent air from leaking into the bagging system during vacuum. This material is strong enough to withstand shear forces caused by the bag, and be able to withstand high temperatures during curing.

Figure 186: Sealant Tape

8. Vacuum Fitting: Metal valve that allows air to be drawn from the bag and connects to vacuum lines leading to the vacuum compressor. The valve is placed on the cotton breather and sandwiched by the vacuum bag.

Figure 187: Vacuum valve (assembled - left; disassembled - right)

9. Hoses: Standard hoses used to draw air from the vacuum fitting to the compressor system.

Figure 188: Vacuum hoses

10. Pressure Gauge: Device used to measure the vacuum pressure in the bagging systems to verify correct pressure readings for successful part curing.

Figure 189: Vacuum pressure gauge

7.4.2 Vacuum Bagging Process

The vacuum process used to manufacture the carbon-parts in the side-pod system is as follows:

1. Clean the mold by applying acetone to all surfaces in contact with carbon-fiber and allowed to dry.
2. Prepare the mold by coating it with 2-3 layers of mold release, while waiting approximately 5 minutes to allow each coat to dry before reapplying.
3. Build up the part by placing layers of pre-preg and/or core in desired areas and in proper lay-up schedule.
4. Place peel ply over the laminate (pre-preg) stack, allowing for extra to leave slack to fill in all areas.
5. Place release film over the same areas of the peel ply of the same shape and size, also allowing some extra for slack.
6. Apply the cotton breather material across the part. Typically strips will work fine, making sure that there are no long distances where breather is absent. Improper distribution of the vacuum due to lack of breather can lead to insufficient pressure needed during curing. This can lead to a decrease in strength of the final part.
7. Fit the bottom half of the vacuum valve on top of the breather, making sure that the valve does not contact any pieces of the carbon. This will lead to a damaged part.
8. Apply sealant tape around the entire assembly.

9. Lay the vacuum bag over the assembly; push the top-half of the vacuum valve through the bag. Press onto the sealant to create an air-tight seal.
10. Activate the vacuum and check for leaks. Attach pressure gauge to verify bagging system pressure is less than 1 inHg of compressor unit. If not, check for leaks or re-bag.

7.4.3 Issues - Bridging

The main issue that was encountered during the manufacturing process was bridging of the carbon-fiber. As mentioned in Section 2.3, bridging occurred as a result of inadequate pressure due to insufficient contact between the vacuum bag and the part. This occurred primarily with the use of the Rohacell® foam core. To eliminate this, the core was chamfered at 45°, using sanding blocks, to eliminate any right angles that may not come in contact with the vacuum bag. The core was also cut at 45° angles to eliminate any bridging in corner areas where two pieces of car meet with one another, as seen by the angled cut in the lower-left of Figure 190.

Figure 190: 45° chamfer of Rohacell foam core

7.5 Oven Curing

Curing the carbon-fiber components is unique to the type of molds used to manufacture all of the aerodynamics parts. This section will outline the cure cycles for the two different molds used to manufacture parts.

Figure 191: Oven curing of RenShape molds

7.5.1 Curing RenShape Molds

With the use of RenShape, the cure cycle must be carefully chosen. The RenShape molds are particularly brittle and in the event of rapid cooling, they can easily crack and break, requiring manufacturing of completely new molds. Recommended cure

cycles begin at room temperature (~75°F) and only ever reaches a maximum of 250°F. The typical cycle temperature used for aerodynamic manufacturing is ramped up and down at +30°/-30°F. This ensures that too large of a temperature gradient will not cause thermal stresses in the mold and cause cracking. Once the oven has reached 250°F, the oven was held at this temperature for 10-12 hours in order to fully cure the T800 carbon-fiber pre-preg.

7.5.2 Overview of Curing with Sheet-Metal Molds (GK Machine)

Initially, the sheet-metal molds were cured in a cure cycle of 350°F temperature with ramp-up and down rates of +180/-300°F. Although this temperature is suitable for T800, the final products were complete failures. At this temperature, the sheet-metal began to expand more than anticipated, causing the carbon-fiber to adhere strongly to the molds. It was also assumed that the extreme ramp-down rate lead to some kind of vaporization and solidification of the resin in too short of a duration, causing extreme difficulty in removing the parts. In order to remove the carbon-fiber, all parts run in this cure cycle were damaged. The high thermal conductivity of steel also may have led to residual stresses in the carbon-fiber. With extreme temperature differentials between the outer surfaces of the pre-preg and the still high temperature sheet-metal during the -300°F ramp-down cycle, this would have caused significant stresses in the parts, causing removal difficulties. This also required a lot of post processing work to clean up the sheet-metal and remove hardened resin, carbon-fiber residue and re-finishing the surfaces in order to salvage the molds.

This led to a more conservative approach in which all parts were cured with the same cure cycle as the RenShape molds. This cure cycle allowed for much easier removal of parts, and a much better surface finish.

7.6 Parts Manufacturing

This section will outline the manufacturing of each component for the 2014 side-pod system.

7.6.1 Side-Pod Profile

The side-pod utilized the top profile of the undertray mold. In order to accurately maintain the necessary airfoil profile designed in CAD, two printed templates were used. One template was used to locate key locations on the mold for proper lay-up and positioning, while the other was used to cut out the correct carbon-profile. The positioning template is shown in Figure 192 and the carbon-fiber cutting template is shown in Figure 193.

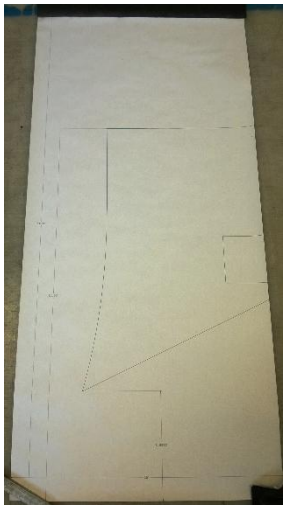

Figure 192: Positioning of side-pod

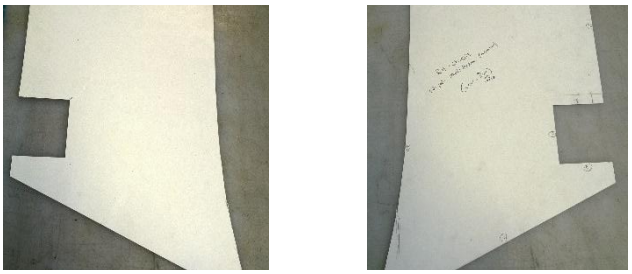

Figure 193: Side-pod template

This template was placed in the undertray mold by starting at the leading edge. Marks were made on the edge of the undertray to locate the position of the part. In order to maintain the slanted profile of the leading edge, tape was placed on the mold at the correct angle and location. Five layers of tape were used to offset the side-pod equivalent to the thickness of three layers of carbon used to make the leading edge. This allowed for flush interfacing between the two parts after curing. This also had to change for the left-hand side-pods which were manufactured using exactly the same process.

Figure 194: Leading edge offset

The side-pod carbon was cut slightly longer than the desired shape in order to wrap around the core laid around the designated perimeter. Initially, the carbon was cut to size, and each piece of core was individually wrapped with its own piece of carbon,

however this led to structural weaknesses in the part, a poor edge quality, and a heavier part than desired.

Once the carbon was placed in the mold, each piece of pre-cut and chamfered core was wrapped in the adhesive film and placed in the correct location on the mold.

Figure 195: Side-pod lay-up process

The extended portions were then wrapped around the core and trimmed to the correct length to reduce material and weight. This part was then vacuum bagged and cured.

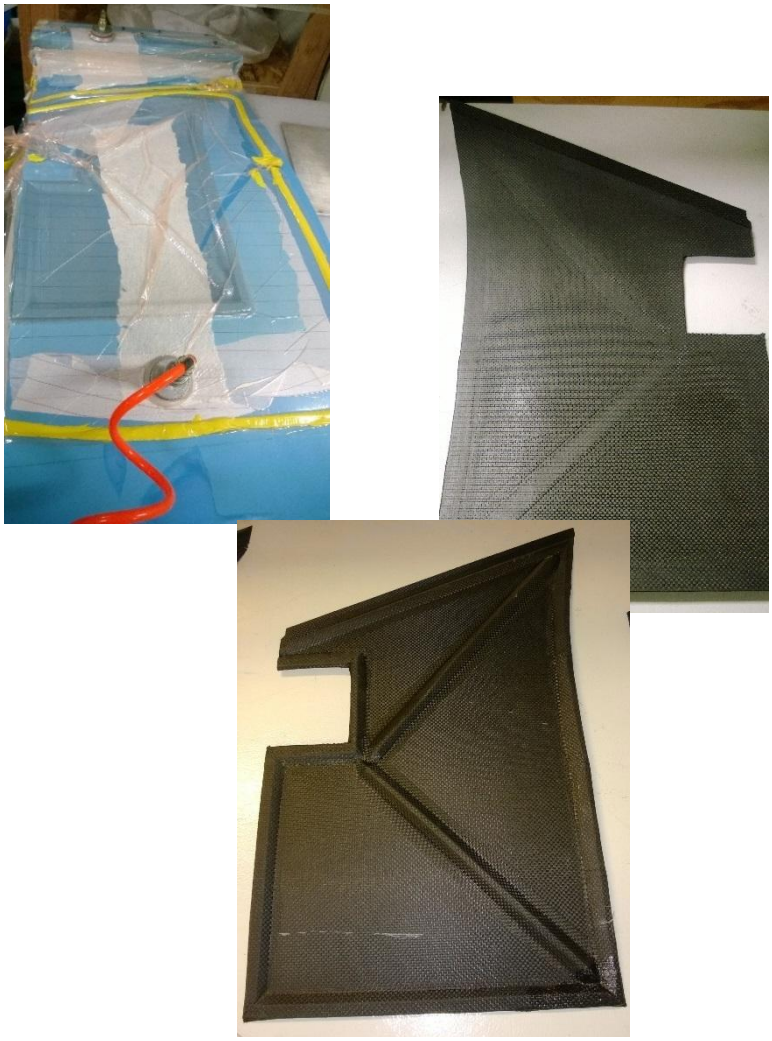

Figure 196: Vacuum bag and final side-pod

Some issues that occurred with the core lattice structure was bridging on the first side-pod. The vacuum bag was not properly placed in the necessary areas, and was too tight around the lower trailing edge, as well as around the cut-out for the radiator cap.

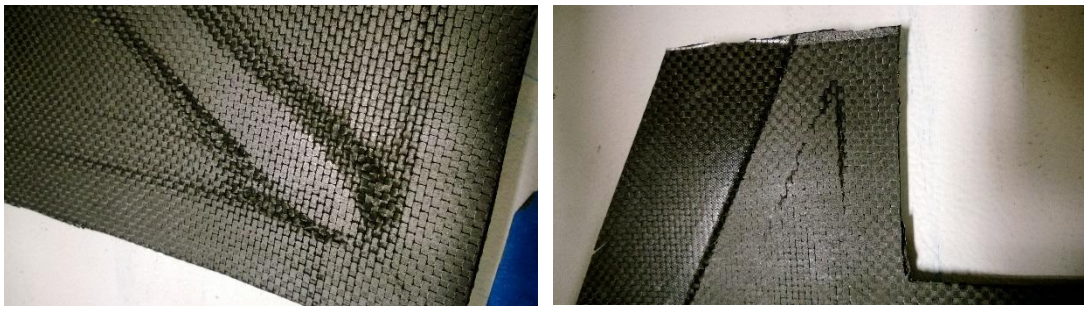

Figure 197: Bridging of carbon-fiber on initial side-pod

This was eliminated with better bagging techniques which utilized pleats along the perimeter of the assembly for better placement of bags in the chamfered areas. Figure 198 shows the final four side-pods (right-hand only).

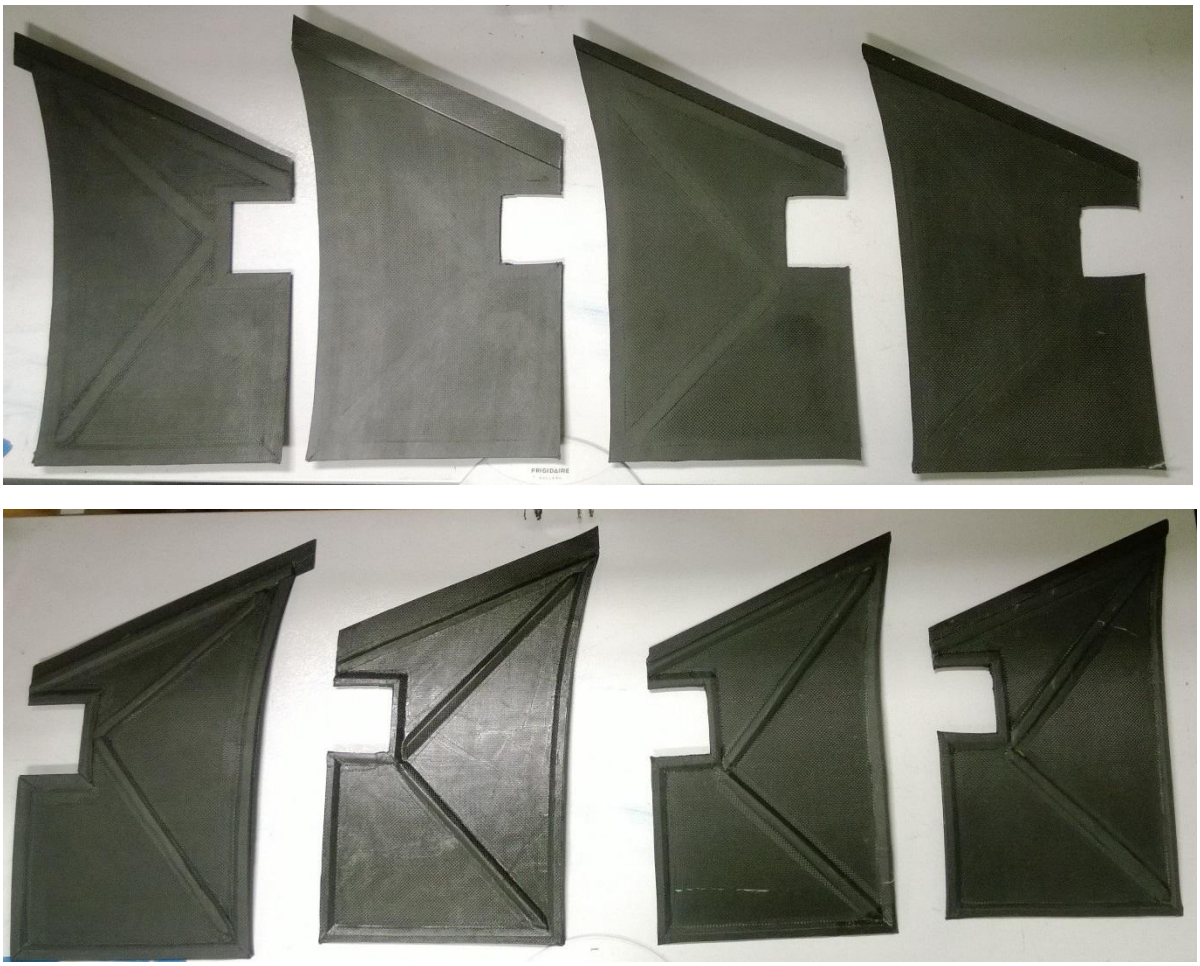

Figure 198: Final side-pods (right-hand) - 2 cCar and 2 eCar

7.6.2 Leading Edge

Manufacturing the leading edge was a rather simple task, but one that required a lot of scheduling of the molds between the side-pod and undertray engineer. The leading edges require both molds to be used to create one complete edge, and eliminated the possibility of making any other parts with those molds until after they are cured. The process was as follows:

1. Cut layers of carbon to the full width of the mold.

2. Vacuum bag and cure.

3. Once cured, top mold with the joggle offset was trimmed to remove excess carbon.

4. Two halves were then epoxied together using *Loctite 9430 Hysol* ® epoxy adhesive and hardener. Halves were then clamped down and allowed to dry for 24 hours.

5. Using printed templates, trim leading edges to fit chassis and endplate shape.

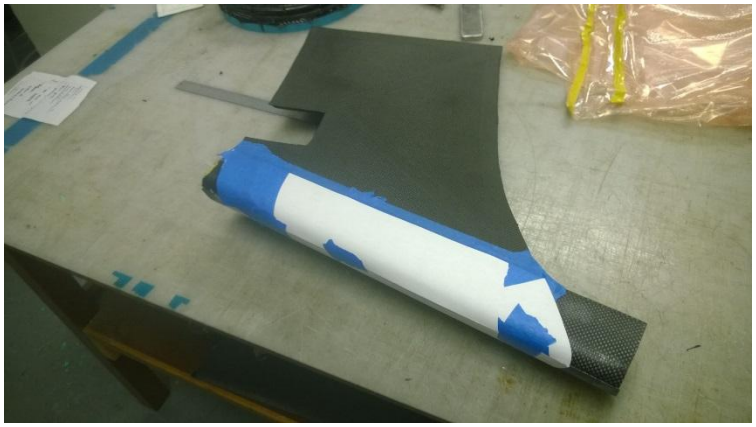

6. Epoxy side-pod front flange and leading edge and allow to bond.

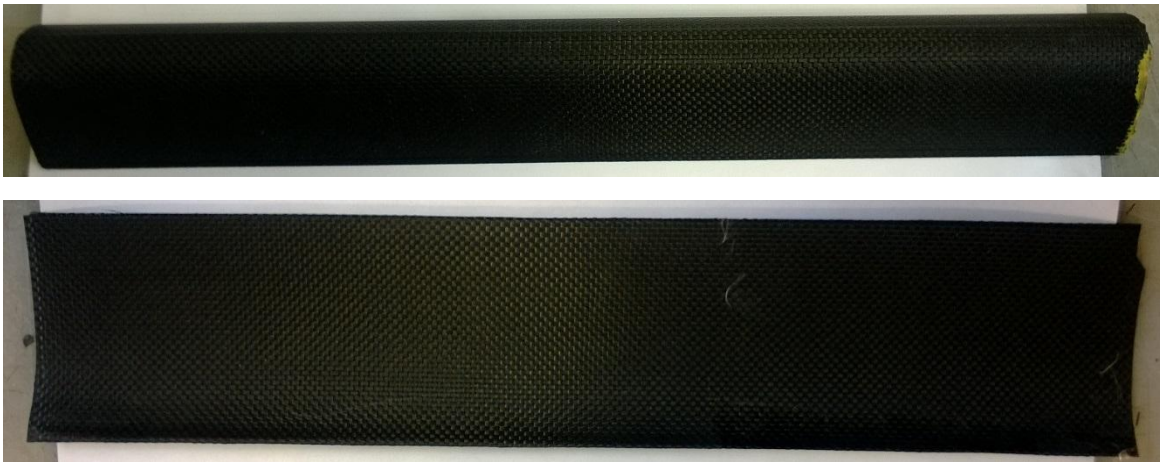

Figure 199: Top and bottom components of leading edge

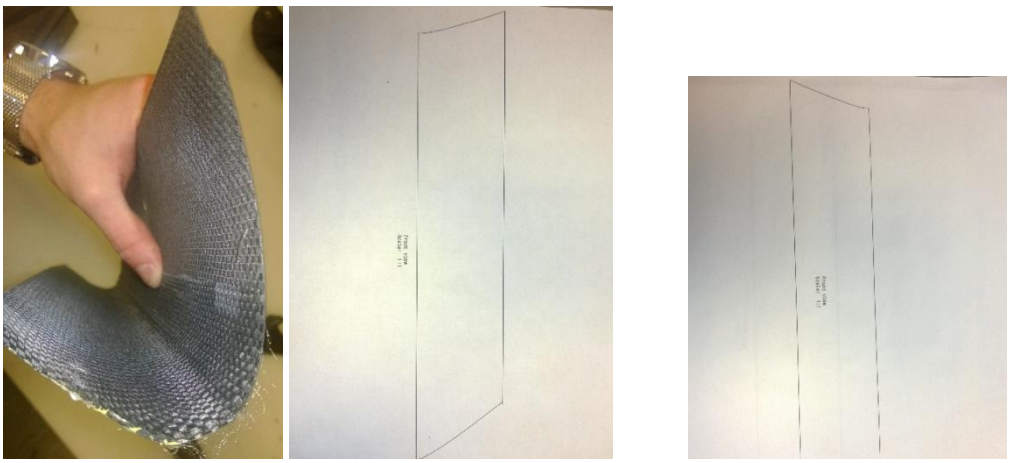

Figure 200: Leading edge profile and templates used for shaping

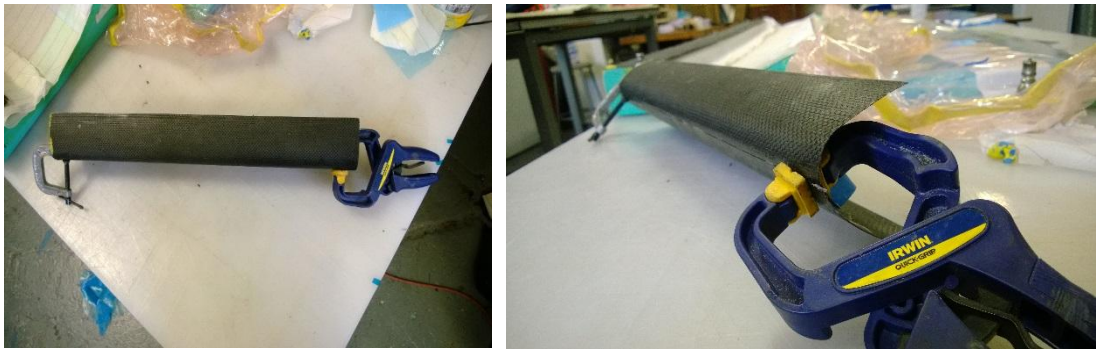

Figure 201: Leading edge epoxy process

Figure 202: Side-pod and leading edge mounting configuration

7.6.3 Endplate

This section will discuss the construction of the endplate. Much like the side-pod, the endplate consisted of a core lattice structure that required inner edges of the core to be chamfered at 45°, and wrapped with extended carbon-edges to maintain a 1-core-1 structure. This component also dealt with hard points (squares of twenty-five ply carbon-fiber pre-preg) which were used to be inserted into the core in order to absorb the load from the clamping force of fasteners. These hard points were countersunk to allow the countersunk fasteners to sit flush with the edge of the endplate. The endplate utilized the sheet-metal mold from GK Machine to cut the carbon template and for curing. The important aspect of this manufacturing was to make sure that both the peel ply and release film had enough slack as to not create any bridging. The finished left-hand endplate can be seen in Figure 204.

Figure 203: Endplate mold (left); core lattice design (middle); hard point chamfering (right)

Figure 204: Final endplate

7.6.3.1 Gurney Slot

This component was not a complex part to manufacture, and required a U-channel aluminum rod to use as a mold. This utilized eight layers of carbon fiber. The mold and final product is shown in Figure 205.

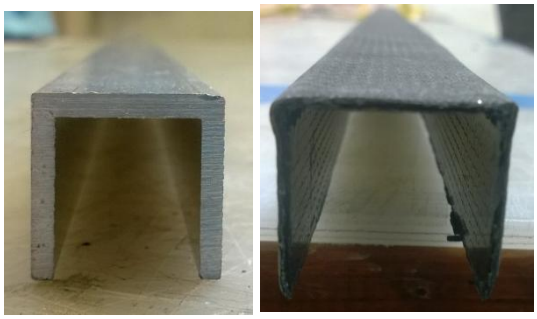

Figure 205: Gurney Slot

7.6.4 Fan Shroud

The fan shroud was one of the most difficult components to manufacture. Given the multiple bends that carbon-fiber must be laid on, this required the most preparation in terms of core cutting, core overlapping to eliminate bridging, wrapping all core with adhesive, and folding oversized carbon to match the final shape. Having bottom layer of carbon cut oversize, allowed the fan to maintain a true, 1-core-1 lay-up schedule. This

particular component utilized 3 mm, versus the 6 mm foam used on the side-pod and endplate. The lay-up and construction process can be seen in Figure 206 which includes the carbon and core cutting, adhesive wrapping, vacuum bagging, and the finished cured product.

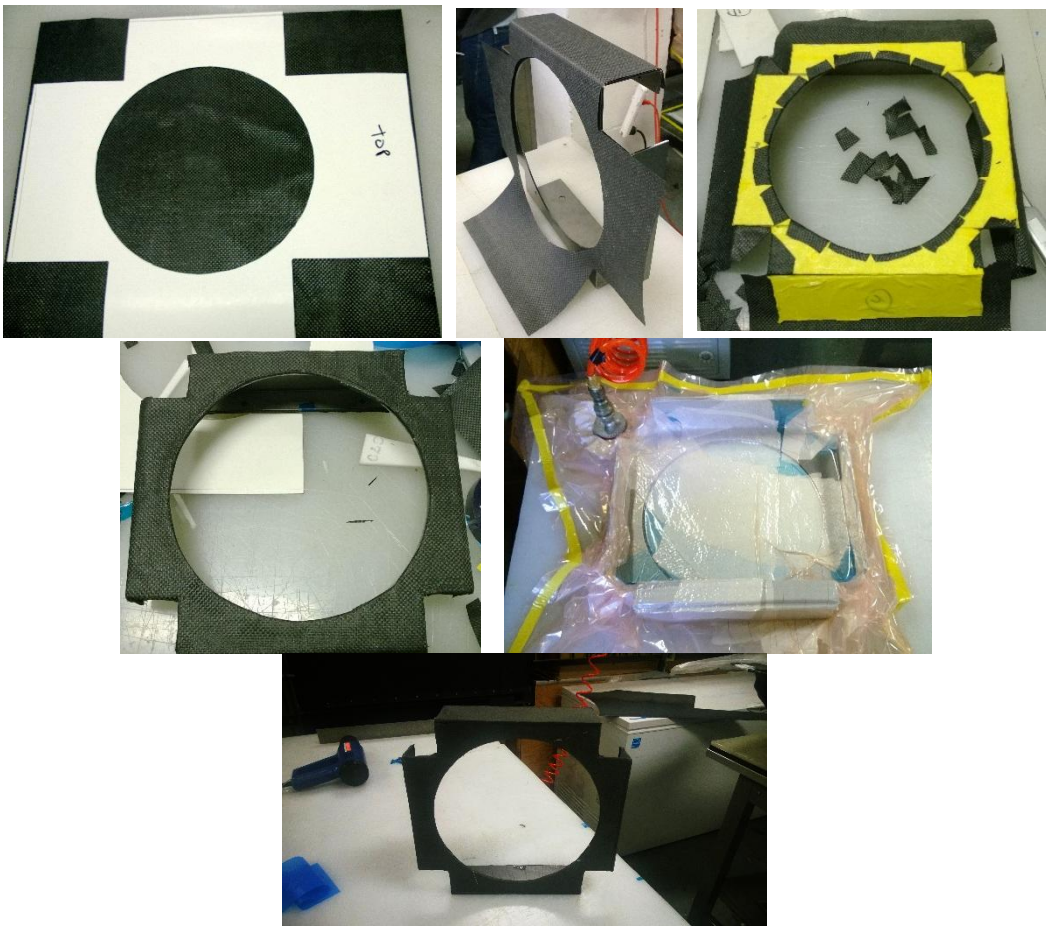

Figure 206: Fan shroud lay-up and final cured part.

Removing the fan shroud was the most difficult part but the flexibility of the part made it manageable. Integration with the radiator fan itself was perfect. The fan holes from the sheet-metal mold were in exactly the correct position where holes needed to be drilled post-cure to mount the fan. This can be seen in Figure 207: Air fan and shroud.

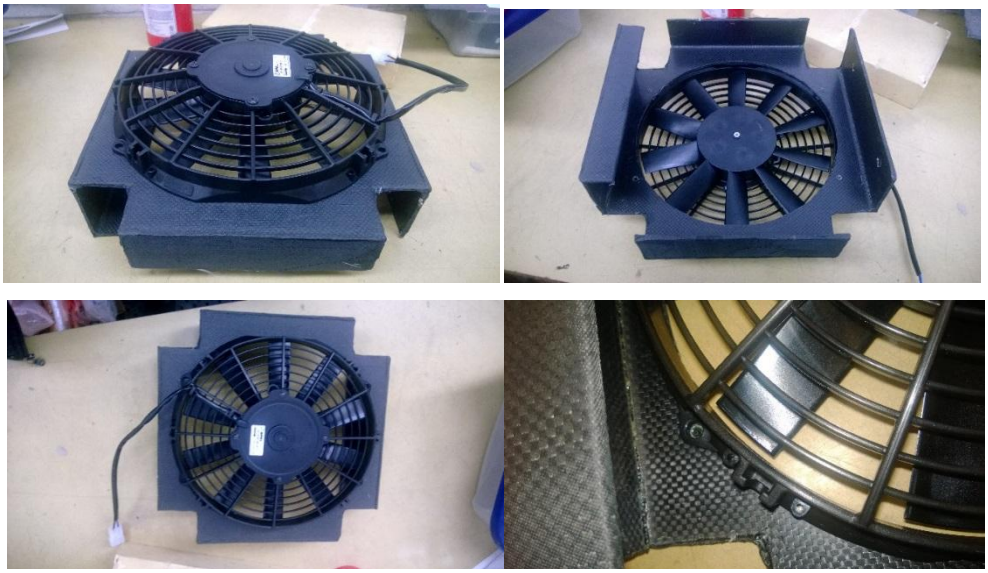

Figure 207: Air fan and shroud

The next step was to check its compatibility with the radiators. The holes in the bottom of the fan shroud needed to be offset by 8 mm due to errors in the hole locations in the mold, however the shroud and fan mounted very nicely with the radiator. The finished product is shown in Figure 208.

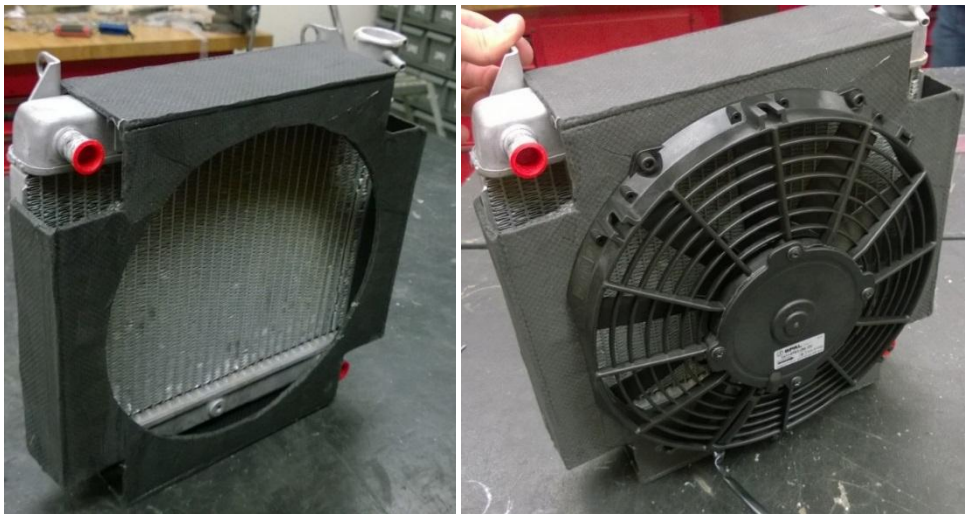

Figure 208: Fan shroud integration with radiator (left) and air fan assembly (right)

7.6.5 Front Brackets

The front brackets simple to manufacture, but due to the small size and bends of the mold, these were some of the most time consuming parts to manufacture and vacuum bag correctly. Using printed templates, carbon-fiber pre-preg was cut-to-size and laid up all at once. Once they were laid-up on the mold, the excess carbon was then cut flush with the mold edges. The flanges were then taped to the mold, to prevent any of the laminate from moving. They were then vacuum bagged, and cured.

Figure 209: Bracket construction process: templates, lay-up, cured part, and post-processing work

7.6.6 Rear Bracket

These brackets were also rather simple, yet required rather long manufacturing times. The brackets used printed templates to cut out the carbon-fiber pre-preg. These were then laid up with four plies of 0° T800 plain weave, and two plies of 45° T800 plain weave. The 45° plain weave was included in the lay-up schedule to help with the in-plane torsional stress from turning the main switch on and off. An additional strip of plain

weave was laid up along the bend radius of the rear bracket to provide additional strength against deflection. All eight brackets can be seen in Figure 213.

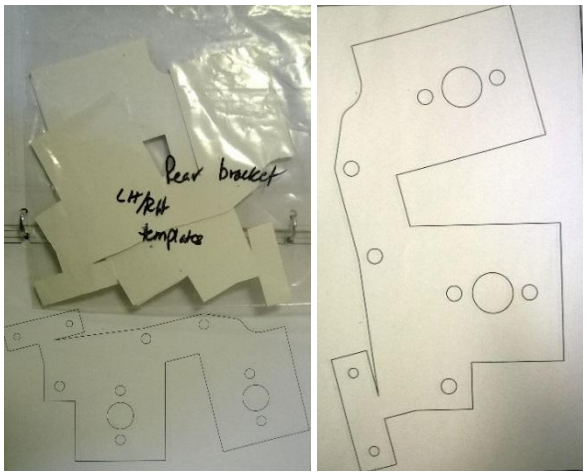

Figure 210: Paper and cardstock templates used to cut carbon-fiber

Figure 211: Carbon-fiber lay-up on sheet metal mold

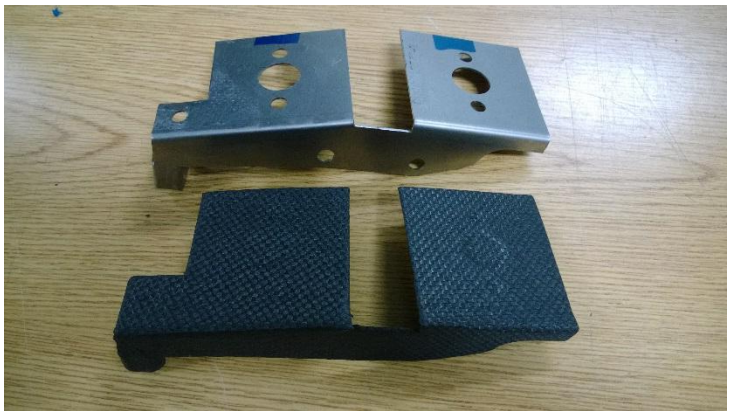

Figure 212: Final cured part

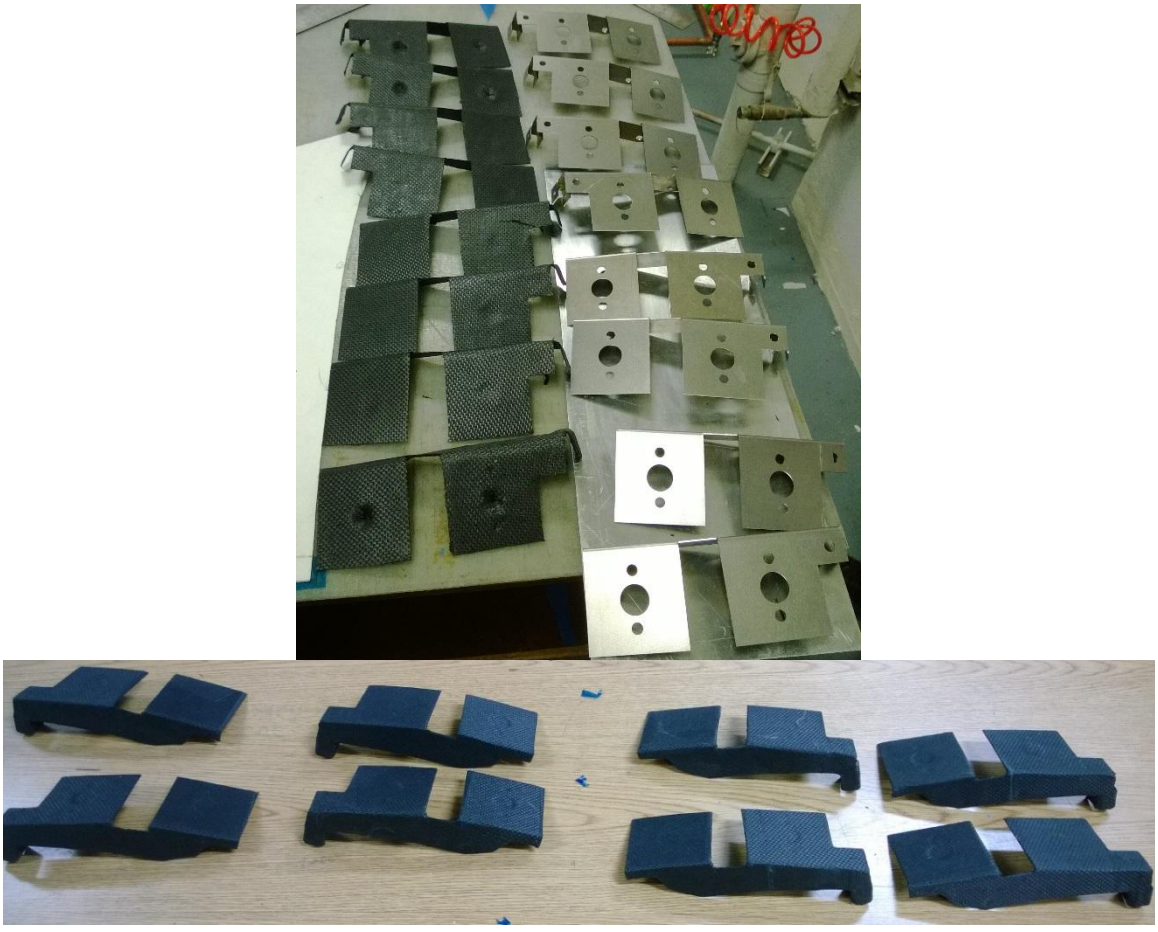

Figure 213: One oven cure cycle batch of eight finished brackets

7.6.7 Side-Pod/Endplate Brackets

These brackets were cut to simple 2” x 10” carbon-fiber plies, and were laid up within the L-bracket mold provided by GK Machine. This part was very simple to manufacture. For vacuum bagging, this part utilized a pressure intensifier as discussed in Section 2.3.

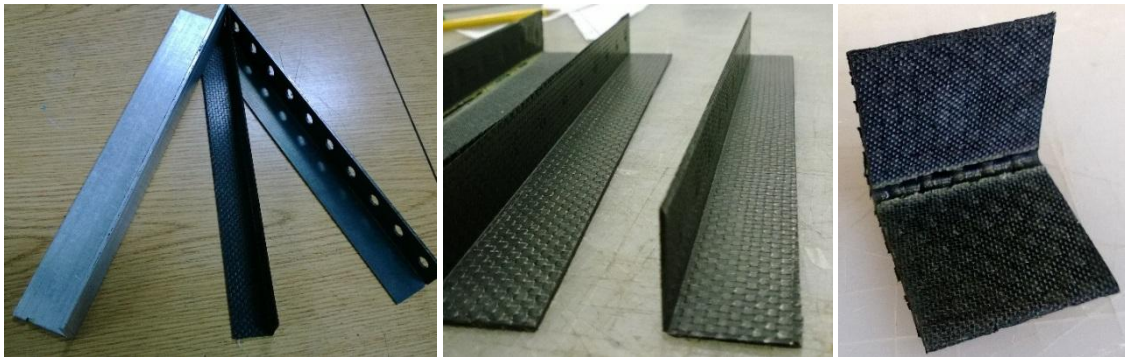

Figure 214: Side-pod/endplate bracket molds and pressure intensifier (left); final cured bracket strip (middle); and individual cut bracket (right)

7.6.8 Front Ducting

The front ducting has a relatively obscure shape. Each piece was cut individually and but was epoxied together after curing. Each piece was cut using printed templates, and vacuum bagged with metal pieces to create flanges for bonding. The final ducting is seen in the bottom image of Figure 215.

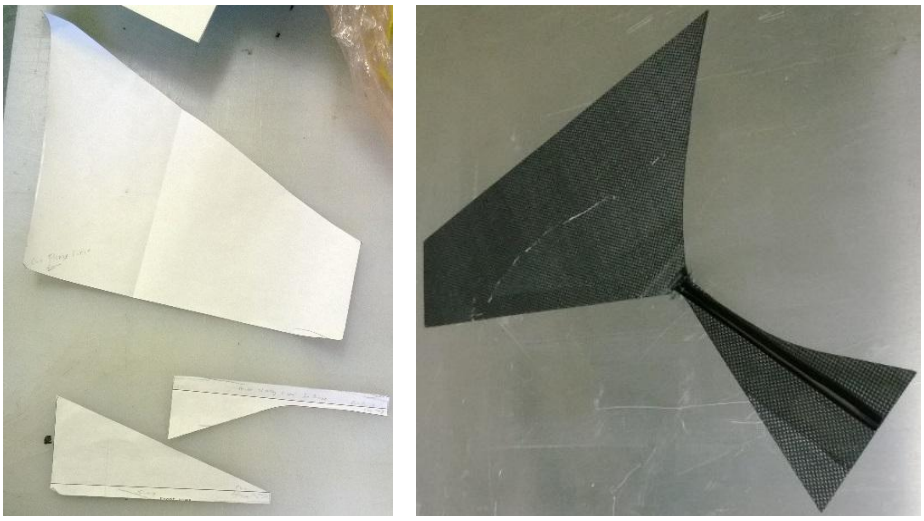

Figure 215: Front ducting template (top-left); individual components; finished ducting (bottom)

7.6.9 Rear Ducting

The rear ducting required the use of the wing flaps, shared by both the front and rear wing. The profile of this mold was crucial to the shape and performance of the rear ducting as it provided the best aerodynamic performances. This ducting utilized the printed location templates to locate the correct starting point for the ducting profile. The carbon was cut using printed templates, and was vacuum bagged in the flap mold. The individual vertical supports were cured separately on a flat plate, and the support flanges were epoxied after curing.

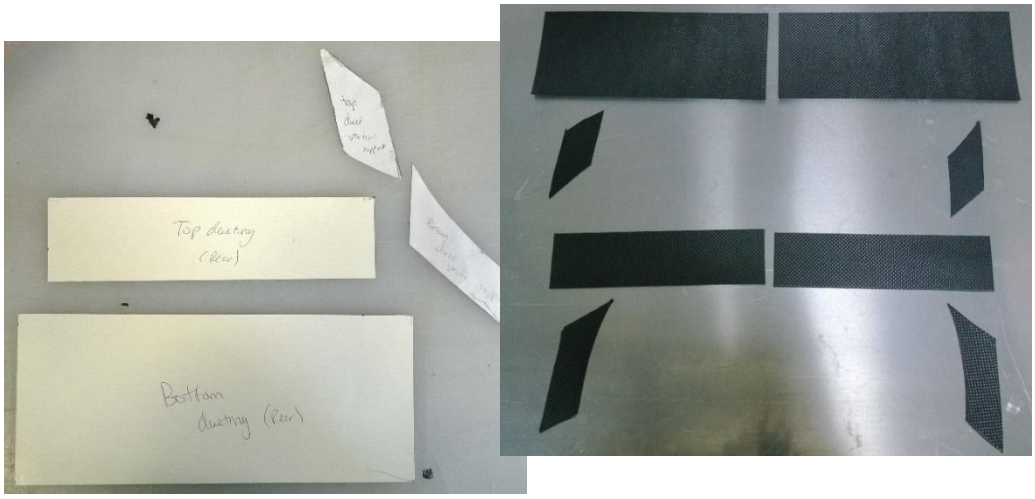

Figure 216: Rear ducting templates (left) and cured components (right)

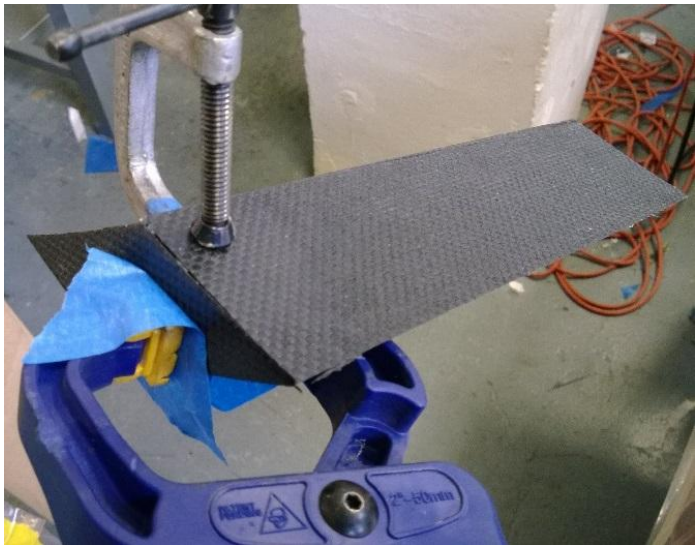

Figure 217: Epoxy process of assembling rear ducting components

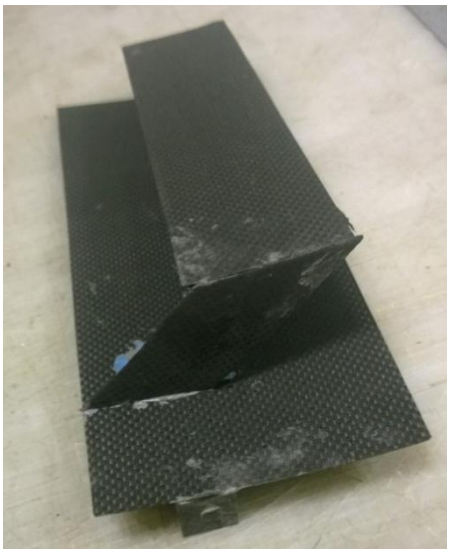

Figure 218: Final rear ducting assembly

7.6.10 Fill Cap Cover

This piece was the last component to be manufactured. This part is extremely simple and is cut out of a rectangular template. After being laid-up, this part was cured. The leading and trailing edges were attached to the side-pod using Velcro™.

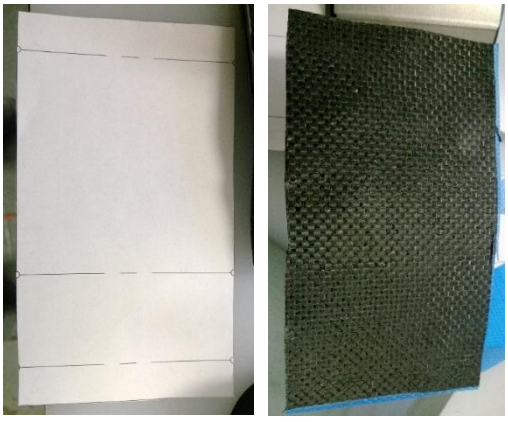

Figure 219: Template (left) and carbon-fiber ply

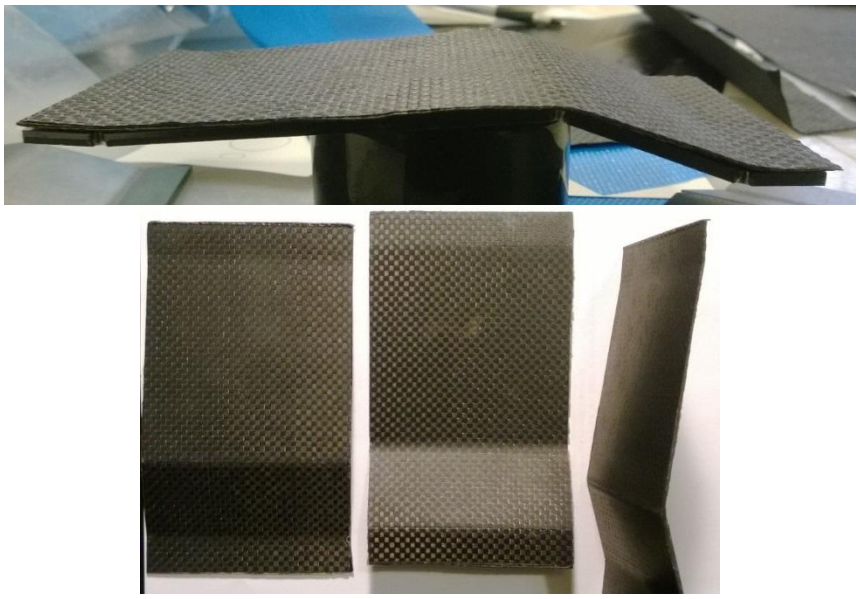

Figure 220: Fill cap cover lay-up (top) and cured part profiles (bottom)

7.7 Part Weights

This section will outline the overall final weights of the manufactured parts in comparison to the predicted weights, as well as the correlation to competition points.

7.7.1 Part Weight Comparison to Calculated Weights

Table 53: Part weight comparison of manufactured vs. predicted values

Part	Manufactured Weight	Predicted Weight	% Differential
Side-Pod w/ leading edge	409 g	336.34	12%
Endplate	590 g	556.1 g	6%
Fan Shroud	302 g	423.44 g	-29%
Front Bracket	10 g	24.12 g	-59%
Rear Bracket	72 g	152.76 g	-53%
Side-Pod/Endplate Bracket	4.6 g	12.06 g	-62%
Front Ducting	108 g	203.68 g	-47%
Rear Ducting	142 g	277.38 g	-49%
Fill Cap Cover	24 g	17.42 g	38%
Total Weight of Composite Parts:	1661.6 g	2033.3 g	-18%
Plastic Rivet	0.8 g (Qty. 8)	0.8 g (Qty. 8)	0%
Potted Inserts	0.9 g (Qty. 10)	0.9 g (Qty. 10)	0%
Total Side-Pod Package Weight:	1677 g	2050.7 g	-18%

7.8 Side-Pod/Endplate Integration

The following figure shows the integration and compatibility of the 2014 side-pod and leading edge with the modular endplate design.

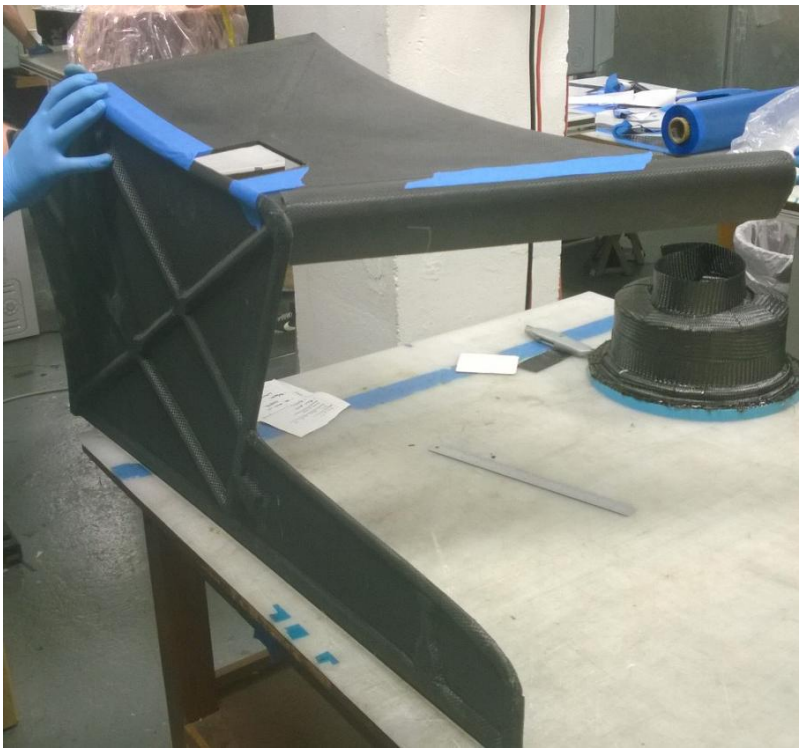

Figure 221: 2014 Side-pod and endplate integration

8. Testing

8.1 Airflow Performance

In order to validate some of the airflow performance of the new radiator and fan components of the 2014 combustion vehicle, a simple test was established to provide data collection for both the combustion powertrain and aerodynamics team.

The layout of this experiment incorporated the radiator, fan and shroud assembly, attached to a 12 volt power source to run the fan, and is shown in
Figure 222. Using an Amprobe® TMA-21 HW hotwire anemometer portable probe, air flow velocities were measured in front of the radiator with the fan at full-power. These velocities can be seen in Figure 223 of the radiator core velocity distribution matrix. These values were then compared to measured airspeed values of the fan attached to a shroud, with no radiator to measure true air flow speed produced by the fan alone. This allowed for a basic understanding of the air flow resistance of the radiator core, as well as the air flow performance of the cooling package without external forced air conduction through a side-pod during vehicle motion.

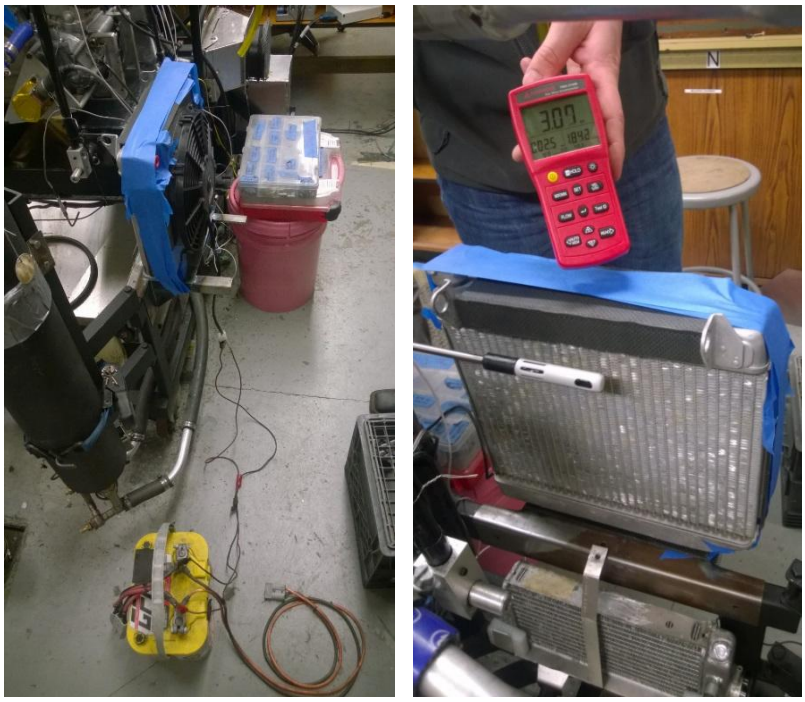

Figure 222: Test fixture and measurement

Figure 223: Radiator core grid and velocity matrix

The above described test produced the results for air velocity through the radiator and fan assembly. Figure 223 shows a velocity matrix across the front face of the radiator core. The average of all of these velocities produces a mass flow rate of 0.565 kilograms per second. The average velocity of the fan without the radiator attached produced a mass flow rate of approximately 0.821 kilograms per second. This results in a 31% loss in mass flow rate with the addition of the porous radiator core. However, there is still significant cooling power provided by the fan only in a static position, and will only be increased with additional vehicle velocity forcing more air through the ducting system.

8.2 Recommendations for Future Testing

Due to the time limitations and vehicle construction scheduling, the final 2014 vehicle was not fully assembled and before the completion of this thesis. Thus, there are a few experiments that are recommended for physical validation once the vehicle is fully assembled

8.2.1 Radiator Pressure Drop and Loss Coefficients – Wind Tunnel Validation

This particular experiment includes theoretical CFD validation of radiator performance characteristics, complimented by experimental wind-tunnel testing. Using Pitot Tubes, described in Section 2.4.2, the pressure at the inlet and outlet of the radiator core can be measured in order to accurately gain pressure drop information across the radiator specific to *Global Formula Racing.* The pressure drop can be empirically defined as a function of air velocity, a controlled parameter in the wind-tunnel. Using Equation

6**Error! Reference source not found.**, the correlation between pressure drops across the radiator versus wind speed can also help to determine the loss coefficient caused by the resistance of the fins and radiator core according to Equation 8. Using this would allow for better understanding of how the radiators will cool the engine, and can thus be translated into settings and parameters in CFD software for more accurate modeling.

8.2.2 Autocross and Endurance Configuration Performance

Using adequately paired hotwire anemometers with the onboard vehicle Data Acquisition System (DAQ) using USB or CAN type connectivity, permanent anemometers should be placed within both the left and right hand side-pod ducts, near the middle of the radiator core. This would allow for a better understanding of the airflow into the vehicle components during physical racing situations. Continuous, on-board data collection would allow future engineering design to utilize data in various racing situations including straight-line and yaw scenarios, varying ambient temperatures, vehicle speeds, and other various factors. This is an area of extreme recommendation for future work on the 2014 side-pod package as validation and benchmarking for continuous improvement in the 2015 season.

9. Conclusion

As discussed throughout this thesis, the need for engine cooling solutions is of vital importance to the success of Formula SAE vehicle performance. This problem requires design solutions that remove enough heat to prevent engine damage and failure. As was seen with the side-pod design for the 2014 *Global Formula Racing* combustion and electric vehicles, it is a lengthy design process that must take into account multiple factors across multiple iterations. For *Global Formula Racing*, the side-pod also plays an important role in the aerodynamic performance of the vehicle in addition to impacting cooling.

The research, design, and analysis completed in this study led to a significant improvement in both aerodynamic and cooling performance for the 2014 Formula SAE vehicle. In comparison to the 2013 vehicle, projected airflow and downforce performance were improved dramatically due to the newly designed inverted air profile for the side-pod and its internal components. It is projected from this study that the 2014 combustion and electric vehicle powertrain will be able to perform more reliably at Formula SAE competitions in the 2014 season.

Recommendations for Future Research:

Due to the extensive amount of additional research that could be conducted on both the aerodynamic and cooling performance of Formula SAE vehicles, with side-pods in particular, a few recommendations for future study are summarized next.

These recommendations focus on the engine cooling performance and the shape of the side-pod ducts for aerodynamic purposes. Based on the external research and familiarization of adequate side-pod duct design, future work should focus on the benefits of shape design similar to those in Section 5.1 – Designs Considered. These concepts utilized a smaller inlet, combined with an internal diverging-converging ducting shape incorporated with the chassis body and undertray. As seen in most Formula 1 type vehicles, this duct shape provides adequate heat management abilities on a much larger scale than those of Formula SAE and should be further evaluated. Evaluation should include CFD simulation and physical testing, potentially using small scale rapid-prototype models.

Due to time constraints, manufacturing requirements, and a need for simplicity and reliability in the 2014 season, the side-pod designs evaluated for this study weighed various trade-offs. Further investigation could be conducted into incorporating an inverted airfoil profile and still maintaining the converging-diverging-converging duct shape for adequate airflow through the radiators. This would require new molds to be made at *Global Formula Racing.* Thus, design and manufacturing would need to be conducted early in the season.

Bibliography

[1] "2014 Formula SAE Rules." *SAE International*. Web. 1 Nov. 2013. <http://students.sae.org/cds/formulaseries/rules/2014_fsae_rules.pdf>.

[2] Bergman, Theodore L., Adrienne S. Lavine, Frank P. Incropera, and David P. Dewitt. *Fundamentals of heat and mass transfer*. 7th ed. Hoboken: J. Wiley & Sons, 2011. Print.

[3] Christoffersen, L., Söderblom, D., and Löfdahl, L., "Improving the Cooling Airflow of an Open Wheeled Race Car," SAE Technical Paper 2008-01-2995, 2008, doi:10.4271/2008-01-2995.

[4] Crouse, William H. . "Engine Cooling System." *Automotive Fuel Lubricating and Cooling System*. Second ed. New York: McGraw-Hill Book Company, Inc., 1959. 354-375. Print.

[5] Daimler Trucks North America. “Side-Pod Analysis”. *Daimler Trucks North America Engineering Department.* Powerpoint. 2010. 1 November 2013. <https://docs.google.com/a/ba-racing-team.de/file/d/0B-bcPZrGWlR7SXZIODBUYW5lVDg/edit?pli=1>

[6] Dang, Victor Q.,“The Design, Manufacturing, and Testing of an Undertray for Formula SAE,” Oregon State University, Corvallis, OR. 2013.

[7] De Silva, C.M., M. Nor Azmi, T. Christie, E. Abou-Saba, and A. Ooi. "Computational Flow Modelling of Formula-SAE Sidepods for Optimum Radiator Heat Management." *Engineering Science and Technology* 6 (2011): 94-108. Print.

[8] Dyverfors, N., Borre, K., Arnell, C., and Rice, J., "Interaction of Downforce Generating Devices and Cooling Air Flow - A Numerical and Experimental Study on Open Wheeled Race Cars," SAE Technical Paper 2012-01-1165, 2012, doi:10.4271/2012-01-1165.

[9] "Equating design parameters to points." *Global Formula Racing Private*. Global Formula Racing - Oregon State University. Web. 1 Oct. 2013. <https://sites.google.com/a/ba-racing-team.de/global-formula-racing-general/wike/theory-and-analysis/1_general-design-theory/equating-design-parameters>.

[10] “2014 Formula Student Combustion Rules,” Formula Student Germany, 2014. <https://www.formulastudent.de/uploads/media/FSC_Rules_2014_v1.0.0.pdf>

[11] “2014 Formula Student Electric Rules,” Formula Student Germany, 2014. < http://www.formulastudent.de/uploads/media/FSE_Rules_2014_v1.1.0.pdf>

[12] Jenson, Karl, “Aerodynamic Undertray Design for Formula SAE,” Oregon State University, Corvallis, OR, 2010.

[13] Kamath, S., M P, P., S N, S., Damodaran, V. et al., "CFD and Experimental Optimization of Formula SAE Race Car Cooling Air Duct," SAE Technical Paper 2013-01-0799, 2013, doi:10.4271/2013-01-0799.

[14] Knowles, Don. "Cooling Systems." *Automotive fuel, lubrication, and cooling systems*. Reston, Va.: Reston Pub. Co., 1985. 331-346. Print.

[15] MacBeath, Simon. *Competition Car Aerodynamics: A Practical Handbook*. 2 ed. Sparkford: Haynes, 2011. Print.

[16] "Monash Motorsport." Monash Motorsport - Facebook. Monash University, n.d. Web. 1 Jan. 2014. <https://www.facebook.com/monashmotorsport>

[17] Salvio Chacko, Dr, et al. "Numerical Simulation for Improving Radiator Efficiency by Air Flow Optimization.”

[18] Strid, Logan, Bryan Kilgore, and Wyeth Crawford. "2011 Aerodynamics Report." Global Formula Racing. Oregon State University, Corvallis, OR. 2011. <https://sites.google.com/a/ba-racing-team.de/body-team/project-groups/Aerodynamics/reports/2011-osu-aerodynamic-report>.

[19] Strong, A. Brent. *Fundamentals of composites manufacturing materials, methods and applications*. 2nd ed. Dearborn, Mich.: Society of Manufacturing Engineers, 2008. Print.

[20] "Technical Information." Rohacell. Evoniks Industries AG, 1 Jan. 2014. Web. 1 Feb. 2014. <http://www.rohacell.com/sites/dc/Downloadcenter/Evonik/Product/ROHACELL/product-information/ROHACELL%20IG_IG-F%20Product%20Information.pdf>.

[21] Terry, Len, and Alan Baker. “The Cooling System.” *Racing car design and development.* Cambridge, Mass.: R. Bentley, 1973. 189-197. Print

[22] Toray Carbon Fibers America – T800H - Data Sheet <http://www.toraycfa.com/pdfs/T800HDataSheet.pdf>.

[23] "TU Graz Racing." TU Graz Racing Team - Facebook. Technischen Universität Graz. Web. 1 Jan. 2014. <https://www.facebook.com/pages/TU-Graz-Racing-Team/261700161521>.

[24] White, Frank M. . *Fluid Mechanics*. Seventh ed. New York: McGraw-Hill, 2011. Print.

Appendices

Appendix A – Design Tables

Table A 1: Comparison of side-pod designs from 2011-2013

Side-Pod Structure Comparison	2013		2012		2011	
	Oil	*Water*	*Oil*	*Water*	*Oil*	*Water*
Mounting Strategy	4 plastic hex head bolts with corresponding nut. Small L-shape brackets: 2 Upper-Inboard chassis mounted brackets. 2 Lower-Outboard undertray mounted brackets. All L-brackets mounted using epoxy. Non-removable. Side-pod placed directly on top of undertray wings.	Same as 2013 Oil	4 plastic hex head bolts with corresponding nut. Individual carbon flanges at front of side-pod (inboard and outboard) epoxied onto chassis with through bolt 3 sheet metal brackets with rivets through lower-outboard surface of side-pod and undertray for mounting rigidity. Small wire from undertray to chassis. Rear upper-inboard attachment mechanism with hex head screw through full-length chassis side flange. Rear lower-inboard attachment flange attached to undertray with rivet and plastic hex head bolt to side-pod.	4 plastic hex head bolts with corresponding nut. Upper-inboard mounting directly to chassis carbon fiber mounted flange. 3 sheet metal brackets lower inboard to undertray. Lower outboard mounted directly to undertray piece using thing sheet-metal brackets. Rear lower-inboard attachment flange attached to undertray with epoxy and two metal rivets. Flange attaches to side-pod via plastic hex head bolts (1 of 4).	4 main torx head screws with washer, mounted into chassis hard points (2 upper-inboard/2 lower-inboard). Side-pod individualized flanges allow for through bolt into chassis hard points versus length-wise chassis mounted flange. Upper-inboard flanges individual pieces as well as lower-inboard flanges. No out-board mounting pieces. 2 small torx head screws on external upper side of side-pod connecting flange to side pod. 1 of main torx head screws to connect epoxied side-pod flange to chassis body.	Same as 2011 Oil
Assembly Notes	Difficult to get tools in to properly fit over plastic nuts on internals of side-pod. Hidden behind frontal radius of part. Requires tools on external and internals of side-pod for removal. Removal also difficult due to cross member linkage interference with tool.	Same as 2013 Oil	Difficult to remove plastic hex bolts due to location within internals of side-pod. Hidden behind frontal radius and under the upper chassis flange. Requires tools on external and internals of side-pod. Difficult rear attachment removal due to radiator cooling lines, air-intake components and louvers.	Same as 2012 Oil	Relatively easy to remove 2 main torx head screws on lower inboard flange. Rather difficult to reach upper-inboard torx heads with tool.	Same as 2011 Oil
Features	No external louvers. Louvers were removed and top surface of side-pod contains large cut-out opening allowing access to radiator and fan package.	Same as 2013 Oil	External louvers. Converging shape towards the rear of side-pod. Attached and secured using Velcro and epoxy. Uncertainty as to if they can be removed without being damaged. Undertray complete piece spanning entire width under the vehicle chassis for upper-inboard attachment.	Same as 2012 Oil	External Louvers. Epoxied onto main side-pod body. Undertray does not span entire wide under vehicle chassis. Flat carbon panels attached to bottom of side-pods to support radiator.	Same as 2011 Oil
Internal Ducting	Post-processing required. Inefficient design using cut-to-fit foam and few carbon fiber pieces (1-ply) to fill in gaps between side-pod faces and radiator body. Inefficient and difficult to properly replace during assemble and disassemble processes. Wire mesh in front of radiator.	Same as 2013 Oil. No wire mesh in front of radiator.	Metal wire connecting undertray/side-pod interface to chassis. Wire used to dampen vibration during race. Post-processing required. Carbon fiber pieces (1-ply) to fill in gaps between side-pods faces and radiator body. Attached to chassis using Velcro to frontal inner radius and top of side-pod above radiator. Wire mesh placed in front of radiator for protection of "fins".	Carbon fiber piece (1-ply) with epoxied brackets and attached using Velcro to side pod surface internally. No wire mesh placed in front of radiator. Excess gaps where carbon plies did not cover are filled in with electrical tape.	Wire mesh in front of radiator. Foam and tape cut-to-fit around gaps between side-pod walls and radiator body. Tight fit, well done in post-processing, however not an integrated system into side-pod.	Same as 2011 Oil

Table A 2: Weight calculations and velocity ratios for initial design concepts considered for initial GFR14 aerodynamics package

Part #/ Aero Run-Ran Code	Iteration Name	Side-Pod End Plate SA (m^2)	Undertray Endplate SA (m^2)	Total Endplate SA (m^2)	Side Pod Top SA (m^2)	Side Pod Bottom Leading Edge Radius SA (m^2)	Total Surface Area of Side-Pod/Complete Endplate (m^2)	Part Weight (kg)	Weight Addition to Full Car (kg)	Velocity Ratio
10_41_201_PRT_A	Concept #1	0.182	0.151	0.333	0.239	0.019	0.591	0.565	1.129	1.58
10_41_201_PRT_B_It1	Concept # 2	0.205	0.151	0.356	0.238	0.002	0.596	0.569	1.139	1.15
10_41_201_PRT_B_It2	Concept # 3	0.251	0.151	0.402	0.236	0.005	0.643	0.614	1.229	0.96
10_41_201_PRT_C	Concept # 4	0.202	0.151	0.353	0.187	0.007	0.547	0.523	1.045	1.45
10_41_201_PRT_D_It2	Concept # 6	0.12	0.151	0.267	0.182	0.094	0.565	0.540	1.080	1.45

Table A 3: CFD simulation results, weights, and competition points

	Part #/ Aero Run-Ran Code	Iteration Name	Leading Edge Offset from Undertray Leading Edge	Side-Pod End Plate SA (m^2)	Undertray Endplate SA (m^2)	Total Endplate SA (m^2)	Side Pod Top SA (m^2)	Side Pod Bottom Leading Edge Radius SA (m^2)	Total Surface Area of Side-Pod/Complete Endplate (m^2)	Part Weight (kg)	Weight Addition to Full Car (kg)	Velocity Ratio
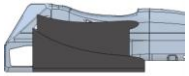	201_G 14_SP_1.2	Side-Pod 55 mm offset/low AOA	-50	0.193	0.151	0.344	0.312	0.038	0.694	0.66	1.33	1.58
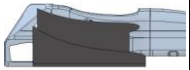	201_E 14_SP_1.3	Side-Pod 50 mm offset/undertray angle	-50 mm	0.197	0.151	0.348	0.318	0.038	0.704	0.67	1.35	1.15
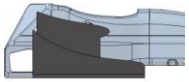	201_F 14_SP_1.4	Side-Pod 250 mm offset/undertray angle	-250 mm	0.13	0.151	0.281	0.219	0.032	0.532	0.51	1.02	0.96
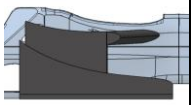	201_H 14_SP_1.5	Slanted Opening/Undertray Angle	-83 mm to front edge	0.116	0.151	0.267	0.256	0.042	0.565	0.54	1.08	1.45
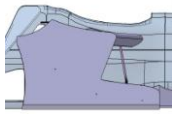	201_J 14_SP_1.16	2014 Final Side-Pod/Endplate	-83 mm to front edge	0	0.337	0.337	0.186	0.035	0.558	0.53	1.07	2.03

Table A 4: CFD simulation results, weights, and competition points

Part #/ Aero Run-Ran Code	Side Pod (Description)	Mass Flow Kg/s	DF	DR	Points DF	Points DR	Net Points	Total DF N	Total Drag N	L/D	Total Points DF	Total Points DR	Total Car Net Points
201_G 14_SP_1.2	Long entry, low angle	0.37	-26.4	-0.2	-4.75992	0.01174	-4.74818	1156.8	420	2.75	208.57	-24.65	**183.92**
201_E 14_SP_1.3	Long entry (50 mm offset), undertray angle	0.43	-7.6	2.4	-1.37028	-0.14088	-1.51116	1166.8	415.4	2.81	210.37	-24.38	**185.99**
201_F 14_SP_1.4	Short entry (250 mm offset), undertray angle	0.49	-11	-0.14	-1.9833	0.008218	-1.975082	1174.4	415.8	2.82	211.74	-24.41	**187.34**
201_H 14_SP_1.5	Slanted entry, undertray angle	0.45	-20	-3.4	-3.606	0.19958	-3.40642	1177.6	421.2	2.80	212.32	-24.72	**187.60**
201_J 14_SP_1.16	new small front ducting, Rear Ducting Iteration 5 - Lowered, Final Side-pod location, Final endplate, Undertray trailing edge gurney	0.45	-12	-0.4	-2.1636	0.02348	-2.14012	1143.8	419	2.73	206.23	-24.60	**181.63**

Appendix B – Engineering Drawings

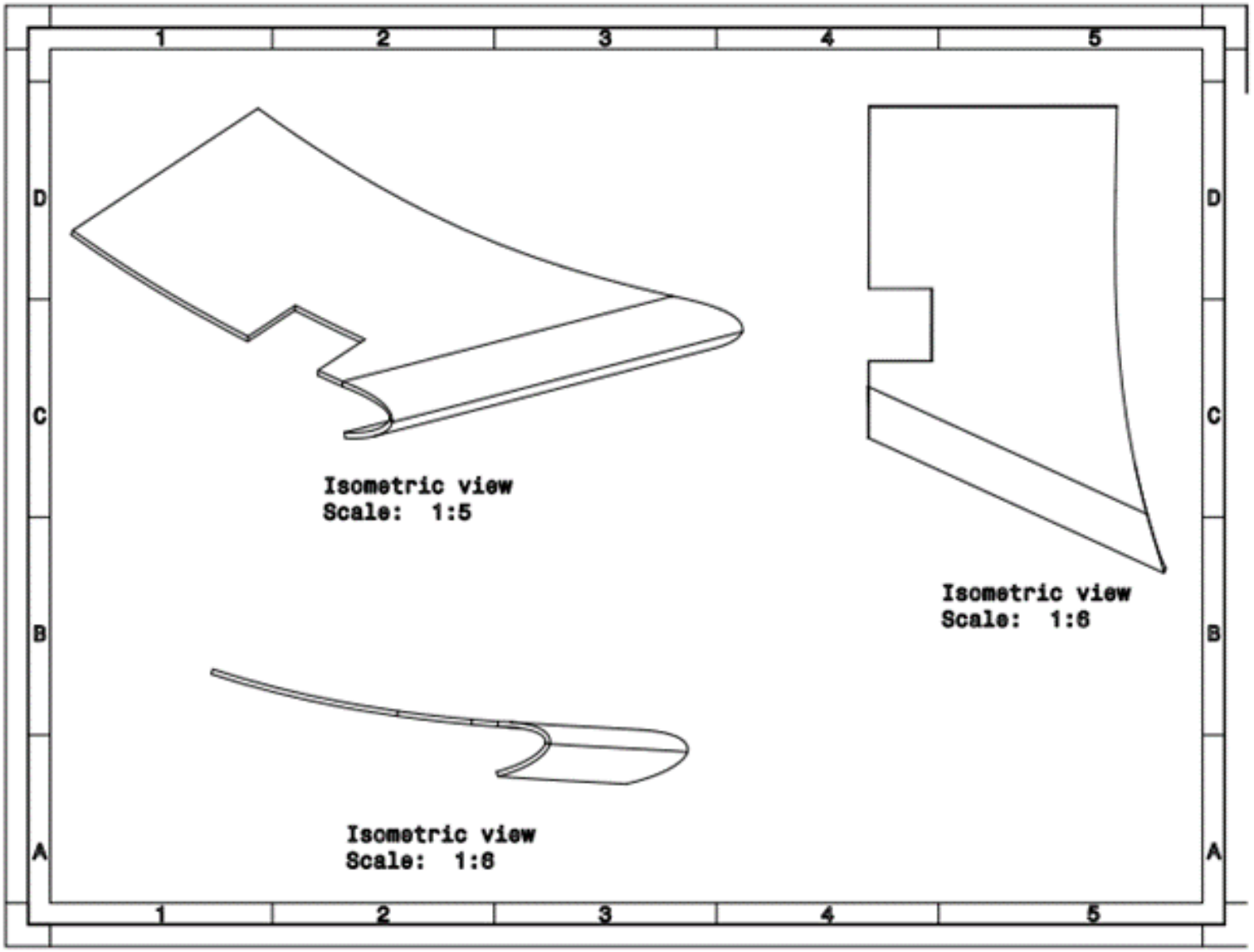

Figure B 1: Three view engineering drawing of 2014 side-pods.

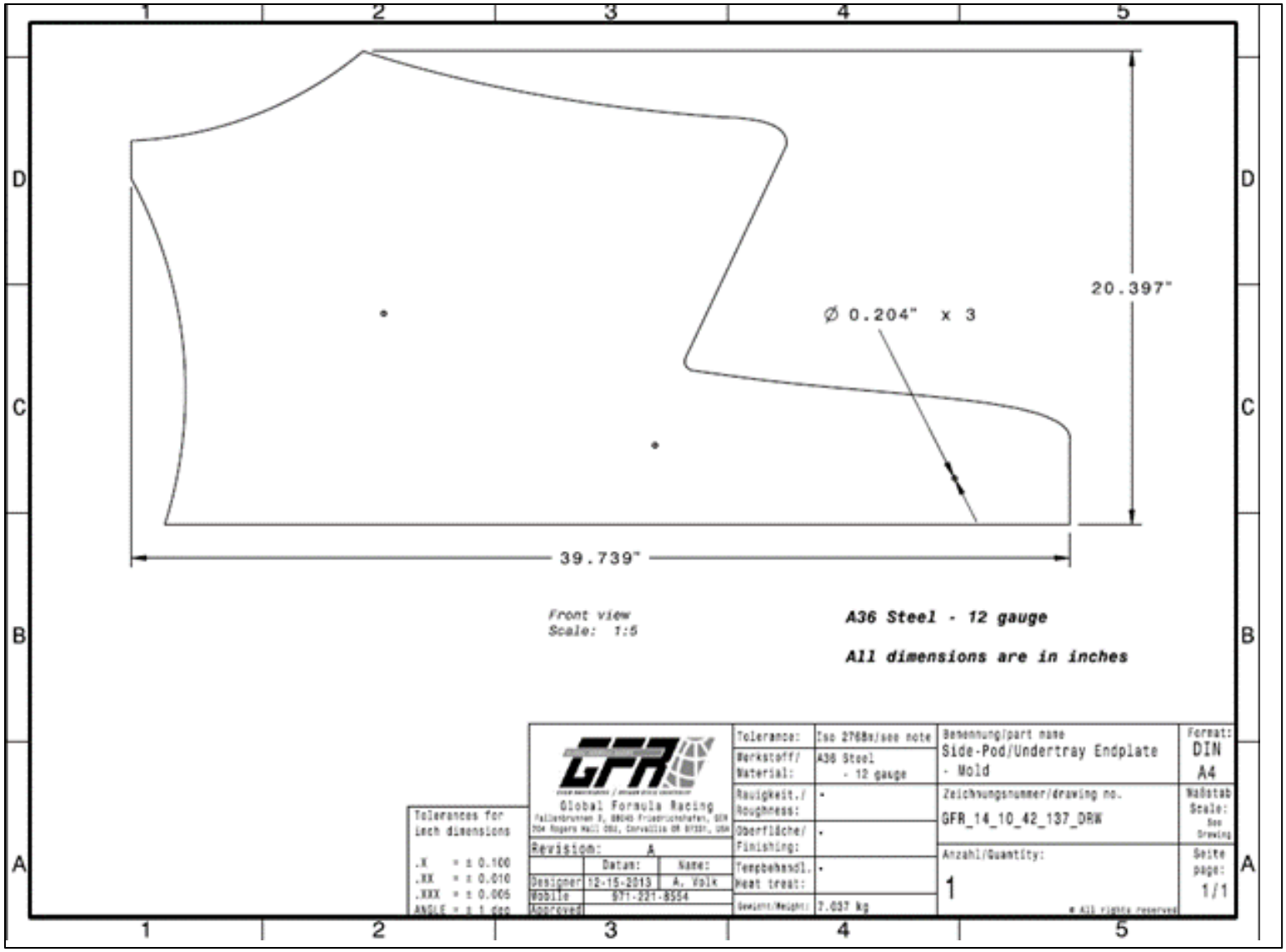

Figure B 2: Endplate engineering drawing sent to GK Machining.

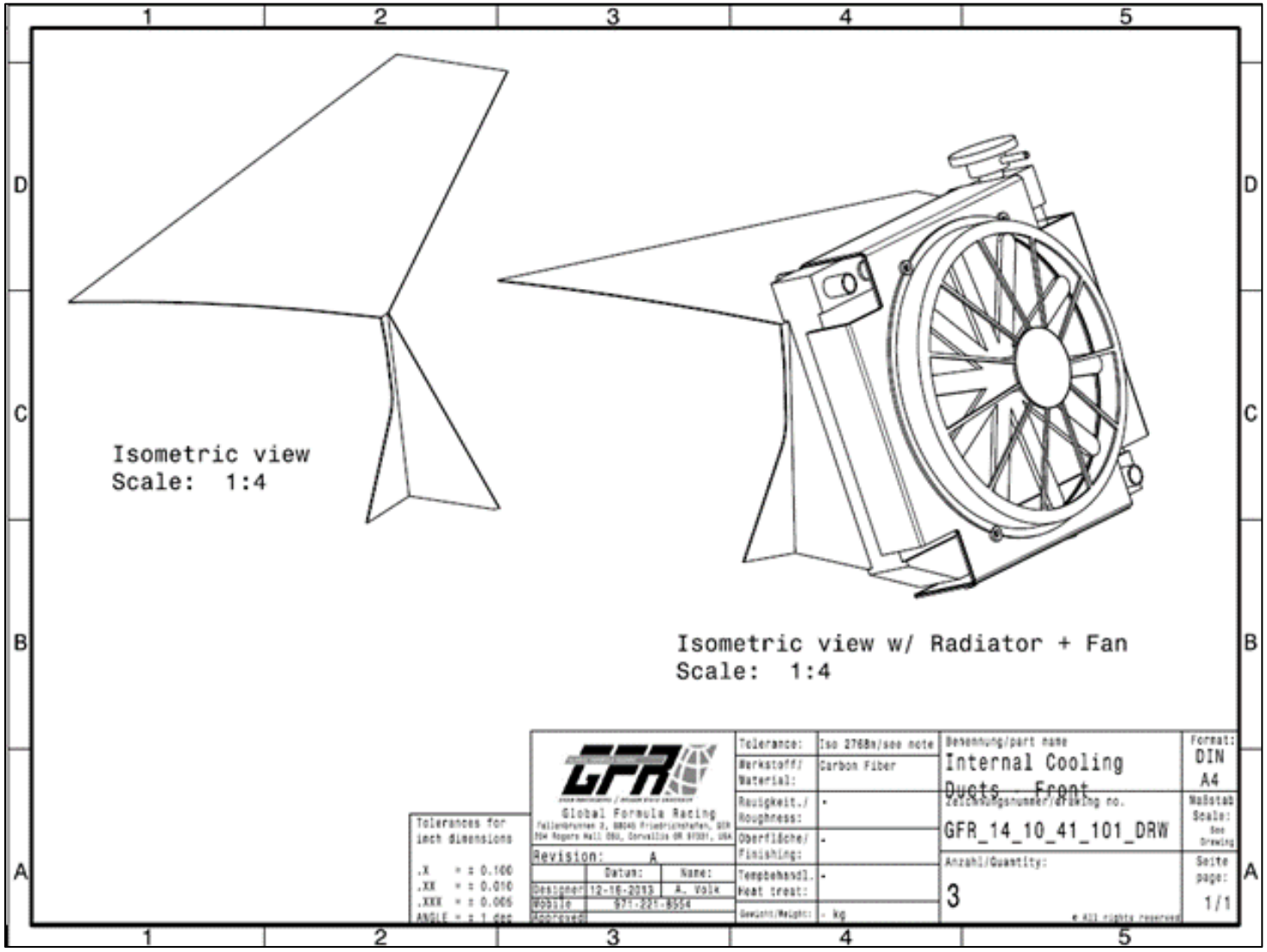

Figure B 3: Front ducting engineering drawing.

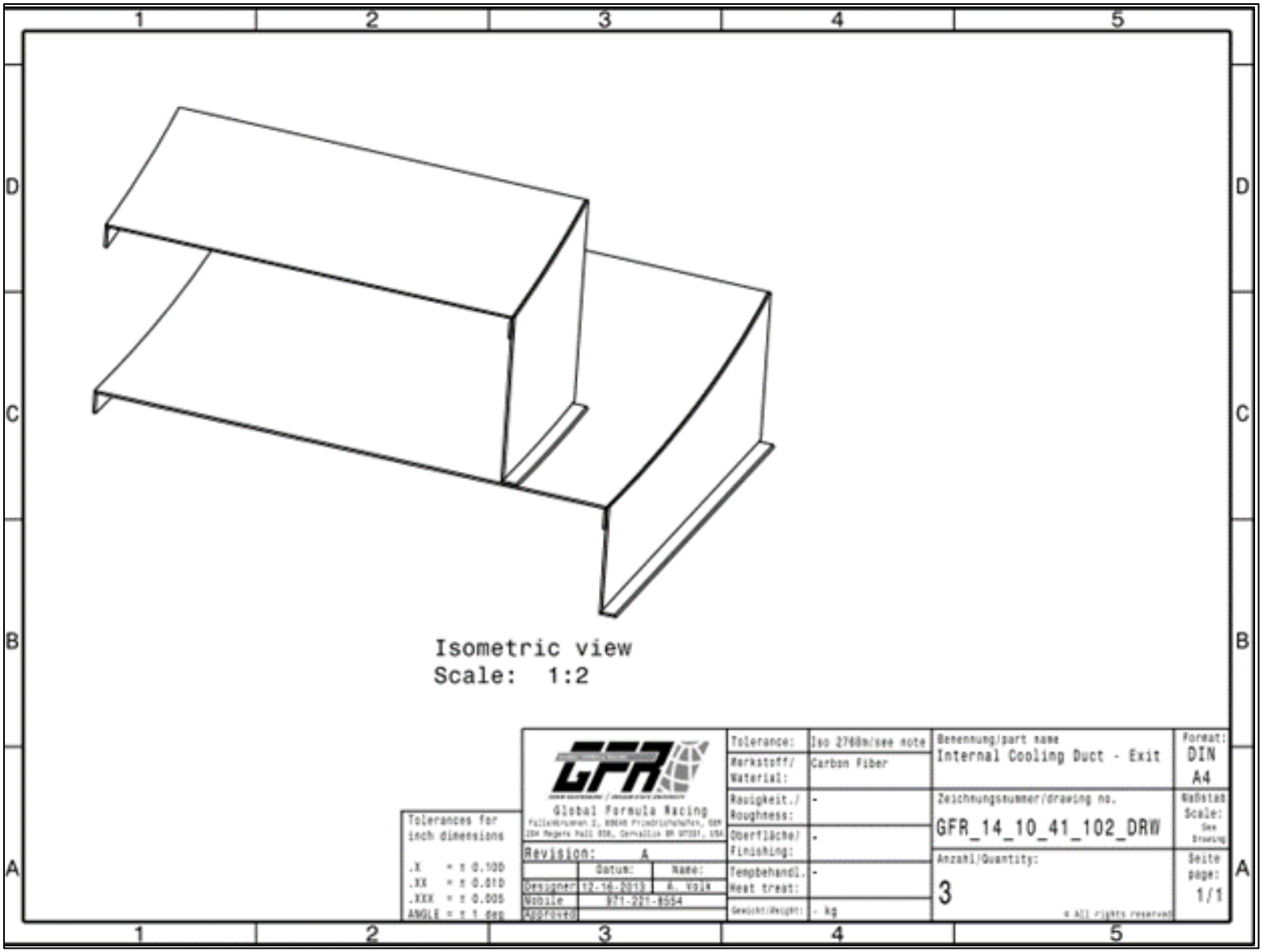

Figure B 4: Engineering drawing of rear ducting

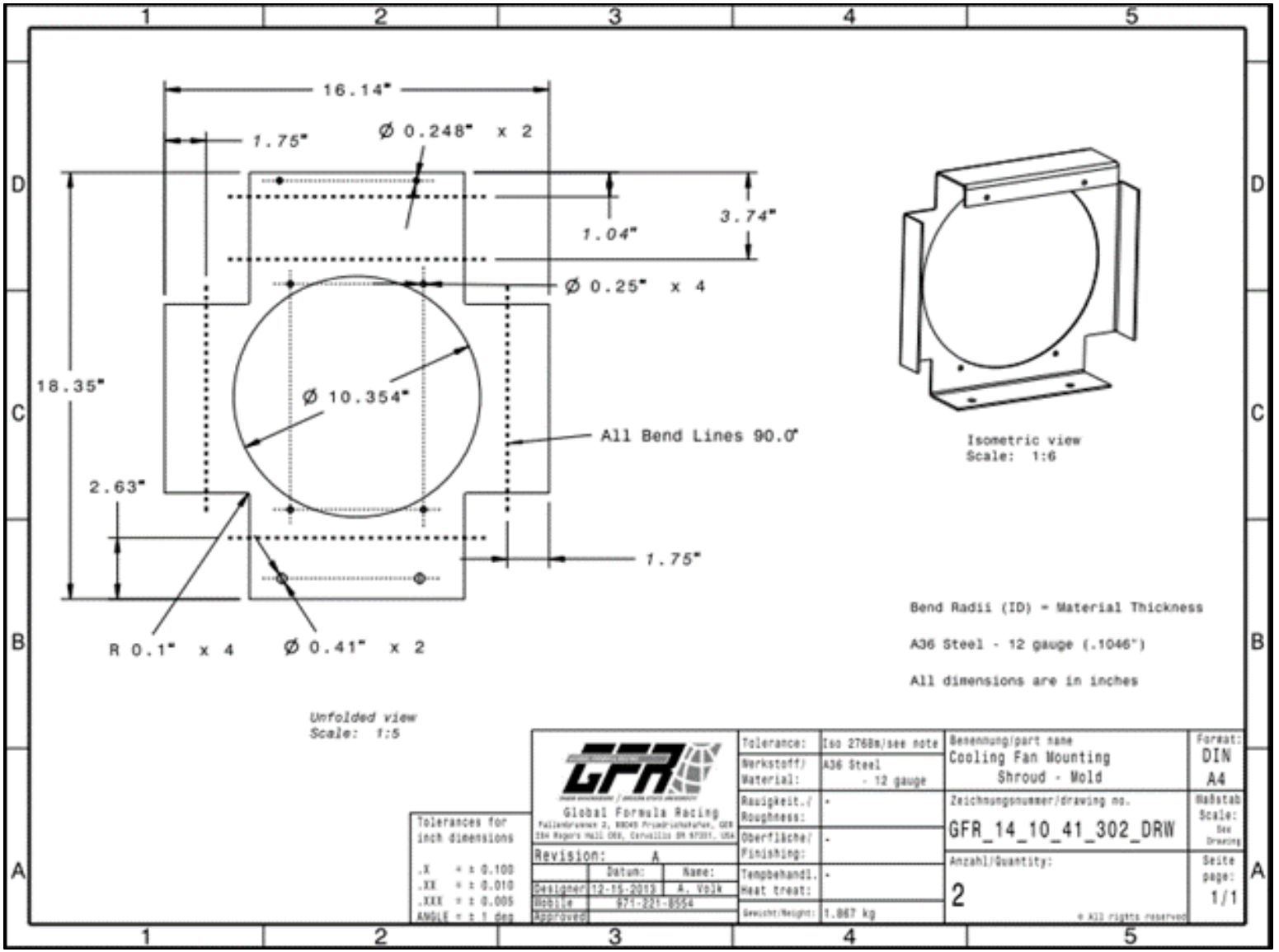

Figure B 5: Fan shroud sheet-metal mold engineering drawing

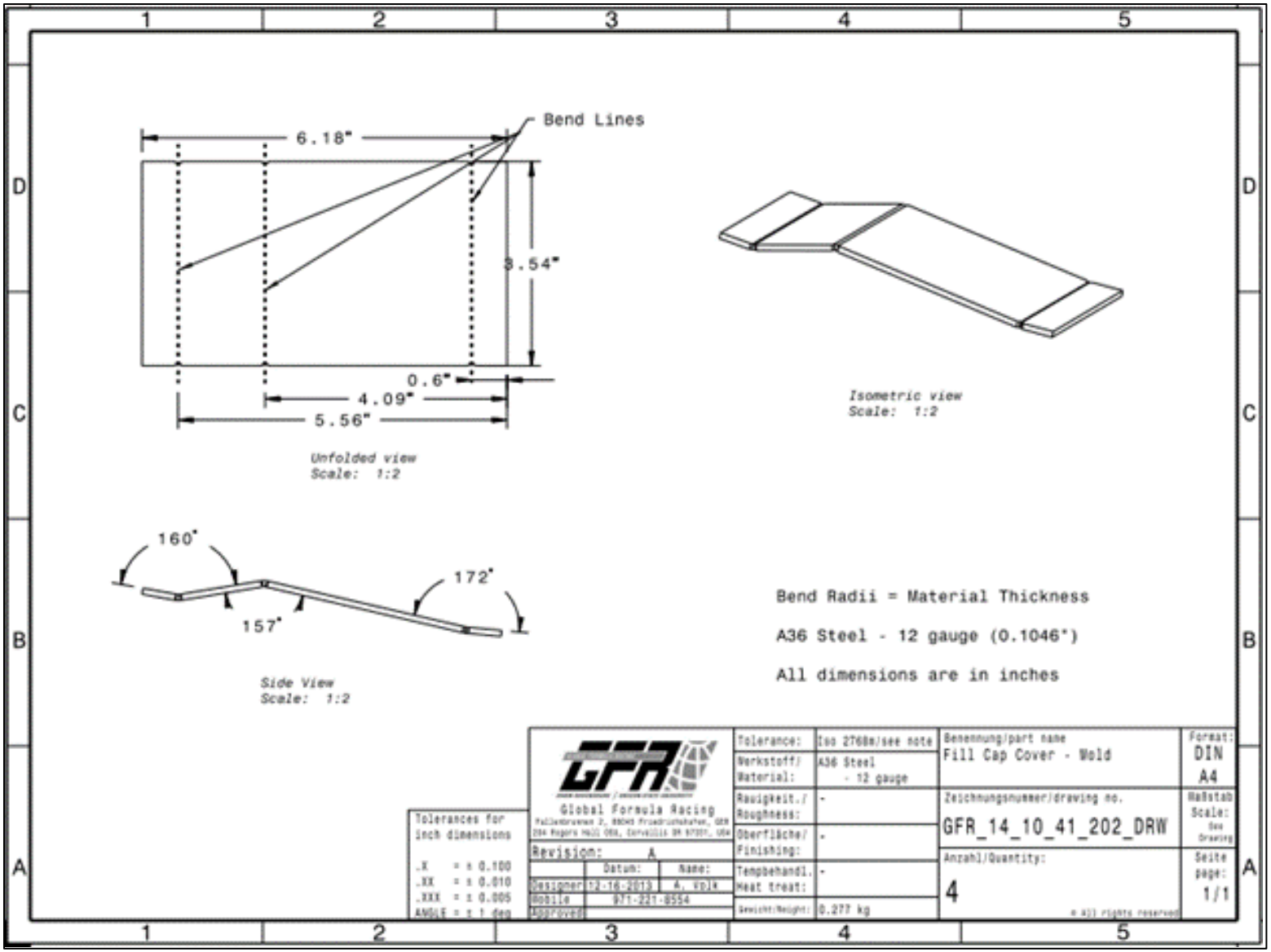

Figure B 6: Fill cap cover sheet metal mold three-view engineering drawing

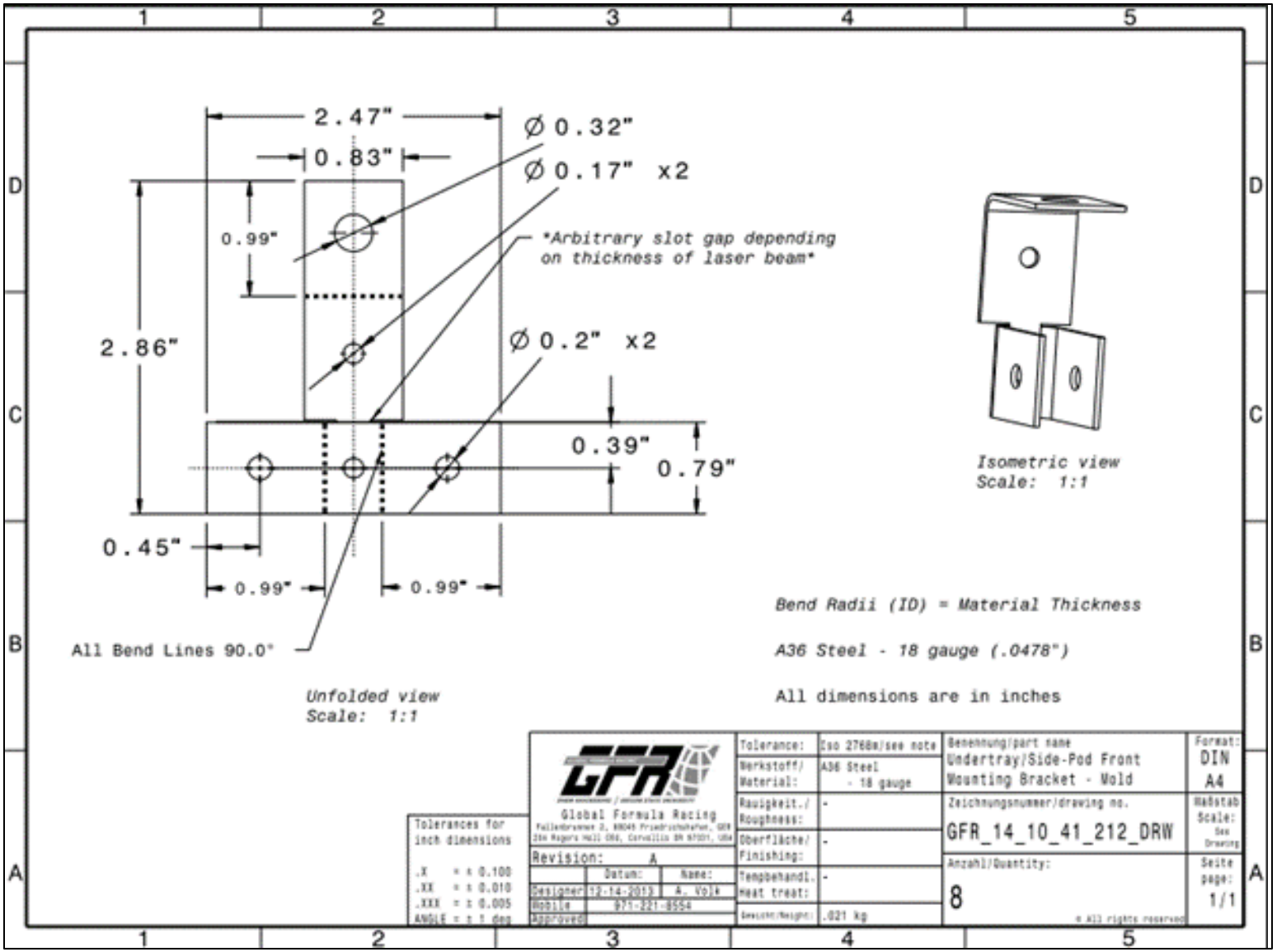

Figure B 7: Engineering drawing of the front bracket sheet metal mold.

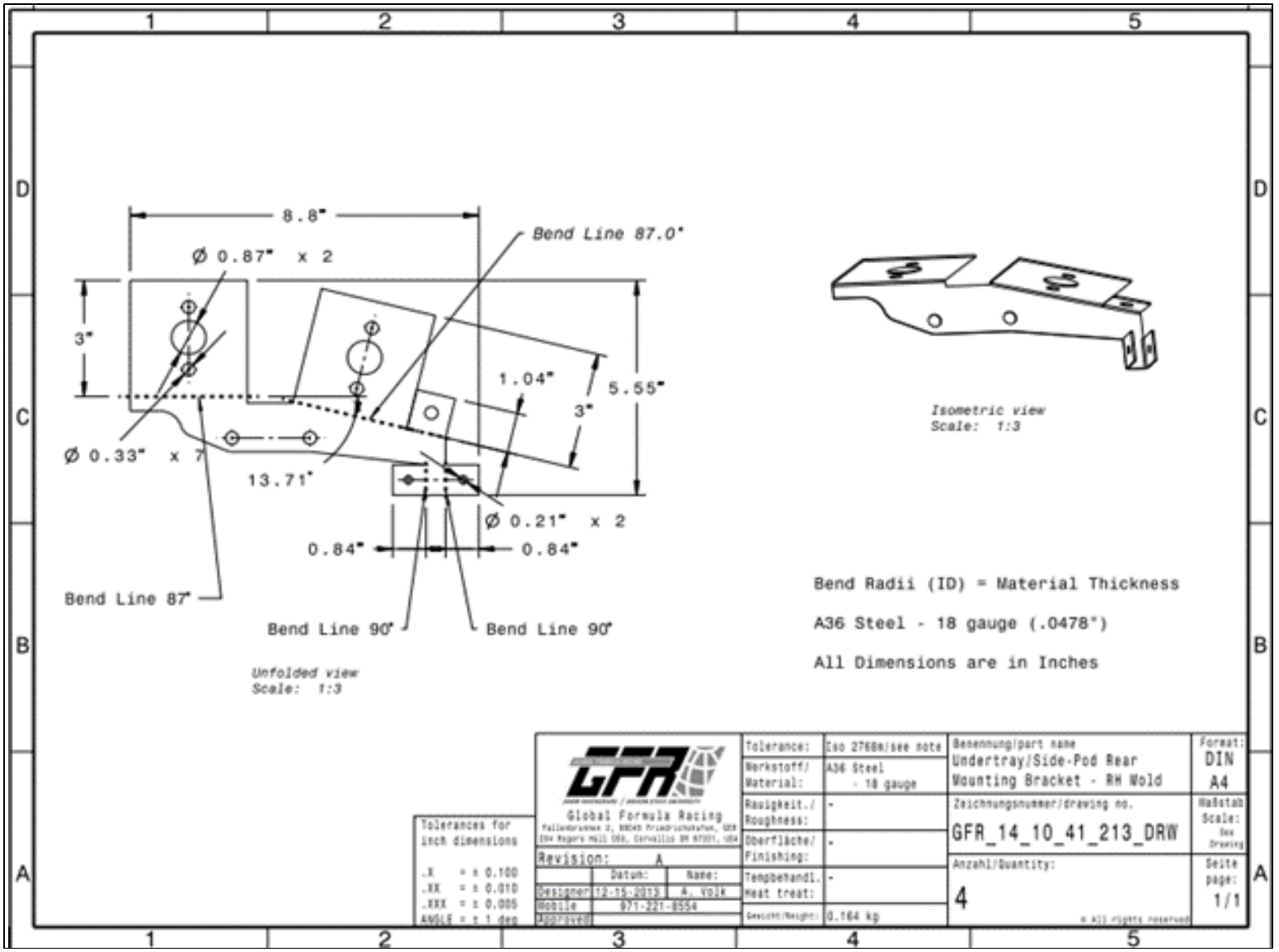

Figure B 8: Engineering drawing of RH mold for rear mounting bracket.

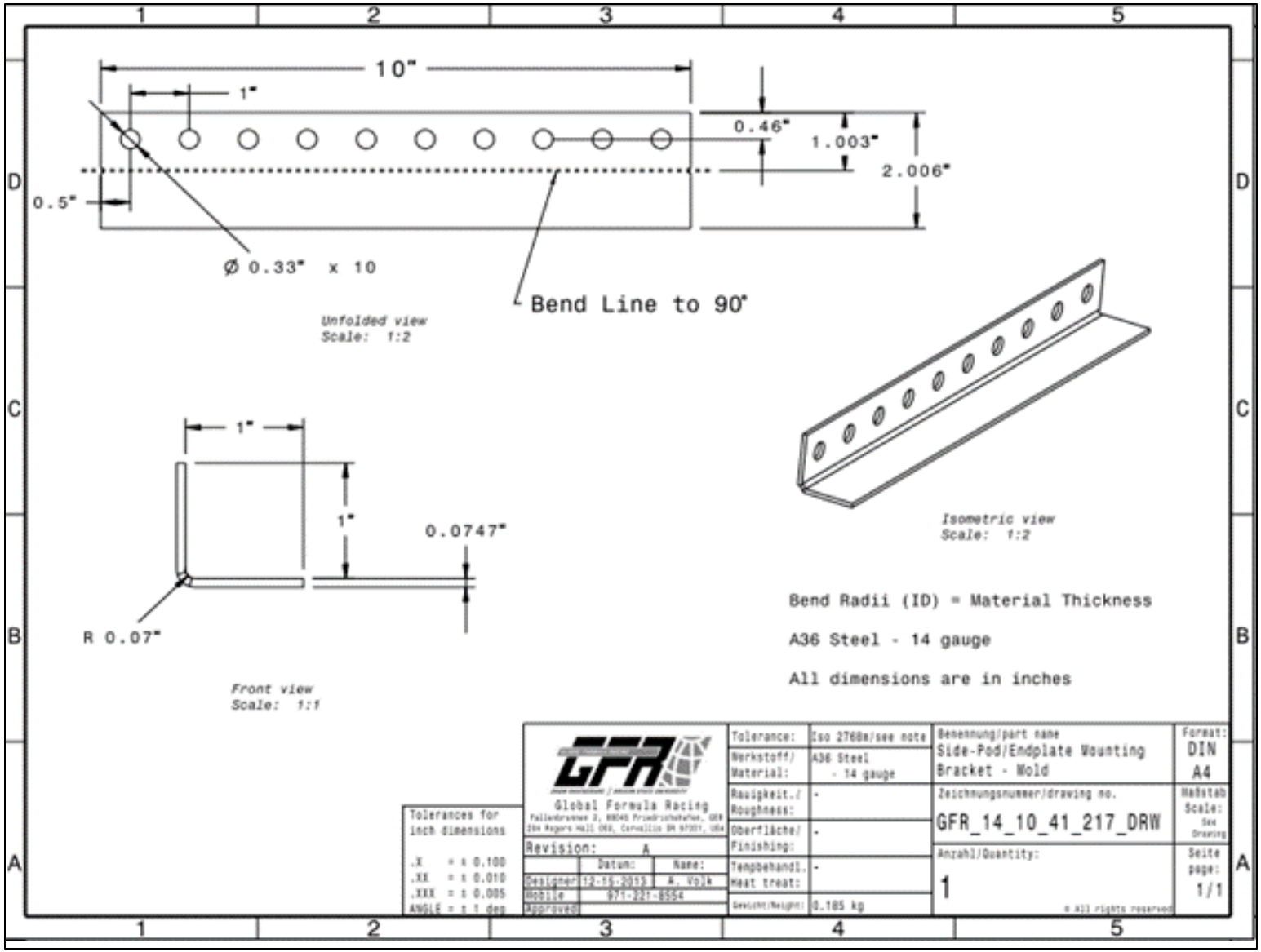

Figure B 9: Engineering drawing for the side-pod/endplate mounting bracket mold.

Appendix C – Templates

Front Ducting:

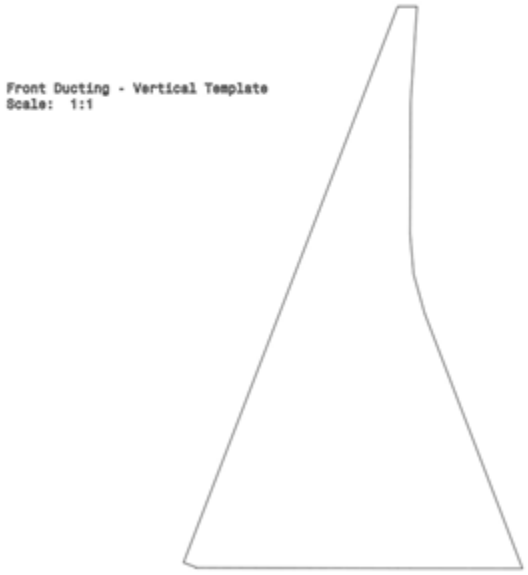

Figure C 1: Vertical template for front ducting

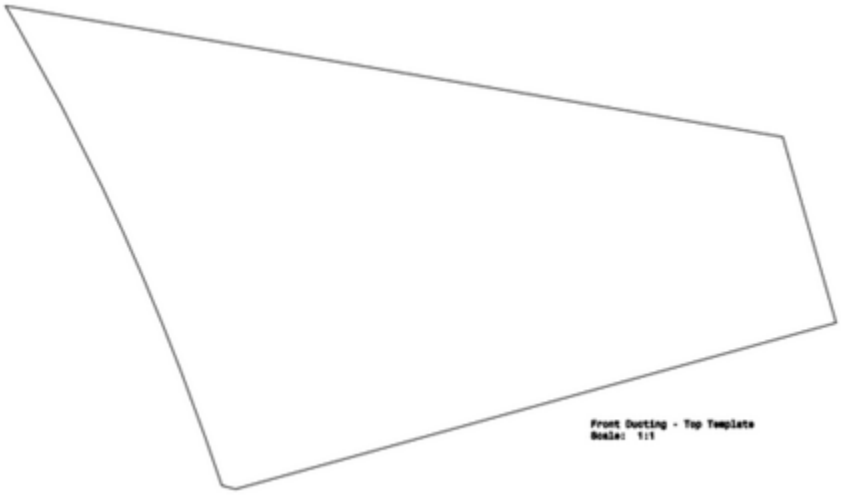

Figure C 2: Horizontal template for front ducting

Rear Ducting:

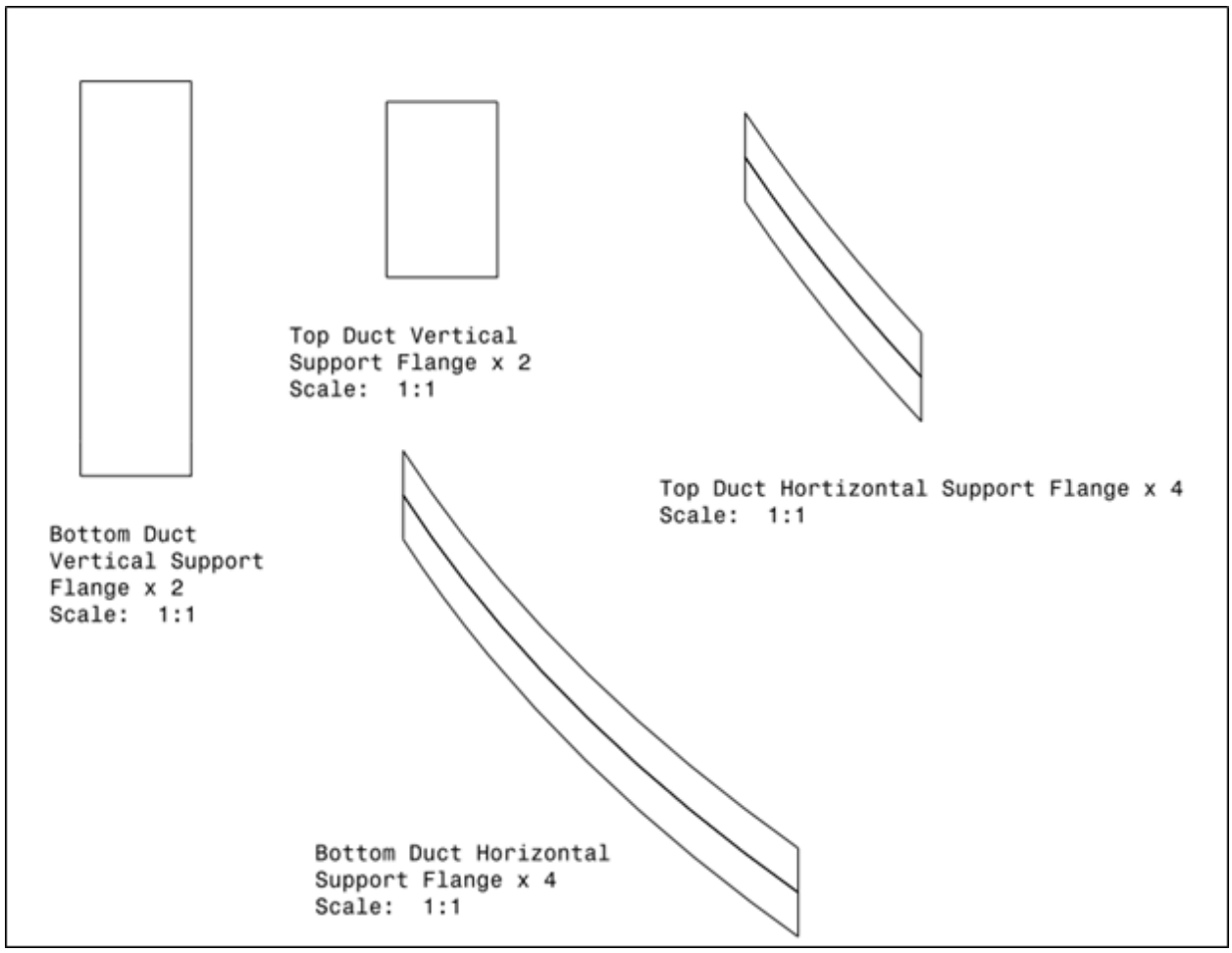

Figure C 3: Templates for vertical supports and flanges

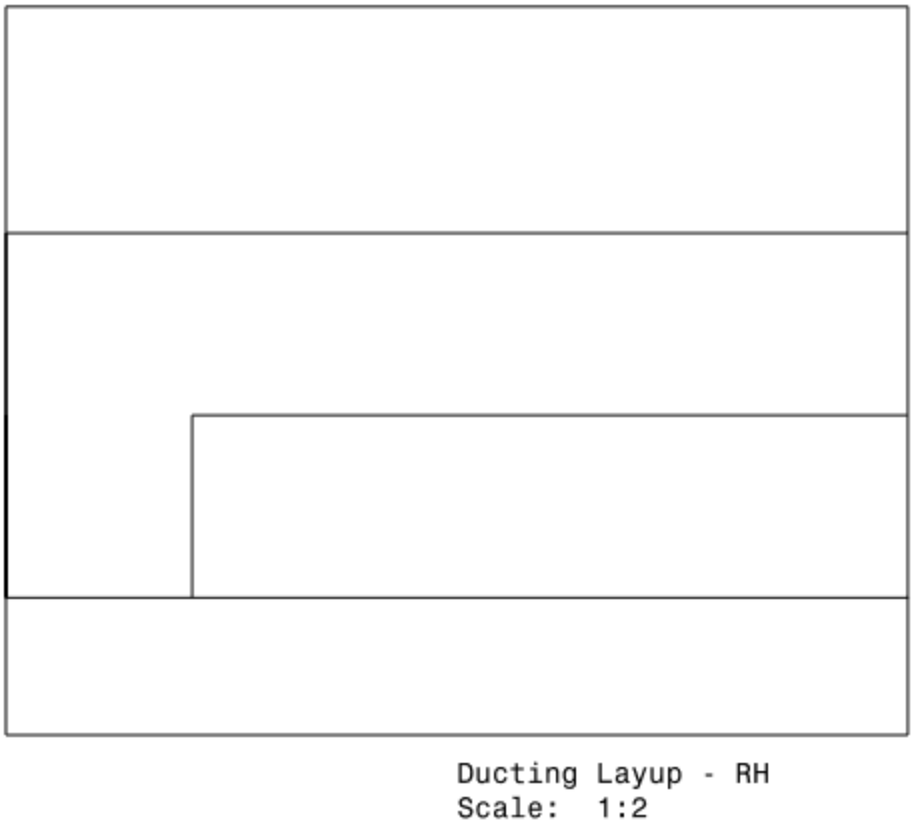

Figure C 4: Wing flap ducting elements and positioning in wing flap mold. (RH shown)

Fan Shroud:

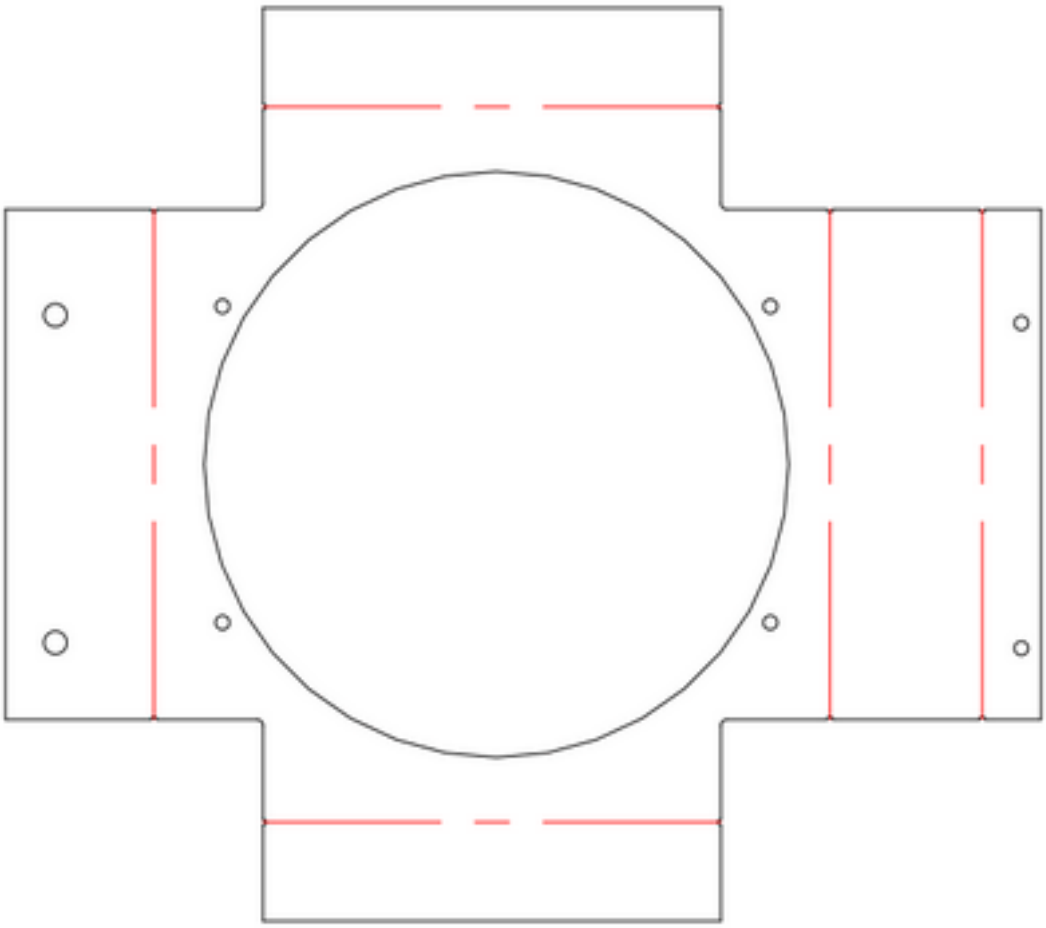

Figure C 5: Unfolded sheet-metal mold template. Bend lines are indicated by the red lines